SEDIMENTARY, MICROBIAL AND DEFORMATION FEATURES IN THE LOWER BELT SUPERGROUP (*ca*. 1.45 Ga), WESTERN NORTH AMERICA: PSEUDOFOSSILS, FACIES, TIDES AND SYNDEPOSITIONAL TECTONIC ACTIVITY IN A MESOPROTEROZOIC INTRACRATONIC BASIN

A Thesis Submitted to the
College of Graduate and Postdoctoral Studies
In Partial Fulfillment of the Requirements
For the Degree of Doctor of Philosophy
In the Department of Geological Sciences
University of Saskatchewan
Saskatoon

By

Roy Gregory Rule

PERMISSION TO USE

In presenting this thesis in partial fulfilment of the requirements for a Postgraduate degree from the University of Saskatchewan, I agree that the Libraries of this University may make it freely available for inspection. I further agree that permission for copying of this thesis in any manner, in whole or in part, for scholarly purposes may be granted by the professor or professors who supervised my thesis work or, in their absence, by the Head of the Department or the Dean of the College in which my thesis work was done. It is understood that any copying or publication or use of this thesis or parts thereof for financial gain shall not be allowed without my written permission. It is also understood that due recognition shall be given to me and to the University of Saskatchewan in any scholarly use which may be made of any material in my thesis.

Requests for permission to copy or to make other uses of materials in this thesis in whole or part should be addressed to:

Head of the Geological Sciences
Geology Building
University of Saskatchewan
Saskatoon, Saskatchewan S7N 5E2, Canada

Or

Dean
College of Graduate and Postdoctoral Studies
University of Saskatchewan
116 Thorvaldson Building, 110 Science Place
Saskatoon, Saskatchewan S7N 5C9, Canada

ABSTRACT

Sedimentary, microbial and deformation features in the lower Belt Supergroup (*ca.* 1.45 Ga), western North America: pseudofossils, facies, tides and syndepositional tectonic activity in a Mesoproterozoic intracratonic basin

The Belt Supergroup, called the Purcell Supergroup in Canada, accumulated in a broad, rapidly subsiding basin that formed during the oblique collision of an Australian craton with western Laurentia around 1.45 Gyr ago. These rocks are exposed in southwestern Alberta, southeastern British Columbia, and adjacent northwestern Montana, Idaho and northeastern Washington. Emplaced over Upper Cretaceous rocks by the Lewis Thrust fault, the northeastern exposures of the Lower Belt succession are in Waterton and Glacier national parks of Alberta and Montana, as well Castle Wildland Provincial Park of Alberta. The Lower Belt in this region was deposited initially as a west-facing carbonate platform while the basin had considerable bathymetric relief, but it shallowed due to voluminous siliciclastic mud input from the eroding orogen to the west.

The Lower Belt has not been studied since the 1980s when the carbonate rocks were interpreted as tidal flat deposits, and a few years later the 'string-of-beads' features in mudstones of the lower Appekunny Formation were formally named *Horodyskia* and regarded as the oldest eukaryotic macrofossils. Thus, the aim of thesis is to approach these rocks in a modern perspective, using a combination of measured sections, photography, serial sectioning, petrography, scanning electron microscopy, X-ray diffraction, CT scanning and synchrotron XRF analysis.

Horodyskia has been interpreted as a eukaryotic fossil, and algal, animal and fungal-like affinities have been suggested. Instead, it is shown here to be not a fossil but the preferential binding of mud flakes and flocs onto a wrinkled and tufted microbial benthic mat. The mat, or biofilm, was characterized by elevated pinnacles and ridges that bound these particles creating the appearance of an organised curvilinear structure as the mat continued to build up over time. Although *Horodyskia* is not a eukaryotic fossil, it is not simply a pseudofossil but a kind of microbially-induced sedimentary structure.

The underlying Haig Brook, Tombstone Mountain and Waterton formations indicate that a broad, eastward-shallowing carbonate ramp developed. The carbonate factory was dominated by lime mud production. The overlying Altyn Formation records a prograding carbonate platform succession that culminated in a shallow shelf setting. Five main facies are identified in the Waterton and Altyn formations: laminated mudstone, ribbon limestone, grainstone, oolite and stromatolite patch reefs. The last three were deposited under relatively high energy conditions. In northern sections the quartz and carbonate sand formed shoals reworked by tidal action, whereas in the southern area this facies occurs as allochthonous beds in a deeper, outer shelf setting. Oolite and grainstone locally exhibit large clinoforms which are interpreted as westward-migrating sand bars formed by tidal currents. Extensive tidal flats and sabkhas are inferred to have been present along the coastline on the basis of silicified oolite and anhydrite grains admixed in the grainstone. Not only did tsunamis impact the coast, tsunami off-surge is interpreted as the main agent of transporting coarse inner shelf grains to the middle and outer shelf, and occasionally down the ramp. Tidal effects diminished, then ceased after burial of the carbonate platform by muds from a western source which led to a shallowing of the Belt Basin.

Although it was probably major faults in the basin centre that caused the tsunamis, tectonic activity also caused the platform to be wracked by strong earthquakes which generated a variety of syndepositional deformation structures depending on the rheology of the sediments. These seismites include folds, ball-and-pillow structure, cracks, microfaults, breccias, cataclastites, veins and rare molar-tooth structure. Molar-tooth structure also formed in inner-shelf lime muds as evidenced by transported microspar grains in grainstone. The facies-dependent nature of these features corroborates previous work on the Belt Supergroup and other units of pre-Cambrian and Phanerozoic ages.

The salient achievements of this study are: (1) elucidation of *Horodyskia* and the intricacies of mud deposition and microbial mats in the Appekunny Formation; (2) a new interpretation of the sedimentology of the Lower Belt carbonate platform based on facies and inferred environments; (3) the recognition of the effects of strong tides in the Belt Basin early in its development; (4) the recognition of the role of tsunamis in sediment transport on and off the platform; and (5) a better appreciation of the range and attributes of synsedimentary deformation features.

ACKNOWLEDGEMENTS

I thank the staff of Waterton and Glacier national parks, especially B. Johnson of the Ecology Team, for their aid, hospitality and support. I am grateful to field assistants A. Spragg, T. Magee and S. Elmer for sharing their adventuresome spirit and companionship. M.J. Pushie and G.N. George carried out the synchrotron XRF element analysis and D.M.L. Cooper and Y. Carter provided access and help with the micro-CT scanner. I thank T. Bonli for help with scanning electron microscopy and B. Novakovski for thin section preparation. S. Butler, C. Holmden, J.F. Basinger and C. Strachan-Crossman were helpful in departmental matters. Thanks also to E. King and S. Unsworth of the Student Wellness Centre, and S. Mamer-Dauvin of Access and Equity Services. I am very grateful to the College of Graduate and Postdoctoral Studies for granting the needed extensions. I thank P.R. Fermor for discussion of structural relationships in the study area, and for commenting on the thesis text.

I offer my sincere thanks to my supervisory committee: S. Butler, C. Holmden, E. Robertson, R. Renaut, and of course my supervisor, B.R. Pratt.

Funding for field work was from Natural Sciences and Engineering Research Council of Canada Discovery Grants to B.R. Pratt. I am grateful to the Department of Geological Sciences for providing Graduate Teaching Fellowships and the opportunity to serve as a teaching assistant in undergraduate courses.

I thank my family in the United Kingdom for their constant support and encouragement. Finally, a note of appreciation for my professors at the University of Plymouth, especially R.J. Twitchett, for urging me to undertake graduate studies.

TABLE OF CONTENTS

LIST OF FIGURES

CHAPTER 1

Introduction to the study

1. Introduction

Resting at the 'dog leg' of the Rocky Mountains, the Mesoproterozoic rocks of the Belt Supergroup rise up from the Prairies due to the sudden bend in the trace of the Lewis Thrust fault. This brings up these strata from the depths to overlie the softer Cretaceous rocks of the foothills and prairies. It is within this uplifted pre-Cambrian section the Waterton Lakes and Glacier national parks were established, and later linked as the international peace park astride the U.S.A.–Canada border as a symbol of friendship between the two countries. The Belt Supergroup is present in the adjacent subsurface in southeastern British Columbia, and it extends beyond the park boundaries across southwestern and western Montana and northern Idaho as far as easternmost Washington, and northwards through the recently established Castle Wildland Provincial Park of southwestern Alberta, westward into south-eastern British Columbia, and eastward to central Montana.

The Belt Supergroup is a strikingly thick and colourful succession that lends a spectacular uniqueness to the mountain scenery in this section of the Rocky Mountains. Despite the wide distribution and thickness of the Belt Supergroup, it has received much less study than might be expected. In particular, even the most fundamental aspects of the sedimentology of the various units remain controversial, even though the national parks have been visited by many geologists over the past century and more.

The purpose of this thesis is to tackle important aspects of two of the units in the lower part of the Belt Supergroup. The first aspect to be evaluated is the sedimentary structures, suggested to be macrofossils, in the siliciclastic Appekunny Formation. The aim here is to reevaluate the possibility of biological formation and offer a more comprehensive and plausible interpretation. The second is to make a sedimentological study of the underlying carbonate units, the Altyn and Waterton formations. These comprise a carbonate platform succession that accumulated on the northeastern margin of the basin. The results of these efforts have considerable application to the rock record in general, identifying the processes and depositional facies, the behaviour of mud-sized particles before bioturbation, and the effects of earthquakes, tides, storms and tsunamis in sediment movement and reworking.

2. The Proterozoic of North America

The Proterozoic eon lasted from ~2500 Ma to ~541 Ma, and was the time when atmospheric and environmental changes began to move towards their modern state. Changes in sea water chemistry, the production of oxygen by stromatolites and planktic cyanobacteria and algae, and the formation of major cratons and two supercontinents, Columbia (also known as Nuna) and Rodinia (Zhao et al., 2004; Bogdanova et al., 2015; Pehrsson et al., 2016) are just some of the characteristics of this time period. Information gleaned from the sedimentary material deposited during this time shows how sediments were affected by different events and processes, at most under microbial influence, without faunal or floral interaction, as well as giving insight into the formation of material in Mars' ancient seas and oceans (Noffke, 2015).

2.1. The Paleoproterozoic

The Paleoproterozoic lasted between ~2500 Ma and ~1600 Ma, and makes its mark due to the presence of the Great Oxidation Event during ~2400 Ma to ~2000 Ma. At the beginning of this event, seawater began to evolve towards a more modern composition; due to the changes in atmospheric oxygen, increased terrestrial erosion and the flow of metals and sulphides into the seawater causing a diversification of the biota and, in turn, the subsequent changes towards a more oxygenated atmosphere (e.g., Konhauser et al., 2009; Steadman et al., 2020). Paleosols began to form during the Paleoproterozoic, and it has been suggested that there was significantly elevated carbon dioxide level during the Paleoproterozoic which led to a higher rate of chemical weathering than during the Meso- and Neoproterozoic (Mitchell and Sheldon, 2010).

There is evidence that during this time there was extensive glacial cover in what is now North America based on attributes of the Snowy Pass and Huronian supergroups, where carbonate rocks deposited between ~2.4 and ~2.2 Ga show carbon-isotopic values and sedimentary structures that could suggest the presence of cap carbonates (Bekker et al., 2005).

In North America, the Trans-Hudson orogeny took place between ~2070 Ma and ~1800 Ma with first the opening of the Manikewan Ocean and then its closing (Corrigan et al., 2009). This makes up the final phase of the assembly of the supercontinent. Over time and possibly starting during the Great Oxidation Event, Columbia began to break up. While the initial growth and evolution of the supercontinent was during the Paleoproterozoic, it was still mostly intact until around ~1600 Ma, but then separated into an array of cratons, such as Laurentia and Baltica, by ~1400 Ma (Pisarevsky et al., 2014). The early phase of the disassembly of Columbia was the precursor for the rifting associated with the formation of the Belt Basin.

2.2. The Mesoproterozoic

The Mesoproterozoic, comically referred to by some as "the Boring Billion" (Lyons et al., 2012; Roberts, 2013), is an era associated with slow but steady changes in the environment as microbial life developed in a wider range of biological and sedimentary structures, such as the proliferation of different types of stromatolites (Grotzinger and Knoll, 1999), fungal forms (Loron et al, 2019) and microbial mats (Noffke, 2010). These changes exerted a more important influence on biological factors during sedimentation, for example the binding of sediment on microbial mats and polysaccharides acting as an adhesive for sediment grains during flocculation. The proliferation of stromatolites and microbial mat features during the Mesoproterozoic (Grotzinger and Knoll, 1999; Noffke, 2010; Noffke et al., 2002) in shallow-marine regions and other aquatic environments associated with the widespread formation of carbonate platforms and reefs. The Belt Supergroup itself houses many stromatolites, such as the branching *Baicalia* and the domal stromatolites conforming to *Collenia*.

Seawater chemistry had already begun to move towards a more modern composition during the Paleoproterozoic (Strauss, 2002), and the increasing oxygen content and decreasing carbon dioxide levels in the atmosphere changed the weathering and chemical pathways of erosion (Sheldon, 2013). Mesoproterozoic chromium isotopes, as well as oxidized sulphur and molybdenum have been interpreted to indicate a continuing increase in atmospheric and seawater oxygen levels, to at least >1% of modern atmospheric level (Cox et al., 2016; Canfield et al., 2018). Carbonate platforms were the world's first major carbon sinks, locking in the carbon over a billion years before trees ever took root. The chemistry would have further been affected as certain microorganisms in microbial mats interacted with silica (Dong et al., 2008; Manning-Berg and Kah, 2017).

Mesoproterozoic rocks were the inspiration for the idea of shales and mudstones being deposited in shallower, higher energy waters than hitherto believed. Lenticular lamination in shales of the Newland and Greyson formations of the Belt Supergroup led Schieber (1998) to propose that muds could flocculate in the water column and later be compressed into small lenses, a process now observed in many other units (Schieber and Southard, 2009).

Rifting caused widespread volcanism across Laurentia, Baltica and Siberia (Bingen et al., 2008). Part of the evidence for a Siberian connection to western Laurentia was the presence of volcanic dykes in the Udzha basin of the same age and same volcanic event as those in the Belt Supergroup (Sears, 2004; Sears and Price, 2003). It has also been suggested that the Belt Basin's "sister" in Western Australia could be the Bangemall Supergroup, both sharing similar ages (Martin et al., 2008), isotopic compositions (Ross et al., 1992; Ross and Villeneuve, 2003), sedimentary facies and pseudofossils (Calver et al., 2010; Grey et al., 2010; Martin et al., 2008). However, the Western Australian craton is now considered to be not directly adjacent to Laurentia, and oblique collision with the Mawson craton (East Antarctica) is implicated in the formation of the Belt Basin (Pisarevsky et al., 2014; Medig et al., 2014; Pehrsson et al., 2016).

2.3. The Neoproterozoic

By ~1000 Ma Laurentia was part of the supercontinent Rodinia, formed from the re-assembly of the cratons, including collisions that caused the Grenville orogeny along the eastern side (Hynes and Rivers, 2010). Later rifting and passive margin formation along the western side led to deposition of the Windermere Supergroup (Ross and Arnott, 2007).

During the Neoproterozoic when the development of the storied but controversial Snowball Earth state took place (Hoffman et al., 1998), based on glacially influenced deposits and cap carbonates from many places around the earth. The Sturtian and Marinoan glaciations (Evans, 2009; Eyles and Januszczak, 2004; Zhao et al., 2002) in the Cryogenian (Rooney et al., 2015) suggest a phase where the seas, continents or the entire planet were frozen over (Pierrehumbert et al., 2011). It was after this phase when complex animal life appeared, the precursor to the Cambrian Explosion (Wood et al., 2019).

3. The Belt Supergroup

3.1. History of study

Although the first stratigraphic scheme was presented by Willis (1902), the geology along the U.S.A.–Canada border, in the area now known as Waterton-Glacier International Peace Park, had been examined by H. Bauerman in the 1860s, but not published until twenty years later (Bauerman, 1885). Charles Walcott first laid eyes on the Belt Supergroup in 1895, and by the time he returned to study the rocks in 1905, Waterton Lakes National Park had already been the site of western Canada's first producing oil well, drilled in 1902 on an oil seep. Based on the occurrence of stromatolites Walcott realized that these rocks are pre-Cambrian in age and deposited prior to the evolution of animal life. The Fentons (Fenton and Fenton., 1937) elaborated on this in their study of the stratigraphy in 1937, and the stromatolites in particular were described in some detail by Rezak (1957). The geology of the Glacier National Park and neighbouring Flathead Range was described by Ross (1959).

Early stratigraphers concentrated on two separate areas: The Belt Supergroup, named after the Little Belt Mountains of central Montana, and the Purcell Supergroup, named by Daly (1912) after the Purcell Mountains of south-eastern British Columbia. Two sets of partly overlapping formational names were erected. Rocks of the 'Belt–Purcell Supergroup' turned

out to host important ore deposits, and that of the Sullivan district of south-eastern British Columbia was studied in particular detail. The regional context in British Columbia was enhanced by stratigraphic and structural work by Price and his students, McMechan and Fermor, as well as Höy (McMechan, 1981; Fermor and Price, 1983; Höy, 1993).

'Modern' sedimentological research started in the 1970s, by Horodyski (Horodyski, 1976, 1977) and Winston (inter alia 2007, 2016; Winston et al., 2013) who over nearly 50 years published numerous descriptions of stratigraphic units and field guide contributions, and supervised a number of graduate students who focused on individual formations. He reinterpreted the Belt Basin as a lake (Winston, 1985, 1990, 2016), although this was challenged by Schieber (1998) based on study of units in the Helena Embayment in the eastern part of the basin. Horodyski studied the stromatolites and other sedimentary features in Glacier National Park. Later, Pratt (1998a, 1999, 2001) focused mainly on the sedimentology and deformation features—especially molar-tooth structure—in the Helena Formation and then on the younger Grinnell Formation (Pratt and Ponce, 2019).

In the last nearly 30 years there have been a number of studies of detrital zircon geochronology in siliciclastic units of the Belt Supergroup. These have up to now corroborated the suggestion based on petrographic characteristics that the source of compositionally immature fine-grained siliciclastic sediment was mainly from a now-vanished orogenic belt to the west, whereas mature silt- and sand-sized sediment was from the Archean-cored cratonic area to the east (Ross and Villeneuve, 2003; Link et al., 2016).

3.2. Location

The Belt Supergroup stretches across an area greater than 200,000 km^2, with U.S. outcrops located in northern Idaho, eastern Washington and western to central Montana. On the Canadian side of the border, the Belt Supergroup dominates the southernmost Canadian Rocky Mountains of southwestern Alberta and southeastern British Columbia. Outcrops in the Cordillera are located within areas of considerable uplift from major thrust faults, with the most continuous successions in the Waterton–Glacier International Peace Park, but additional ones are present in the Big Belt and Little Belt mountains and the western Rocky Mountains of the U.S., and in the Castle Wildland Provincial Park, Clark Range and Purcell Mountains of Canada.

3.3. Paleogeography

Deposition of the Belt Supergroup took place post 1.47 Ga. Most agree that it was a rift basin formed in the western part of the Medicine Hat Block, Great Falls Tectonic Zone, and Wyoming craton (Ross and Villeneuve, 2003). Mawsonia (East Antarctic craton) is currently thought to have collided against northwestern Laurentia (Medig et al., 2014, Pisarevsky et al., 2014)

Geochemistry of the Belt Supergroup suggests a salty water body, with freshwater influxes off the land from fluvial input (Lyons et al., 2000). The argument is whether the rocks were deposited within a sea connected to the ocean, or if the basin was a fully intracratonic lake (Winston et al., 1993). The presence of stromatolites and microbial mat structures similar to those recorded elsewhere, such as *Horodyskia* and the stromatolites *Baicalia* and *Conophyton* (Horodyski, 1977; Winston et al., 2013), argue for marine conditions. Halite as the dominant evaporite mineral where evidence for evaporites is present, with only rare evidence for sulfates, has been explained as due to bottom-hugging brines rather than a non-marine hypersaline water chemistry (Pratt, 2001; Pratt and Ponce, 2019).

3.4. Stratigraphy

3.4.1. Basin formation

Rifting of the Belt Basin began at ~1.47 Ga, after the breakup of the supercontinent Columbia. A series of rifts may have developed along the now western margin of Laurentia. Rifting involved volcanism based on sills drilled in the lower Prichard Formation (= Aldridge Formation in Canada) and thought to be imaged in the subsurface (Harrison et al., 1985; Cook and Van der Velden, 1995). The initial tectonic activity led to deposition of fluvial sands of the Neihart and Fort Steele formations followed by rapid subsidence and marine flooding (Ross and Villeneuve, 2003). Deposition of the Prichard Formation (= Aldridge Formation in Canada) involved turbidites and hemipelagic argillaceous silts and volcanics, along with volcanogenic massive sulphide Sullivan deposit of southern British Columbia (Lydon, 2007).

3.4.2. Lower Belt

The Haig Brook, Tombstone Mountain, Waterton and Altyn formations mark the early record of transgression and regression in the Belt Supergroup. These rocks show the mixing of the products of the shallow-water carbonate factory with clay and silt from the adjacent land surface. The Altyn Formation passes stratigraphically upwards into the argillaceous siltstone and very fine-grained sandstone of the overlying Appekunny Formation. The source of this sediment was the developing orogen on the western side of the basin (Pratt, 2017; Rule and Pratt, 2019).

3.4.3. Ravalli Group

The Ravalli Group, consisting in the eastern area of the Belt Basin of the Grinnell and Creston formations, overlies the Lower Belt carbonates. This succession is characterised by strikingly colourful siliciclastic rock types (Pratt and Ponce, 2019). They may have been deposited in a series of transgressions and regressions, but without shallow-water equivalents this cannot be ascertained. These units have been debated as to original bathymetry and sedimentary environment, with interpretations ranging from relatively deep water to subaerial (Winston, 2016; Pratt and Ponce, 2019). They exhibit abundant evidence for frequent soft-sediment deformation by syndepositional earthquakes generated by faulting in the basin (Pratt, 2017; Pratt and Ponce, 2019).

The Appekunny Formation is discussed in Chapter 2 (focusing on microbial textures and the pseudofossil *Horodyskia*), and the lower part of the formation at least is argued to be a deeper-water depositional environment with clay, silt and very fine-grained sand having smothered the underlying carbonate ramp and shelf.

The Grinnell Formation is the most controversial in terms of depositional environment. Composed of mudstones interbedded with sandstones, the Grinnell Formation is renowned for its deep red or maroon colouration. It has been identified as being both marine, fluvial and alluvial in origin. Both the Appekunny and Grinnell formations exhibit textures which point to ‘sticky mud’ properties that are not understood, although likely involve mineralogical, chemical and biological factors (Pratt and Ponce, 2019). This led to unusual features like mud intraclasts and mudballs in the Grinnell Formation and muddy flocs and flakes in the Appekunny Formation (Chapter 2).

3.4.4. Piegan Group

This group, hitherto often referred to as the Middle Belt Carbonate, was deposited around ~1.45 Ga, and consists of the Helena and Wallace formations (= Siyeh and Kitchener formations in Canada). These units are thick, stromatolite-bearing strata. They are riddled with molar-tooth structure (Pratt, 1998b, 1999, 2001; Winston, 2007). As with other units, the depositional setting has been controversial, with not only the lacustrine versus marine environment being debated but also water depth: peritidal versus a continuously submerged environment (Frank et al., 1997; Pratt, 2001).

Molar-tooth structure was ignored for over a century since it was first described, but eventually it was recognized in mainly—but not exclusively—Proterozoic carbonates worldwide. The stromatolites and dolomitic limestone of the Helena Formation have undergone cracking, rupturing and shrinkage, depending on facies and rheology, and fissures were infilled with lime mud expelled and injected as a slurry during dewatering. While many have tried to detect a biological or chemical origin for these features (Furniss et al., 1998), the preponderance of evidence favours a tectonic origin (Pratt, 1998b, 1999).

3.4.5. Missoula Group

The uppermost part of the Belt Supergroup consists of a succession of subaqueous deposits comprising the Snowslip and Shepard (= Gateway and Sheppard formations in Canada) and overlying units, with one exception, the Bonner Formation (= Phillips Formation in Canada) which is fluvial, at least in part.

In the upper part of the Gateway Formation in the northeastern part of the Belt Basin the Purcell Lava consists of a 10 m thick amygdaloidal pillow basalt unit overlain by a series of pahoehoe flows, suggesting a ~10 m water depth in that area (Pratt, 2001). The units comprising the Missoula Group have largely escaped modern, detailed sedimentological study.

4. This Study

The aim of this study is to examine in detail the Lower Belt carbonates and lower Appekunny Formation, and identify and analyse the sedimentology and sedimentary structures of the Waterton, Altyn and the lower Appekunny formations. To do this, I have focused on sections mainly in Waterton Lakes and Glacier national parks.

The Lower Belt carbonate platform provides a snapshot of carbonate sedimentation and facies development long before the advent of bioturbation, and a case study where the effects of tectonic, storm and tidal processes can be evaluated. Microbial activity was locally important. This plexus of processes is relevant for other Precambrian platforms but also their Phanerozoic equivalents, especially lower Paleozoic examples which share similar sediment types.

The pseudofossil *Horodyskia*, a structure often described as “the string-of-beads fossil” or “problematic bedding plane markings”, is evaluated in detail, which is crucial to the understanding of the oldest eukaryotic fossil record. This is the first part of this thesis (Chapter 2).

The second section of this thesis (Chapter 3) is the stratigraphic record and facies analysis of the Lower Belt carbonate platform. The focus here is defining and describing the sedimentary structures and facies in order to reconstruct the architecture and bathymetry of the platform and determine its evolution over time. Two other processes are elucidated. The role of tsunamis is interpreted as a mechanism for delivering coarse, nearshore sediment onto the offshore carbonate platform. Secondly, features interpreted as migrating bar deposits in the upper part of the carbonate platform are ascribed to strong tidal currents. This is a novel

take on the processes that operated in the Belt Basin, and pose interesting and relevant questions, but also supports a tidal interpretation for dune deposits in the upper part of the succession. The interpretation of the overall sedimentary environment is markedly different from those of previous views (Horodyski, 1983; White, 1984; Hill and Mountjoy, 1984; Pratt, 1994).

In the final section of this thesis (Chapter 4), the record of synsedimentary deformation on the ramp and platform is analyzed. This includes structures that are common to many other units in the stratigraphic record, and also are both similar to but also contrasting with other carbonate facies of the Belt Supergroup. The stratigraphic variation of these features helps elucidate which facies were vulnerable to the various effects of synsedimentary earthquake-induced deformation and how they responded.

By describing the facies and sedimentary processes of the lower Belt carbonate units the carbonate platform and adjacent ramp is reconstructed. This is relevant for the understanding of how these environments formed at other times. Discrimination of various processes that disrupt and deform the sediments is also important for interpreting counterparts in other platforms. The insight gained from the pseudofossil *Horodyskia* in the Appekunny Formation aid in the appreciation of the impact of biological factors muddy siliciclastic environments.

References

Anbar, A.D., Duan, Y., Lyons, T.W., Arnold, G.L., Kendall, B., Creaser, R.A., Kaufman, A.J., Gordon, G.W., Scott, C., Garvin, J., Buick, R., 2007. A whiff of oxygen before the Great Oxidation Event?. Science 317, 1903–1906.

Baird, D.J., Knapp, J.H., Steer, D.N., Brown, L.D., Nelson, K.D., 1995. Upper-mantle reflectivity beneath the Williston basin, phase-change Moho, and the origin of intracratonic basins. Geology 23, 431–434.

Bauerman, H., 1885, Report on the geology of the country near the forty-ninth parallel of the north latitude west of the Rocky Mountains. Canadian Geological Survey, Report of Progress 1882–1884, pt. B, 1–42.

Bekker, A., Kaufman, A.J., Karhu, J.A., Eriksson, K.A., 2005. Evidence for Paleoproterozoic cap carbonates in North America. Precambrian Research, 137, 167–206.

Bingen, B., Andersson, J., Soderlun, U., Moller, C., 2008. The Mesoproterozoic in the Nordic countries. Episodes 31, 1–6

Bogdanova, S., Gorbatschev, R., Skridlaite, G., Soesoo, A., Taran, L., Kurlovich, D., 2015. Trans-Baltic Palaeoproterozoic correlations towards the reconstruction of supercontinent Columbia/Nuna. Precambrian Research, 259, 5–33.

Calver, C.R., Grey, K., Laan, M., 2010. The ‘string of beads’ fossil (*Horodyskia*) in the mid-Proterozoic of Tasmania. Precambrian Research 180, 18–25.

Canfield, D.E., Zhang, S., Frank, A.B., Wang, X., Wang, H., Su, J., Ye, Y., Frei, R., 2018. Highly fractionated chromium isotopes in Mesoproterozoic-aged shales and atmospheric oxygen. Nature Communications 9, 1–11.

Cook, F.A., Van der Velden, A.J., 1995. Three-dimensional crustal structure of the Purcell anticlinorium in the Cordillera of southwestern Canada. Geological Society of America Bulletin 107, 642–664.

Corrigan, D., Pehrsson, S., Wodicka, N., Kemp, E. de, 2009. The Palaeoproterozoic Trans-Hudson Orogen: a prototype of modern accretionary processes. In: Murphy, J.B., Keppie, J.D., Hynes, A.J. (Eds.), Ancient Orogens and Modern Analogues, Geological Society Special Publication 327, 457–479.

Cox, G.M., Jarrett, A., Edwards, D., Crockford, P.W., Halverson, G.P., Collins, A.S., Poirier, A., Li, Z.-X., 2016. Basin redox and primary productivity within the Mesoproterozoic Roper Seaway. Chemical Geology 440, 101–114.

Daly, R.A., 1912. Geology of the North American Cordillera at the Forty-ninth Parallel. Geological Survey of Canada, Memoir 38, xxvii + 546 pp.

Dong, L., Xiao, S., Shen, B., Zhou, C., 2008. Silicified *Horodyskia* and *Palaeopascichnus* from upper Ediacaran cherts in South China: tentative phylogenetic interpretation and implications for evolutionary stasis. Journal of the Geological Society 165, 367–378.

Evans, D.A.D., 2009. The palaeomagnetically viable, long-lived and all-inclusive Rodinia supercontinent reconstruction. In: Murphy, J.B., Keppie, J.D., Hynes, A.J. (Eds), Ancient Orogens and Modern Analogues. Geological Society Special Publication 327, 371–404.

Eyles, N., Januszczak, N., 2004. 'Zipper-rift': a tectonic model for Neoproterozoic glaciations during the breakup of Rodinia after 750 Ma. Earth-Science Reviews 65, 1–73.

Fenton, C.L., Fenton, M.A., 1937. Belt Series of the North: stratigraphy, sedimentation, paleontology. Geological Society of America Bulletin 48, 1873–1970.

Frank, T.D., Lyons, T.W., Lohmann, K.C., 1997. Isotopic evidence for the paleoenvironmental evolution of the Mesoproterozoic Helena Formation, Belt Supergroup, Montana, USA. Geochimica et Cosmochimica Acta 61, 5023–5041.

Furniss, G., Rittel, J.E., Winston, D., 1998. Gas bubble and expansion crack origin of molar tooth calcite structures in the middle Proterozoic Belt Supergroup Western Montana. Journal of Sedimentary Research 68, 104–117.

Grey, K., Yochelson, E.L., Fedonkin, M.A., Martin, D.M., 2010. *Horodyskia williamsii* new species, a Mesoproterozoic macrofossil from Western Australia. Precambrian Research 180, 1–17.

Grotzinger, J.P., Knoll, A.H., 1999. Stromatolites in Precambrian carbonates: evolutionary mileposts or environmental dipsticks? Annual Review of Earth and Planetary Sciences 27, 313–358.

Harrison, J.E., Cressman, E.R., Kleinkopf, M.D., 1985. Regional structure, the Atlantic Richfield-Marathon Oil No. 1 Gibbs borehole, and hydrocarbon resource potential west of the Rocky Mountain trench in northwestern Montana. U.S. Geological Survey, Open-File Report 85-249, 8 pp.

Hill, R., Mountjoy, E.W., 1984. Stratigraphy and sedimentology of the Waterton Formation, Belt-Purcell Supergroup, Waterton Lakes National Park, southwest Alberta. Montana Geological Society, 1984 Field Conference, Northwestern Montana, 91–100.

Hoffman, P.F., Kaufman, A.J., Halverson, G.P., Schrag, D.P., 1998. A Neoproterozoic snowball earth. Science 281, 1342–1346.

Horodyski, R.J., 1976. Stromatolites from the Middle Proterozoic Altyn Limestone, Belt Supergroup, Glacier National Park, Montana. In: Walter, M. R. (Ed.), Stromatolites, pp. 585–597. Elsevier, Amsterdam.

Horodyski, R.J., 1977. Environmental influences on columnar stromatolite branching patterns: Examples from the Middle Proterozoic Belt Supergroup, Glacier National Park, Montana. Journal of Paleontology 51, 661–671.

Horodyski, R.J., 1983. Sedimentary geology and stromatolites of the Middle Proterozoic Belt Supergroup, Glacier National Park, Montana. Developments in Precambrian Geology 7, 283–317.

Höy, T., 1993. Geology of the Purcell Supergroup in the Fernie west-half map area, southeastern British Columbia. British Columbia Mineral Resources Division Bulletin 84, 157 pp.

Hynes, A., Rivers, T., 2010, Protracted continental collision - evidence from the Grenville Orogen. Canadian Journal of Earth Sciences, 47, 591–620.

Konhauser, K.O., Pecoits, E., Lalonde, S.V., Papineau, D., Nisbet, E.G., Barley, M.E., Arndt, N.T., Zahnle, K., Kamber, B.S., 2009. Oceanic nickel depletion and a methanogen famine before the Great Oxidation Event. Nature 458, 750–753.

Link, P.K., Stewart, E.D., Steel, T., Sherwin, J., Hess, L.T., and McDonald, C., 2016, Detrital zircons in Mesoproterozoic upper Belt Supergroup in the Pioneer, Beaverhead, and Lemhi ranges, Montana and Idaho: The Big White Arc. In*:* MacLean, J.S., and Sears, J.W. (Eds.), Belt Basin: Window to Mesoproterozoic Earth. Geological Society of America Special Paper 522, 163–183.

Lydon, J.W., 2007. Geology and metallogeny of the Belt–Purcell Basin, In: Goodfellow, W.D. (Ed.), Mineral Deposits of Canada: A Synthesis of Major Deposit Types, District Metallogeny, the Evolution of Geological Provinces, and Exploration Methods: Geological Association of Canada, Mineral Deposits Division Special Publication 5, pp. 581–607.

Lyons, T.W., Luepke, J.J., Schreiber, M.E., Zieg, G.A., 2000. Sulfur geochemical constraints on Mesoproterozoic restricted marine deposition: lower Belt Supergroup, northwestern United States. Geochimica et Cosmochimica Acta 64, 427–437.

Lyons, T.W., Reinhard, C.T., Love, G.D., Xiao, S., 2012. Geobiology of the Proterozoic eon. In: Knoll, A.D., Canfield, D.E., Konhauser, K.O. (Eds.), Fundamentals of Geobiology, pp. 371–402. Wiley-Blackwell, Chichester.

Manning-Berg, A.R., Kah, L.C., 2017. Proterozoic microbial mats and their constraints on environments of silicification. Geobiology 15, 469–483.

Martin, D.M., Sircombe, K.N., Thorne, A.M., Cawood, P.A., Nemchin, A.A., 2008. Provenance history of the Bangemall Supergroup and implications for the Mesoproterozoic paleogeography of the West Australian Craton. Precambrian Research, 166, 93–110.

McMechan, M.E., 1981. The Middle Proterozoic Purcell Supergroup in the southwestern Rocky and southeastern Purcell Mountains, British Columbia and the initiation of the Cordilleran miogeocline, southern Canada and adjacent United States. Bulletin of Canadian Petroleum Geology 29, 583–621.

Mitchell, R.L., Sheldon, N.D., 2010. The ~1100 Ma Sturgeon Falls paleosol revisited: Implications for Mesoproterozoic weathering environments and atmospheric CO_2 levels. Precambrian Research 183, 738–748.

Noffke, N., 2010. Geobiology: Microbial Mats in Sandy Deposits from the Archean Era to Today. Springer, Heidelberg, 194 pp.

Noffke, N., 2015. Ancient sedimentary structures in the < 3.7 Ga Gillespie Lake Member, Mars, that resemble macroscopic morphology, spatial associations, and temporal succession in terrestrial microbialites. Astrobiology 15, 169–192.

Noffke, N., Knoll, A.H., Grotzinger, J.P., 2002. Sedimentary controls on the formation and preservation of microbial mats in siliciclastic deposits: A case study from the Upper Neoproterozoic Nama Group, Namibia. Palaios 17, 533–544.

Pehrsson, S.J., Eglington, B.M., Evans, D.A.D., Huston, D., Reddy, S.M., 2016. Metallogeny and its link to orogenic style during the Nuna supercontinent cycle. In: Li, Z.X., Evans, D.A.D, Murphy, J.B., (Eds), Supercontinent Cycles Through Earth history, Geological Society Special Publication 424, 83–94.

Pierrehumbert, R.T., Abbot, D.S., Voigt, A., Koll, D., 2011. Climate of the Neoproterozoic. Annual Review of Earth and Planetary Sciences 39, 417–460.

Pisarevsky, S.A., Elming, S.-Å., Pesonen, L.J., Li, Z.-X., 2014. Mesoproterozoic paleogeography: Supercontinent and beyond. Precambrian Research 244, 207–225.

Planavsky, N.J., Asael, D., Hofmann, A., Reinhard, C.T., Lalonde, S.V., Knudsen, A., Wang, X., Ossa Ossa, F., Pecoits, E., Smith, A.J.B., Beukes, N.J., Bekker, A., Johnson, T.M.,

Konhauser, K.O., Lyons, T.W., Rouxel, O.J., 2014. Evidence for oxygenic photosynthesis half a billion years before the Great Oxidation Event. Nature Geoscience 7, 283–286.
Pratt, B.R., 1994. Seismites in the Mesoproterozoic Altyn Formation (Belt Supergroup), Montana: A test for tectonic control of peritidal carbonate cyclicity. Geology 22, 1091–1094.
Pratt, B.R., 1998a. Syneresis cracks: subaqueous shrinkage in argillaceous sediments caused by earthquake-induced dewatering. Sedimentary Geology 117, 1–10.
Pratt, B.R., 1998b. Molar-tooth structure in Proterozoic carbonate rocks: Origin from synsedimentary earthquakes, and implications for the nature and evolution of basins and marine sediment. Geological Society of America Bulletin 110, 1028–1045.
Pratt, B. R., 1999. Gas bubble and expansion crack origin of molar-tooth calcite structures in the Middle Proterozoic Belt Supergroup, western Montana—Discussion. Journal of Sedimentary Research 69, 1136–1140.
Pratt, B.R., 2001. Oceanography, bathymetry and syndepositional tectonics of a Precambrian intracratonic basin: integrating sediments, storms, earthquakes and tsunamis in the Belt Supergroup (Helena Formation, ca. 1.45Ga), western North America. Sedimentary Geology 141–142, 371–394.
Pratt, B.R., 2017. The Mesoproterozoic Belt Supergroup in Glacier and Waterton Lakes national parks, northwestern Montana and southwestern Alberta: Sedimentary facies and syndepositional deformation. In: Hsieh, J.C.C. (Ed.), Geologic Field Trips of the Canadian Rockies, 2017 Meeting of the GSA Rocky Mountain Section. Geological Society of America Field Guide 48, 123–135.
Pratt, B.R., Ponce, J.J., 2019. Sedimentation, earthquakes, and tsunamis in a shallow, muddy epeiric sea: Grinnell Formation (Belt Supergroup, ca. 1.45 Ga), western North America. GSA Bulletin 131, 1411–1439.
Roberts, N.M.W., 2013. The boring billion? – Lid tectonics, continental growth and environmental change associated with the Columbia supercontinent. Geoscience Frontiers 4, 681–691.
Rooney, A.D., Strauss, J.V., Brandon, A.D., Macdonald, F.A., 2015, A Cryogenian chronology: Two long-lasting synchronous Neoproterozoic glaciations. Geology 43, 459–462
Ross, C.P., 1959. Geology of Glacier National Park and the Flathead region, northwestern Montana. US Geological Survey Professional Paper 296, 125 pp.
Ross, G.M., Arnott, R.W.C., 2007. Regional geology of the Windermere Supergroup, southern Canadian Cordillera and stratigraphic setting of the Castle Creek study area, Canada, in: Nilsen, T.H., Shew, R.D., Steffens, G.S., Studlick, J.R.J. (Eds.), Atlas of Deep-Water Outcrops, AAPG Studies in Geology 56, 16 pp.
Ross, G.M., Parrish, R.R., Winston, D., 1992. Provenance and U-Pb geochronology of the Mesoproterozoic Belt Supergroup (northwestern United States): implications for age of deposition and pre-Panthalassa plate reconstructions. Earth and Planetary Science Letters 113, 57–76.
Ross, G.M., Villeneuve, M., 2003. Provenance of the Mesoproterozoic (1.45 Ga) Belt basin (western North America): Another piece in the pre-Rodinia paleogeographic puzzle. Geological Society of America Bulletin 115, 1191–1217.
Rule, R.G., Pratt, B.R., 2019. The pseudofossil Horodyskia: flocs and flakes on microbial mats in a shallow Mesoproterozoic sea (Appekunny Formation, Belt Supergroup, western North America). Precambrian Research 333, 105439.
Schieber, J., 1998. Possible indicators of microbial mat deposits in shales and sandstones: examples from the Mid-Proterozoic Belt Supergroup, Montana, U.S.A. Sedimentary Geology 120, 105–124.

Schieber, J., Southard, J.B., 2009. Bedload transport of mud by floccule ripples—Direct observation of ripple migration processes and their implications. Geology 37, 483–486.
Sears, J., 2004. Linking the Mesoproterozoic Belt-Purcell and Udzha basins across the west Laurentia–Siberia connection. Precambrian Research 129, 291–308.
Sears, J.W., Price, R.A., 2003. Tightening the Siberian connection to western Laurentia. Geological Society of America Bulletin 115, 943–953.
Sheldon, N.D., 2013. Causes and consequences of low atmospheric pCO2 in the Late Mesoproterozoic. Chemical Geology 362, 224–231.
Steadman, J.A., Large, R.R., Blamey, N.J., Mukherjee, I., Corkrey, R., Danyushevsky, L.V., Maslennikov, V. Hollings, P., Garven, G., Brand, U., Lécuyer, C., 2020. Evidence for elevated and variable atmospheric oxygen in the Precambrian. Precambrian Research 343, 105722.
Strauss, H., 2002. The isotopic composition of Precambrian sulphides—seawater chemistry and biological evolution. In: Alterman, W., Corcoran, P.L. (Eds.), Precambrian Sedimentary Environments: a Modern Approach to Ancient Depositional systems. International Association of Sedimentologists, Special Publication 33, 67–105.
Willis, B., 1902. Stratigraphy and structure, Lewis and Livingston ranges, Montana. Geological Society of America Bulletin 13, 305–352.
Winston, D., 1985. Tectonics and Sedimentation of Middle Proterozoic Belt Basin, and Their Influence on Cretaceous Compression and Tertiary Extension in Western Montana and Northern Idaho. AAPG Bulletin 69, 871–871.
Winston, D., 1990. Evidence for intracratonic, fluvial and lacustrine settings of Middle to Late Proterozoic basins of western U.S.A. In: Gower, C. F., Rivers, T., Ryan, B. (Eds.), Mid-Proterozoic Laurentia–Baltica. Geological Association of Canada Special Paper 38, 535–564.
Winston, D., Rittel, J.F., Furniss, G., 1998. Gas Bubble and Expansion Crack Origin of Molar-Tooth Calcite Structures in the Middle Proterozoic Belt Supergroup, Western Montana. Journal of Sedimentary Research 68, 104–114.
Winston, D., 2016. Sheetflood sedimentology of the Mesoproterozoic Revett Formation, Belt Supergroup, northwestern Montana, USA. In: MacLean, J.S. and Sears, J.W. (eds.), 2016. Belt Basin: Window to Mesoproterozoic Earth. Geological Society of America, Special Publication 522, 1–56
Winston, D., Link, P.K., 1993. Middle Proterozoic rocks of Montana, Idaho and eastern Washington: The Belt Supergroup. In: Link, P.K. (Ed.), Middle and Late Proterozoic stratified rocks of the western U.S. Cordillera, Colorado Plateau, and Basin and Range Province. In: Reed, J.C., Bickford, M.E., Houston, R.S., Link, P.K., Rankin, D.W., Sims, P.K., Van Schmus, W.R. (Eds.), Precambrian: Conterminous U.S. Geological Society of America, The Geology of North America C-2, pp. 487–517.
Winston, D., Horodyski, R.J., Whipple, J.W., 1989. Stromatolites of the Belt Supergroup, Glacier National Park, Montana. Middle Proterozoic Belt Supergroup, Western Montana: Great Falls, Montana to Spokane, Washington, American Geophysical Union Field Trip Guidebooks, 334, 27–42.
White, B., 1984. Stromatolites and associated facies in shallowing-upward cycles from the Middle Proterozoic Altyn Formation of Glacier National Park, Montana. Precambrian Research 24, 1–26.
Wood, R., Liu, A.G., Bowyer, F., Wilby, P.R., Dunn, F.S., Kenchington, C.G., Hoyal Cuthill, J.F., Mitchell, E.G., Penny, A., 2019. Integrated records of environmental change and evolution challenge the Cambrian Explosion. Nature Ecology & Evolution 3, 528–538.
Zhao, G., Cawood, P.A., Wilde, S.A., Sun, M., 2002. Review of global 2.1–1.8 Ga orogens: implications for a pre-Rodinia supercontinent. Earth-Science Reviews 59, 125–162.

Zhao, G., Sun, M., Wilde, S.A., Li, S., 2004. A Paleo-Mesoproterozoic supercontinent: assembly, growth and breakup. Earth-Science Reviews 67, 91–123.

CHAPTER 2

The pseudofossil *Horodyskia*: flocs and flakes on microbial mats in a shallow Mesoproterozoic sea (Appekunny Formation, Belt Supergroup, western North America)[1]

ABSTRACT

Horodyskia moniliformis Yochelson and Fedonkin, 2000 is found abundantly in its type area, the lower Appekunny Formation (Belt Supergroup; *ca*. 1.45 Ga) of northwestern Montana and adjacent southwestern Alberta. It has a distinct curving to meandering string-of-beads appearance on bedding planes of thin-bedded, laminated argillaceous siltstone, and has been regarded by some as one of the oldest eukaryotic organisms in the fossil record. The beads are disc-shaped to lenticular, ~1–5 mm in diameter, circular to elliptical to polygonal in outline, and composed of variably silty clay. They are interpreted as mud flocs and intraclasts. The beads in individual specimens are fairly uniform in size and spacing, but string length varies from about one to 15 cm depending in part on bead size. The radius of curvature varies from tight to open, but strings never form loops. Isolated beads are also present and smaller ones become indistinguishable from pustules which, along with mud-cored wrinkles and blisters, are associated on many bedding surfaces. These are regarded as evidence for a benthic microbial mat with variable topography ranging from crudely linear or stellate ridges to small domes and pinnacles. Rather than representing a semi-infaunal colonial eukaryote, fungal bladders or macroalgae, *Horodyskia* is here interpreted to be large mud particles that were trapped on tufts of the microbial mat. Commonly, the tufts were oriented in rows of similar-sized and generally evenly spaced pinnacles and these bound suspended flocs and flakes of a more or less uniform size, resulting in the features that appear organized as strings-of-beads. *Horodyskia* is therefore a microbially-induced sedimentary structure specific to a muddy, relatively low-energy, subtidal marine setting with just the right combination of sediment type depositional factors.

1. Introduction

The search for the oldest multicellular animal fossils has been a key paleontological quest since the Sir William E. Logan and then J. William Dawson introduced *Eozoan canadense* to the scientific world in the middle of the 19th century. Efforts have intensified over the past more than half a century after the enigmatic Ediacaran macrofossils were discovered and the scale and tempo of the Cambrian 'explosion' became apparent (e.g., Seilacher, 1992; Grazhdankin, 2014; Droser and Gehling, 2015; Budd and Jensen, 2017). At the same time, it has been necessary but often problematic to distinguish pre-Cambrian sedimentary features that may be biogenic from those that definitively are biogenic, and if the latter: microbially influenced or metazoan in origin. This is particularly critical for the interpretation of burrow-like structures well before the Cambrian (e.g., Bengtson et al., 2007; Buatois et al., 2018; El Albani et al., 2019) and the role of microbial mats in the taphonomy of metazoan compression fossils (Gehling, 1999).

'String-of-beads' features named *Horodyskia moniliformis* Yochelson and Fedonkin, 2000 were first identified in mudstone belonging to the Mesoproterozoic Appekunny Formation of

[1] Published as: Rule, R.G., and Pratt, B.R., 2019. The pseudofossil *Horodyskia*: Flocs and flakes on microbial mats in a shallow Mesoproterozoic sea (Appekunny Formation, Belt Supergroup, western North America): Precambrian Research, v. 333, article 105439, 15 pp. Analysis of the samples was carried out by Roy Rule and the manuscript was prepared jointly with Brian Pratt.

the Belt Basin of west-central North America. Initially regarded as a 'dubiofossil' (Horodyski, 1982), these were later interpreted to be tissue-grade colonial eukaryotic fossils (Fedonkin and Yochelson, 2002). A biological lifestyle was elaborated in which a row of stationary conical structures living on and just under the sediment–water interface was connected by a stolon. It was suggested that nutrition could have been via photosynthesis but, more likely, chemosynthesis. Other examples of *Horodyskia* and similar forms have since been discovered in Western Australia (Grey and Williams, 1990; Grey et al., 2010), Tasmania (Calver et al., 2010), South China (Dong et al., 2008) and North China (Shen et al., 2007), ranging in age from Mesoproterozoic to Ediacaran. A variety of interpretations has been proposed, yet despite the additional examples and newly named species as well as re-investigation of *Horodyskia* from its type area (Retallack et al., 2013), the origin of this feature has remained uncertain.

Recent work on the sedimentology of the lower and middle parts of the Belt Supergroup (Pratt, 2001, 2017; Pratt and Ponce, 2019) calls into question the contrasting environmental settings and depositional processes envisaged by Fedonkin and Yochelson (2002) and Retallack et al. (2013) for the *Horodyskia*-bearing strata. The purpose of this paper is to present new observations that show that these features are part of a range and perhaps a continuum of sedimentary features influenced by microbial mats that bound aggregates or flocs and intraclastic flakes of cohesive mud in a permanently submerged marine environment. We argue that they are not evidence for colonial eukaryotes, fungi, algae or other biological affinities that have been advanced, and that, rather, *Horodyskia* represents a microbially-induced sedimentary feature that formed due to the unusual nature of the muddy Belt Basin under specific sedimentological conditions that developed during deposition of the lower Appekunny Formation.

2. Methods

The Appekunny Formation crops out in Glacier National Park of northwestern Montana and Waterton Lakes National Park and Castle Wildland Provincial Park in adjacent southwestern Alberta (Fig. 2.1A, B). In Glacier National Park samples were collected mostly from the scree slope plus some from the adjacent outcrop on Apikuni Mountain (48°49'N, 113°38.5'W), as well a few from the Going-to-the-Sun Road cut at Dead Horse Point (48°41.3'N, 113°31.6'W) which is along strike 16.5 km to the south-southeast. In Waterton Lakes National Park samples were collected at Crypt Lake (48°59.8'N, 113°50.2'W) by the international border, from Sofa Mountain (49°02'N, 113°56'W) about 5 km to the northeast, and Bertha Lake (49°02'N, 113°56.2'W) 8 km to the west-northwest. Some were also collected from the eastern side of St. Eloi Mountain in Castle Wildland Provincial Park, Alberta (49°18.5'N, 114°28'W), 57 km northwest of Crypt Lake. Specimens have also been collected from the flank of Rising Wolf Mountain at Two Medicine Lake (48°29.5'N, 113°22.1'W) in Glacier National Park (Horodyski, 1982; Fedonkin and Yochelson, 2002; Retallack et al., 2013).

Samples of fresh and naturally weathered bed surfaces were photographed under incandescent light, both dry and wetted with ethanol. Selected samples exhibiting surface textures were painted with photographic opaque or diluted black gouache then dusted with ammonium chloride sublimate before photography under oblique lighting from the upper left, in accordance with standard paleontological practice. Several samples were serially ground parallel to bedding with 600 mesh carborundum grit and photographed wetted with ethanol. Approximately 60 thin sections were prepared both normal and parallel to bedding and photographed with the petrographic microscope or scanned with a flat-bed scanner. The lighting and contrast of most bedding plane images were digitally slightly enhanced using

Photoshop™. Selected examples of rock specimens and polished thin sections were examined under a scanning electron microscope. Synchrotron-based X-ray fluorescence imaging was performed on the upper surface of a thin bed exhibiting *Horodyskia* beads (at the Stanford Synchrotron Radiation Lightsource, Menlo Park, California; see Pushie et al. [2014] for analytical details). With a desktop micro-CT scanner an X-ray projection was made straight down on a specimen 5 mm thick. In addition, a 3x3x6 mm block with a *Horodyskia* bead on the top was scanned at 0.5 degree intervals, and these were compiled to create a three-dimensional image of the bead and its matrix, but this did not yield useful information about the internal structure.

3. Geological Setting

3.1. Belt Supergroup

The Belt Supergroup (= Purcell Supergroup in Canada) is a thick and geographically widespread succession of Mesoproterozoic (*ca*. 1.48–1.25 Ga) strata exposed in central-western North America (Fig. 2.1A), specifically southwestern Alberta, southeastern British Columbia, western Montana, northern Idaho, and northeastern Washington (e.g., Winston, 1986a, b; Hein and McMechan, 1994; Pratt, 2017). The Belt Basin was likely an intracratonic rift that opened to the ocean to the northwest (e.g., Höy, 1989; Winston and Link, 1993; Chandler, 2000; Pratt, 2001; Luepke and Lyons, 2001). Rifting may have been caused by oblique collision of a continent consisting of the East Antarctic (Mawson) and Australian cratons with present-day northwestern Laurentia (Pisarevsky et al., 2014; Medig et al., 2014; Pehrsson et al., 2016). This apparently also led to major uplift along the western side of the basin, as well as considerable syndepositional faulting in the basin itself, with rapid subsidence and sediment accumulation (Winston, 1986c; Evans et al., 2000; Sears, 2007; Pratt 2017). The western side of the basin is not preserved, but as subsidence continued following deposition of the carbonate platform represented by the Altyn Formation, the sea probably extended considerably farther into central Montana and over more of southwestern Alberta than is suggested by present-day outcrop distribution (Pratt, 2001; Pratt and Ponce, 2019). It was dominated by siliciclastic sedimentation with several episodes of carbonate sedimentation (Fermor and Price, 1983; Pratt, 1994, 2001). Petrology and detrital zircon dating indicate that siliciclastic sediment provenance was dominantly from the west with subordinate coarse sand from the east, at least until late in the history of the basin (Ross and Villeneuve, 2003; Link et al., 2007, 2016; Stewart et al., 2010; Pratt and Ponce, 2019). The Belt Basin was lake-like in that it was semi-enclosed and generally fairly shallow, but all indications are that it was normal-marine (Lyons et al., 2000), although hypersaline brines are thought to have concentrated at times in shallow areas along the eastern margin which occasionally flowed into deeper areas (Pratt, 2001; Pratt and Ponce, 2019).

The Belt Supergroup is subdivided into four units: lower Belt, Ravalli Group, Piegan Group (‘middle Belt carbonate’ of some past usage) and Missoula Group (e.g., Whipple et al., 1984; Winston, 1989, 2007; Winston and Link, 1993). The bedding plane features of interest here occur in the Appekunny Formation which comprises the upper part of the lower Belt or lowest part of the Ravalli Group, depending on nomenclatural preference. In the area of the Waterton Lakes and Glacier national parks, it rests on the shallow-water carbonate platform represented by light grey- to cream-coloured dolomites of the Altyn Formation (Fig. 2.2). Depending on the location, the basal contact is sharp and erosional (Whipple et al., 1984) or is gradational (Horodyski, 1983) and is marked by interbedding over a few metres of greenish fine-grained sandstone, dolomite, and coarse-grained dolomitic sandstone. The Appekunny Formation in turn is overlain gradationally by mudstones and subordinate

interbedded sandstones of the Grinnell Formation whose dominantly reddish or maroon colour contrasts markedly with the dominantly greenish colour of the Appekunny Formation (Pratt, 2017; Pratt and Ponce, 2019).

3.2. Appekunny Formation

3.2.1. Description

In the eastern side of Glacier National Park, the Appekunny Formation is about 670 m thick (Ross, 1959; Whipple et al., 1984). The type section is on Apikuni Mountain above and to the east of Apikuni Falls (Fig. 2.3A; Willis, 1902). The formation was first subdivided into three members by Fenton and Fenton (1937), from lowest to highest: Singleshot, Appistoki and Scenic Point members, with the middle member being the thickest. Subsequently it was subdivided into five informal members, from lowest to highest: 135 m, 165 m, 165 m, 135 m, and 60 m in approximate thickness (Whipple et al., 1984; Whipple, 1992). Member 1 is distinguished from member 2 largely on the basis of the presence of some maroon-coloured intervals. For mapping and structural geological purposes Yin and Kelty (1991) subdivided the formation into four mudstone units separated by resistant quartz sandstone beds above a basal sandstone.

The lower members consist dominantly of "siltite" whereas the uppermost member consists mostly of "argillite" with lenticular "quartz arenite" interbeds, exhibiting "mud-chip breccias," "fluid-escape structures" and "subaqueous shrinkage cracks" (Whipple et al., 1984; Whipple, 1992). Silt is angular to subangular and dominantly quartz with subordinate feldspar; sand is mostly rounded to well-rounded. Member 1 contains a 24 m thick sandstone unit on Apikuni Mountain (Slotznick et al., 2016). Member 2 contains sporadic thin sandstone beds and laminae. Members 3–5 are not treated here.

In detail, the *Horodyskia*-bearing lower two members consist mostly of thin-bedded, planar-laminated argillaceous siltstone, with lesser, variably silty claystone, and rare, very fine-grained sandstone laminae (Figs. 2.3B, C, 2.4A–C, 5A–C; Retallack et al., 2013, fig. 8A–E). The scree from the weathering of these rocks consists of tabular plates ~5–50 mm thick. Normal grading is locally present in laminae, and some laminae contain isolated clay intraclasts (Fig. 2.5C). Low-relief, small-scale hummocky cross-stratification (i.e. lamination) is fairly common (Fig. 2.4A), whereas, unidirectional cross-lamination in thin lenses occurs rarely (Fig. 2.5B; Retallack et al., 2013, fig. 8D). Low-relief symmetrical ripples with a wavelength of ~50–100 mm and interference ripples are present on some bedding planes. Common are scour surfaces a few millimetres up to about 10 mm deep (Fig. 2.4A–C; also Fig. 2.9G; Retallack et al., 2013, figs. 8B, C, E, 10E). Present very rarely are slightly more deeply eroded gutter fills and thick laminae consisting of fine-grained sandstone with intraclasts (Figs. 2.5C, 2.6A–C). In the gutters, intraclasts vary in size up to ~20 mm, while in the laminae they are typically 3–5 mm across; they range from rounded to subangular or polygonal in outline. Metre-scale intervals of low-relief hummocky cross-stratified, very fine-grained sandstone occur locally (Fig. 2.3C; Winston et al., 1989, fig. 24; Whipple et al., 1997, fig. 14).

The lower members show a variety of post-depositional soft-sediment deformation features. These include slightly distorted laminae (Fig. 2.5A), rare vertical dikelets, criss-crossing arrays of normal microfaults with a few millimetres of throw, and numerous horizons with ball-and-pillow structures (Slotznick et al., 2016, fig. 3B; Pratt, 2017, fig. 6C).

Retallack et al. (2013) noted the presence of carbonaceous "fragments," "laminae," and a "compression" or "zone" in what was regarded as the same 'carbonaceous-swirl shale facies' of Schieber (1989). No carbonaceous material was detected in this study, however, and opaque particles and laminae are iron minerals (see Slotznick et al., 2016). Moreover, the

'carbonaceous-swirl facies' in the Newland Formation of central Montana consists distinct, vertically crumpled carbonaceous seams in argillaceous dolomudstone (also Pratt, 2011, fig. 2C), neither of which is present in the Appekunny Formation.

3.2.2. Interpretation

The overall fine-grained lithological uniformity of the lower Appekunny Formation for a considerable thickness and distance along strike indicates a permanently submerged depositional environment located a significant distance from shore. It lacks the coarse sand that is present in the upper Altyn Formation, and the contact between the two represents a flooding event. Horodyski (1983) noted that because ripple cross-lamination is uncommon, deposition took place below wave base (presumably meaning fair weather wave base). Fedonkin and Yochelson (2002) considered the environment to be poorly oxygenated, but widespread presence of traction features argues that it was well circulated. Dominance of planar-laminated argillaceous siltstone points to hemipelagic fall-out of cohesive mud aggregates or flocs from muddy plumes and low flow-regime bottom currents, often coupled with some reworking. Fedonkin and Yochelson (2002) suggested that the clay was wind-borne, but its admixture with silt suggests subaqueous transport entirely (see Manning et al., 2013). Source is likely from the west (e.g., Link et al., 2007; Pratt, 2017; Pratt and Ponce, 2019).

Lenses and unidirectional cross-lamination record slightly elevated current velocities that produced starved ripples. Symmetrical and interference ripples indicate occasional gentle wave action, and scattered small-scale hummocky cross-stratification (i.e. lamination) suggests impingement of slightly stronger storm-induced oscillatory and combined flows. The scours and rare gutters indicate erosional events, some of which were from unidirectional currents, while others may have been due to oscillatory currents. In cases where the intraclasts are poorly sorted they were probably eroded from stiff mud layers, but where well sorted some may be *Horodyskia* beads (see below).

On the other hand, sporadic larger scale but low-relief hummocky cross-stratified, very fine-grained sandstone intervals with sharp bases record anomalous events of sand influx and stronger oscillating bottom currents compared to background conditions. They could be tempestites. However, their volume and the jump in energy levels and grain size do not appear to be adequately explained by invoking stronger storms and in situ reworking of pre-existing sediment. Instead, these beds seem to involve a combination of coarser sediment influx combined with wave action of atypical magnitude, and for these reasons they may be tsunami-generated (see Pratt, 2017; Pratt and Ponce, 2019). The sediment was probably still derived from the west or northwest, perhaps from backwash flows, and reworked by seiche-like oscillatory currents. The rare thin beds and laminae composed of rounded, coarser grained sand mainly in members two and three are likely derived from coastal areas broadly to the east (Whipple et al., 1984; Pratt and Ponce, 2019). Whether or not they can be ascribed to tsunami backwash or storm-induced flows is unclear, but their overall rarity in this part of the basin suggests considerable distance from the coast to the east, possibly combined with the impact of only fairly small tsunamis.

By contrast, Retallack et al. (2013) concluded that the lower Appekunny Formation was deposited in a sedimentary setting consisting of lakes, braided streams and occasionally subaerially exposed, microbial mat-stabilized muds intercalated with soil horizons. Retallack et al. (2013) claimed to have encountered climbing ripples and a bed with trough cross-bedding which "may have been a shallow paleochannel in temporarily exposed mudflats." No such structures were observed in this study or recorded in previous descriptions (Whipple et al., 1984; Slotznick et al., 2016). The identification of paleosols was based on reddish iron staining in the lowermost member. However, cross-cutting relationships here and in the

Grinnell Formation indicate that the red colouration is a diagenetic phenomenon (Pratt and Ponce, 2019). It is also not directly indicative of oxygen in the atmosphere as contemplated by others (e.g., Slotznick et al., 2016). Thus, the environmental setting as envisaged by Retallack et al. (2013) is unsupported and, rather, the evidence indicates permanently submerged subtidal conditions under relatively low energy.

The presence of ball-and-pillow structures was suggested to be due to loading from rapid sedimentation (Whipple et al., 1997) or slumping on a slope (Winston et al., 1989). However, lack of independent evidence for an inclined sea floor, the broad lateral extent of facies, the fact that deformation took place after deposition, and the morphological attributes of these and other soft-sediment deformation features in the succession, indicate that they are earthquake-induced features, i.e. seismites (Pratt, 2017). Intact preservation of sedimentary structures, seismites and scoured contacts is evidence that distortion due to burial compaction did not appreciably affect the lower Appekunny Formation.

4. Bedding surfaces

4.1. Wrinkles, blisters and pustules

4.1.1 Description

The upper surfaces of most beds in the lower Appekunny Formation are flat and appear featureless or slight pitted due to weathering (Fig. 2.7A). Wrinkle marks conforming to *Kinneyia*, often considered a type of 'microbially induced sedimentary structure,' are uncommon. On the other hand, many beds exhibit a wrinkled, blistered or finely pustular upper surface. These features stand out in positive epirelief, and the overlying bed sole correspondingly shows them in negative hyporelief. A range of shapes is present. Pustules are discrete, millimetre-sized pimples (Fig. 2.7B). Also common are numerous, discontinuous, crudely linear, reticulate or radiating or stellate ridge-like wrinkles up to a millimetre high, a few millimetres wide, and up to about 30 mm long (Fig. 2.7C–E, I; also Fig. 11A, B). Blisters up to 10 mm across with a circular to irregularly polygonal outline often co-occur with wrinkles, isolated or merged (Fig. 2.7F–H; also Fig. 11A). Typically they are separate from each other, although the distance apart is variable. Some examples of blisters have been misidentified as *Horodyskia* beads (Retallack et al., 2013, fig. 5D, E). In cross-section these protuberances have a lenticular core covered by several claystone laminae (Fig. 2.7H). Some surfaces are densely covered by fine wrinkles and tiny pustules ~0.3–1 mm across and with minimal relief (Figs. 2.7I, 2.9A–F, 10A–G, 11A–D; also Fig. 13A). The wrinkles, blisters and pustules are composed of clay and appear light-coloured.

Serial sections parallel to lamination show a fine mottling due to variable proportion of silt and clay, and lighter coloured, short, arcuate to linear clay features and irregular to lobate clay patches (Fig. 2.8A–E). Both locally intersect each other; some patches appear to be *Horodyskia* beads revealed as the strings-of-beads on the weathered surface were ground off. Successive surfaces show vertical changes in the shapes of the linear features and patches, i.e. the clay-cored wrinkles, blisters and pustules, and their eventual disappearance.

4.1.2. Interpretation

Most bedding planes are smooth because the planar lamination is mainly a low-flow regime traction structure. There is no evidence of post-depositional deformation causing the surface textures, such as shearing along bedding planes, a combination of lateral compression and stretching, or injection which are known to have taken place in other facies of the Belt Supergroup (Pratt, 1994, 1998, 2001, 2017; Pratt and Ponce, 2019). Instead, the wrinkled, blistered and pustular bedding surfaces are considered to be due to benthic microbial mats

that had a variable primary topography that trapped and bound silt and clay in pockets or on slightly elevated irregularities consisting of ridges, domes and tufts. Blisters are cored with a mud lens, which likely represents preferential trapping by locally somewhat regularly spaced tufts or depressions that then built up. Presumably the mats were dominated by cyanobacteria, and the different surfaces features suggests vagaries of growth, shaping by bottom currents and possibly some variation in microbial composition. Similar surfaces have been described from both modern settings and ancient counterparts (e.g., Noffke et al., 2013; Cuadrado and Pan, 2018) and those in the lower Appekunny Formation appear to fulfil the most reliable criteria (Noffke, 2009; Davies et al., 2016). Wrinkled surfaces have been termed 'elephant skin' in some studies (Porada and Bouougri, 2006) but in detail they appear to be different than the surfaces described here.

4.2. Horodyskia

4.2.1. Description

Horodyskia moniliformis occurs on innumerable bedding planes in the lower Appekunny Formation; it is often more visible on the undersides of rocks in the scree due to differential weathering. It appears as roughly straight to curving to sinuous rows of clay-dominated beads which are discs, flakes or thin lenses that are of more or less uniform size and have typically, although not always, roughly equidistant spacing – the string-of-beads aspect – and maximum length is ~150 mm (Figs. 2.9A–F, 2.10A–H, 2.11A–D; Horodyski, 1982, fig. 3; Fedonkin and Yochelson, 2002, fig. 5). The radius of curvature is commonly as low as 3–5 mm, with the tightest curves 1–1.5 mm (Fig. 10C; Fedonkin and Yochelson, 2002, fig. 5). However, strings-of-beads are never seen to form closed loops.

The beads are oriented bedding-parallel. They are variable in outline but dominantly circular, although many are elliptical, lobate, or polygonal – mostly square or triangular – and they range from about 1 mm to 5 mm in diameter (also Retallack et al., 2013, figs. 6, 7A–H). In some specimens the beads have slight positive epirelief (Figs. 2.7A, 10C; Fedonkin and Yochelson, 2002, figs. 4B, 6A–C, 7A–C). The smaller ones appear to grade into pustules. In a few specimens on bed soles the beads are surrounded by an irregular ridge which has been interpreted as the cast of a scour feature (Fedonkin and Yochelson, 2002, fig. 11C). In rare cases the beads are crescentic in outline and have the same orientation and tilt angle along the length of the string (Fedonkin and Yochelson, 2002, fig. 11A, D).

Spacing between beads ranges from about half to just over one times the diameter and is usually fairly consistent, although it can vary in some specimens (Fig. 2.9B, E, F). There is a broadly linear relationship between bead size and distance apart (Horodyski, 1982, fig. 4; Retallack et al., 2013, fig. 11; also Grey and Williams, 1990, fig. 7; Calver et al., 2010, fig. 10). Fedonkin and Yochelson (2002, fig. 18) reconstructed small forms as having laterally juxtaposed beads, but this is not observed. Contrary to the assertion in Fedonkin and Yochelson (2002, p. 23), the strings can overlap or lie adjacent to each other (Fig. 2.9B–D; Horodyski, 1983, pl. 1.3A) or appear clustered (Figs. 2.7A, 2.9A, C, D, 2.11D). In some cases beads occur instead as isolated discs (Fig. 2.9E), and rarely as dense accumulations without evidence for rows, although still exhibiting a roughly even spacing between discs (Fig. 2.9F). Some laminae composed of claystone intraclasts (Fig. 2.6B, C) may be in part accumulations of redeposited *Horodyskia* beads. Strings consisting of different-sized beads are seemingly present on the same surface and may cross each other (Fig. 2.10A, C; Fedonkin and Yochelson, 2002, fig. 8B). In some specimens the rows lie directly across low-relief rippled surfaces (Fig. 2.9F) or on planed-off ripples (Fig. 2.10G). *Horodyskia* is most conspicuous on bed surfaces that appear smooth or densely pustulate, and less commonly on blistered or wrinkled surfaces (Figs. 2.10G, H, 2.11A–D; also 13A; Retallack et al., 2013, fig.

7D, E). The darker aura around many examples appears to be due to weathering and oxidation of iron in the immediately adjacent clay and silt matrix. Many bed surfaces also exhibit isolated argillaceous objects that are similar to *Horodyskia* beads, and in some cases there it is difficult to distinguish small ones from pustules (Figs. 2.9A, C, 2.10G, H, 2.11A–D). Indeed, some submillimetre-sized pustules are also oriented in rows forming miniature strings-of-beads (Fig. 2.10H).

Thin sections cut parallel to lamination that intersect *Horodyskia* beads reveal a densely mottled background fabric distinguished by small variations in clay versus silt content (Fig. 2.14A, B). The mottles are dominated by variably distinct, isolated or juxtaposed, roundish to lobate clay patterns about 0.5–1 mm across surrounded by darker coloured clay-dominated material which locally appears like a mud matrix. *Horodyskia* beads appear as round to lobate clay objects that are denser than the surrounding sediment.

Synchrotron XRF analysis (Fig. 2.12A–L) confirms that the mudstone is rich in the major elements, especially K and Fe, associated with the illite and chlorite composition of the clay minerals. The Ca is likely from plagioclase silt. The elevated Ti is due to ilmenite which occurs in the silty laminae and in the beads if they are siltier (Fig. 2.12B; also Fig. 2.15D). The Fe-rich spots are due to pyrite, magnetite or goethite (Slotznick et al., 2016). The trace element composition accords with previous determinations although the concentrations differ somewhat (Fedonkin and Yochelson, 2002, p. 14; Slotznick et al., 2016).

An X-ray scan of a thin piece of mudstone with *Horodyskia* and densely arranged pustules on the surface shows variable attenuation, with the most caused by superimposed *Horodyskia* beads possibly along with blisters in successive laminae under the surface (Fig. 2.13A, B).

Thin sections cut perpendicular to bedding reveal variably silty argillaceous flakes and lenses many of which are *Horodyskia* (Fig. 2.15A–D). Not all objects signalled by Retallack et al. (2013, fig. 8A–D, 10E) are *Horodyskia* beads and some are blisters which are larger, laminated and lenticular in shape.

4.2.2. Interpretation

Horodyski (1982) regarded the strings-of-beads as ‘dubiofossils’ of uncertain origin, but he did not discount the possibility that they represent a macroscopic organism.

The fairly regular spacing of beads in individual strings regardless of the size of the beads and length of the strings, and serial grinding to determine the three-dimensional structure and what lies under the beads, indicate that the model of formation proposed by Fedonkin and Yochelson (2002, fig. 19), involving juxtaposed small bodies that grew upward from a stolon into large beads separated by spaces, is untenable. Strings-of-beads do overly wrinkled surfaces but clay-cored, ridge-like wrinkles are not integral to the strings as would be required if they were stolons. Thus, the interpretation that *Horodyskia moniliformis* represents a colonial, tissue-grade organism is unlikely.

Retallack et al. (2013) proposed that the beads in the Appekunny Formation may be the bladder-like cells of an endocyanotic fungus (a fungus with a symbiotic intracellular bacterium; incorrectly also termed an “endolichen fungus”). Extant endocyanotic fungi live in soils, not marine settings. Apart from the evidence that the sediments were permanently submerged and deposited below fairweather wave base, not only is the string-of-beads morphology unlike clusters of fluid-filled bladders, but also there is no indication that the beads were once tissues or fluid-filled objects that were somehow replaced by mud or left cavities that were subsequently filled with mud.

Strings-of-beads in sandstone of the Mesoproterozoic Stag Arrow and Backdoor formations, Bangemall Group of Western Australia, are similar in shape as *Horodyskia*, but overall beads are smaller and exhibit a narrower size range, the strings are shorter, and they are preserved in concave hyporelief on bed soles (Grey and Williams, 1990; Grey et al.,

2010). Considered a separate species mainly due to their smaller size, specimens of *H. williamsii* Grey, Yochelson, Fedonkin and Martin, 2010 were considered to have been in epirelief when formed, and interpreted to have been originally spheroidal and hollow, and connected by a thin strand; common is a slight central dimple and a surrounding ring-shaped depression. On some surfaces they are quite linear and oriented subparallel (Grey et al., 2010, fig. 2A). The surrounding depressions were ascribed to current scour. Similar strings-of-beads, assigned to *H. williamsii*, are present in the upper Mesoproterozoic to lower Neoproterozoic Cassiterite Creek Quartzite of Tasmania, mostly occurring in positive epirelief on siltstone laminae and as coloured patches in shale (Calver et al., 2010). This is evidence that bead composition reflects the host sediment. Some on siltstone surfaces exhibit a ring-shaped depression or rim, depending on style of preservation.

In examples from the Stag Arrow Formation, "chevron-shaped" markings formed by beads flanked on one side (all on the same side) by a short trough were also ascribed to current scour (Grey and Williams, 1990). The nearly parallel sides of the depressions argue against this, however. Another possibility is bedding-parallel shear and lateral translation of the string-of-beads which left behind a short gouge behind each bead on the bed surface.

A macrophytic algal affinity was considered most likely by Grey and Williams (1990) who compared *Horodyskia* to extant branching phaeophycean algae (brown algae), specifically with the *Hormosira banksia* whose thalli consist of chains of bubble-like pneumatocysts filled with gas, as well as with *Scaberia agardhii* which has lobate branches that have a circular cross-section. Apart from the fact that most brown algae branch whereas *Horodyskia* does not, they implied that the beads are preserved as pit-shaped impressions in the sediment. However, *Horodyskia* beads in the Appekunny Formation appear to consist of mud flocs and intraclasts.

Horodyskia minor Dong, Xiao, Shen and Zhou, 2008 was named for strings-of-bead structures preserved in three dimensions in cherts of the Ediacaran Liuchapo Formation, in South China, which co-occur with *Palaeopascichnus minimus* Shen, Xiao, Dong Zhou and Liu, 2007, the latter differing primarily in the crescentic outline of the concavo-convex lenticular segments. The composition of the beads and segments was speculated to be dark due to organic carbon or pyrite, but Al and Mg enrichment of the segments indicates that they have an argillaceous component, and the petrographic similarity with the beads suggests they may too be argillaceous. In contrast to those of *H. moniliformis*, the beads in *H. minor* were originally spheroidal, smaller in size – 0.2–0.7 mm in diameter – and commonly more closely spaced; string length is correspondingly less, up to 5.5 mm. The beads and segments are thought to be connected by a filamentous structure similarly regarded as a stolon. In both forms the strings are encased in a halo of microquartz that is more limpid than the rest of the matrix. Dong et al. (2008) interpreted both forms as possibly akin to uniseriate foraminifers. The small size and contrasting style of preservation makes it problematical to relate *H. minor* to *Horodyskia* in siltstones and shales (Calver et al., 2010).

4.2.3. New Models

The composition, varied shape and size of the beads, their discrete nature, and their bedding-parallel orientation are evidence that, in the Appekunny Formation, they are argillaceous particles consisting of large flocs and small intraclasts and are not compacted spheroids. The intraclastic flakes could have been eroded from mud laminae on the adjacent sea bottom, although some could be due to flocculation in the water column. The variable shape of the rounded to lobate beads may be related to clay flocculation, although the rounding of some beads may indicate grain-to-grain abrasion before settling.

The apparent intergradation between the smallest beads and pustules is suggestive of a common or related origin. The rarely developed crescentic beads were probably originally

disc-shaped but were tilted by gentle, unidirectional shear under shallow burial. This, and polygonal shapes, imply that the beads were somewhat rigid. Rheological evidence in the Grinnell Formation also points to stiffening of argillaceous sediment on the sea floor (Pratt and Ponce, 2019). The source for the shear stress is uncertain, but the presence of seismites throughout the Appekunny Formation (Pratt, 2017) suggests that gentle shaking of the sea bed could have been the source.

4.2.3.1. Filaments Revised

While the suggestion of Grey and Williams (1990) that the thalli of macroalgae left beaded impressions in the sediment is not directly tenable as an explanation for *Horodyskia* in the Appekunny Formation, it is conceivable that the strings-of-beads may have formed in some way by a large filamentous thallus. Argillaceous flakes would have had to adhere to the filament, and the spacing of the beads implies that the filament had more or less regular subdivisions, with one kind of subdivision favourable for this and the adjacent one not. Smaller strings-of-beads suggest narrower filaments and consequently closer subdivisions. If instead of distinct intraclasts, mud adhered to the filament, no evidence of the filament would have been preserved. If so, *Horodyskia* would be the record of intraclasts suspended near the sea bottom and available to stick to the filaments. According to this scenario, accumulations of beads and strings-of-beads can be explained as concentrations due to current activity, before or after attachment to filaments, and possibly involving decay of the filament and release of the intraclasts.

4.2.3.2. Microbial Mats

Bedding surfaces with wrinkles, blisters and pustules, which are interpreted as reflecting the varied and changing topography of a growing benthic microbial mat, suggest the possibility that biomats or biofilms may have played a role in *Horodyskia* formation. This is also suggested by the patterns revealed by transverse thin sections and serial sectioning. Mud – mostly clay with or without small amounts of silt – would have been flocs and small intraclastic flakes suspended in the water column and captured by the sticky exopolymeric substances (exopolysaccharides) of the filamentous cyanobacteria comprising the upper surface of the mat, leading to accretion of the mat surface. If these particles were trapped by closely spaced tufts of filaments that were arranged loosely in a row or along a ridge and broadly equidistant from each other, then an apparent chain or string-of-beads could conceivably form. The tufts would have been smaller than the mat irregularities that are preserved as centimetre-scale wrinkles and blisters which have a different cross-section and were seemingly not trapping intraclasts. This is a possible explanation for the differences in their preserved pattern on bed surfaces versus the curving strings-of-beads, where the latter are the sole evidence for subtle surface topography consisting of rows of tufts, in addition to a pustular or wrinkled surface if present. Rows of pustules may also be inferred to be rows of tiny tufts. Apparent overlap of strings-of-beads could represent separate events of floc or intraclast formation and trapping. Bedding surfaces with two populations of bead sizes may represent separate trapping events involving different sizes of flocs or intraclasts. Accumulations of beads not obviously in chains might represent successive trapping of flocs and intraclasts on a microbial mat without well-developed rows of tufts or later redistribution by currents. Overall, the benthic microbial mat would have exhibited a variety of surface irregularities, which explains the variation in *Horodyskia* morphology.

5. Discussion

A purely physical origin for *Horodyskia* has yet to be formulated, as it is difficult to explain the linear arrangement of beads as some sort of self-organized feature arising during sedimentation. Previous biological explanations for *Horodyskia* suffer from several handicaps: (1) misunderstanding of the sedimentary environment (of the lower Appekunny Formation); (2) mischaracterization of the nature of the beads; (3) misinterpretation of locally associated ridge-like wrinkles as a stolon beneath and connecting the strings-of-beads; and (4) the absence of a convincing modern analogue. Here we entertain two new models for the strings-of-beads, one that considers them to be flocs and flakes attached to segmented filaments, and the other that the beads were trapped by rows of tufts or other irregularities on the upper surface of a benthic microbial mat.

The revised filament origin may be superficially appealing, despite the absence of a clear-cut modern analogue. Some specimens of the late Ediacaran putative brown alga *Miaohephyton* possess rows and clusters of conceptacle-like structures along the thallus although they are not arranged as alternating node and node-free portions or segments (Xiao et al., 1998). In addition, there are aspects of *Horodyskia* that are difficult to explain by the action of filaments. The absence of looping is problematic given the local tight curving and taking that as evidence for flexibility of the filament. Explaining different sizes of strings-of-beads as representing different sizes of microbial or macroalgal filaments is difficult to envisage if they belonged to the same taxon, because extant filamentous cyanobacteria and algae do not exhibit this kind of intraspecific morphological variation (e.g., Graham et al., 2009). Although the extant filamentous cyanobacterium *Microcoleus* consists of multiple trichomes within a common sheath, the large size variation is unlikely to be due to trichome or filament bundles of different diameters because that would require that the sticky nodes of the component filaments be aligned. The bedding-parallel orientation of beads implies that the filaments were flat, because if flake-shaped particles were attached to the nodes of a cylindrical thallus then they would likely show various orientations with respect to bedding, assuming the nodes were sticky right around. Moreover, the curving shape of the strings-of-beads, especially examples with a small radius of curvature, is difficult to reconcile with a flat, ribbon-shaped filament or a bladed form, shapes that resist lateral bending without tearing or folding.

Ascribing the rows of beads to trapping of flocs and flakes by a variably oriented surface features of a microbial mat removes the impediments posed by a macrophytic filamentous origin and the absence of a modern analogue for this mechanism. In both subaerially exposed and submerged mats filaments can exhibit both prostate and upright orientations (e.g., Wierzchos et al., 2006). Intertidal and supratidal microbial mats are commonly wrinkled, pustular or blistered (e.g., Pratt, 2010; Court et al., 2017; Cuadrado and Pan, 2018), and submerged versions may exhibit pinnacle-like tufts of upward-gliding polytrichomous filaments such as *Microcoleus* (e.g., Gerdes, 2007; Flannery and Walter, 2012). Such tufts have the right size range to trap beads.

Filamentous cyanobacteria are known from upper Archean to Neoproterozoic strata, but primarily from silicified examples in early diagenetic cherts in shallow-marine, tidal flat and restricted lagoonal carbonates, whereas larger filaments belonging to the rhodophytes and chlorophytes made their appearance in the late Mesoproterozoic (Sergeev et al., 2012; Butterfield, 2015). Mesoproterozoic to Neoproterozoic *Eomicrocoleus* is similar to its extant counterpart, *Microcoleus* (Horodyski and Donaldson, 1980; Hofmann and Jackson, 1991) but examples preserving pinnacle-like tufts have yet to be discovered. On the other hand, many stromatolitic laminae are cuspate in cross-section and form reticulate patterns in plan view, providing evidence for microbial mat topography caused by upward growth (e.g., Flannery and Walter, 2011). Conical microbial laminae, similar in size to the blisters in the Appekunny Formation, have been observed in Mesoproterozoic limestones (e.g., Upfold, 1984) and

Archean sandstones interpreted to have been deposited in the upper intertidal and supratidal zones (Homann et al., 2015). Vertical filament growth is probably more likely to have formed pinnacle-like tufts, but reticulate ridges and peaks can form due to lateral motility as well (Shepard and Sumner, 2010).

6. Conclusions

Strings-of-beads structures confined to laminated argillaceous siltstones of the lower Appekunny Formation of the lower Belt Supergroup (*ca*. 1.45 Ga) have been named *Horodyskia moniliformis* and regarded as a macrofossil and possibly as the oldest colonial eukaryotic fossils in the rock record. Similar structures have been identified in several units elsewhere, and likewise have been taken as having a biological origin albeit involving other possible affinities. Here, we show that, instead, that the string-of-beads aspect is more likely due to trapping of suspended, large clay-dominated flocs and intraclastic flakes on a benthic microbial mat. The mat possessed a variable topographic relief that included wrinkles, blisters, pustules, and rows of pinnacle-like tufts with often a regular-enough distribution to impart an apparently organized, curving chain-like aspect to trapped particles, that masquerades as a filament, ribbon or a stolon connecting a row of globular organic structures. In the Belt Supergroup, *Horodyskia* is highly facies-specific 'microbially induced sedimentary structure' that formed only with the precise confluence of factors including sediment type, flocculation, bottom currents, and microbial mat growth.

References

Bengtson, S., Rasmussen, B., Krapež, B., 2007. The Paleoproterozoic megascopic Stirling biota. Paleobiology 33, 351–381.

Buatois, L.A., Almond, J., Mángano, M.G., Jensen, S., Germs, G.J.B., 2018. Sediment disturbance by Ediacaran bulldozers and the roots of the Cambrian explosion. Scientific Reports 8, no. 4514 [9 pp].

Budd, G.E., Jensen, S., 2017. The origin of the animals and a 'Savannah' hypothesis for early bilaterian evolution. Biological Reviews 92, 446–473.

Butterfield, N.J., 2015. Proterozoic photosynthesis – a critical review. Palaeontology 58, 953–972.

Calver, C.R., Grey, K., Laan, M., 2010. The 'string of beads' fossil (*Horodyskia*) in the mid-Proterozoic of Tasmania. Precambrian Research 180, 18–25.

Cuadrado, D.G., Pan, J., 2018. Field observations on the evolution of reticulate patterns in microbial mats in a modern siliciclastic coastal environment. Journal of Sedimentary Research 88, 24–37.

Chandler, F.W., 2000. The Belt–Purcell Basin as a low-latitude passive rift: implications for the geological environment of Sullivan type deposits, in: Lydon, J.W., Höy, T., Slack, J.F., Knapp, M.E. (Eds.), The Geological Environment of the Sullivan Deposit, British Columbia. Geological Association of Canada, Mineral Deposits Division Special Publication 1, pp. 82–112.

Court, W.M., Paul, A., Lokier, S.W., 2017. The preservation potential of environmentally diagnostic sedimentary structures from a coastal sabkha. Marine Geology 386, 1–18.

Davies, N.S., Liu, A.G., Gibling, M.R., Miller, R.F., 2016. Resolving MISS conceptions: A geological approach to sedimentary surface textures generated by microbial and abiotic processes. Earth-Science Reviews 154, 210–246.

Dong, L., Xiao, S., Shen, B., Zhou, C., 2008. Silicified *Horodyskia* and *Palaeopascichnus* from upper Ediacaran cherts in South China: tentative phylogenetic interpretation and

implications for evolutionary stasis. Journal of the Geological Society, London 165, 367–378.
Droser, M.L., Gehling, J.G., 2015. The advent of animals: The view from the Ediacaran. PNAS 112, 4865–4870.
El Albani, E., Mángano, M.G., Buatois, L.A, Bengtson, S., 19 others, 2019. Organism motility in an oxygenated shallow-marine environment 2.1 billion years ago. PNAS 116, 3431–3436.
Evans, K.V., Aleinikoff, J.N., Obradovich, J.D., Fanning, C.M., 2000. SHRIMP U-Pb geochronology of volcanic rocks, Belt Supergroup, western Montana: evidence for rapid deposition of sedimentary strata. Canadian Journal of Earth Sciences 37, 1287–1300.
Fedonkin, M.A., Yochelson, E.L., 2002. Middle Proterozoic (1.5 Ga) *Horodyskia moniliformis* Yochelson and Fedonkin, the oldest known tissue-grade colonial eukaryote. *Smithsonian Contributions to Paleobiology no. 94*, 29 pp.
Fenton, C.L., Fenton, M.A., 1937. Belt Series of the north: Stratigraphy, sedimentation, paleontology. Geological Society of America Bulletin 48, 1873–1969.
Fermor, P.R., Price, R.A., 1983. Stratigraphy of the lower part of the Belt-Purcell Supergroup (Middle Proterozoic) in the Lewis thrust sheet of southern Alberta and British Columbia. Bulletin of Canadian Petroleum Geology 31, 169–194.
Flanner, D.T., Walter, M.R., 2011. Archean tufted microbial mats and the Great Oxidation Event: new insights into an ancient problem. Australian Journal of Earth Sciences 59, 1–11.
Gehling, J.G. 1999. Microbial mats in terminal Proterozoic siliciclastics: Ediacaran death masks. Palaios 14, 40–57.
Gerdes, G., 2007. Structures left by modern microbial mats and their host sediments, in: Schieber, J., Bose, P.K., Eriksson, P.G., Banerjee, S., Sarkar, S., Altermann, W., Catuneanu, O. (Eds.), Atlas of Microbial Mat Features Preserved within the Siliciclastic Rock Record. Elsevier, Amsterdam, pp. 5–38.
Graham, L.E., Graham, J.M., Wilcox, L.W., 2009. Algae [2nd Edn.]. Benjamin Cummings, San Francisco, 616 pp. [+ glossary, literature cited, indices].
Grazhdankin, D., 2014. Patterns of evolution of the Ediacaran soft-bodied biota. Journal of Paleontology 88, 269–283.
Grey, K., Williams, I.R., 1990. Problematic bedding-plane markings from the Middle Proterozoic Manganese Subgroup, Bangemall Basin, Western Australia. Precambrian Research 46, 307–327.
Grey, K., Yochelson, E.L., Fedonkin, M.A., Martin, D.M., 2010. *Horodyskia williamsii* new species, a Mesoproterozoic macrofossil from Western Australia. Precambrian Research 180, 1–17.
Harrison, J.E., 1972. Precambrian Belt basin of northwestern United States: Its geometry, sedimentation, and copper occurrences. Geological Society of America Bulletin 83, 1215–1240.
Hein, F.J., McMechan, M.E., 1994 Proterozoic and Lower Cambrian strata of the Western Canada Sedimentary Basin, in: Mossop, G.D., Shetsen, I. (Compilers), Atlas of the Western Canada Sedimentary Basin. Canadian Society of Petroleum Geology and Alberta Research Council, pp. 57–67.
Hofmann, H.J., Jackson, G.D., 1991. Shelf-facies microfossils from the Uluksan Group (Proterozoic Bylot Supergroup), Baffin Island, Canada. Journal of Paleontology 65, 361–382.
Homann, M., Heubeck, C., Airo, A., Tice, M.M., 2015. Morphological adaptations of 3.22 Ga-old tufted microbial mats to Archean coastal habitats (Moodies Group, Barberton Greenstone Belt, South Africa). Precambrian Research 266, 47–64.

Horodyski, R.J., Donaldson, J.A., 1980. Microfossils from the Middle Proterozoic Dismal Lakes Group, Arctic Canada. Precambrian Research 11, 125–159.
Horodyski, R.J., 1982. Problematic bedding-plane markings from the Middle Proterozoic Appekunny Argillite, Belt Supergroup, northwestern Montana. Journal of Paleontology 56, 882–889.
Horodyski, R.J., 1983. Sedimentary geology and stromatolites of the Middle Proterozoic Belt Supergroup, Glacier National Park, Montana. Precambrian Research 20, 391–425.
Höy, T., 1989. The age, chemistry, and tectonic setting of the Middle Proterozoic Moyie sills, Purcell Supergroup, southeastern British Columbia. Canadian Journal of Earth Sciences 26, 2305–2317.
Höy, T., 1992. Geology of the Purcell Supergroup in the Fernie west-half map area, southeastern British Columbia. British Columbia Mineral Resources Division, Bulletin 84, 157 pp.
Link, P.K., Fanning, C.M., Lund, K.I., Aleinikoff, J.N., 2007. Detrital-zircon populations and provenance of Mesoproterozoic strata of east-central Idaho, U.S.A.: Correlation with the Belt Supergroup of southwest Montana, in: Link, P.K., Lewis, R.S. (Eds.), Proterozoic Geology of Western North America and Siberia. SEPM Special Publication 86, pp. 101–128.
Link, P.K., Stewart, E.D., Steel, T., Sherwin, J., Hess, L.T., and McDonald, C., 2016, Detrital zircons in Mesoproterozoic upper Belt Supergroup in the Pioneer, Beaverhead, and Lemhi ranges, Montana and Idaho: The Big White Arc, in*:* MacLean, J.S., and Sears, J.W. (Eds.), Belt Basin: Window to Mesoproterozoic Earth. Geological Society of America Special Paper 522, pp. 163–183.
Luepke, J.J., Lyons, T.W., 2001. Pre-Rodinian (Mesoproterozoic) supercontinental rifting along the western margin of Laurentia: geochemical evidence from the Belt-Purcell Supergroup. Precambrian Research 111, 79–90.
Lyons, T.W., Luepke, J.J., Schreiber, M.E., Zieg, G.A., 2000, Sulfur geochemical constraints on Mesoproterozoic restricted marine deposition: lower Belt Supergroup, northwestern United States. Geochimica et Cosmochimica Acta 64, 427–437.
Manning, A.J., Spearman, J.R., Whitehouse, R.J.S., Pidduck, E.L., Baugh, J.V., Spencer, K.L., 2013. Flocculation dynamics of mud:sand mixed suspensions, in: Manning, A. (Ed.), Sediment Transport, Processes and Their Modelling Applications. IntechOpen, London, p. 119–164.
McMechan, M.E., 1981. The Middle Proterozoic Purcell Supergroup in the southwestern Rocky and southeastern Purcell Mountains, British Columbia and the intitiation of the Cordilleran miogeocline, southern Canada and adjacent United States. Bulletin of Canadian Petroleum Geology 29, 583–621.
Medig, K.P.R., Thorkelson, D.J., Davis, W.J., Rainbird, R.H., Gibson, H.D., Turner, E.C., Marshall, D.D., 2014. Pinning northeastern Australia to northwestern Laurentia in the Mesoproterozoic. Precambrian Research 249, 88–99.
Noffke, N., 2009. The criteria for the biogeneicity of microbially induced sedimentary structures (MISS) in Archean and younger, sandy deposits. Earth-Science Reviews 96, 173–180.
Noffke, N., Christian, D., Wacey, D., Hazen, R.M., 2013. Microbially induced sedimentary structures recording an ancient ecosystem in the *ca*. 3.48 billion-year-old Dresser Formation, Pilbara, Western Australia. Astrobiology 13, 1103–1124.
Pehrsson, S.J., Eglington, B.M., Evans, D.A.D., Huston, D., Reddy, S.M., 2016. Metallogeny and its link to orogenic style during the Nuna supercontinent cycle, in: Li, Z.X., Evans, D.A.D., Murphy, J.B. (Eds.), Supercontinent Cycles Through Earth History. Geological Society, London, Special Publication 424, pp. 83–94.

Pisarevsky, S.A., Elming, S.-Å., Pesonen, L.J., Li, Z.-X., 2014. Mesoproterozoic paleogeography: Supercontinent and beyond. Precambrian Research 244, 207–225.
Porada, H., Bouougri, E., 2007. 'Wrinkle structures' – a critical review, in: Schieber, J., Bose, P.K., Eriksson, P.G., Banerjee, S., Sarkar, S., Altermann, W., Catuneanu, O. (Eds.), Atlas of Microbial Mat Features Preserved within the Siliciclastic Rock Record. Elsevier, Amsterdam, pp. 135–144.
Pratt, B.R., 1994. Seismites in the Mesoproterozoic Altyn Formation (Belt Supergroup), Montana: A test for tectonic control of peritidal carbonate cyclicity. Geology 22, 1091–1094.
Pratt, B.R., 1998. Syneresis cracks: subaqueous shrinkage in argillaceous sediments caused by earthquake-induced dewatering. Sedimentary Geology 117, 1–10.
Pratt, B. R., 2001. Oceanography, bathymetry and syndepositional tectonics of a Precambrian intracratonic basin: integrating sediments, storms, earthquakes and tsunamis in the Belt Supergroup (Helena Formation, ca. 1.45 Ga), western North America. Sedimentary Geology 141, 371–394.
Pratt, B.R., 2010. Peritidal carbonates, in: James, N.P., Dalrymple, R.W. (Eds.), Facies Models 4, GEOtext 4. Geological Association of Canada, St. John's. pp. 401–420.
Pratt, B.R., 2011. Molar-tooth structure, in: Reitner, J., Thiel, V. (Eds.), Encyclopedia of Geobiology. Springer, Dordrecht, pp. 662–666.
Pratt, B.R., 2017. The Mesoproterozoic Belt Supergroup in Glacier and Waterton Lakes national parks, northwestern Montana and southwestern Alberta: Sedimentary facies and syndepositional deformation, in: Hsieh, J.C.C. (Ed.), Geologic Field Trips of the Canadian Rockies, 2017 Meeting of the GSA Rocky Mountain Section. Geological Society of America Field Guide 48, pp. 123–135.
Pratt, B.R., Ponce, J.J., 2019. Sedimentation, earthquakes, and tsunamis in a shallow, muddy epeiric sea: Grinnell Formation (Belt Supergroup, ca 1.45 Ga), western North America. Geological Society of America Bulletin 132, #–#. [in press]
Price, R., 1964. The Precambrian Purcell System in the Rocky Mountains of southern Alberta and British Columbia. Bulletin of Canadian Petroleum Geology 12, 399–426.
Pushie, M.J., Pratt, B.R., Pickering, I.J., George, G.N., MacDonald, T.C., 2014. Evidence for biogenic copper (hemocyanin) in the Middle Cambrian arthropod *Marrella* from the Burgess Shale. Palaios 29, 512–524.
Retallack, G.J., Dunn, K.L., Saxby, J., 2013. Problematic Mesoproterozoic fossil *Horodyskia* from Glacier National Park, Montana, USA. Precambrian Research 226, 125–142.
Ross, C.P., 1959. Geology of Glacier National Park and the Flathead region, northwestern Montana. U.S. Geological Survey Professional Paper 296, 125 pp.
Ross, G. M., Villeneuve, M., 2003. Provenance of the Mesoproterozoic (1.45 Ga) Belt basin (western North America): Another piece in the pre-Rodinia paleogeographic puzzle. Geological Society of America Bulletin 115, 1191–1217.
Schieber, J., 1989. Facies and origin of shales from the mid-Proterozoic Newland Formation, Belt Basin, Montana, USA. Sedimentology 36, 203–219.
Sears, J.W., 2007. Rift destabilization of a Proterozoic epicontinental pediment: A model for the Belt-Purcell Basin, North America, in: Link, P.K., Lewis, R.S. (Eds.), Proterozoic Geology of Western North America and Siberia. SEPM Special Publication 86, pp. 55–64.
Seilacher, A., 1992. Vendobionta and Psammocorallia: lost constructions of Precambrian evolution. Journal of the Geological Society, London 149, 607–613.
Sergeev, V.N., Sharma, M., Shukla, Y., 2012. Proterozoic fossil cyanobacteria. The Palaeobotanist 61, 189–358.
Shen, B., Xiao, S., Dong, L., Zhou, C., Liu, J., 2007. Problematic macrofossils from Ediacaran successions in the North China and Chaidam blocks: Implications for their

evolutionary root and biostratigraphic significance. Journal of Paleontology 79, 1396–1411.
Shepard, R.N., Sumner, D.Y., 2010. Undirected motility of filamentous cyanobacteria produces reticulate mats. Geobiology 8, 179–190.
Slotznick, S.P., Winston, D., Webb, S.M., Kirschvink, J.L., Fischer, W.W., 2016. Iron mineralogy and redox conditions during deposition of the mid-Proterozoic Appekunny Formation, Belt Supergroup, Glacier National Park, in: MacLean, J.S., Sears, J.W. (Eds.), Belt Basin: Window to Mesoproterozoic Earth. Geological Society of America Special Paper 522, pp. 221–242.
Stewart, E.D., Link, P.K., Fanning, C.M., Frost, C.D., McCurry, M., 2010 Paleogeographic implications of non-North American sediment in the Mesoproterozoic upper Belt Supergroup and Lemhi Group, Idaho and Montana, USA. Geology 38, 927–930.
Upfold, R.L., 1984. Tufted microbial (cyanobacterial) mats from the Proterozoic Stoer Group, Scotland. Geological Magazine 121, 351–355.
Whipple, J.W., compiler, 1992. Geologic map of Glacier National Park, Montana. U.S. Geological Survey, Miscellaneous Investigations Series Map I-1508-F, scale 1:100,000.
Whipple, J.W., Connor, J.J., Raup, O.B., McGimsey, R.G., 1984. Preliminary report on the stratigraphy of the Belt Supergroup, Glacier National Park and adjacent Whitefish Range, Montana, in: McBane, J.D., Garrison, P.B. (Eds.), Northwest Montana and Adjacent Canada. Montana Geological Society Guidebook, 1984 Field Conference and Symposium, pp. 33–50.
Whipple, J.W., Binda, P.L., Winston, D., 1997. Geologic guide to Glacier National Park, Montana and areas adjacent to Waterton, Alberta, in: Geologic Guidebook to the Belt-Purcell Supergroup, Glacier National Park and Vicinity, Montana and Adjacent Canada, Field Trip Guidebook for the Belt Symposium III. Belt Association, Pocatello, Idaho, pp. 125–155.
Wierzchos, J., Berlanga, M., Ascaso, C., Guerrero, R., 2006. Micromorphological characterization and lithification of microbial mats from the Ebro Delta (Spain). International Microbiology 9, 289–295.
Willis, B., 1902. Stratigraphy and structure, Lewis and Livingston ranges, Montana. Geological Society of America Bulletin 13, 305–325.
Winston, D., 1986a. Sedimentology of the Ravalli Group, middle Belt carbonate and Missoula Group, Middle Proterozoic Belt Supergroup, Montana, Idaho and Washington, in: Roberts, S.M. (Ed.), Belt Supergroup: A Guide to Proterozoic Rocks of Western Montana and Adjacent Areas. Montana Bureau of Mines and Geology, Special Publication 94, pp. 85–124.
Winston, D., 1986b, Middle Proterozoic tectonics of the Belt basin, western Montana and northern Idaho, in: Roberts, S.M. (Ed.), Belt Supergroup: A Guide to Proterozoic Rocks of Western Montana and Adjacent Areas. Montana Bureau of Mines and Geology, Special Publication 94, pp. 245–257.
Winston, D., 1986c. Sedimentation and tectonics of the Middle Proterozoic Belt Basin and their influence on Phanerozoic compression and extension in western Montana and northern Idaho, in: Peterson, J.A. (Ed.), Paleotectonics and Sedimentation in the Rocky Mountain Region, United States. American Assocation of Petroleum Geologists, Memoir 41, pp. 87–118.
Winston, D., 1989a. Introduction to the Belt, in: Winston, D., Horodyski, R.J., Whipple, J.W. (Eds.), Middle Proterozoic Belt Supergroup, Western Montana. American Geophysical Union, 28th International Geological Congress, Washington, Field trip Guidebook T334, pp. 1–6.

Winston, D., 1989b. A sedimentologic and tectonic interpretation of the Belt, in: Winston, D., Horodyski, R.J., Whipple, J.W. (Eds.), Middle Proterozoic Belt Supergroup, western Montana. American Geophysical Union, 28th International Geological Congress, Washington, Field trip Guidebook T334, pp. 46–69.
Winston, D., 1990. Evidence for intracratonic, fluvial and lacustrine settings of Middle to Late Proterozoic basins of western U.S.A., in: Gower, C. F., Rivers, T., Ryan, B. (Eds.), Mid-Proterozoic Laurentia–Baltica. Geological Association of Canada Special Paper 38, pp. 535–564.
Winston, D., 2007. Revised stratigraphy and depositional history of the Helena and Wallace formations, mid-Proterozoic Piegan Group, Belt Supergroup, Montana and Idaho, U.S.A., in: Link, P.K., Lewis, R.S. (Eds.), Proterozoic Geology of Western North America and Siberia. SEPM Special Publication 86, pp. 65–100.
Winston, D., 2016. Sheetflood sedimentology of the Mesoproterozoic Revett Formation, Belt Supergroup, northwestern Montana, USA, in: MacLean, J.S., Sears, J.W. (Eds.), Belt Basin: Window to Mesoproterozoic Earth. Geological Society of America Special Paper 522, pp. 1–56.
Winston, D., Link, P.K., 1993. Middle Proterozoic rocks of Montana, Idaho and eastern Washington: the Belt Supergroup, in: Link, P.K. (Ed.), Middle and Late Proterozoic stratified rocks of the western U.S. Cordillera, Colorado Plateau, and Basin and Range Province, in: Reed, J.C., Bickford, M.E., Houston, R.S., Link, P.K., Rankin, D.W., Sims, P.K., Van Schmus, W.R. (Eds.), Precambrian: Conterminous U.S. Geological Society of America, The Geology of North America C-2, pp. 487–517.
Winston, D., Horodyski, R.J., Whipple, J.W., 1989. A sedimentologic and tectonic interpretation of the Belt: Middle Proterozoic Belt Supergroup, Western Montana: Middle Proterozoic Belt Supergroup, western Montana, in: Winston, D., Horodyski, R.J., Whipple, J.W. (Eds.), American Geophysical Union, 28th International Geological Congress, Washington, Field trip Guidebook T334, pp. 47–70.
Xiao, S., Knoll, A.H., Yuan, X., 1998. Morphological reconstruction of *Miaohephyton bifurcatum*, a possible brown alga from the Neoproterozoic Doushantuo formation, South China. Journal of Paleontology 72, 1072–1086.
Yin, A., Kelty, T.K., 1991. Structural evolution of the Lewis plate in Glacier National Park, Montana: Implications for regional tectonic development. Geological Society of America Bulletin 103, 1073–1089.
Yochelson, E.L., Fedonkin, M.A., 2000. A new tissue-grade organism 1.5 billion years old from Montana. Proceedings of the Biological Society of Washington 113, 843–847.

Figure Captions

Fig. 2.1. (A) Map of central western North America showing outcrop distribution of Belt Supergroup rocks and Glacier and Waterton Lakes national parks (Waterton–Glacier International Peace Park astride the border between Montana and Alberta). (B) Map of the parks showing the location of the type section on the lower flank of Apikuni Mountain and the main sample locality above Apikuni Falls.

Fig. 2.2. West-to-east-to-north cross-section across the Belt Basin from Idaho to Glacier National Park, Montana, showing the main subdivisions of the Belt Supergroup and formations in the lower and middle portion (based on the most recent compilation by Winston, 2016, fig. 1; revised from Winston, 1989a, fig. 3; Winston, 1990, fig. 5; Winston and Link, 1993, fig. 13). The Appekunny Formation has been placed in the Ravalli Group in some schemes (Harrison, 1972; Horodyski, 1983; Whipple et al., 1984). The Wallace

Formation was not originally mapped in Glacier National Park (Whipple, 1992), so the boundary is shown with a dashed line. The Belt Supergroup is called the Purcell Supergroup in Canada and the lithostratigraphic nomenclature has some differences (e.g., McMechan, 1981; Höy, 1992; Chandler, 2000).

Fig. 2.3. (A) View of Altyn Peak and Apikuni Mountain, Glacier National Park, Montana, from the road to Many Glacier. Grey strata forming the lower part of the cliff above the forest belong to the Altyn Formation. Banded but dominantly greenish strata above comprise the Appekunny Formation. The maroon unit in the background is the Grinnell Formation. Apikuni Falls is located in the notch in the Altyn Formation to the right of centre. (B) Outcrop of lower Appekunny Formation and adjacent scree slope above and to the east of Apikuni Falls, showing dominantly thin, planar bedding. (C) Outcrop of lower Appekunny Formation at Crypt Lake, Waterton Lakes National Park, Alberta, showing thin, planar argillaceous siltstone beds overlain by low-relief hummocky cross-stratified, very fine-grained sandstone. Crypt Lake (48°59.8'N, 113°50.2'W), Waterton Lakes National Park, is along strike 25 km north-northwest of Apikuni Falls. Scale in centimetres.

Fig. 2.4. Argillaceous siltstone in the lower Appekunny Formation, viewed parallel to bedding. A is a natural surface, B and C are sawn surfaces, all wetted with ethanol and the brightness and contrast enhanced. Darker laminae are more argillaceous. (A) Gently dipping laminae cut by a scour surface overlain by gently dipping to planar laminae. (B) Planar, gently dipping and lenticular laminae. (C) Planar laminae cut by a scour surface and overlain by gently convex-upward plane laminae; lower laminae affected by slight soft-sediment deformation.

Fig. 2.5. Optical scans of thin sections of argillaceous siltstone. Darker areas are more clay-rich, and lighter areas are siltier. Scale bar same for all. (A) Planar laminae with scattered discontinuous millimetre-sized clay seams in lower part, with a slightly deformed lenticular layer containing gently dipping cross laminae at lower right. (B) Planar laminae with discontinuous clay-rich seams and lenses near the bottom, overlain near the top in turn by gently dipping cross laminae filling a shallow scour, then planar laminae with scattered millimetre-sized clay seams. (C) Planar laminae with millimetre- to centimetre-sized clay intraclasts and discontinuous seams near the bottom and top.

Fig. 2.6. Bedding surfaces exhibiting mudstone intraclasts. (A) Shallow gutter filled with fine-grained sandstone containing intraclasts up to 20 mm in size. (B) Lamina of fine-grained sandstone containing intraclasts up to 10 mm in size. (C) Lamina of fine-grained sandstone containing intraclasts 3–5 mm in size.

Fig. 2.7. Bedding surfaces exhibiting blistered and wrinkled textures. A–G and I blackened and dusted with ammonium chloride sublimate; H wetted with ethanol. (A) Gently pitted surface with several centimeter-scale mudstone intraclasts and a patch of crowded *Horodyskia* beads in slight epirelief at lower right. (B) Smooth surface with pimple-shaped pustules. (C) Irregular to crudely linear wrinkles and low-relief pustules. Linear fractures are tectonic. (D) Irregular and crudely radiating wrinkles and low-relief pustules. (E) Elongate wrinkles and ridges with subordinate blisters. (F) Elongate and polygonal blisters and fine wrinkles. (G) Polygonal and subordinate elongate blisters and ridges with *Horodyskia* string-of-beads at the centre of the lower edge (shown close-up in Figure 2.10C). (H) Sawn surface cut perpendicular to bedding along the lower right side of the slab shown in G (and continuing beyond the edge of the photograph). Planar argillaceous siltstone laminae are

truncated and overlain by gently convex-upward laminae (becoming concave in the shallow depression beyond to the edge), in the upper part containing several mudstone lenses, some with domical lamination and some with oblique lamination. The upper edge exhibits clay lenses conforming to cross-sections of surface blisters. (I) Crudely elongate blisters on a finely wrinkled surface.

Fig. 2.8. Mudstone cut parallel to lamination and ground to produce serial sections approximately 0.5 mm apart, showing successive morphological change of microbial surfaces. Wetted with alcohol. Light-coloured material is clay; darker coloured is clay and silt. (A–C) is one sample. (D and E) is a second sample.

Fig. 2.9. Bedding surfaces exhibiting *Horodyskia* beads. Wetted with ethanol. (A) Numerous strings-of-beads of various diameters, lengths and curvatures, on a finely wrinkled and pustular surface. (B) Crisscrossing strings-of-beads. (Oblique fractures are tectonic.) (C) Several, partly tangled strings-of-beads showing a bimodal size, along with seemingly isolated beads, on a finely wrinkled and pustular surface. (D) Overlapping to clustered strings-of-beads on a finely pustular surface. (E) String-of-beads and scattered beads on a finely wrinkled surface. (F) Densely clustered beads and possibly strings-of-beads oriented diagonally down the left side.

Fig. 2.10. Bedding surfaces exhibiting *Horodyskia* beads. A, B, D–H wetted with alcohol; C blackened and dusted with ammonium chloride sublimate. (A) String-of-beads oriented in a sinuous shape. (B) String-of-beads of variable diameter and with varying distances apart oriented in a U shape, on a finely pustular surface. (C) String-of-beads oriented in a U shape on a blistered surface. (Close-up of part of surface shown in Figure 2.7F.) (D) Curving string-of-beads. (E) Meandering string-of-beads. (F) String-of-beads in a U shape, with varying distances apart. (G) Scoured ripples with a nearly straight string-of-beads (right) and possibly scattered beads on a finely pustular surface. (H) Curving strings-of-beads of variable sizes on a finely pustular surface; aligned pustules or small string-of-beads at left.

Fig. 2.11. Bedding surfaces exhibiting *Horodyskia* beads and wrinkled or pustular textures. Wetted with ethanol. (A) Several strings-of-beads on a wrinkled and pustular surface. (B) Several strings-of-beads oriented subparallel and transverse to crudely linear wrinkles. (C) Curving string-of-beads on a sparsely, coarsely pustular surface. (D) Lower surface showing several beads (top centre) on a finely wrinkled and pustular surface.

Fig. 2.12. Elemental composition of argillaceous siltstone with *Horodyskia* string-of-beads, determined with synchrotron X-ray fluorescence. (A) Bed surface (wetted with alcohol) showing row of six clay-rich beads (same specimen as Figure 2.13A, B). (B–K) Key elemental maps. Ti, titanium; K, potassium; Ca, calcium; As, arsenic; Fe, iron; Ca, calcium; S, sulphur; Mn, manganese; Ni, nickel; Zn, zinc; As, arsenic; Cu, copper. "Hot" colours indicate increased concentration. (Streaks in G are an artefact.) (L) Map of degree of scatter of X-rays due to surface irregularities (which affects apparent concentration).

Fig. 2.13. (A) Specimen 5 mm thick bearing a *Horodyskia* string-of-beads on a finely pustular surface (same specimen as Figure 2.12A). (B) CT X-ray scan oriented perpendicular to lamination, with denser areas (more clay-rich) appearing lighter and more transmissive areas appearing darker. Various amounts of strings-of-beads and probable blisters give variable densities to the scan, and orientation of strings-of-beads in successive laminae are unrelated to each other.

Fig. 2.14. Optical scans of thin sections of mudstone cut parallel to lamination through *Horodyskia* beads (dark). (A) String-of-beads oriented lower right to upper left (upper two partly plucked during preparation) showing somewhat irregular shape, in mottled mudstone. (B) Two beads, one lobate and the other roughly circular in outline, in mottled mudstone.

Fig. 2.15. Thin section photomicrographs (A–C) and backscattered electron micrograph (D) of laminated argillaceous siltstone containing mudstone (silt- or clay-rich) lenses comprising *Horodyskia* beads and blisters. Surfaces cut perpendicular to lamination. Scale in C is same for A and B. (A) Clay seams and silt-rich lenses. (B) Clay-rich lenses in lower part. (C) Clay seams and lenses. (D) Argillaceous siltstone composed of angular quartz (dark-grey), feldspar (medium-grey), and scattered ilmenite (bright), overlain by clay lens (at top). (Scattered black spots are due to grain plucking from sample cutting and polishing.)

Fig. 2.16. Diagrammatic portrayal of the formation of *Horodyskia* strings-of-beads from trapping of clay flocs and flakes on filament tufts growing as pinnacles on a benthic microbial mat, which also exhibits ridge-like wrinkles, blisters and pustules on which mud accumulates.

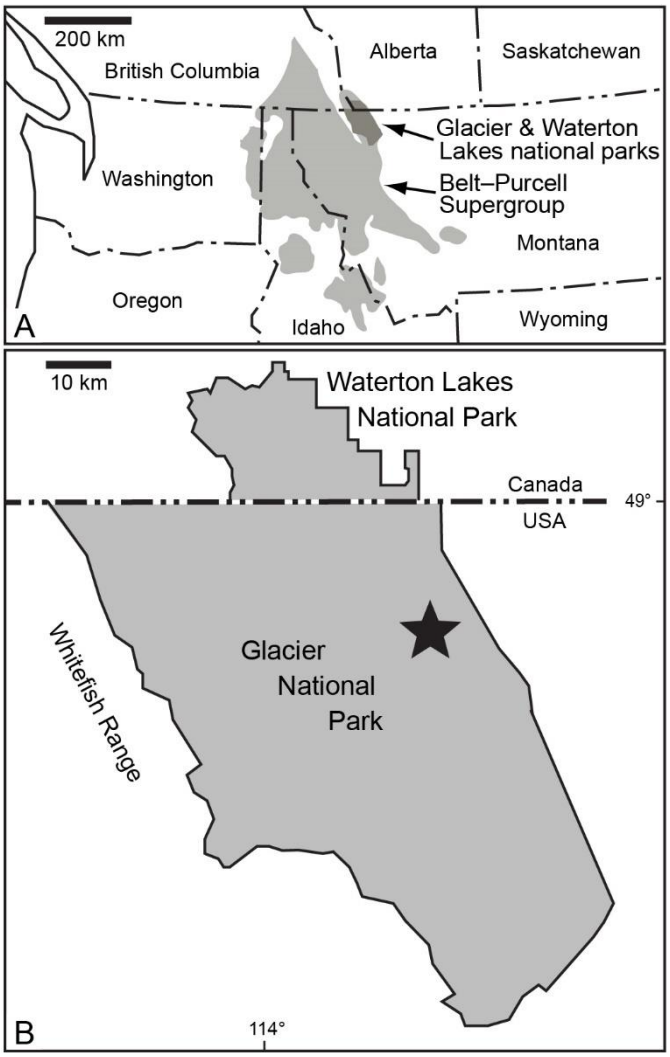
200 km
British Columbia
Alberta
Saskatchewan
Glacier & Waterton
Lakes national parks
Belt–Purcell
Supergroup
Washington
Montana
Oregon
Idaho
Wyoming
A
10 km
Waterton Lakes
National Park
Canada
USA
49°
Glacier
National
Park
Whitefish Range
B
114°

Fig. 2.1

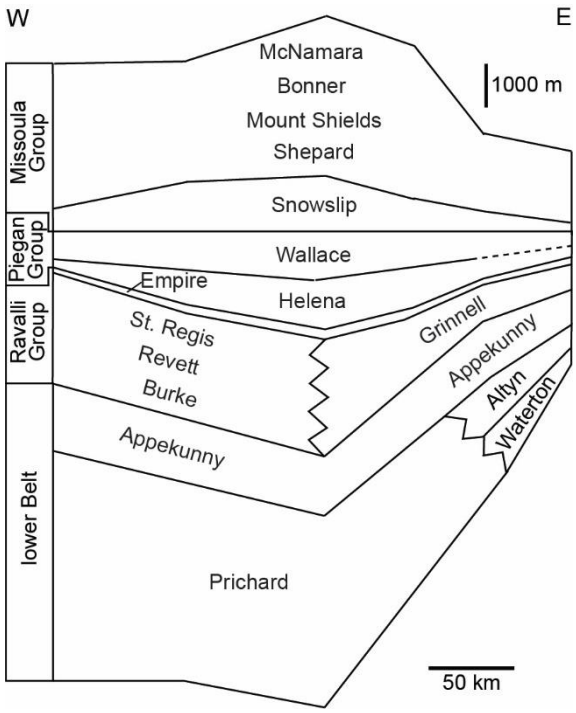
W
E
McNamara
Bonner
Mount Shields
Shepard
1000 m
Missoula Group
Snowslip
Piegan Group
Wallace
Empire
Helena
Ravalli Group
St. Regis
Revett
Burke
Grinnell
Appekunny
Altyn
Waterton
lower Belt
Appekunny
Prichard
50 km

Fig. 2.2

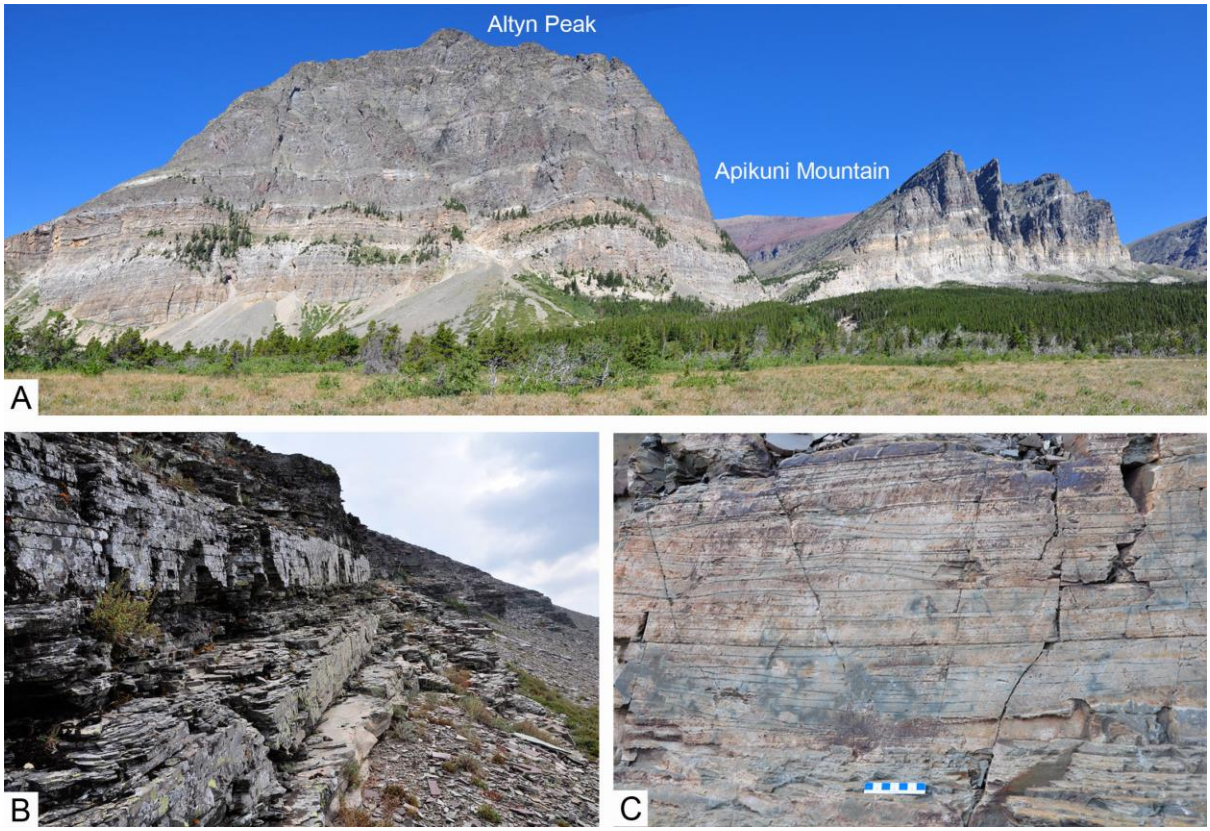

Fig. 2.3

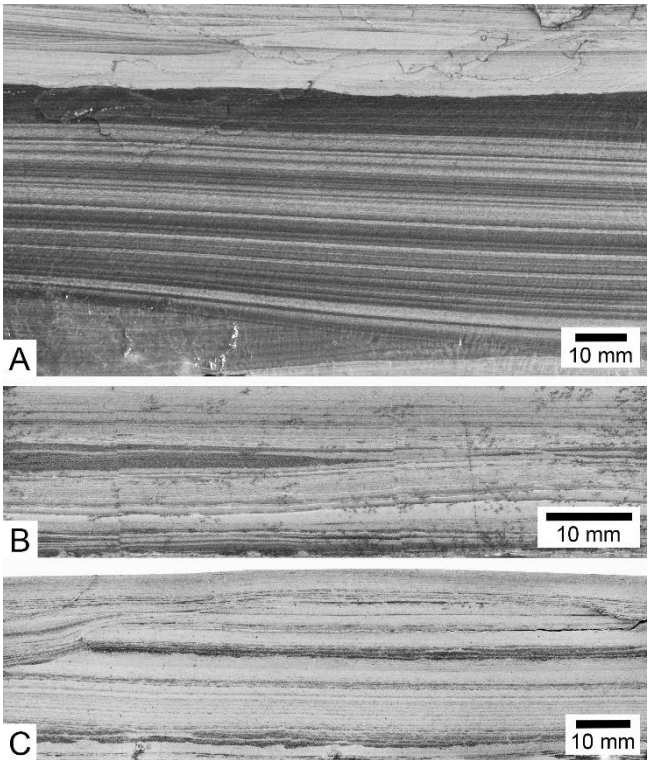

Fig. 2.4

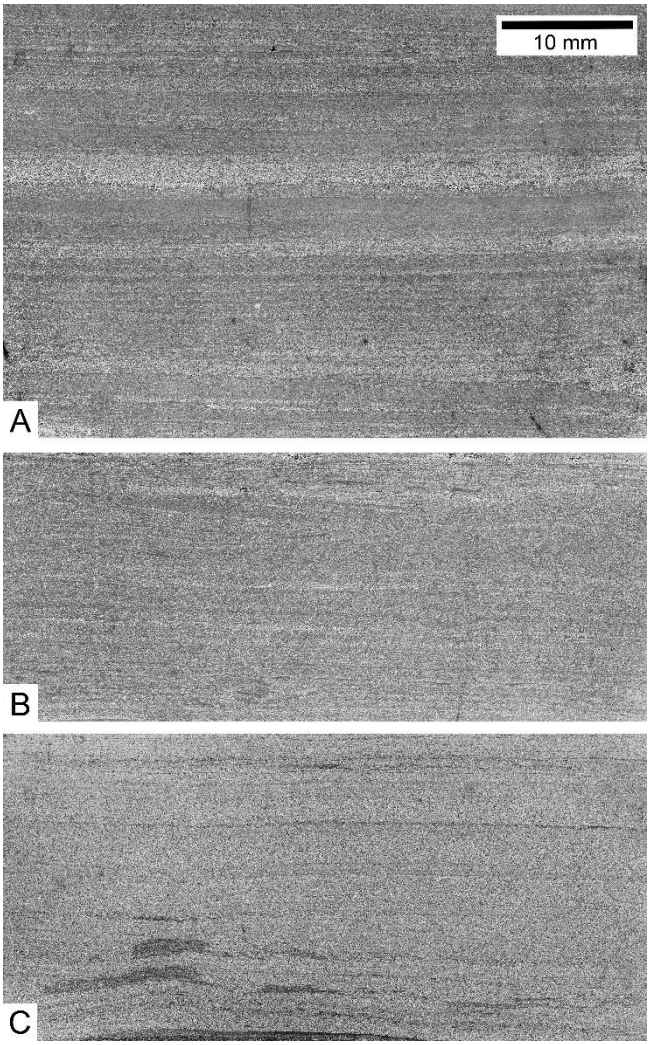

Fig. 2.5

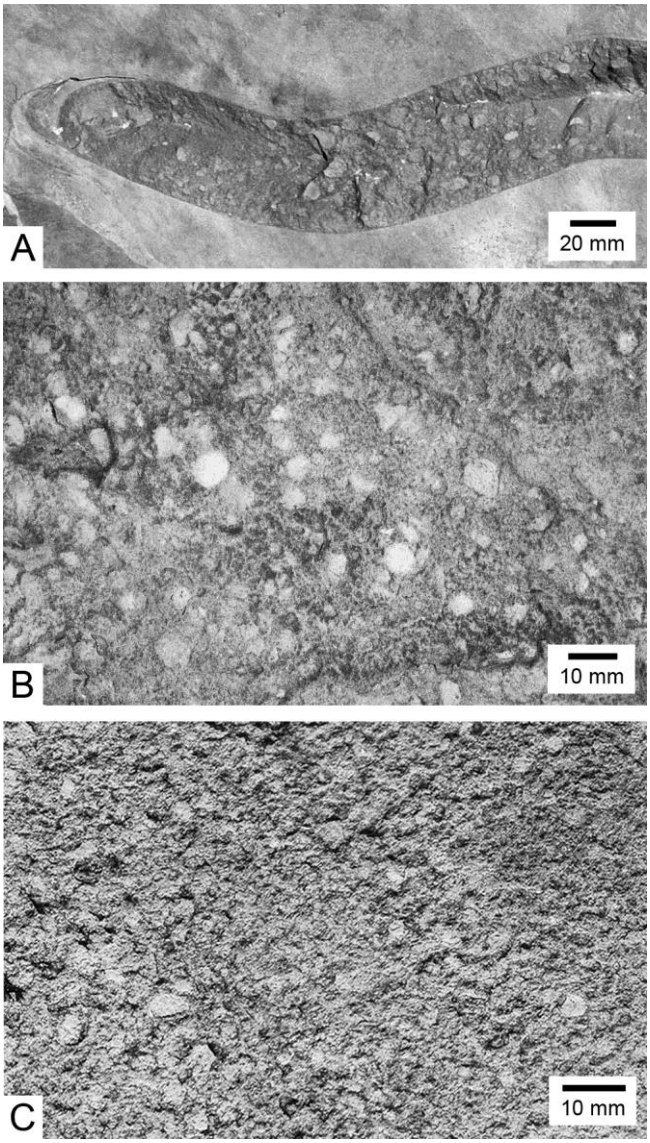

Fig. 2.6

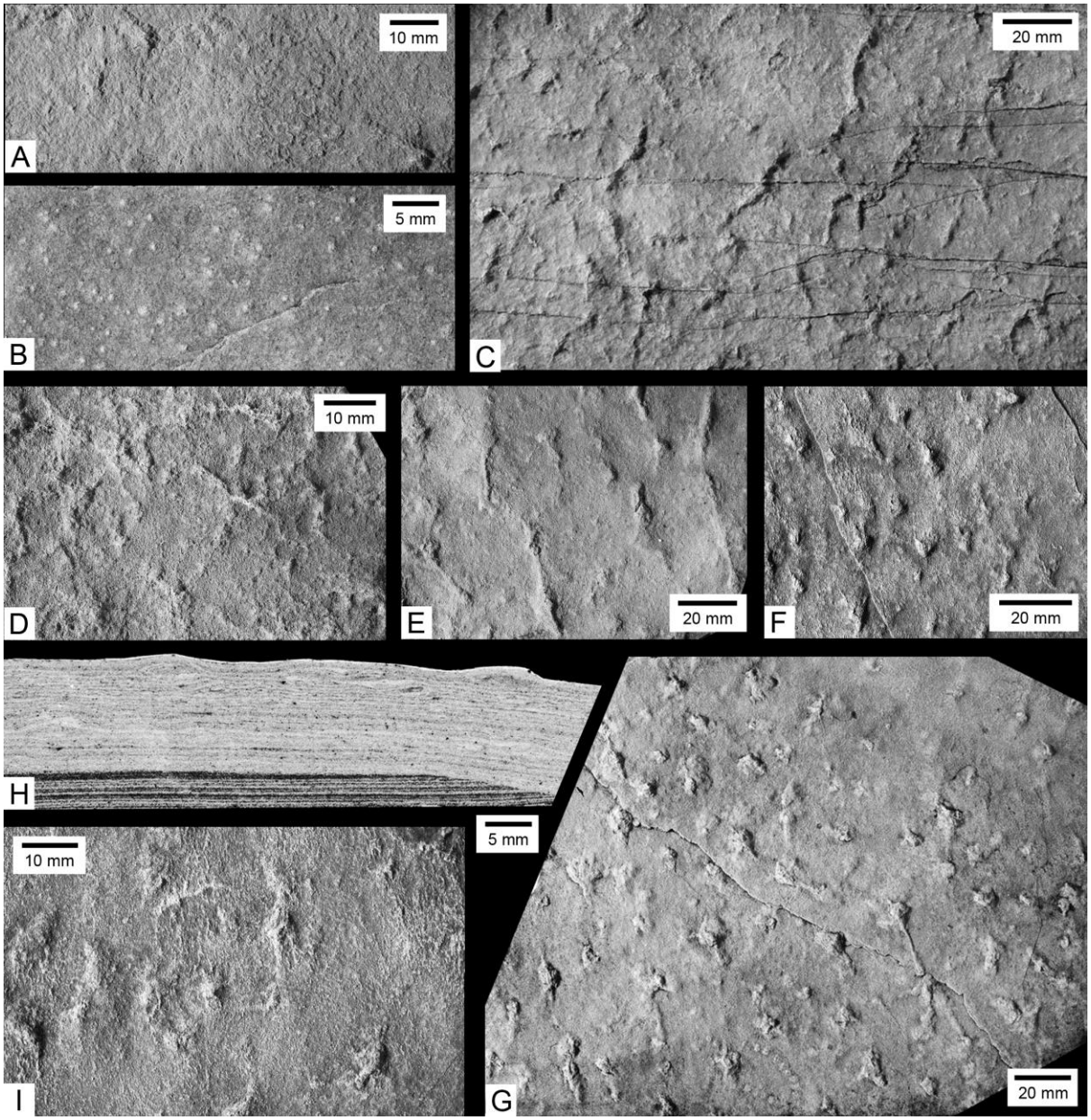

Fig. 2.7

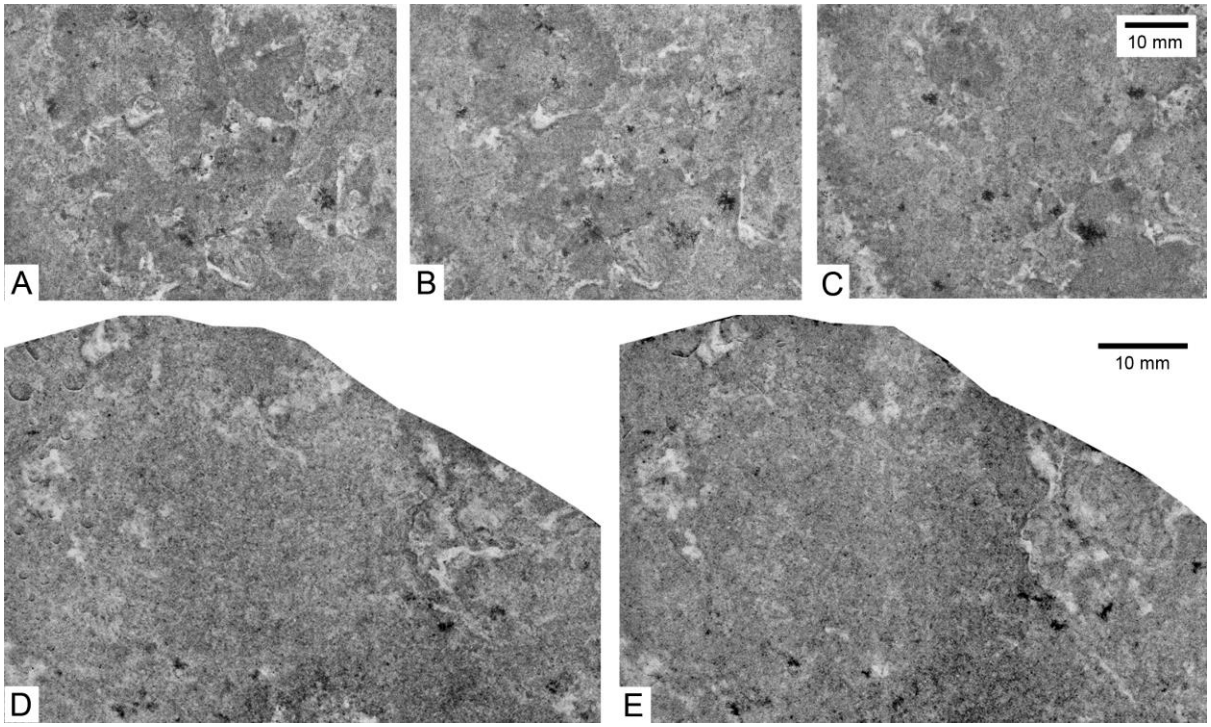

Fig. 2.8

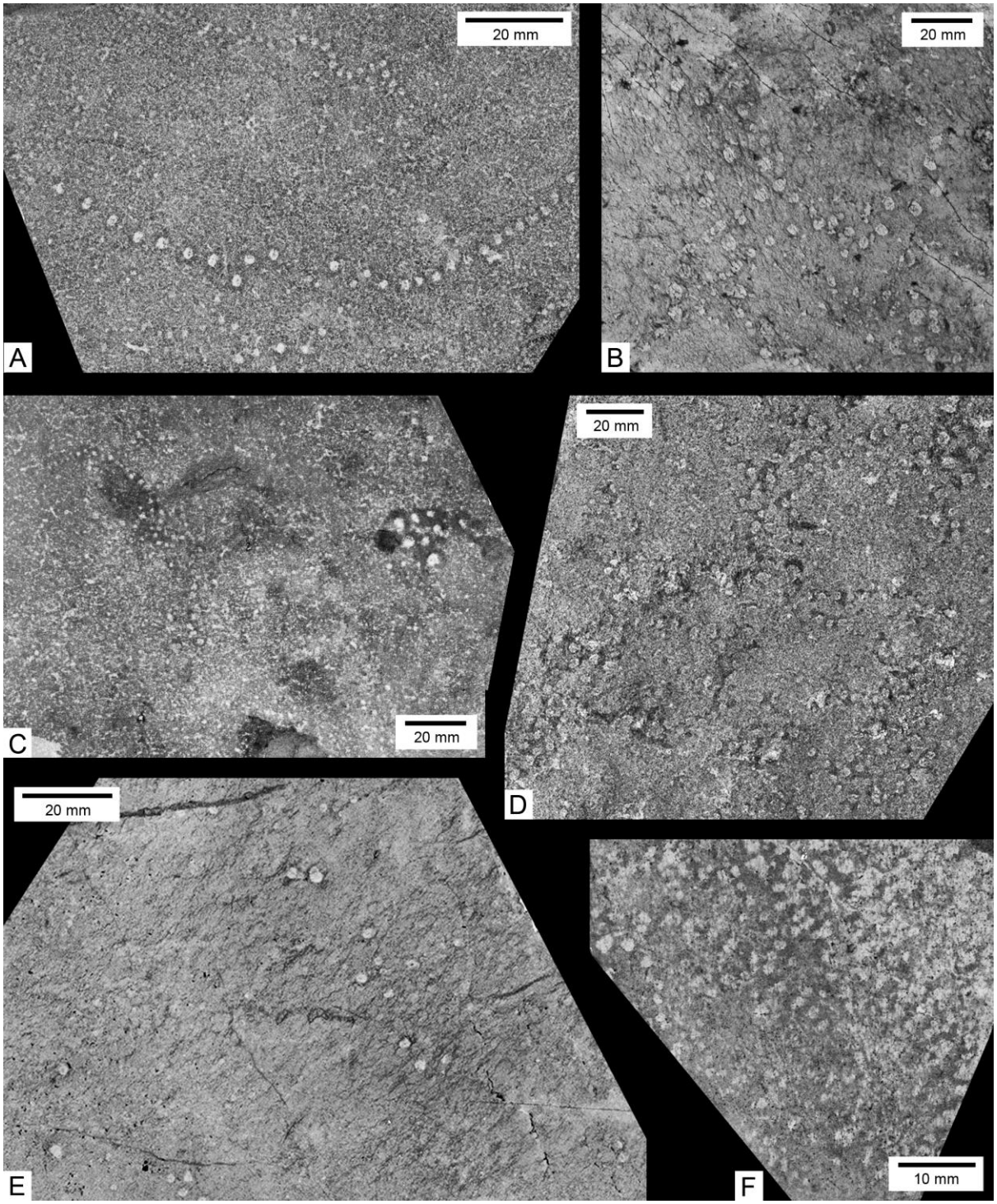

Fig. 2.9

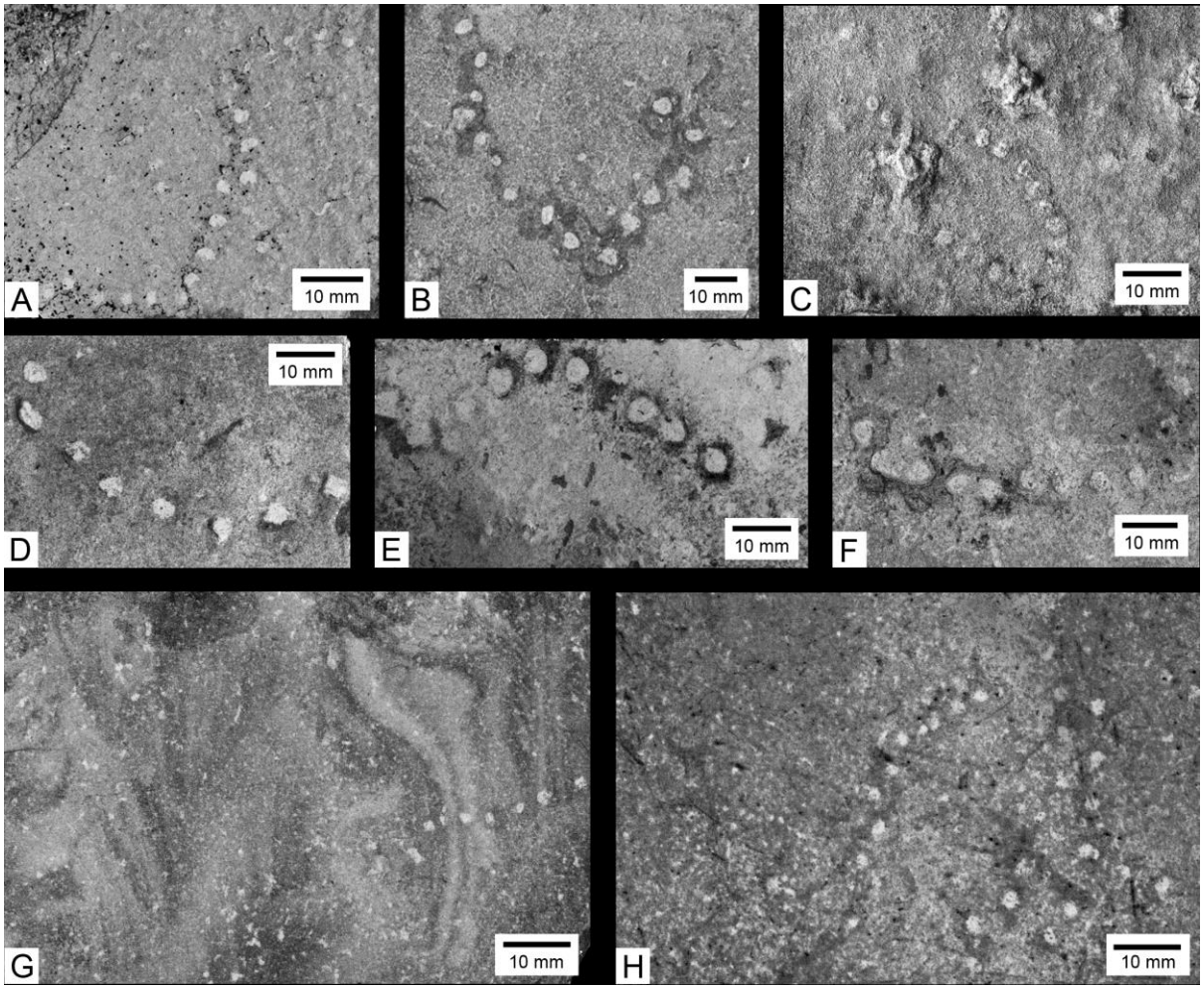

Fig. 2.10

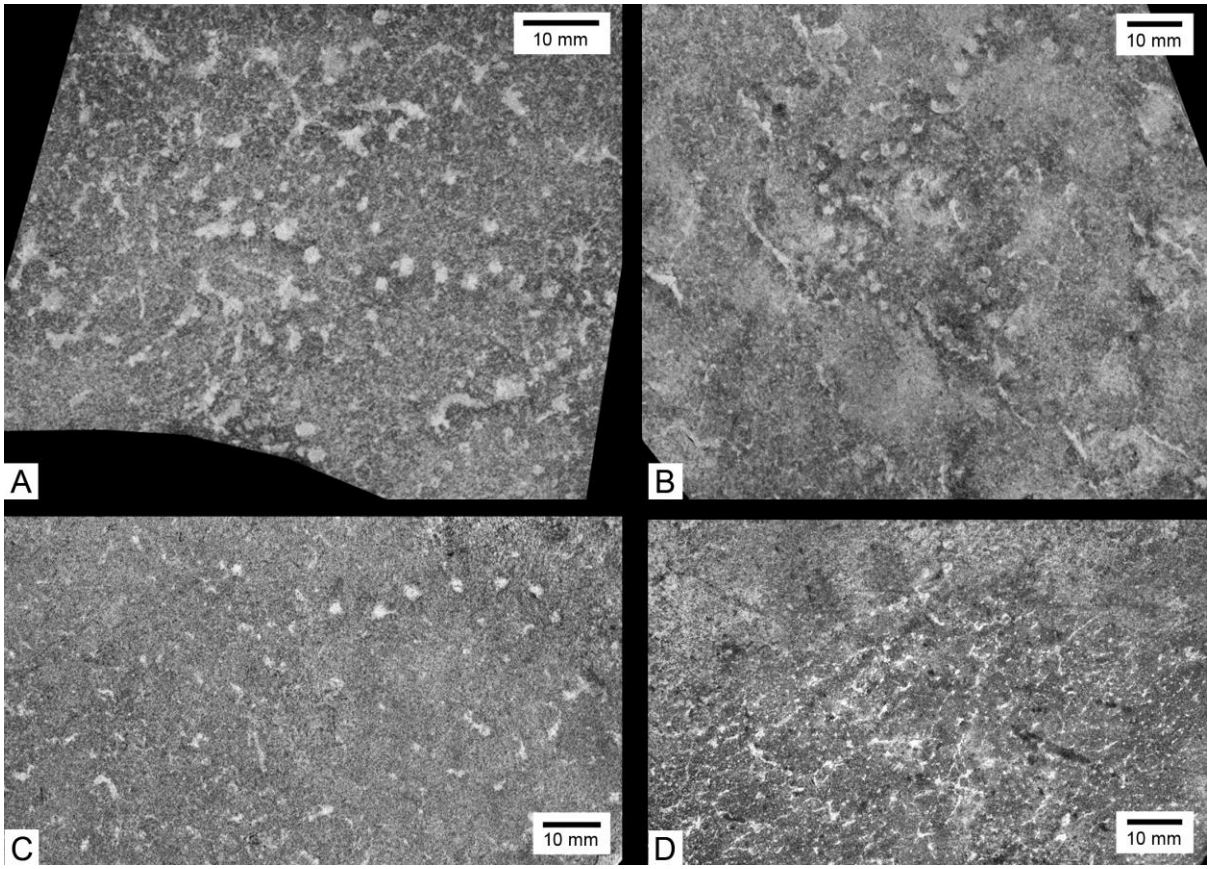

Fig. 2.11

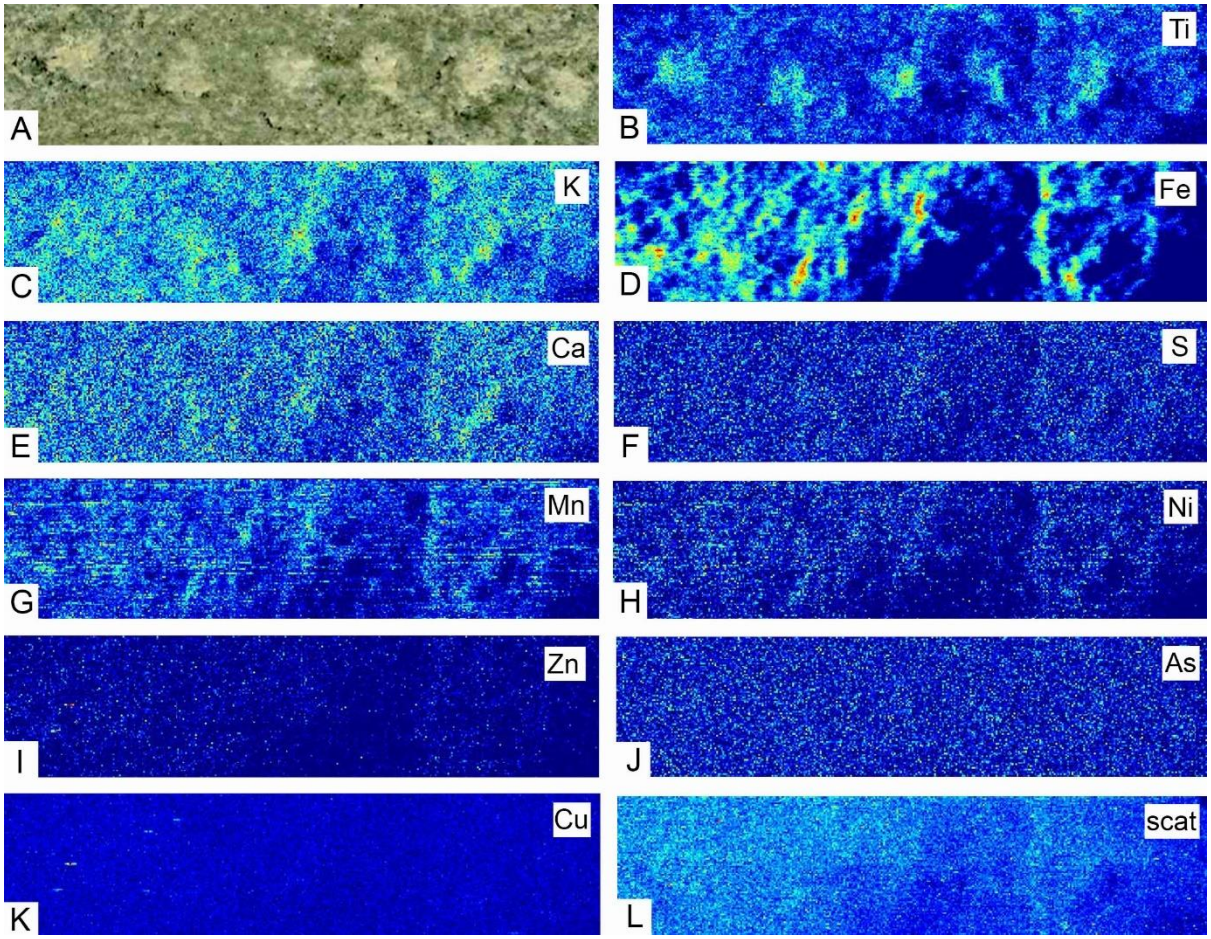

Fig. 2.12

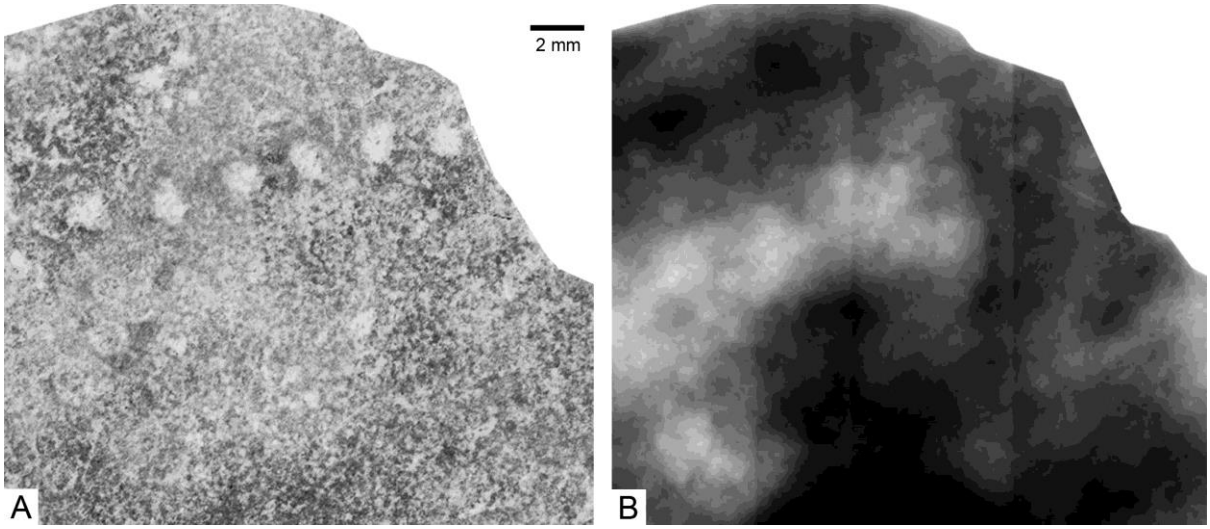

Fig. 2.13

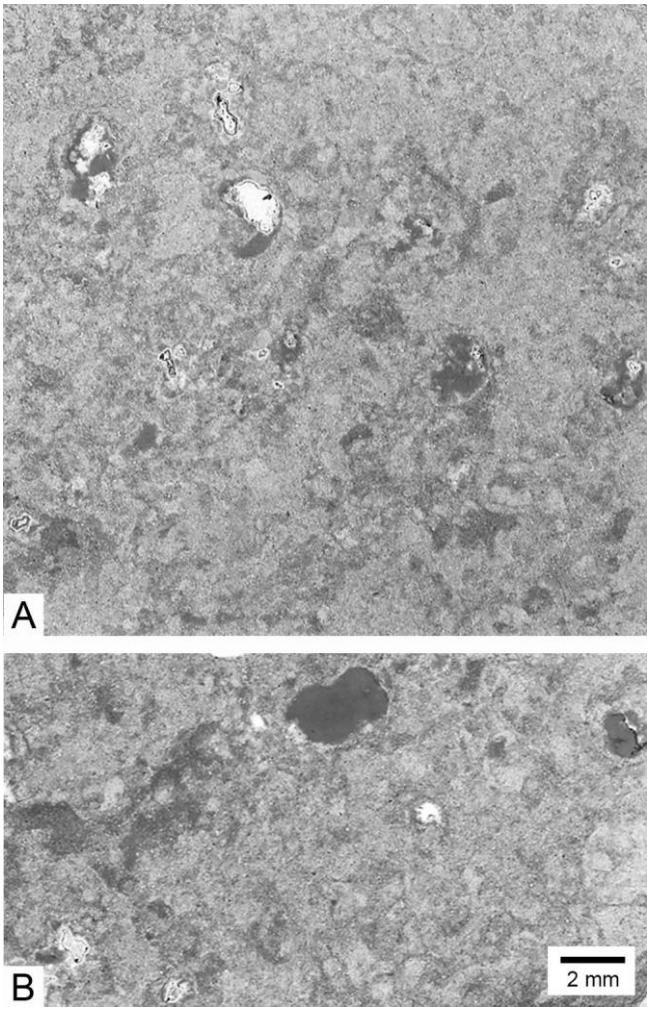

Fig. 2.14

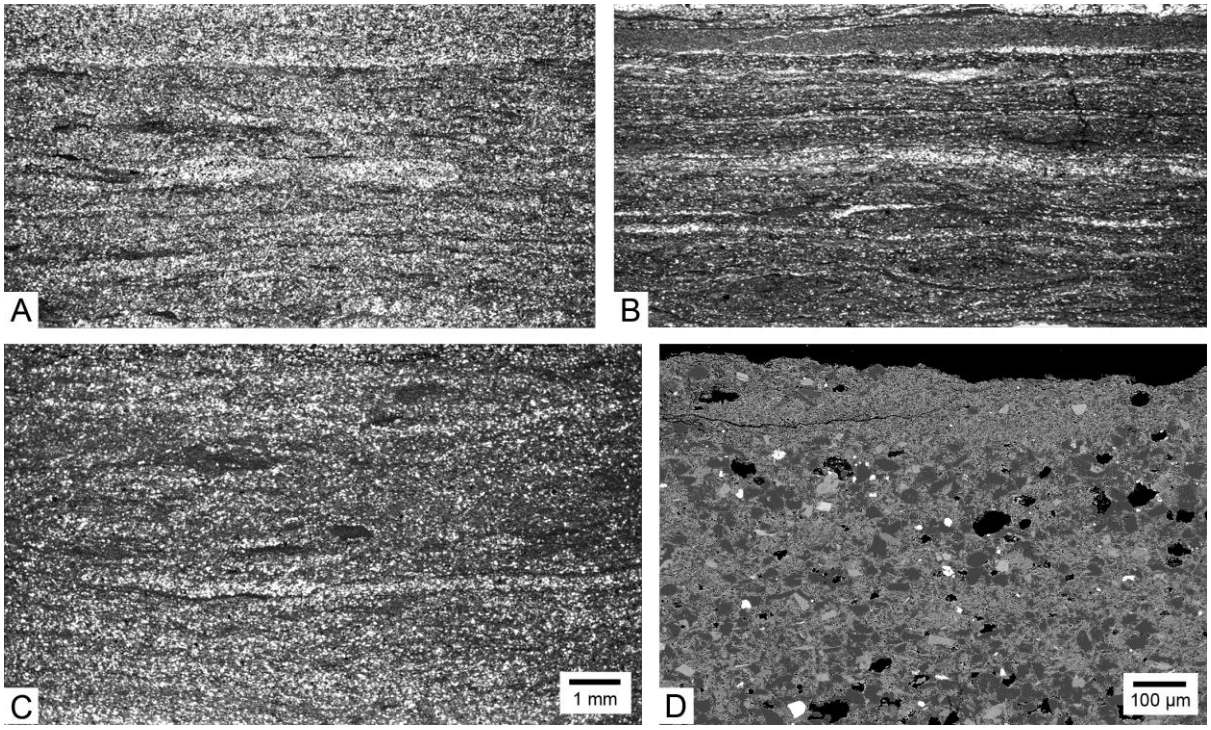

Fig. 2.15

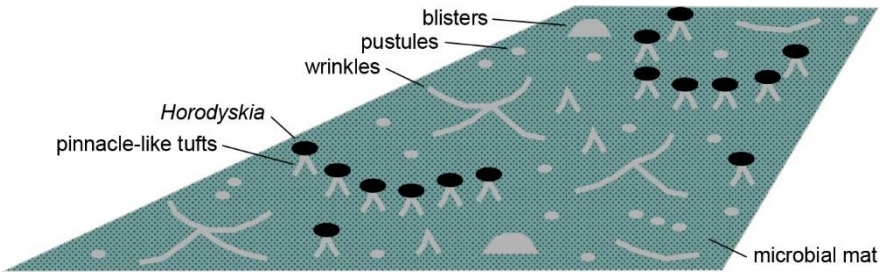
blisters
pustules
wrinkles
Horodyskia
pinnacle-like tufts
microbial mat

Fig. 2.16

CHAPTER 3

Evolution of a Mesoproterozoic carbonate platform in a tectonically active, intracratonic basin, lower Belt Supergroup (*ca.* 1.45 Ga), western North America

ABSTRACT

Carbonate rocks of the lower Belt (Purcell) Supergroup comprise the Haig Brook, Tombstone Mountain, Waterton and Altyn formations which crop out in the eastern Rocky Mountains of northwestern Montana, southwestern Alberta and adjacent southeastern British Columbia. They record the development on the present-day northeastern side of the Belt Basin of a ramp-style carbonate platform while the basin was deep and before water depth was reduced due to voluminous siliciclastic mud input from the west. The Waterton–Altyn succession records a shallowing-upward, westward prograding carbonate platform. Five main facies types are recognized: laminite, ribbon, grainstone, oolite and stromatolite. The first two consisted of lime muds deposited in deeper water at and below the limit of the ambient, shallow storm wave-base. The grainstone facies consists of sand-sized peloids, aggregates and intraclasts plus admixed siliciclastic sand, microspar grains and ooids, while ooids dominate the oolite facies. These are allochthonous coarse-grained particles interpreted to have been transported westward mainly by tsunami off-surge from the inner platform, coastal shoals and tidal flat sabkhas, outcrops of which are not preserved. In the outer platform this sediment lay undisturbed, but in the mid-platform it was reworked by strong tidal currents, which led to variably directed cross-lamination from dune migration and locally large sand bars with northwestward-dipping clinoforms. Tidal currents may also have been an agent of lime mud transport into deeper areas. By contrast, evidence for strong storms, such as hummocky or swaley cross-stratification, is absent. Consequently, intraclastic conglomerates in deeper water down the ramp are ascribed instead to episodic tsunami-induced wave action which caused localized scour and reworking. Deformation features due to synsedimentary earthquakes are common but in the Altyn Formation are not coincident with individual tsunami deposits in the outer platform, indicating that the faults that generated these two sets of features were generally not the same. The carbonate factory was eventually shut down because the platform was suffocated by siliciclastic mud derived from the west, and tidal currents diminished as the whole basin shallowed. Previously interpreted to consist of shallow subtidal and tidal-flat deposits, these strata reveal a different depositional system that invokes processes not typically considered in studies of carbonate platforms.

1. Introduction

Relatively few carbonate platform successions have been described from Mesoproterozoic strata deposited during the so-called ‘Boring Billion’, a protracted phase of apparent tectonic, climatic and evolutionary stability on Earth (Brasier and Lindsay, 1998). Many of these successions were deposited in shallow epeiric seas of limited bathymetric differentiation (e.g., Bertrand-Sarfati and Moussine-Pouchkine, 1985; Pratt, 2001; Mei, 2007; Banerjee and Jeevankumar, 2007; Mei and Tucker, 2013; Bartley et al., 2015), although there are others where rapid basin subsidence led to comparatively steep shelf-to-basin geometry (e.g., Sherman et al., 2000, 2001; Turner, 2009; Turner et al., 2016; Medig et al., 2016). Despite study of many examples (Medig et al., 2016, table 2), there is much to be determined about

the nature and origin of carbonate allochems and facies, lateral relationships, how and why facies are arranged stratigraphically, and what is the overall platform architecture. It is also unclear if certain carbonate facies could be considered typical of this phase, as has been contemplated in some discussions of Precambrian carbonates (e.g., Grotzinger and James, 2000; Sumner and Grotzinger, 2000; James et al., 2010; Pratt, 2010; Hood et al., 2011; James and Jones, 2016; Wang et al., 2020), or if they are due to specific environmental attributes of individual basins, or both. The nature of shallow-marine carbonate facies evolved through the subsequent Neoproterozoic and into the early Paleozoic, before biomineralization expanded during Ordovician diversification and took greater control of precipitation (e.g., Schlager, 2005; Pruss et al., 2010; Pratt et al., 2012). However, the similarity of some carbonate facies between the Proterozoic and lower Paleozoic, such as ribbon limestone (e.g., Sherman et al., 2000; Bayet-Goll et al., 2015), along with a broadly analogous facies architecture of many carbonate platforms of both Precambrian and Phanerozoic ages, demonstrate the long history of basically the same paleoceanographic and paleoclimatic controls regardless of how carbonate allochems formed (e.g., Grotzinger, 1986; Lehrmann et al., 1998; Clough and Goldhammer, 2000; Jiang et al., 2003; Da Silva et al., 2012).

The Mesoproterozoic Belt Supergroup (= Purcell Supergroup in Canada) in central-western North America is an enormously thick package of dominantly fine-grained siliciclastic sediments (e.g., Winston, 1986c; Winston and Link, 1993; Pratt, 2017; Pratt and Ponce, 2019). The lowest unit, the 'lower Belt,' consists of a >6 km thick succession of siliciclastic turbidites (Cressman, 1989). Even though direct evidence is not observed, the carbonate platform units on the northeastern side are considered to be the comparatively thin shallow-water equivalents (Smith and Barnes, 1966; Harrison, 1972), and comprise the Haig Brook, Tombstone Mountain, Waterton and Altyn formations (Fermor and Price, 1983, 1984). This bathymetric differentiation became subdued by the onset of sedimentation of the overlying Appekunny Formation, as attested to by its lithological similarity across the Belt Basin (Winston, 1986a).

One of the obstacles to interpreting the sedimentology of these carbonate units is that they lie at the base of the Lewis thrust sheet (e.g., Stockmal and Fallas, 2015) and consequently have been extensively deformed. Nonetheless, the succession has received some study, albeit not in a modern context (Horodyski, 1976, 1983; Fermor and Price, 1983, 1984; Hill and Mountjoy, 1984; White, 1984; Hill, 1985; Pratt, 1994). It exhibits carbonate facies that are not recorded in the younger Piegan Group, or 'middle Belt carbonate,' consisting of the Helena and Wallace formations (= Siyeh and Kitchener formations in Canada), and vice versa (Pratt, 2001; Winston, 2007). The Altyn Formation has been regarded as peritidal (Horodyski, 1976, 1983, White, 1984, Hill, 1985; Pratt, 1994) whereas the Helena and Wallace formations were deposited under fully submerged conditions (Pratt, 2001). Moreover, studies of the overlying Appekunny, Grinnell and Helena formations in the same region point to the widespread effects of synsedimentary earthquake-induced deformation and tsunamis (Pratt, 1998a, b; 2001, 2017; Pratt and Ponce, 2019). These notions and the intervening advances in carbonate sedimentology over the past few decades suggest that the lower Belt carbonate succession can be approached afresh. The purpose of this paper is to present an updated sedimentological study of the lower Belt carbonate platform, integrating depositional facies and paleoenvironmental factors with the effects of early diagenesis in a seismically active basin. The results have relevance for the interpretation of other Precambrian and early Paleozoic platforms, especially in evaluating ostensibly peritidal carbonate facies.

2. Geological Setting

2.1. Belt Supergroup

The Belt Supergroup is a thick and geographically widespread succession of Mesoproterozoic (*ca*. 1.48–1.25 Ga) strata exposed in central-western North America (Fig. 3.1A), specifically southwestern Alberta, southeastern British Columbia, western Montana, northern Idaho, and northeastern Washington (e.g., Winston, 1986a, b; Hein and McMechan, 1994; Pratt, 2017). The Belt Basin was likely an intracratonic rift that opened to the ocean to the northwest (e.g., Höy, 1989; Winston and Link, 1993; Chandler, 2000; Pratt, 2001; Luepke and Lyons, 2001). Rifting may have been induced by oblique collision of a continent consisting of the East Antarctic craton (Mawsonia) and Australian cratons with Laurentia (Pisarevsky et al., 2014; Medig et al., 2014; Pehrsson et al., 2016). This also seems to have led to dramatic uplift along the western side of the basin, as well as syndepositional faulting in the central parts of the basin, causing rapid subsidence (Winston, 1986c; Evans et al., 2000; Sears, 2007; Pratt 2017).

The Belt Basin was lake-like in that it was semi-enclosed and, after deposition of the bulk of the lower Belt, remained relatively shallow, likely less than a few tens of metres' water depth as suggested by sedimentary facies and stratigraphy of the Purcell Lava (Pratt, 2001), until deposition of the Bonner Formation which is fluvial (Winston et al., 1986). It was largely normal-marine (Lyons et al., 2000) although based on the occurrence of halite casts in some units, hypersaline brines are presumed to have concentrated along the margin and at times flowed into deeper areas (Pratt, 2001; Pratt and Ponce, 2019). Fresh feldspar sand grains and evidence for evaporites indicate that the climate was arid, and the absence of specific high-energy facies suggests that it was not prone to major storms and hurricanes (Pratt and Ponce, 2019).

The western side of the basin is not preserved, but as subsidence continued the sea probably extended considerably farther eastward into central Montana and over more of southwestern Alberta than is suggested by present-day outcrop and facies distribution (Pratt, 2001). The basin was dominated by siliciclastic sedimentation with several episodes of carbonate deposition (Fermor and Price, 1983; Horodyski, 1983; Hill and Mountjoy, 1984; Pratt, 1994, 1998b, 2001, 2017). Petrology and detrital zircon dating indicate that for most of the history of the basin fine-grained siliciclastic sediment provenance was dominantly from the west, as suggested by ~1.6–1.5 Ga grains, with subordinate medium to coarse sand from the east, reflected by late Archean grains presumed to be derived from the Wyoming craton plus ~1.8 Ga grains from the Trans-Hudson orogen (Ross and Villeneuve, 2003; Link et al., 2007, 2016; Stewart et al., 2010). It has been argued that fairly late in the history of the basin that supply shifted to mostly from the south (Ross and Villeneuve, 2003; Link et al., 2007, 2016; Stewart et al., 2010).

The Belt Supergroup is subdivided into four units: lower Belt, Ravalli Group, Piegan Group ('middle Belt carbonate' of some past usage) and Missoula Group (e.g., Whipple et al., 1984; Winston, 1989, 2007; Winston and Link, 1993). The Waterton and Altyn formations, and the underlying Haig Brook and Tombstone Mountain formations (Fermor and Price, 1983), comprise the lower Belt in the area of the Waterton Lakes and Glacier national parks and Castle Wildland Provincial Park and in the Clark Range of immediately adjacent southeastern British Columbia (Figs. 3.1B, 3.2). The base is not exposed, and thrust faults associated with the Lewis thrust complicate the stratigraphic units.

2.2. Lower Belt Supergroup

2.2.1. Stratigraphic correlation

The lowest unit of the lower Belt Supergroup in the U.S.A. is the >6 km thick succession of distal, fine-grained siliciclastic turbidites and hemipelagic mudstones belonging to the Prichard Formation (Cressman, 1989). The equivalent unit in southeastern British Columbia is the Aldridge Formation, but beneath that is the Fort Steele Formation which is sandstone-rich and may be fluvial (McMechan, 1981; Höy, 1993; Chandler, 2000; Goodfellow, 2000). Carbonaceous laminae in the mudstones can be correlated over wide areas of the northern part of the basin which is suggestive of a frequently stagnant water body (Huebschman, 1973; Höy, 1993). Geochemical composition argues for a stratified water column with H_2S-rich bottom waters (Goodfellow, 2000). The upper part of the formation exhibits a shallowing trend indicating progressive filling of the previously deep basin (McMechan, 1981; Chandler, 2000).

The carbonate succession in the northeastern side of the Belt Basin is considered correlative, with the upper part of the Prichard Formation (Smith and Barnes, 1966). This suggests that any carbonate sediment shed from the platform did not reach the deeper part of the basin more than 100 km to the west. However, interbedded dolomitic mudstone occurs near the top of the Aldridge Formation in the northern part of the basin (Goodfellow, 2000). It is possible that this may equate with the onset of platform development, but no nearby equivalents of the Haig Brook–Tombstone Mountain–Waterton–Altyn succession are present in that area to allow a more precise correlation.

2.2.2. Carbonate succession

At its type section in the Clark Range immediately to the west of northern Castle Wildland Provincial Park, the Haig Brook Formation consists of ~150 m of laminated to thin-bedded, variably argillaceous, finely crystalline dolomudstone and subordinate lime mudstone (Fermor and Price, 1983). Cross-lamination in silty beds, intraclastic rudstone and synsedimentary folds are locally present. Dark-coloured 'argillite,' that is, siliciclastic mudstone, is interbedded in the lower part, and comprises a unit near the top as well as possibly below the base, as suggested by the nearby Sage Creek Well (Pacific-Atlantic Flathead No. 1, d-34-E/82-G-1). Cuttings indicate that there may be over 850 m of similar rock types below the Haig Brook Formation (Fermor and Price, 1983).

The Tombstone Mountain Formation at its type section in the same area consists of ~175 m of primarily thin-bedded and planar-laminated, dark-coloured argillaceous and silty lime mudstone; argillaceous content appears to increase over a short distance to the southwest (Fermor and Price, 1983). Wavy- and lenticular-bedded lime mudstone is also locally present.

The base of the Waterton Formation is not exposed in its type 'area' around Waterton townsite in Waterton Lakes National Park (Daly, 1912), but a complete section is exposed in the Clark Range where it attains a thickness of ~250 m (Fermor and Price, 1983). It consists of mainly thin-bedded lime mudstone and dolomudstone and dolomitic mudstone, nodular- and lenticular-bedded lime mudstone, and rare 'argillite' (Fermor and Price, 1983; Hill and Mountjoy, 1984; Hill, 1985; Jardine, 1985). It is locally cherty. Dolomitic beds are commonly buff-coloured; the uppermost unit in southeastern exposures is a distinctive reddish dolomite. The upper part in the northwestern part of the study area is thicker bedded.

The Altyn Formation (Willis, 1902; Daly, 1912) has its type 'area' at Apikuni Mountain, Glacier National Park, although its lower part is not exposed there. It consists of light-coloured sandy dolograinstone, oolite, columnar-branching stromatolite patch reefs, laminated, variably argillaceous and silty dolomudstone, intraclastic dolorudstone, and rare 'argillite' (Horodyski, 1976; Fermor and Price, 1983; White, 1984; Hill, 1985; Jardine, 1985; Pratt, 1994, 2017). Dolomudstone is commonly buff-coloured. The formation is thought to reach ~375 m in thickness in Waterton Lakes National Park (Fermor and Price, 1983),

although structural complications make this uncertain. In the Waterton Lakes and northeastern part of Glacier national parks it has been subdivided into three informal members (Douglas, 1952; Hill and Mountjoy, 1984; Hill, 1985; Jardine, 1985).

Depending on the location, the contact with the overlying Appekunny Formation is sharp and erosional (Whipple et al., 1984) or is gradational and marked by interbedding of greenish coloured mudstone, fine-grained sandstone, and coarse-grained dolomitic sandstone or sandy dolograinstone over a few metres (Horodyski, 1983). Quartz and chert pebbles are present at the contact at Crypt Lake. An interval 32 m thick of Altyn-like sandy dolograinstone with quartz and chert pebbles at the top is present in the Appekunny Formation on the easternmost spur of Pincher Ridge and nearby mountainsides in Castle Wildland Provincial Park.

2.2.3. Structural Context

These carbonate units are underlain by the Lewis thrust fault and they have been extensively deformed by splays of imbricate thrust faults along with development of duplex structures in places (Douglas, 1952; Fermor and Price, 1983, 1987; Davis and Jardine, 1984; Jardine, 1985; Hudec and Davis, 1989; Yin and Kelty, 1991; Stockmal and Fallas, 2015). These structures, not all of which are easily apparent in some outcrops, govern the choice of intact sections that can be measured.

The Altyn Formation is extensively faulted in southeastern Glacier National Park, such as near Two Medicine Lake and Marias Pass (Hudec and Davis, 1989), and usefully coherent sections are not available. The middle and upper Altyn Formation is exposed along the base of Singleshot Mountain above St. Mary Lake and along strike in the hillside and in Going-to-the-Sun road cuts by Rising Sun. The originally studied section is at Apikuni Falls in the lower part of Apikuni Mountain, although the lower part of the formation is not exposed. A short distance to the northeast at and near the mountain front the Waterton Formation and lower part of the Altyn Formation, including the distinctive reddish-stained dolomite interval at the top of the Waterton Formation, contain numerous thrust faults (Davis and Jardine, 1984; Jardine, 1985; P.R. Fermor pers. comm., 2020). At Yellow Mountain and Chief Mountain and environs, the lower Waterton Formation is also faulted, but the formation has been subdivided into five informal units estimated to be ~200 m thick, with the upper four units above the Yellow Mountain thrust comprising a coherent package (Jardine, 1985). Sofa Mountain, along strike to the north in southeastern Waterton Lakes National Park, also has thrust faults in the lower part, including offsetting the same reddish interval, but most of the Altyn Formation appears intact (Hill and Mountjoy, 1984; Hill, 1985). Immediately to the northwest, the Altyn Formation exposed at and below Crypt Lake appears uninterrupted. However, whether the nearly 350 m measured thickness is affected by thrust faults is not clear. On adjacent Mount Boswell the Altyn Formation was measured to be almost twice as thick as that on Sofa Mountain, ~7 km to the east, considered to be due to a much thicker lower part of the formation (Hill and Mountjoy, 1984; Hill, 1985). However, the large number of northeastward-directed thrust faults there (Douglas, 1952; Stockmal and Fallas, 2015) may have caused structural thickening. The section at Ruby Ridge, shown as nearly 350 m thick by Hill (1985), was deemed here to be unsuitable due to faulting and poor exposure. In general, the wide range of thicknesses of the Altyn Formation given by Douglas (1952) and Jardine (1985) over a fairly small area may be evidence for these structural complications. On the other hand, the section at Sofa Mountain measured here is thinner than that shown by Hill and Mountjoy (1984; Hill, 1985), and the section at Apikuni Falls shown in Hill (1985) is ~30% thicker than that determined by White (1984) and in this study.

The Waterton Formation exposed along the west side of Upper Waterton Lake is also cut by numerous thrusts and there is considerable duplication. This seems to have been mostly

overlooked in early studies (Douglas, 1952, 1977) in which almost 190 m were regarded as a continuous section. Douglas (1952) and Hill and Mountjoy (1984; Hill, 1985) considered that there are two limestone intervals but this appears to be due to fault repetition because only one is present on Yellow Mountain and Chief Mountain. A few kilometres to the north, along the Akamina Highway, Akamina Creek and on the flank of Mount Crandell, the upper Waterton and lower Altyn formations are faulted. The Altyn and Appekunny formations on Bear's Hump are cut by the Mount Crandell thrust and associated imbricates (Douglas, 1952, 1977; Stockmal and Fallas, 2015).

In Castle Wildland Provincial Park, the upper Waterton and Altyn formations are exposed on both sides of West Castle River where it crosses the Lewis thrust, and an undeformed section is accessible on the west side on a ridge trending from Syncline Mountain (Fermor and Price, 1983) and Barnaby Ridge across the river (Hill, 1985). The contact between the two formations is uncertain. In Fermor and Price (1983) it was placed 120 m above base of the section at the base of an apparent argillite. Here, the lowest sandy limestones were encountered 92.5–93 m and 106–107.5 m above base, suggesting that that interval may correlate with the upper part of the lower Altyn Formation which elsewhere sees the first influx of sand. The headwall of Syncline Brook 7 km to the south-southwest exposes the Waterton Formation that is laterally equivalent to the nearby Altyn Formation. The Tombstone Mountain Formation is exposed locally in the creek bed where it is cut by faults (Fermor and Price, 1983). Some 3 km to the southwest, the Haig Brook, Tombstone Mountain and Waterton formations are underlain by the Lewis thrust which has brought them upward in imbricate thrusts forming large duplexes (Fermor and Price, 1983, 1987). The Haig Brook Formation is exposed on mountainsides above Cate Creek and nearby Haig Brook, but is extensively deformed such that its thickness can only be estimated (Fermor and Price, 1983).

3. Methods

The Waterton and Altyn formations were studied in Glacier National Park of northwestern Montana and Waterton Lakes National Park and Castle Wildland Provincial Park in adjacent southwestern Alberta (Fig. 3.1A, B). Sections of Waterton Formation and lower Altyn Formation in the Waterton area are in thrust-bounded intervals. The lowermost part of the Waterton Formation, consisting of cherty dolomite as identified by Jardine (1985), which crops out in Yellow Mountain and Chief Mountain, Glacier National Park, below the Yellow Mountain thrust, was not studied. The Altyn Formation there and along the base of Singleshot Mountain and west along strike to Rising Sun was also not measured. An interval of Altyn-like dolomite within the Appekunny Formation was measured on Pincher Ridge in the eastern part of Castle Wildland Provincial Park.

The upper Waterton Formation and a small exposure of the underlying Tombstone Mountain were examined in Syncline Brook headwall and valley, respectively, in Castle Wildland Provincial Park, and the Haig Brook Formation was examined on the flank of Packhorse Peak in the Clarke Range just to the southwest. Due to the limited observations of these two formations, they are included in the stratigraphic picture (Fig. 3.3) but are not incorporated into the sedimentological interpretation.

This study is based on outcrop-level observations (Fig. 3.4A–F) augmented with slabbed samples, acetate peels and thin sections.

4. Mineralogical and diagenetic context

4.1. Description

The Haig Brook, Tombstone Mountain and Waterton formations as a whole consist of argillaceous dolomite and lime mudstone that are locally slightly silty and argillaceous. By contrast, the Altyn Formation almost everywhere is dolomite with minor clay and varying amounts of silt and sand; the exception is at Syncline Mountain where dolomitization of sandy grainstone is locally incomplete. The clay is illite (Ross, 1959). Dolomite in the Waterton and lower Altyn formations weathers buff-coloured due to slight Fe enrichment. However, localized orange and reddish to maroon colouration close to thrust faults, such as at Chief Mountain, Sofa Mountain and Bosporus ridge, may be due to alteration from late-stage fluid flow related to faulting.

Lime mudstone of the Ribbon facies in the Waterton Formation consists of micrite 3–5 µm in size and calcisiltite composed of microspar 5–10 µm in size. The matrix between intraclasts in rudstone interbeds tends to be coarser microspar. Some limestone laminae appear finely peloidal. Silt-sized, doubly terminated, authigenic quartz euhedra with calcite inclusions are locally common.

The Laminite facies contains micrite, silt-sized peloids, angular silt, and sporadically interbedded sand. The Grainstone facies contains peloids, peloidal micritic aggregates, small, rounded intraclasts, angular quartz silt, and fine- to coarse-grained sand (Fig. 3.5A–B). Sand is mostly well-rounded but is locally subrounded or subangular, and includes some feldspar (Fig. 3.5C). This facies contains scattered radial ooids, subangular to rounded intraclasts of oolite, and rounded to angular sand-sized grains of silicified oolite with either concentric or radial fabrics (Fig. 3.5B). It also contains varying amounts of rounded grains composed of distinctive, uniform calcite microspar, and whose margins are replaced by quartz euhedra in some cases (Fig. 3.5E). These grains are mostly dolomitized.

In the Oolite facies of the upper Altyn Formation the ooid cortices are concentric or structureless, or both, often with sand nuclei (Fig. 3.5D, F). The cement is composed of elongate but isopachous crystals followed by finely blocky spar, both composed of limpid dolomite. In other beds the dolomite is coarser, 5–10 µm across. Where cortical layers have dissolved the pore is filled with large quartz crystals. In upper beds there are also rounded sand-sized grains composed of microsparry dolomite 5–15 µm in size (Fig. 3.5D). Dolomite that replaces quartz grains consists of limpid euhedra.

The Grainstone facies of the upper middle Altyn Formation at Apikuni Falls contains rare clusters of radiating and bundles of subparallel bladed crystals up to ~2 mm long with pointed terminations that extend beyond micritic grain boundaries into the micrite matrix (Fig. 3.6A; Pratt, 2017, fig. 5H). The contain microcrystalline dolomite inclusions. There are also individual and patches of clustered short blades or prisms (Fig. 3.6B). The crystals extend beyond micritic grain boundaries. The original mineral has been replaced by blocky megaquartz crystals ~30–50 and rarely up to 100 µm across. There are also silicified grains composed of tight meshworks of lath-shaped crystals typically ~20–100 µm and up to ~300 µm in length, replaced by microquartz. (Fig. 3.6C). Chert nodules are locally present in the Ribbon facies and in the lower Altyn Formation. In the Altyn Formation at Apikuni Falls, isolated and clustered, quartz-rimmed geodes, individually up to about 5 cm across, are sporadically present. No anhydrite inclusions were observed in them. They also occur sporadically in younger, siliciclastic units.

Dolomite in the Oolite facies consists of planar-s dolomite crystals 1–3 µm across. By contrast, replacive dolomite in the Ribbon facies is 5–15 µm in size, with mostly planar-s idiotopic fabric along with sporadic rhombic euhedra. The dolomite is located mostly in argillaceous interbeds but also occurs as nodular patches in the limestone. Dense laminae in stromatolites are composed of dolomite crystals 5–20 µm in size. Dolomite in the Laminite, Grainstone and in components of the Stromatolite facies is also planar-s idiotopic with

scattered euhedra, and crystals are typically 20–50 µm and locally up to about 70 µm across. Dolomite is coarser in the Altyn Formation on Syncline Mountain and in the Altyn-like unit on Pincher Ridge.

4.2. Interpretation

Siliciclastic silt and sand were derived from the adjacent land surface, with the silt perhaps involving eolian transport en route. Sand grains were reworked in coastal areas where enhanced grain abrasion took place due to protracted, wind-induced wave action (Folk, 1980). While mostly rounded, the presence of subrounded and subangular grains reflects varying residence time in the coastal setting before transport to the offshore.

Primary products of the carbonate factory were lime mud ranging in size from clay to silt, sand-sized peloids and ooids, and granule-sized micritic intraclasts and aggregates, along with micrite precipitated in stromatolite-forming microbial mats. The lime mud was probably mostly precipitated in the water column (Turner et al., 1997; Grotzinger and James, 2000; Pratt, 2001; Medig et al., 2016; Greenman et al., 2020). Microbial activity may have participated in grain formation, both in triggering lime mud precipitation and in binding and cementing particles to form peloids, aggregates and intraclasts (e.g., Robbins and Blackwelder, 1992; Pratt et al., 2012).

The small crystal meshes are interpreted as silicified felted anhydrite that precipitated under elevated temperature in the supratidal zone of coastal tidal flats. The geodes have been interpreted as silicified evaporite nodules (Chandler, 2000). However, the absence of anhydrite inclusions, presence in subaqueous facies, cross-cutting nature of their localization, and presence in younger units suggest that they are a late-diagenetic phenomenon.

The silicified bladed crystals contain inclusions and extend beyond micritic grain boundaries indicating that they formed in situ, mostly by replacement. Horodyski (1976) interpreted these "rosettes," including some with tabular crystals, as pseudomorphs after barite based on the presence of hyalophane (a barium-rich potassium feldspar) detected by XRD. However, it is more likely that these crystals were originally gypsum, given the shallow-marine setting, as opposed to areas of high siliciclastic sedimentation rate such as continental margins (Hesse and Schacht, 2011, p. 689) as well as areas with a hydrothermal influence (e.g., Jamieson et al., 2016) that are considered to be settings conducive to barium enrichment. They may have precipitated out of temporary hypersaline bottom waters that had flowed in from coastal areas, as proposed for halite in younger units (Pratt and Ponce, 2019).

Because already silicified oolite and anhydrite grains were eroded from coastal areas and often rounded (see section 5.3.) this silicification was an early-diagenetic phenomenon (e.g., Noble and van Stempvoort, 1989; Chafetz and Zhang, 1998). It is unclear, however, when silicification of the large bladed crystals occurred. The source of the silica is unknown, as it also is for the chert nodules. Authigenic quartz precipitation in lime mudstone and replacive euhedra in molar-tooth grains may have taken place during subsequent burial (Molenaar and de Jong, 1987; Mišík, 1995).

The distinctive microspar grains and their dolomitized counterparts in the Grainstone and Oolite facies were eroded from molar-tooth structure (Pratt, 1998b, 1999). Although molar-tooth structure was not observed in the upper part of the Altyn or lower Appekunny formations, these grains also must have had their source elsewhere, likely in the inner platform because they co-occur with silicified anhydrite and oolite grains. The lime mud there was at least in part granular (Pratt, 1998b, 2011).

The dolomite in the Ribbon facies is identical to the slightly ferroan burial dolomite that occurs ubiquitously in ribbon and parted limestones in Cambro-Ordovician successions (e.g., Wanless, 1979; Demicco, 1983; Aitken, 1997; Bayet-Goll et al., 2015). The dolomite in the

Laminite, Grainstone and Stromatolite facies also represents a burial diagenetic stage, but most of the replacement is at a fine scale. This implies that the lime mud that was replaced was crypto- or microcrystalline with many nucleation sites (Sibley, 2003). For the truly mimetic fabrics in the Oolite facies, a case might be made that the cryptocrystalline dolomite is a primary seawater precipitate as proposed for some Neoproterozoic platforms and ascribed to ocean anoxia (Hood et al., 2011; Shuster et al., 2018). However, it is not realistic to expect changes in the oxic state of the shallow sea in upper Altyn time, especially given the relatively high-energy aspect of this facies (see section 5.4.). On the other hand, dissolution of cortical layers in many ooids is suggestive of a primary aragonite mineralogy, and the mimetic style of replacement may have been due to replacement of aragonite (Zempolich and Baker, 1993).

5. Lithofacies

The lower Belt carbonate platform in the northeastern side of the Belt Basin is represented by a suite of recurring facies. This study focuses on the Waterton and Altyn formations. These strata also host a variety of synsedimentary deformation features which are specific to facies type (see Chapter 4).

5.1. Laminite facies

5.1.1. Description

This facies occurs in the Waterton and lower and middle Altyn formations, and rarely in the upper Altyn Formation at Apikuni Falls. It consists of laminated, variably silty dolomudstone that displays a weathering aspect varying from fissile to medium- and thick-laminated and massive (Fig. 3.7A–C; also Fig. 3.9A). Laminae are laterally persistent for metres at least. Sedimentary structures in silty intervals include planar lamination and wavy and lenticular bedding locally with wave-ripple cross-lamination, including starved ripples (Fig. 3.7D–F); deeply scoured surfaces are absent. At Apikuni Falls, laminae drape over symmetrical ripples that are locally developed in dolomitic sandstone interbeds. Laminae in the Waterton and lower Altyn formations are at the sub-millimetre scale (Fig. 3.8A), whereas in the middle Altyn Formation thicker ones are intercalated (Fig. 3.8B, C). Laminae in the middle Altyn Formation at Apikuni Falls contain more silt and, rarely, sand-sized grains (Fig. 3.8B, C). Wispy, black carbonaceous seams are also locally present, and small pyrite euhedra are commonly preferentially localized on them.

5.1.2. Interpretation

The Laminite facies represents a low-energy, subtidal environment with hemipelagic lime mud deposition, from particles precipitated in the water column or brought in from shallower areas or both, along with varying amounts of silt and occasionally sand from coastal areas. Tidal currents may have been involved in transport. This was punctuated sporadically by weak oscillatory and combined-flow bottom currents, giving rise to planar, wavy and lenticular laminae. It is possible that microbial mats established themselves in shallower areas and that these account for the carbonaceous seams in this interval, or they are due to water-column productivity. The laminae that drape over ripples may also have been microbially bound, but it may also have been the fine grain-size and clay that caused them to be sufficiently cohesive.

5.2. Ribbon facies

5.2.1. Description

'Ribbon limestone' composed of interbedded planar-, wavy-, lenticular- and nodular-bedded lime mudstone and argillaceous dolomudstone, or marlstone, comprises a large part of the Waterton Formation. This facies can be intercalated at the metre scale with intervals of Laminite facies (Fig. 3.9A). Lenses of lime mudstone are variably silty and exhibit uni-directional and combined-flow ripple cross-lamination in beds up to ~5 cm thick (Fig. 3.9B–D). In horizons with nodules, they range from lenticular to round to elliptical in cross-section and are enclosed in dolomudstone (Fig. 3.9E).

5.2.2. Interpretation

This facies records hemipelagic deposition lime mud and clay alternating with current-transported and reworked coarser lime mud, silt and locally silt-sized peloids. The lime mud probably represents originally suspended sediment, plus land-derived clay that may have been blown onto the platform by winds. The mud was probably reworked by weak storm-induced combined flow, that is, low flow-regime, unidirectional and oscillatory currents. Tidal currents may have helped transport the mud, given the evidence for tides in the Altyn Formation (section 5.3.2), but direct evidence is lacking. The nodules formed by selective early cementation followed by compaction and eventual dolomitization of intercalated and laterally adjacent, uncemented mud (e.g., Ricken, 1986; Møller and Kvingan, 1988; Westphal et al., 2008).

5.3. Grainstone facies

5.3.1. Description

Variably sandy and silty dolograinstone and dolomitic sandstone with peloids, micritic aggregates and intraclasts along with radial ooids, microspar intraclasts, and rare silicified anhydrite and oolite comprise most of the middle and upper Altyn Formation. At Sofa Mountain and Bosporus ridge the lower part of the middle Altyn Formation is thin-bedded, relatively well-sorted, medium-grained sandy dolograinstone exhibiting planar lamination, uni-directional cross-lamination, including some herringbone-style reversals, and local concave and convex laminae (Fig. 3.10A). Cross-laminated beds are mostly lenticular and scour surfaces occur sporadically. This passes upwards in those localities, at Bear's Hump and at Apikuni Falls into very coarse sandy dolograinstone with planar bedding and tabular cross-bedding showing varying and seemingly reversing current directions (Fig. 3.10B). At Sofa Mountain and Bosporus ridge these beds are overlain by distinctly light grey-coloured, less coarse-grained, sparsely sandy grainstone that is planar and cross-bedded.

At Syncline Mountain, the Grainstone facies is well sorted and medium grained, and is planar- and locally cross-laminated in the lower part, grading upward into very coarse-grained dolograinstone with planar bedding and tabular cross-bedding. By contrast, the Altyn-like unit in the Appekunny Formation on Pincher Ridge consists entirely of uniformly well-sorted dolograinstone that is mainly medium- to coarse-grained. It exhibits hummocky cross-stratification, some planar bedding, and wave ripples, with some trough cross-bedding at the top. Interbedded dololaminite or siliciclastic mudstone is absent.

In the lower part of the middle Altyn Formation at Apikuni Falls, however, the Grainstone facies forms thin to medium beds with sharp erosive bases (Fig. 3.10C, D). Siliciclastic

grains, up to granule-sized, are both irregularly distributed and concentrated in individual laminae, and beds are moderately to poorly sorted (Fig. 3.10E); normal grading is locally present. Planar and uni-directional ripple cross-lamination is common whereas symmetrical ripples are rarer (Fig. 3.10D, E).

The upper middle and upper Altyn Formation at Apikuni Falls is characterized by tabular and broadly lenticular medium to thick bedding that is apparent across strike and down-dip to the west (Fig. 3.11A). The upper part of the middle Altyn Formation at Bosporus ridge consists of a stack of broadly lenticular beds ~10 m thick, overlain by ~10 m of superimposed, northwest-dipping wedge-shaped beds (Fig. 3.11B; Hill, 1985, fig. 5.2). Internally, these beds exhibit planar bedding and tabular cross-bedding. No channelform features are apparent.

5.3.2. Interpretation

The thin beds with variably directed and combined-flow cross-lamination in the lower middle Altyn Formation in the Waterton area indicate that this part of the platform was subject to low flow-regime, variably directed and occasionally reversed, uni-directional currents forming planar lamination and 3D ripples, plus occasional subordinate combined flow producing concave and convex lamination (e.g., Dumas et al., 2005). These structures suggest a tidal regime affected occasionally by wave action in intermediate water depths. Higher in the upper Altyn Formation, the larger scale cross-bedding indicates formation of dunes under stronger and often reversing currents, pointing to the dominance of tidal currents reworking a sand sheet on a shallow shelf. The succession at Syncline Mountain is similar. The sparsely sandy dolograinstone in the upper Altyn Formation in the Waterton area indicates a reduction of sand input, but no obvious depositional change. The absence of hummocky cross-stratification suggests either that strong combined flows did not develop, or that bedforms were reworked.

The thick, broadly lenticular bodies in the middle Altyn Formation are probably stacked compound dunes that grew by forward accretion, whereas the clinoforms at Bosporus ridge are interpreted as due to lateral accretion of a larger sand bar or sand ridge, both types likely also due to tidal currents (Dalrymple et al., 2003; Dalrymple, 2010; Steel et al., 2012; Olariu et al., 2012; Desjardins et al., 2012; Durbano et al., 2015). The currents responsible for the tidal ridge may have been oriented broadly north–south leading to westward lateral accretion. This interpretation contrasts with that presented by Hill (1985) who considered the clinoforms to represent beach deposits which were overlain by subaerial dunes and washover sediments comprising the upper part of the middle Altyn Formation. However, the steepness of the clinoforms, the evidence for reversing currents, the presence of grains indicative of landward but distant lagoonal, nearshore and peritidal environments (section 4.2), and absence of evidence for a nearby land surface argue for an offshore, submerged setting. The cross-bedding in the dolograinstone does not exhibit the typical high-angle lee surfaces of eolian cross-bedding and indicates variable current direction, and the clinoforms also have a lesser dip than that of the slip face of eolian dunes and there is no evidence for dune climbing (e.g., Mountney, 2006).

Dolograinstone in the middle Altyn Formation at Apikuni Falls records the deposition under moderate to high-energy conditions of uni-directional flow. The overall poor sorting and absence of variably directed cross-lamination are evidence that once the grainy sediment was deposited it was not reworked by protracted ambient current activity. However, sporadic symmetrical ripples suggest some local, minor modification by wave action of thin beds interbedded with Laminite facies.

By contrast, the Altyn-like unit in the Appekunny Formation records allochthonous carbonate and siliciclastic sand that was probably deposited over a relatively short period of time, given the well-sorted aspect and absence of interbedded lithologies. The predominance of hummocky cross-stratification points to reworking by strong oscillatory and combined flow. Absence of uni-directional cross-bedding except at the top suggests that there was little influence from tidal currents.

5.4. Oolite facies

5.4.1. Description

Oolite makes up a thick interval in the upper Altyn Formation at Apikuni Falls. Planar cross-lamination is present locally. The interval includes a lower unit 5.5 m thick that exhibits steeply westward-dipping sigmoidal clinoforms (Fig. 3.11C). Quartz sand, subrounded micritic intraclastic peloids, and rounded, sand-sized microspar intraclasts of molar-tooth structure are admixed with the ooids.

5.4.2. Interpretation

Ooids form in wave-induced turbulence, with or without the influence of tides (e.g., Harris et al., 2019). This facies was deposited by relatively strong currents, and the clinoform-bearing unit represents a large compound dune that migrated by forward accretion in a broadly westward direction (Olariu et al., 2012; Desjardins et al., 2012). There is no evidence of strong wave action. The mixture of ooids, peloidal intraclasts, siliciclastic sand, grains of molar-tooth structure microspar, and fragments of silicified oolite represents the gamut of sand-sized grains deposited on the shallow shelf and coastal tidal flats, including recording the presence of molar-tooth structure. Thus, the sediment was transported from its original place of origin, out onto this part of the platform where it was reworked. The dominance of ooids compared to comparable beds of the Grainstone facies suggests that the primary source area was a large ooid shoal that briefly developed in the shallow mid-shelf, rather than a complex mosaic of carbonate sediment types which would have led to a more heterogeneous particle composition.

5.5. Stromatolite facies

5.5.1. Description

Rare beds in the Ribbon facies of the Waterton Formation host small *Cryptozoan*-like encrustations on lime mudstone beds, forming low-relief domes ~10 cm high. By contrast, several horizons of stromatolites form mounds 0.5–1 m thick and up to ~2 m wide in the lower Altyn Formation at Syncline Mountain. In the middle Altyn Formation at Apikuni Falls, one bed near the base consists of mounds 0.3 m thick and 2 m in diameter, whereas higher they are up to 3 m thick and many metres across (Fig. 3.12A), and near the top stromatolites form a mound ~2 m thick. Most stromatolites are branching-columnar, conforming to *Baicalia* (Fig. 3.12B). Columns are typically ~10–15 cm wide, more or less circular in plan view, divergent in the lowermost mound at Apikuni Falls but more upright higher up. Some intervals at both Syncline Mountain and at Apikuni Falls, however, possess columns inclined in a single direction (Fig. 3.12B, C), although the same mound, if large enough, can exhibit suprajacent intervals exhibiting leaning in opposing directions (Horodyski, 1976, fig, 5C). In at least one mound domical stromatolites, conforming to

Collenia, are elongated west–east (Fig. 3.12D). Locally columns do not branch and approach a *Conophyton* morphology by virtue of the axial portion forming a blunt point (Fig. 3.12E).

Stromatolites are composed of smooth and somewhat irregular laminae of micrite and intercalated, variably silty, normally graded microspar (Fig. 3.12F). Irregular laminae have a wavy upper surface and are discontinuous in places, and the micrite is denser than that of other laminae. Apart from large intraclasts of brecciated Laminite facies collected against the lowermost and uppermost mounds (see Chapter 4, section 2.9.), flanking deposits belong to the Grainstone facies.

5.5.2. Interpretation

Metre-scale and larger stromatolite mounds are microbial patch reefs that grew in the photic zone. Small ones in the Waterton Formation formed near storm-wave base, as suggested by the cross-lamination in the lime mudstone of the enclosing Ribbon facies. Those in the Altyn Formation accreted in a setting of episodic moderate turbulence, as suggested by flanking Grainstone facies. Accretion was by a combination of microbial mat-stabilized silty lime mud as well as microbially induced precipitated micrite (Horodyski (1976, 1977). The precipitated laminae are denser and more finely crystalline, forming a 'filmy' microstructure (e.g. Knoll and Semikhatov, 1998), and their irregular and discontinuous nature suggests the microbial mat surfaces possessed some topographic relief. Domical stromatolites are present but those described by White (1984) are folds (see Chapter 4, section 2.2.). *Collenia* forms that are elongated west–east suggest the influence of dominant current orientation (Hoffman, 1967) due to onshore-directed winds. Inclined stromatolite columns may be due to the influence of directed currents (Horodyski, 1976, 1983) or caused by dislocation during a high-energy event (see section 6.4.1.).

5.6. Discussion

Prior study regarded the laminated dolomite of the Waterton Formation as a low-energy subtidal deposit, whereas the ribbon limestone was interpreted as representing shallow subtidal and intertidal to supratidal conditions, due to the presence of wave-generated features, local stromatolites, 'beach rosettes' composed of edgewise flat pebbles (see section 6.1.1.), and supposed desiccation cracks (Hill and Mountjoy, 1984; Hill, 1985). Similarly, the Altyn Formation was seen as composed of shallow subtidal to supratidal facies (Horodyski, 1983; White, 1984; Hill, 1985). The stromatolites and oolite were considered to have formed in shallow, turbulent conditions, while the sandy dolomite possibly records tidal channels and the laminated dolomite was deposited on tidal flats as locally desiccation-cracked and ripped up microbial laminites (Horodyski, 1983; White, 1984; Hill, 1985). Parts of the Altyn Formation were interpreted as being barrier island, beach and eolian deposits (Hill, 1985). These interpretations were in the context of the level of understanding of carbonate sedimentology at the time. The peritidal setting was provisionally accepted by Pratt (1994) in order to explore the apparent cyclicity in the Altyn Formation.

These interpretations, however, are largely not borne out by lithological detail. The Laminite facies in both the Waterton and Altyn formations was deposited mostly by hemipelagic fall-out at the limit of storm-wave base, as indicated by the lateral persistence of laminae, although small-scale erosion surfaces and cross-lamination suggest low-energy bottom scour. Cracks and locally folded and disrupted laminae do not represent desiccation on tidal flats but seismic activity (see Chapter 4, section 2.4; Pratt, 1994). There are no channel deposits or short-distance lateral variation of the kind that would be expected on a tidal flat, based on modern analogues (e.g., Hardie, 1977; Rankey, 2002). Despite a similarity

with siliciclastic tidal-flat deposits (Demicco, 1983), the Ribbon facies records transport followed by reworking by relatively weak oscillating and combined flow of allochthonous, coarser grained lime mud alternating with hemipelagic fall-out. The edgewise intraclasts formed by disruption and reworking by wave action (see section 6.2.2; e.g., Bayet-Goll et al., 2015), but under ambient conditions, not from an episode of exposure on a beach or tidal flat. Similarly, small stromatolites in the Ribbon facies accreted in these subtidal conditions but within the photic zone.

Because beds of the Laminite and Ribbon facies occur stratigraphically juxtaposed and there is some intergradation between the two in sedimentary attributes, it is unlikely that water depth changed abruptly, and rather the facies change was due to the difference in the type of sediment that was input: hemipelagic clay-sized lime mud versus coarse silt-sized particles that were within the appropriate grain size to develop traction structures such as ripples. This points to control by particle source rather than water depth. The two classes of mud may reflect variable geography and types of mud production in shallow areas, source of the currents, or differing levels of energy during transport leading to size-sorting, or all of these factors.

Patch reefs of the Stromatolite facies formed under a range of conditions from relatively deeper to shallower depths where there was a higher degree of ambient turbulence. The dominance of this facies in the upper part of the middle Altyn Formation in the southeastern area suggests an upward decrease in bathymetry. However, stromatolites in the lower Altyn Formation at Syncline Mountain suggest that the shallow, high-energy setting indicated by the Grainstone facies in the upper part was not conducive to their development.

Sandy grainstone, dolomitic sandstone and sandy oolite are composed of allochthonous sediments transported from the middle and inner shelf and coastal areas. In the lower middle Altyn Formation at Apikuni Falls, beds of the Grainstone facies were for the most part not reworked, and thus they did not form shifting sand shoals within fairweather wave base, nor were they repeatedly reworked by storms, based on the absence of hummocky cross-stratification. Thus, these beds do not seem to indicate individual shallowing episodes. On the other hand, broadly equivalent cross-laminated beds in the Waterton area indicate frequent reworking by dominantly uni-directional currents. This is suggestive of tidal currents affecting a somewhat shallower region of the platform. The Grainstone facies in the upper Altyn Formation was reworked, and planar and trough cross-bedding suggests the shallow platform was characterized by dunes, and the variable current directions were due to tidal flows. The sigmoidal beds in the Oolite facies at Apikuni Falls were westward-migrating compound dunes, indicating strong uni-directional flow. The large clinoforms in Grainstone facies in Waterton record lateral accretion of a large sand bar or ridge. Given the clinoform geometry and because the sediment was not reworked by waves, water depths of ~5–10 m are likely.

Clusters of large blades of presumed gypsum are evidence for the rare development of hypersalinity during deposition of the middle Altyn Formation at Apikuni Falls. However, there is no evidence for in situ evaporites elsewhere, suggesting that the waters of the platform did not become hypersaline. On the other hand, coarse particles composed of silicified gypsum and anhydrite are evidence for common evaporite precipitation on tidal flats. What is envisaged is evaporation and concentration in shallower, coastal areas that occasionally led to bottom-hugging brines that flowed onto the outer shelf. This mechanism has been invoked for the precipitation of halite elsewhere in the Belt Supergroup (Pratt and Ponce, 2019).

6. Events of extraordinary erosion

The Waterton–Altyn succession contains evidence for episodic events of anomalously high energy that led to scouring of lithifying sediment and the creation of pebble- and cobble-size intraclasts, followed by local reworking or transport by bottom currents. Incipient cementation was due to microcrystalline calcite precipitation in interparticle pores, similar to early diagenesis seen in the younger Helena Formation (Pratt, 1998b, 2001), as well as in many other comparable examples of Precambrian and early Paleozoic age (e.g., Lee and Kim, 1992; Mount and Kidder, 1993; Pratt, 2002; Kwon et al., 2002; Myrow et al., 2004; Awramik and Buchheim, 2009; Bayet-Goll et al., 2015; Wright and Cherns, 2016; Wang et al., 2019). The Ribbon, Grainstone and Stromatolite facies contain intraclastic layers, and consequently the lithology of the intraclasts varies with the host facies. Beds exhibiting these features punctuate the succession and do not show any obvious stratigraphic regularity.

6.1. Ribbon facies

6.1.1. Description

Dololaminite in the Laminite facies in the Waterton Formation preserves some silty lenses but no intraclasts. By contrast, the Ribbon facies of the Waterton Formation exhibits common evidence for localized disruption of lime mudstone laminae, thin beds, lenses and nodules into intraclasts, which are enclosed in the host lime mudstone and laminated argillaceous dolomite laminae and thin beds (Fig. 3.13A–G). Intraclasts are equant to tabular, ranging from less than 1 cm to 15 cm in length and up to ~1 cm in thickness. In rare lenses they are smaller, with length and width of several millimetres. They are subangular to subrounded, and are composed of lime mudstone and laminated silty lime mudstone, and the matrix is lime mudstone or grainstone (Fig. 3.14A–C). They occur as lenticular layers typically in depressions typically up to about 10 cm deep and 20 cm to more than 50 cm wide but locally as low-relief mounds. Grading is absent. Tabular intraclasts range from flat-lying to obliquely oriented and commonly imbricated, in places in opposing directions and vertically stacked to splaying (‘rosettes,’ ‘edgewise’) (Fig. 3.13F–H). The direction of imbrication can be opposite in different parts of the same bed, and no beds were observed with intraclasts consistently oriented in a single direction.

6.1.2. Interpretation

The absence of bending of the intraclasts indicates that the source bed, lens or nodule was relatively stiff but had a low tensile (breaking) strength. The shape was a function of the primary rounded shape of many nodules, brittle fracturing of tabular and lenticular beds which generated angular edges, and brief reworking on the sea floor which led to some abrasion of the broken surfaces. The erosive event that scoured the sea floor faced essentially a smooth, gently undulating, commonly rippled pavement probably covered with a layer of uncemented lime mud and small amounts of clay, but due to the laterally discontinuous nature of the cementing lime mud layers underneath found places where scour could lift up beds, lenses and nodules, especially if they were already cracked (see Chapter 4, 2.6.). The varying degree of rounding, local size diminution, and variable orientation, especially direction of imbrication in these rudstones, are evidence for in-situ reworking by oscillatory currents from waves impinging on the sea bottom. The generally shallow level of scour suggests wave action was not strong.

6.2. Grainstone facies

6.2.1. Description

Thin to medium beds of sandy dolograinstone in the middle Altyn Formation at Apikuni Falls and those at Sofa Mountain have sharp and locally scoured bases and many contain varying quantities of tabular intraclasts of Laminite facies (Fig. 3.15A, B). They range from several millimetres to 2 cm in thickness and up to ~15 cm long, angular to subrounded, and range in thickness from laminae to thin beds. Intraclasts are flat-lying to obliquely oriented and locally imbricated where the host bed is cross-laminated. Intraclasts are rare to absent from the Grainstone facies of the upper Altyn Formation.

In the headwall of Syncline Brook valley is an interval of thick to massive beds of planar- and cross-laminated, sand- and granule-rich Grainstone facies at the top of the Waterton Formation. These beds range from sparsely intraclastic to grain-supported with planar-laminated, sandy lime mudstone intraclasts (Fig. 3.15C–E). Intraclasts are mostly tabular, with subordinate equant shapes, up to 20 cm and locally up to ~50 cm in length, and subangular to rounded. They range in orientation from horizontal to imbricated in various directions, including vertically oriented. Also embedded in places are planar- to cross-laminated dolomitic sandstone lenses up to 2 m long and 50 cm thick. A few of these blocks contain ball-and-pillow structures. This unit is considered here to be laterally equivalent to the uppermost Altyn Formation to the northeast at Syncline Mountain, instead of the correlation of Fermor and Price (1983, 1984) who suggested the Altyn Formation grades westward to the lower Appekunny Formation.

6.2.2. Interpretation

The dolograinstone beds at Apikuni Falls are allochthonous and not in situ channel or shoal deposits as earlier assumed (Horodyski, 1984; White, 1984; Pratt, 1994). The intraclasts were created by scour of cementing Laminite facies during transport of the coarse carbonate and siliciclastic sand from shallow, coastal areas and tidal flats. The dominantly platy and angular shape suggests that erosion and deposition comprised a single event, but the rounding of some of the intraclasts suggests enhanced rounding due to the presence of abrasive siliciclastic grains, or that there was more than one event of turbulence before the sediments came to their final resting point. Scour usually extended down 5–20 cm below the sea floor and likely represents erosion over a wide area, but beds in which larger numbers of intraclasts are concentrated suggest that somewhat deeper erosion took place at times.

The thick to massive beds of intraclastic sandy dolograinstone in the uppermost Waterton Formation, on the other hand, point to major scour and repeated movement over a brief time span and seaward transport of large amounts of coarse sediment by uni-directional currents followed by partial reworking by oscillatory currents. This includes erosion and transport of metre-sized blocks of dolomitic sandstone. This locality was in the upper ramp setting a few kilometres seaward of the shallow platform.

6.3. Stromatolite facies

6.3.1. Description

Whereas the broad stromatolitic patch reefs in the upper part of the middle Altyn Formation are flanked by Grainstone facies, the metre-scale stromatolite patch reef in the lower part of the middle Altyn Formation at Apikuni Falls is flanked by poorly sorted intraclastic conglomerate with a variably sandy grainstone matrix (Fig. 3.16A, B). In the upper Altyn Formation there, similar intraclasts are banked up on one side of the patch reef.

Intraclasts also occur between the *Baicalia* columns in most of the patch reefs. Intraclasts vary in size and shape, from tabular to blocky, and angular to rounded, from a few millimetres in size up to ~10 cm across, composed of dolomudstone belonging to the Laminite facies. Most intraclasts are fragments of Laminite facies, but some are pebble- and cobble-size fragments of stromatolites.

6.3.2. Interpretation

The intraclasts, largely belonging to the Laminite facies but some including fragments of stromatolite columns, indicate that laterally adjacent to the patch reefs lithifying laminated lime mud with minor laminae of sand-sized grains was episodically torn up and reworked. Although the microbial patch reefs largely withstood strong current activity and remained mostly intact, parts of them suffered fragmentation.

6.4. Discussion

The ambient energy levels in the Ribbon facies are indicative of alternating low flow-regime current activity. By contrast, sporadic events of much stronger currents were necessary to cause seemingly discontinuous disruption of the underlying cementing thin beds, followed by oscillatory currents that exceeded ambient conditions. These currents shifted the flat-pebble intraclasts back and forth, causing varying degrees of abrasion to the broken edges, mounding, imbrication, and fan-shaped to vertical, edgewise stacking. Once the intraclasts were emplaced, in general there appears to have been no further movement, corroborating the temporal difference between the two events.

Storms are commonly invoked as the standard agents for scour to generate more or less in situ intraclasts in offshore subtidal carbonates like the Ribbon Limestone facies (e.g., Markello and Read, 1981; Whisonant, 1987; Westrop, 1989; Lee and Kim, 1992; Mount and Kidder, 1993; Myrow et al., 2004; Bayet-Goll et al., 2015; Wang et al., 2019). However, the sporadic occurrence of these beds and their laterally discontinuous nature suggest that they may not be due to quasi-predictable meteorological events. Moreover, the abrupt contrast between ambient, comparatively low-energy conditions and the higher level of scour and reworking argues that, instead, a different process was involved in the formation of the flat pebbles (Pratt, 2002; Pratt and Bordonaro, 2007).

While thick cross-bedded Grainstone facies lack large intraclasts, those in the thin to medium beds with sharp and in places distinctly scoured bases in the middle Altyn Formation indicate that during stronger events some of the underlying laminated lime mudstone was eroded and redeposited as floating clasts. The subangular shape of most intraclasts indicates that erosion and deposition were probably a single event, without protracted reworking and abrasion. Unlike the formation of lime mudstone intraclasts in the Ribbon facies, these intraclasts were eroded and transported by the same currents that brought in the allochthonous sands from the inner platform and coast. Once this sediment was deposited it was left undisturbed, because the ambient energy conditions were too low. By contrast, the thick intraclastic rudstones in the upper Waterton Formation at the head of Syncline Brook reflect superimposed, particularly high-energy events of short-distance off-platform transport, coupled with strong wave action which imbricated the intraclasts at some levels.

The large intraclasts in and flanking the stromatolite patch reefs might be taken as evidence for a dominantly high-energy depositional setting. However, the relatively low-energy levels indicated by the parent lithologies of most of the intraclasts, especially of the Laminite facies, and the enclosing beds are evidence that sedimentation was instead

comparably tranquil for protracted periods of time. This argues that the events of disruption and movement were not typical of the ambient meteorological conditions.

The contrasting levels of energy plus the stratigraphic irregularity are regarded here as evidence that storms were not the agents of erosion, reworking and transport. Furthermore, the absence of hummocky cross-stratification in the Altyn Formation is an indication that strong storms did not affect the platform and shallow ramp, and oscillatory and combined flow generated only low flow-regime sedimentary structures. Grading is not developed in the Ribbon and Grainstone facies in the Waterton and middle Altyn Formation, respectively. Although cross-bedding and clinoforms in the Grainstone facies higher in the Altyn Formation are evidence for tidal currents, these deposits lack indication of anomalous scour, and pebble- and cobble-size intraclasts are not present.

Instead, occasional tsunami-induced wave action is invoked to scour out and rework the flat-pebble intraclasts and create and collect intraclasts flanking and within stromatolite patch reefs. Tsunami on-surge probably moved coastal sands onshore and inundated the tidal flat sabkhas, scouring their upper layeres, which accounts for the angular grains of silicified ooids and anhydrite. Tsunami off-surge, or backwash, transported coastal sand-size grains onto the shallow shelf and beyond onto the outer shelf, and in doing so suspended inner platform muds and eroded the cementing outer platform laminites. Given the low topographic relief of the platform plus the lack of independent evidence for strong storms, it is not realistic to explain the off-surge as due to storm-induced coastal flooding. A similar combination of tsunami effects has been invoked for certain facies in the younger Grinnell and Helena formations which are fundamentally low-energy deposits, although leading to some differences in sediment types and effects (Pratt, 1998b, 2001b; Pratt and Ponce, 2019).

The thick intraclastic sandy dolograinstone beds at the top of the Waterton Formation in Syncline Brook suggest not only transport but the impact of strong, repeated tsunami waves, either from the same or multiple tsunamis, on the upper slope. On the other hand, possible tsunami-related features were not recognized in the nearby platform, and this may have been because they were reworked in the ambient tidal regime.

The Altyn-like unit in the overlying Appekunny Formation exhibits common hummocky cross-stratification. The combination of this and its anomalous composition in an otherwise low-energy muddy unit (Rule and Pratt, 2019) suggest not only was it comparatively rapidly deposited but also reworked by strong oscillatory and combined-flow. Both may be explained as tsunami processes: off-surge events that brought sand-size carbonate-rich sediment from the remnant of the platform that had not yet been smothered, plus the impact of repeated events of wave action.

As with terms like ‘seismite’ and ‘tempestite’, labelling certain beds and structures as tsunamites may be useful in some situations, but the term would seem to lose its value in complex successions involving multiple sedimentary processes, repeated events or large-scale features.

7. The carbonate platform

Integrating petrology, facies interpretation and the role of outsized scour and allochthonous sedimentation leads to a radically different interpretation of this Mesoproterozoic carbonate succession, hitherto assumed to represent a shallow, peritidal platform (Horodyski, 1983; White, 1984; Pratt, 1994).

The Waterton Formation, and seemingly most of the underlying Haig Brook and Tombstone Mountain formations judging from their lithological attributes (Fermor and Price, 1983), were deposited on a gently westward- to southwestward-dipping ramp. The overlying Altyn Formation records regional shallowing and westward progradation of a wide and

differentiated carbonate platform which extended considerably eastward well beyond present-day outcrops. In the northwestern area, thicker bedding of the upper Waterton Formation laterally equivalent to the upper Altyn Formation reflects closer proximity to the shallow platform. Eventually, influx of siliciclastic mud from the west abruptly shut down the carbonate factory, except for a small area that persisted for a while and is recorded by an interval of allochthonous sandy dolograinstone in the Appekunny Formation in the northeastern area.

Some lime mud in the ramp setting may have precipitated in the directly overlying water column, but most was probably derived from precipitation in shallower areas to the east. Similarly, the lime mud comprising the Laminite facies in the lower and part of the upper Altyn Formation was probably generated mostly in the middle and inner platform, and that the lamination records depositional events, not precipitation events. The differences between the Ribbon and Laminite facies were largely due to the relative grain size of the lime mud delivered to the ramp, not changing environmental controls such as bathymetry which seem to have remained stable. This is supported by the variable presence of land-derived silt. Tidal currents may have contributed to seaward transport of mud. The landward equivalents of the Waterton and lower Altyn formations were probably a considerable distance away, as suggested by the absence of sand and coarser carbonate particles. It is also possible that the inner platform was largely muddy at the time and had not developed ooid shoals and the conditions to form peloids, aggregates and intraclasts.

The upper part of the lower Altyn Formation at Apikuni Falls saw the increased presence of admixed silt and sand and interbedding of Grainstone facies in dololaminite, as the shallow platform prograded westward. Lack of reworking of these allochthonous dolograinstone beds at Apikuni Falls suggests that this area was a somewhat deeper, outer platform setting which was also conducive to the development of small stromatolite patch reefs. The upper 30 m of the lower Altyn Formation at Sofa Mountain also became sandier. Sedimentation then became dominated by mixed coarse carbonate and siliciclastic sand. These sediments were deposited in fairly shallow water on the platform top, under a mesotidal regime which generated strong tidal currents that reworked the sands into dunes and bars. Larger stromatolite patch reefs developed in the Apikuni Falls area. Coarse carbonate particles in the Grainstone facies show that much of the now-vanished platform to the east was characterized by grainy sediment consisting of peloids and micritic aggregates and small intraclasts. Also there were ooid shoals as well as probably extensive, low-energy, inner platform areas in which lime mud accumulated and became deformed with molar-tooth structure. Coastal areas consisted of sands and broad tidal-flat sabkhas. The upper Altyn Formation at Apikuni Falls and a few kilometres to the east was a mix of dololaminite, sandy grainstone and stromatolite patch reefs, suggesting a return to outer platform conditions, while to the north it was dominated by grainstone with subordinate siliciclastic sand. The platform passed seaward into the ramp and continued to be the site of mainly allochthonous, fine-grained sediment deposition, although in beds somewhat thicker than typical for Ribbon facies in the Waterton Formation underlying the Altyn Formation.

Anomalous events of high energy occasionally scoured and sorted cementing lenses and nodules. The Ribbon facies was susceptible to this because of the contrast between these stiffer layers and the unlithified argillaceous laminae that separated them, along with the occurrence of earthquakes which disrupted the beds (see Chapter 4). Lacking the same kind of interbedding and consequently being more uniformly coherent, the Laminite facies was not so affected. These events reached much deeper than the strongest storms, and they are interpreted to have been from tsunami-induced wave action.

Westward transport of the sand-size sediment was by tsunami off-surge, as this was the only mechanism available to deliver coarse inner platform and nearshore sediment far out on

the outer platform in an arid, tropical climate that seems to lack major storms and hurricanes (Pratt and Ponce, 2019). The one thick oolite recorded was also transported by off-surge from a large shoal that developed fairly nearby. The sharp-based dolograinstone beds in dololaminite were deposited below storm-wave base and below the effects of tidal currents by tsunami off-surge. Water depth is uncertain, but because storm-wave base was probably shallow it might have been some 20–30 m. The apparent absence of sandy dolograinstone beds in the lower Altyn Formation may indicate that tsunami activity was less, or that the shallow source area was too far away. Dolograinstone beds are not uniformly distributed in dololaminite interals, suggesting that tsunami activity was indeed variable. Higher in the succession, tidal action would have erased the evidence for individual tsunami events.

The thick beds with large intraclastic rudstones composed of sandy grainstone in the northwestern area also record the effects of tsunami impact on the upper ramp, first in transporting the sediment by off-surge, then rupturing the thin beds, followed by reworking them through strong wave action. The sandy dolograinstone beds in the Appekunny Formation were also sediments delivered and reworked by tsunamis, probably from multiple events.

The limited number of sections precludes reconstructing the paleogeography of the carbonate platform with certainty. The shallow platform was probably still some distance to the east during deposition of the lower Altyn Formation. The middle Altyn Formation at Apikuni Falls was probably deposited under slightly deeper conditions than around Waterton where stronger tidal currents were felt. In upper Altyn time, coarse sandy grainstones are thicker and more continuous there as well, suggesting that it remained somewhat deeper. Shallow-water facies appear to thin in the northwest where the platform passed into the ramp. Thus, the platform was probably lobate in outline and not strictly parallel to the Lewis thrust. It is also difficult to determine if the area experienced differential subsidence owing to the structural complications.

8. Discussion

The lower Belt carbonate succession consists of an array of carbonate particle types and facies that are both similar to but also somewhat different from those of many other upper Archean, Proterozoic and lower Paleozoic carbonate platforms. In this protracted episode, oolite is a common thread although ooid microstructure varies (e.g., Chow and James, 1987; Trower and Grotzinger, 2010). Laminated carbonate mudstones are a widespread, low-energy facies regardless of geologic age (e.g., Sherman et al., 2001; Coniglio and James, 1990; Medig et al., 2016), reflecting lime mud production in the warm, shallow platform and its off-platform transport (Pomar and Hallock, 2008). Lime mudstone–marlstone alternations conforming to ribbon limestones are also variably common but become rare after the Cambro-Ordovician (e.g., Sherman et al., 2001; Pratt, 2001; Kwon et al., 200; Bayet-Goll et al., 2015). It is possible that clay export from the pre-vegetation landscape played a role in this distribution (cf. Dalrymple et al., 1985).

Whereas stromatolites comprise patch reefs in the lower Belt they do not exhibit the diversity of shapes and microstructures present in some other successions (e.g., Bertrand-Sarfati and Moussine-Pouchkine, 1985; Sami and James, 1993; Kah et al., 2012). Similar to some of these platforms, stromatolites in deeper water, lower energy settings are domical, whereas those in shallower environments exhibit columnar-branching shapes. Unlike some Archean and Proterozoic platforms (e.g., Sumner, 1997; Grotzinger and James, 2000; Hood et al., 2011; Hood and Wallace, 2012), marine precipitates in the form of isopachous and spherulitic fibrous cements are absent, although micritic calcite cementation took place in ribbon limestones, stromatolites and in aggregates and intraclasts. Micritic aggregates and

small intraclasts are dominant allochems in the tidally influenced mid-platform part of the Altyn Formation, but they were probably transported from shallow, wave-washed areas of the middle or inner platform. These kinds of particles seem to have been only rarely noted in other Proterozoic platforms (Medig et al., 2016). Somewhat similar grains are volumetrically important or dominant in some Cambro-Ordovician platforms (Pratt et al., 2012). Lower Paleozoic examples, however, are composed of more distinctly clotted micrite that suggests a direct microbial role in formation. This may also have been so for the Altyn Formation.

The lower Belt records a shallowing-upward, carbonate platform succession that prograded over a ramp. However, only the ramp and outer and possibly mid-platform settings are preserved, and thus the nature of inner platform and coastal deposits can only be inferred on the basis of allochthonous sediments that were transported seaward. Lime mud was produced mostly in the platform interior, likely in the water column, and some of this was exported to the outer shelf and ramp; some may have precipitated in those areas as well. Common round grains of microsopar in dolograinstone attest to extensive, low-energy areas of lime mud accumulation that was deformed to form molar-tooth structure.

Nearshore sediments consisted of fluvial-derived siliciclastic sand, micritic aggregates and locally ooids, reflecting the increase in energy owing to landward shallowing. Tidal flats mantled the low-relief shoreline. Silicified anhydrite grains attest to a hot, arid paleoclimate. While modern tropical coastal areas are microtidal, the clinoforms in the middle Altyn Formation and cross-bedding in sandy dolograinstone in the upper Altyn Formation point to comparatively strong tidal currents, probably reflecting a mesotidal regime. Tidal flats may have been correspondingly extensive because of the greater daily inundation. By contrast, there are no other indicators of tidal activity in the younger units of the Belt Supergroup. This could be due to the fact that no coastal deposits are preserved. On the other hand, when the Belt Basin switched from being fully submerged to subaerial with deposition of fluvial deposits of the Bonner Formation (= Phillips Formation in Canada), no intervening tidal deposits are recorded. Thus, it is probable that the Belt Basin experienced tides during its earliest phase when dramatic subsidence outpaced the rate of sedimentation and the basin was quite deep. With deposition of the Appekunny Formation, tides would have become reduced as the basin shallowed and there was no longer significant bathymetric differentiation (Pratt, 2001, 2017; Pratt and Ponce, 2019). It is also possible that tectonic activity along the western side may have restricted tidal penetration from the ocean.

The lower Belt facies contrast markedly with those in the younger Helena Formation (Pratt, 1998b, 1999, 2001, 2017). At this point the Belt Basin had little depositional relief and the lateral facies variation is almost imperceptible (Winston, 2007). The lime mud was similarly precipitated in the water column but frequently reworked at the limit of a shallow storm-wave base. Clay makes up a significant proportion of the lime mudstone, and some intervals are silty, but this material was derived from the west, not the east. Sporadic beds of allochthonous grainstone composed of oolite with siliciclastic sand were derived from shallow areas to the east. Rare halite molds indicate that the paleoclimate remained hot and arid. Stromatolite patch reefs are confined to the *Conophyton*-bearing interval in the upper part of the Helena Formation, and a few other levels where they accreted on erosional hardgrounds. The Helena and Wallace formations (= Siyeh and Kitchener formations in Canada) are riddled with molar-tooth structure. This facies-dependent deformation feature and is rare in the Waterton Formation (see Chapter 4), but allochthonous microspar grains indicate that it developed extensively in the inner platform of the Altyn Formation.

As well as common earthquakes (see Chapter 4) the Belt Basin was impacted by tsunamis and possibly seiches generated by movement on normal faults in the basin centre (Pratt, 1998b, 2001; 2017; Pratt and Ponce, 2019). The effects were somewhat different, likely because the lower Belt was deposited in a region more proximal to the margin, sediments had

different distributions, and the basin possessed a greater bathymetric differentiation at the time. Tsunami wave action and impact are held responsible for certain kinds of sediment disruption and brecciation. Tsunami off-surge, similarly suggested for the Helena and Grinnell formations, was an important agent of transport of coarse inner platform and coastal sediment into the outer platform and upper ramp. Apparent cyclically arranged beds in the middle Altyn Formation, previously interpreted as peritidal (White, 1984; Pratt, 1994), are not. Instead, they are outer-platform dololaminites punctuated with allochthonous sandy dolograinstones transported by tsunamis, although not reworked by tsunami-induced wave action. Nonetheless, the lack of coincidence between these beds and seismites (Pratt, 1994) suggests that most of the tsunami deposits and seismites were generated by different events. Although analogous facies in other Proterozoic carbonate platform successions have yet to be interpreted this way, there is no reason why tsunami-lain beds should not be present, if the basin experienced normal fault-induced displacement. Their main distinguishing attributes are that they consist either of allochthonous or reworked sediment, have scoured bases, and demonstrate an anomalous level of energy given what is indicated about background conditions. For example, rudstones composed of imbricated intraclasts, similar to those in the Ribbon facies, are common in many Proterozoic strata (e.g., Sherman et al., 2001; Thomson et al., 2014; Medig et al., 2016), and are potential candidates as tsunami-generated, especially if they formed in low-energy successions and there is independent evidence for syndepositional faulting in the basin. Tsunamis have been implicated in the deposition of certain beds in a number of Phanerozoic platforms and basins (e.g., Duringer, 1984; Pratt, 2002; Puga-Bernabéu et al., 2007; Pratt and Bordonaro, 2007; Massari et al., 2009; Pratt et al., 2012; Matysik and Szulc, 2019), indicating that this phenomenon was surely more widespread than currently understood. In terms of invoking tsunamis as an agent of delivering platform interior sediment to the outer platform, this process would be inferred based on preserved tsunami-lain beds. Coastal effects would be difficult to differentiate between those of hurricanes, which means the paleoclimate of the basin would have to be well understood on the basis of independent proxies.

8. Conclusions

The lower part of the Belt Supergroup (= Purcell Supergroup in Canada) offers a valuable glimpse into the workings of a carbonate platform almost 1.5 Gyr old, during a protracted, ostensibly stable phase of earth's history known as the 'Boring Billion.' The Haig Brook–Tombstone Mountain–Waterton–Altyn succession is a broadly shallowing-upward sequence recording the westward progradation of a carbonate platform over the adjacent ramp on the northeastern margin of the Belt Basin. The Waterton and Altyn formations are composed of five main facies: Laminite, Ribbon limestone, Grainstone, Oolite and Stromatolite patch reefs. Particle types include lime mud, peloidal and intraclastic micrite, ooids, siliciclastic clay, silt and sand, and silicified grains including anhydrite. In this regard, they share similarities but also some differences with the components of other Proterozoic carbonate platforms.

The ramp is recorded by dololaminite and ribbon limestone consisting of lime mudstone–marlstone alternations, whereas although the outer platform was dominated by dololaminite it also hosted low-relief stromatolite patch reefs. Inner-platform and coastal deposits are not preserved, but the identity of sediments deposited in these areas can be reconstructed on the basis of the particles in allochthonous beds delivered to the middle and outer part of the platform. This indicates that coastal areas were wave-agitated sands and tidal flat sabkhas in which sulphate evaporites precipitated. The middle to outer platform hosted mixed carbonate–quartz sands deposited under variably directed currents. Cross bedding plus the

presence of large clinoforms and dunes point to the presence of strong tidal currents and likely a mesotidal regime. Tides were present because the during the early existence of the basin it was deep. As bathymetry was reduced and the basin became lake-like, tidal effects diminished and seem to have disappeared altogether. By contrast, the absence of hummocky and swaley cross-stratification argues that the platform was not affected by strong storms.

Besides frequent soft-sediment deformation due to synsedimentary earthquakes (see Chapter 4), the platform was affected by frequent tsunami onrush and off-surge. Tsunamis eroded coastal sediments and sabkhas and redeposited allochthonous coarse-grained sediment in the outer and middle platform. These high-energy beds were previously misinterpreted as shallow-water facies, and the host dololaminites mistakenly regarded as tidal flat deposits. They illustrate the important role in this platform for tsunamis in transporting sediment seaward. In addition, tsunami-induced wave action disrupted limestone beds in the upper ramp, producing flat-pebble conglomerate. Thus, this feature was not intrinsic to the depositional setting.

The lower Belt carbonate succession provides a unique window onto the variety of phenomena that governed the nature of the sediment, depositional processes, paleoceanography and paleoclimate of the Belt Basin early in its history. Superficially seeming to record a conventional, prograding peritidal carbonate platform, here a radical reinterpretation of these rocks reveals the critical importance of syndepositional tectonic activity, especially in generating tsunamis, as well as the role of tides in a mesotidal setting. These insights should have application to other pre-Cambrian and Phanerozoic carbonate platforms.

References

Aitken, J.D., 1997. Stratigraphy of the Middle Cambrian platformal succession, southern Rocky Mountains. Geological Survey of Canada Bulletin 398, 322 p.

Awramik, S.M., Buchheim, H.P., 2009. A giant, Late Archean lake system: The Meentheena Member (Tumbiana Formation; Fortescue Group), Western Australia. Precambrian Research 174, 215–240.

Banerjee, S., Jeevankumar, S., 2007. Facies and depositional sequence of the Mesoproterozoic Rohtas Limestone: eastern Son valley, Vindhyan basin. Journal of Asian Earth Sciences 30, 82–92.

Bartley, J.K., Kah, L.C., Frank, T.D., Lyons, T.W., 2015. Deep-water microbialites of the Mesoproterozoic Dismal Lakes Group: microbial growth, lithification, and implications for coniform stromatolites. Geobiology 13, 15–32.

Bayet-Goll, A., Chen, J., Moussavi-Harami, R., Mahboubi, A., 2015. Depositional processes of ribbon carbonates in Middle Cambrian of Iran (Deh-Sufiyan Formation, Central Alborz). Facies 61, article 9, 18 pp.

Bertrand-Sarfati, J., Moussine-Pouchkine, A., 1985. Is cratonic sedimentation consistent with available models? An example from the Upper Proterozoic of the West African craton. Sedimentary Geology 58, 255–276.

Brasier, M.D., Lindsay, J.F., 1998. A billion years of environmental stability and the emergence of eukaryotes: new data from northern Australia. Geology 26, 555–558.

Chafetz, H.S., Zhang, J., 1998. Authigenic euhedral megaquartz crystals in a Quaternary dolomite. Journal of Sedimentary Research 68, 994–1000.

Chandler, F.W., 2000. The Belt–Purcell Basin as a low-latitude passive rift: implications for the geological environment of Sullivan type deposits, In: Lydon, J.W., Höy, T., Slack, J.F., Knapp, M.E. (Eds.), The Geological Environment of the Sullivan Deposit, British

Columbia. Geological Association of Canada, Mineral Deposits Division Special Publication 1, pp. 82–112.
Chow, N., James, N.P., 1987. Facies-specific, calcite and bimineralic oods from Middle and Upper Cambrian platform carbonates, western Newfoundland, Canada. Journal of Sedimentary Petrology 57, 907–921.
Clough, J.G., Goldhammer, R.K., 2000. Evolution of the Neoproterozoic Katakturuk Dolomite ramp complex, northeaster Brooks Range, Alaska. In: Grotzinger, J.P., James, N.P. (Eds.), Carbonate Sedimentation and Diagenesis in the Evolving Precambrian World. SEPM Special Publication 67, pp. 209–241.
Coniglio, M., James, N.P., 1990. Origin of fine-grained carbonate and siliciclastic sediments in an Early Palaeozoic slope sequence, Cow Head Group, western Newfoundland. Sedimentology 37, 215–230.
Cressman, E.R., 1989. Reconnaissance stratigraphy of the Prichard Formation (Middle Proterozoic) and the early development of the Belt basin, Washington, Idaho, and Montana: U.S. Geological Survey Professional Paper 1490, 80 pp.
Dalrymple, R.W., 2010. Tidal depositional systems. In: James, N.P., Dalrymple, R.W. (Eds.), Facies Models 4, pp. 201–231. Geological Association of Canada, St. John's.
Dalrymple, R.W., Narbonne, G.M., Smith, L., 1985. Eolian action and the distribution of Cambrian shales in North America. Geology 13, 607–610.
Dalrymple, R.W., Baker, E.K., Harris, P.T., Hughes, M.G., 2003. Sedimentology and stratigraphy of a tide-dominated, foreland-basin delta (Fly River, Papua New Guinea). In: Sidi, F.H., Nummedal, D., Imbert, P., Darman, H., Posamentier, H.W. (Eds.), Tropical Deltas of Southeast Asia—Sedimentology, Stratigraphy, and Petroleum Geology. SEPM Special Publication 76, pp. 147–173
Daly, R.A., 1912. Geology of the North American Cordillera, at the Forty-ninth Parallel. Geological Survey of Canada, Memoir 38, xxvii + 546 pp.
Da Silva, A.-C., Boulvain, F., 2012. Analysis of the Devonian (Frasnian) platform from Belgium: a multi-faceted approach for basin evolution reconstruction. Basin Research 24, 338–356.
Davis, G.A., Jardine, E.A., 1984. Preliminary studies of the geometry and kinematics of the Lewis allochthon, Saint Mary Lake to Yellow Mountain, Glacier National Park, Montana. Montana Geological Society, 1984 Field Conference, Northwestern Montana, pp. 201–209.
Demicco, R.V., 1983. Wavy and lenticular-bedded carbonate ribbon rocks of the Upper Cambrian Conococheague Limestone, central Appalachians. Journal of Sedimentary Petrology 53, 1121–1132.
Desjardins, P., Buatois, L.A., Pratt, B.R., Mángano, M.G., 2012. Subtidal sandbody architecture and ichnology in the Early Cambrian Gog Group of western Canada: Implications for an integrated sedimentologic–ichnologic model of tide-dominated shelf settings. Sedimentology 59, 1452–1477.
Douglas, R.J.W., 1952. Preliminary map, Waterton, Alberta. Geological Survey of Canada, Paper 52-10.
Dumas, S., Arnott, R.W.C., Southard, J.B., 2005. Experiments on oscillatory-flow and combined-flow bed forms: Implications for interpreting parts of the shallow-marine sedimentary record. Journal of Sedimentary Research 75, 501–513.
Durbano, A.M., Pratt, B.R., Hadlari, T., Dewing, K., 2015. Sedimentology of an early Cambrian tide-dominated embayment: Quyuk formation, Victoria Island, Arctic Canada. Sedimentary Geology 320, 1–18.

Duringer, P., 1984. Tempêtes et tsunamis: des dépôts de vagues de haute énergie intermittente dans le Muschelkalk supérieur (Trias germanique) de l'Est de la France. Bulletin de la Société géologique de France (s. 7) 26, 11,777–11,785.
Evans, K.V., Aleinikoff, J.N., Obradovich, J.D., Fanning, C.M., 2000. SHRIMP U-Pb geochronology of volcanic rocks, Belt Supergroup, western Montana: evidence for rapid deposition of sedimentary strata. Canadian Journal of Earth Sciences 37, 1287–1300.
Fermor, P.R., Price, R.A., 1983. Stratigraphy of the lower part of the Belt-Purcell Supergroup (Middle Proterozoic) in the Lewis thrust sheet of southern Alberta and British Columbia. Bulletin of Canadian Petroleum Geology 31, 169–194.
Fermor, P.R., Price, R.A., 1984. Stratigraphy of the lower part of the Belt-Purcell Supergroup (Middle Proterozoic) in the Lewis thrust sheet of southern Alberta and British Columbia. Montana Geological Society, 1984 Field Conference, Northwestern Montana, pp. 73–98. [reprint of Fermor and Price, 1983 with a modified Figure 8]
Fermor, P.R., Price, R.A., 1987. Multiduplex structure along the base of the Lewis thrust sheet in the southern Canadian Rockies. Bulletin of Canadian Petroleum Geology 35, 159–185.
Folk, R.L., 1980. Petrology of Sedimentary Rocks. Hemphill, Austin, 185 pp.
Goodfellow, W.D., 2000. Anoxic conditions in the Aldridge Basin during formation of the Sullivan Zn-Pb Deposit: Implications for the genesis of massive sulphides and distal hydrothermal sediments. In: Lydon, J.W., Höy, T., Slack, J.F., Knapp, M.E. (Eds.), The Geological Environment of the Sullivan Deposit, British Columbia. Geological Association of Canada, Mineral Deposits Division Special Publication 1, pp. 218–250.
Gordey, P.L., Frey, F.R., Norris, D.K., compilers, 1977. Geological Guide for the CSPG 1977 Waterton – Glacier Park Field Conference. Canadian Society of Petroleum Geologists, Calgary, 93 pp.
Greenman, J.W., Rainbird, R.H., Turner, E.C., 2020. High-resolution correlation between contrasting early Tonian carbonate successions in NW Canada highlights pronounced global carbon isotope variations. Precambrian Research 346, article 105816, 17 pp.
Grotzinger, J.P., 1986. Evolution of early Proterozoic passive-margin carbonate platform, Rocknest Formation, Wopmay Orogen, Northwest Territories, Canada. Journal of Sedimentary Petrology 56, 831–847.
Grotzinger, J.P., James, N.P., 2000. Precambrian carbonates: evolution of understanding. In: Grotzinger, J.P., James, N.P. (Eds.), Carbonate Sedimentation and Diagenesis in the Evolving Precambrian World. SEPM Special Publication 67, pp. 3–20.
Harris, P.M., Diaz, M.R., Eberli, G.P., 2019. The formation and distribution of modern ooids on Great Bahama Bank. Annual Review of Marine Science 11, 491–516.
Harrison, J.E., 1972. Precambrian Belt basin of northwestern United States: Its geometry, sedimentation, and copper occurrences. Geological Society of America Bulletin 83, 1215–1240.
Hein, F.J., McMechan, M.E., 1994 Proterozoic and Lower Cambrian strata of the Western Canada Sedimentary Basin. In: Mossop, G.D., Shetsen, I. (compilers), Atlas of the Western Canada Sedimentary Basin. Canadian Society of Petroleum Geology and Alberta Research Council, pp. 57–67.
Hesse, R., Schacht, U., 2011. Early diagenesis of deep-sea sediments. In: Hüneke, H., Mulder, T. (Eds.), Deep-Sea Sediments, pp. 557–713. Elsevier, Amsterdam.
Hill, R.E., 1985. Stratigraphy and Sedimentology of the Middle Proterozoic Waterton and Altyn formations, Belt–Purcell Supergroup, Southwest Alberta. Unpublished MSc thesis, McGill University, 165 pp.

Hill, R., Mountjoy, E. W., 1984. Stratigraphy and sedimentology of the Waterton Formation, Belt Purcell Supergroup, Waterton Lakes National Park, southwest Alberta. Montana Geological Society, 1984 Field Conference, Northwestern Montana, pp. 91–100.
Hoffman, P., 1967. Algal stromatolites: Use in stratigraphic correlation and paleocurrent direction. Science 157, 1043–1045.
Hood, A.S., Wallace, M.W., 2012. Synsedimentary diagenesis in a Cryogenian reef complex: ubiquitous marine dolomite precipitation. Sedimentary Geology 255–256, 56–71.
Hood, A.v.S., Wallace, M.W., Drysdale, R.N., 2011. Neoproterozoic aragonite-dolomite seas? Widespread marine dolomitization in Cryogenian reef complexes. Geology 39, 871–874.
Horodyski, R. J., 1976. Stromatolites from the middle Proterozoic Altyn Limestone, Belt Supergroup, Glacier National Park, Montana. In: Walter, M. R. (Ed.), Stromatolites, pp. 585–597. Elsevier, Amsterdam.
Horodyski, R.J., 1977. Environmental influences on columnar stromatolite branching patterns: Examples from the Middle Proterozoic Belt Supergroup, Glacier National Park, Montana. Journal of Paleontology 51, 661–671.
Horodyski, R.J., 1983. Sedimentary geology and stromatolites of the Middle Proterozoic Belt Supergroup, Glacier National Park, Montana. Precambrian Research 20, 391–425.
Höy, T., 1989. The age, chemistry, and tectonic setting of the Middle Proterozoic Moyie sills, Purcell Supergroup, southeastern British Columbia. Canadian Journal of Earth Sciences 26, 2305–2317.
Höy, T., 1993. Geology of the Purcell Supergroup in the Fernie west-half map area, southeastern British Columbia. British Columbia Mineral Resources Division Bulletin 84, 157 pp.
Hudec, M.R., Davis, G.A., 1989. Out-of-sequence thrust faulting and duplex formation in the Lewis thrust system, Spot Mountain, southeastern Glacier National Park, Montana. Canadian Journal of Earth Sciences 26, 2356–2364.
Huebschman, R.P., 1973. Correlation of fine carbonaceous bands across a Precambrian stagnant basin. Journal of Sedimentary Petrology 43, 688–699.
James, N.P. Jones, B., 2016. Origin of Carbonate Sedimentary Rocks. Wiley, Chichester, 446 pp.
James, N.P., Kendall, A.C., Pufahl, P.K., 2010. Introduction to biological and chemical sedimentary facies models. In: James, N.P., Dalrymple, R.W. (Eds.), Facies Models 4, pp. 323–339. Geological Association of Canada, St. John's.
Jamieson, J.W., Hannington, M.D., Tivey, M.K., Hansteen, T., Williamson, N.M.-B., Stewart, M., Fietzke, J., Butterfield, D., Frische, M. Allen, L., Cousens, B., Langer, J., 2016. Precipitation and growth of barite within hydrothermal vent deposits from the Endeavour Segment, Juan de Fuca Ridge. Geochimica et Cosmochimica Acta 173, 64–85.
Jardine, E.A., 1985. Structural Geology Along a Portion of the Lewis Thrust Fault, Northeastern Glacier National Park, Montana. Unpublished MSc thesis, University of Southern California, 201 pp.
Jiang, G., Christie-Blick, N., Kaufman, A.J., Banerjee, D.M., Rai, V., 2003.Carbonate platform growth and cyclicity at a terminal Proterozoic passive margin, Infra Krol Formation and Krol Group, Lesser Himalaya, India. Sedimentology 50, 921–952.
Kah, L.C., Bartley, J.K., Teal, D.A., 2012. Chemostratigraphy of the Late Mesoproterozoic Atar Group, Taoudeni Basin, Mauritania: Muted isotopic variability, facies correlation, and global isotopic trends. Precambrian Research 200–203, 82–103.
Knoll, A.H., Semikhatov, M.A., 1998. The genesis and time distribution of two distinctive Proterozoic stromatolite microstructures. Palaios 13, 408–422.

Kwon, Y.K., Chough, S.K., Choi, D.K., Lee, D.J., 2002. Origin of limestone conglomerates in the Choson Supergroup (Cambro-Ordovician), mid-east Korea. Sedimentary Geology 146, 265–283.
Lee, Y.I., Kim, J.C., 1992. Storm-influenced siliciclastic and carbonate ramp deposits, the Lower Ordovician Dumugol Formation, South Korea. Sedimentology 39, 951–969.
Lehrmann, D.J., Wei, J., Enos, O., 1998. Facies architecture of a large Triassic carbonate platform: The Great Bank of Guizhou, Nanpanjiang Basin, South China. Journal of Sedimentary Research 68, 311–326.
Link, P.K., Fanning, C.M., Lund, K.I., Aleinikoff, J.N., 2007. Detrital-zircon populations and provenance of Mesoproterozoic strata of east-central Idaho, U.S.A.: Correlation with the Belt Supergroup of southwest Montana. In: Link, P.K., Lewis, R.S. (Eds.), Proterozoic Geology of Western North America and Siberia. SEPM Special Publication 86, pp. 101–128.
Link, P.K., Stewart, E.D., Steel, T., Sherwin, J., Hess, L.T., McDonald, C., 2016, Detrital zircons in Mesoproterozoic upper Belt Supergroup in the Pioneer, Beaverhead, and Lemhi ranges, Montana and Idaho: The Big White Arc. In*:* MacLean, J.S., Sears, J.W. (Eds.), Belt Basin: Window to Mesoproterozoic Earth. Geological Society of America Special Paper 522, pp. 163–183.
Luepke, J.J., Lyons, T.W., 2001. Pre-Rodinian (Mesoproterozoic) supercontinental rifting along the western margin of Laurentia: geochemical evidence from the Belt-Purcell Supergroup. Precambrian Research 111, 79–90.
Lyons, T.W., Luepke, J.J., Schreiber, M.E., Zieg, G.A., 2000, Sulfur geochemical constraints on Mesoproterozoic restricted marine deposition: lower Belt Supergroup, northwestern United States. Geochimica et Cosmochimica Acta 64, 427–437.
Markello, J.R., Read, J.F., 1981. Carbonate ramp-to-deeper shale shelf transitions of an Upper Cambrian intrashelf basin, Nolichucky Formation, Southwest Virginia Appalachians. Sedimentology 28, 573–597.
Massari, F., D'Alessandro, A., Davaud, E., 2009. A coquinoid tsunamite from the Pliocene of Salento (SE Italy). Sedimentary Geology 221, 7–18.
Matysik, M., Szulc, J., 2019. Shallow-marine carbonate sedimentation in a tectonically mobile basin, the Muschelkalk (Middle Triassic) of Upper Silesia (southern Poland). Marine and Petroleum Geology 107, 99–115.
McMechan, M.E., 1981. The Middle Proterozoic Purcell Supergroup in the southwestern Rocky and southeastern Purcell Mountains, British Columbia and the initiation of the Cordilleran miogeocline, southern Canada and adjacent United States. Bulletin of Canadian Petroleum Geology 29, 583–621.
Medig, K.P.R., Thorkelson, D.J., Davis, W.J., Rainbird, R.H., Gibson, H.D., Turner, E.C., Marshall, D.D., 2014. Pinning northeastern Australia to northwestern Laurentia in the Mesoproterozoic. Precambrian Research 249, 88–99.
Medig, K.P.R., Turner, E.C., Thorkelson, D.J., Rainbird R.H., 2016. Rifting of Columbia to form a deep-water siliciclastic to carbonate succession: The Mesoproterozoic Pinguicula Group of northern Yukon, Canada. Precambrian Research 278, 179–206.
Mei, M., 2007. Implications of the Precambrian non-stromatolitic carbonate succession making up the Third Member of Mesoproterozoic Gaoyuzhuang Formation in Yanshan area of North China. Journal of China University of Geosciences 18, 191–209.
Mei, M., Tucker, M.E., 2013. Milankovitch-driven cycles in the Precambrian of China: the Wumishan Formation. Journal of Palaeogeography 2, 369–389.
Mišík, M., 1995, Authigenic quartz crystals in the Mesozoic and Paleogene carbonate rocks of the western Carpathians. Geologica Carpathica 46, 227–239.

Molenaar, N., de Jong, A.F.M., 1987. Authigenic quartz and albite in Devonian limestones: origin and significance. Sedimentology 34, 623–640.
Møller, N., Kvingan, K., 1988. The genesis of nodular limestones in the Ordovician and Silurian of the Oslo Region (Norway). Sedimentology 35, 405–420.
Mount, J.F., Kidder, D., 1993. Combined flow origin of edgewise intraclast conglomerates: Sellick Hill Formation (Lower Cambrian), South Australia. Sedimentology 40, 315–329.
Mountney, N.P., 2006. Eolian facies models. In: Posamentier, H., Walker, R.G. (Eds.), Facies Models Revisited. SEPM Special Publication 84, pp. 19–83.
Myrow, P.M., Tice, L., Archuleta, B., Clark, B., Taylor, J.F., Ripperdan, R.L., 2004. Flat-pebble conglomerate: its multiple origins and relationship to metre-scale depositional cycles. Sedimentology 51, 973–996.
Noble, J.P.A., van Stempvoort, D.R., 1989. Early burial quartz authigenesis in Silurian platform carbonates, New Brunswick, Canada. Journal of Sedimentary Petrology 59, 65–76.
Olariu, C., Steel, R.J., Dalrymple, R.W., Gingras, M.K., 2012. Tidal dunes versus tidal bars: The sedimentological and architectural characteristics of compound dunes in a tidal seaway, the lower Baronia Sandstone (Lower Eocene), Ager Basin, Spain. Sedimentary Geology 279, 134–155.
Pehrsson, S.J., Eglington, B.M., Evans, D.A.D., Huston, D., Reddy, S.M., 2016. Metallogeny and its link to orogenic style during the Nuna supercontinent cycle. In: Li, Z.X., Evans, D.A.D., Murphy, J.B. (Eds.), Supercontinent Cycles Through Earth History. Geological Society, London, Special Publication 424, pp. 83–94.
Pisarevsky, S.A., Elming, S.-Å., Pesonen, L.J., Li, Z.-X., 2014. Mesoproterozoic paleogeography: Supercontinent and beyond. Precambrian Research 244, 207–225.
Pomar, L., Hallock, P., 2008. Carbonate factories: A conundrum in sedimentary geology. Earth-Science Reviews 87, 134–169.
Pratt, B.R., 1994. Seismites in the Mesoproterozoic Altyn Formation (Belt Supergroup), Montana: A test for tectonic control of peritidal carbonate cyclicity. Geology 22, 1091–1094.
Pratt, B.R., 1998. Molar-tooth structure in Proterozoic carbonate rocks: Origin from synsedimentary earthquakes, and implications for the nature and evolution of basins and marine sediment. Geological Society of America Bulletin 110, 1028–1045.
Pratt, B. R., 2001. Oceanography, bathymetry and syndepositional tectonics of a Precambrian intracratonic basin: integrating sediments, storms, earthquakes and tsunamis in the Belt Supergroup (Helena Formation, ca. 1.45 Ga), western North America. Sedimentary Geology 141, 371–394.
Pratt, B.R., 2002. Storms versus tsunamis: Dynamic interplay of sedimentary, diagenetic, and tectonic processes in the Cambrian of Montana. Geology 30, 423–426.
Pratt, B.R., 2010. Peritidal carbonates. In: James, N.P., Dalrymple, R.W. (Eds.), Facies Models 4, pp. 401–420. Geological Association of Canada, St. John's.
Pratt, B.R., 2011. Molar-tooth structure, In: Reitner, J., Thiel, V. (Eds.), Encyclopedia of Geobiology, pp. 662–666. Springer, Dordrecht.
Pratt, B.R., 2017. The Mesoproterozoic Belt Supergroup in Glacier and Waterton Lakes national parks, northwestern Montana and southwestern Alberta: Sedimentary facies and syndepositional deformation. In: Hsieh, J.C.C. (Ed.), Geologic Field Trips of the Canadian Rockies, 2017 Meeting of the GSA Rocky Mountain Section. Geological Society of America Field Guide 48, pp. 123–135.
Pratt, B.R., Bordonaro, O.L., 2007. Tsunamis in a stormy sea: Middle Cambrian inner shelf limestones of western Argentina. Journal of Sedimentary Research 77, 256–262.

Pratt, B.R., Ponce, J.J., 2019. Sedimentation, earthquakes, and tsunamis in a shallow, muddy epeiric sea: Grinnell Formation (Belt Supergroup, ca 1.45 Ga), western North America. Geological Society of America Bulletin 131, 1411–1439.
Pratt, B.R., Raviolo, M.M., Bordonaro, O.L., 2012. Carbonate platform dominated by peloidal sands: Lower Ordovician La Silla Formation of the eastern Precordillera, San Juan, Argentina. Sedimentology 59, 843–866.
Pruss, S.B, Finnegan, S., Fischer, W.W., Knoll, A.H., 2010. Carbonates in skeleton-poor seas: new insights from Cambrian and Ordovician strata of Laurentia. Palaios 25, 73–84.
Puga-Bernabéu, A., Martín, J.M., Braga, J.C., 2007. Tsunami-related deposits in temperate carbonate ramps, Sorbas Basin, southern Spain. Sedimentary Geology 199, 107–127.
Rankey, E.C., 2002. Spatial patterns of sediment accumulation on a Holocene carbonate tidal flat, northwest Andros Island, Bahamas. Journal of Sedimentary Research 72, 591–601.
Ricken, W., 1986. Diagenetic bedding: a model for limestone–marl alternations. Lecture Notes on Earth Science 6, Springer, Berlin, 210 pp.
Robbins, L.L., Blackwelder, P.L., 1992. Biochemical and ultrastructural evidence for the origin of whitings: A biologically induced calcium carbonate precipitation mechanism. Geology 20, 464–468.
Ross, C.P., 1959. Geology of Glacier National Park and the Flathead region, northwestern Montana. U.S. Geological Survey Professional Paper 296, 125 pp.
Ross, G.M., Villeneuve, M., 2003. Provenance of the Mesoproterozoic (1.45 Ga) Belt basin (western North America): Another piece in the pre-Rodinia paleogeographic puzzle. Geological Society of America Bulletin 115, 1191–1217.
Rule, R.G., Pratt, B.R., 2019. The pseudofossil *Horodyskia*: Flocs and flakes on microbial mats in a shallow Mesoproterozoic sea (Appekunny Formation, Belt Supergroup, western North America). Precambrian Research 333, article 105439, 15 pp.
Sami, T.T., James, N.P. 1993. Evolution of early Proterozoic foreland basin carbonate platform, lower Pethei Group, Great Slave Lake, north-west Canada. Sedimentology 40, 403–430.
Schlager, W., 2005. Carbonate Sedimentology and Sequence Stratigraphy. SEPM Concepts in Sedimentology and Paleontology 8, 200 pp.
Sears, J.W., 2007. Rift destabilization of a Proterozoic epicontinental pediment: A model for the Belt-Purcell Basin, North America. In: Link, P.K., Lewis, R.S. (Eds.), Proterozoic Geology of Western North America and Siberia. SEPM Special Publication 86, pp. 55–64.
Sherman, A.G., James, N.P., Narbonne, G.M., 2000. Sedimentology of a late Mesoproterozoic muddy carbonate ramp, northern Baffin Island, Arctic Canada. In: Grotzinger, J.P., James, N.P. (Eds.), Carbonate Sedimentation and Diagenesis in the Evolving Precambrian World. SEPM Special Publication 67, pp. 275–294.
Sherman, A.G., Narbonne, G.M., James, N.P., 2001. Anatomy of a cyclically packaged Mesoproterozoic carbonate ramp in northern Canada. Sedimentary Geology 139, 171–203.
Shuster, A.M., Wallace, M.W., Hood, A.v.S., Jiang, G., 2018. The Tonian Beck Spring Dolomite: Marine dolomitization in a shallow anoxic sea. Sedimentary Geology 368, 83–104.
Sibley, D., 2003. Dolomite textures. In: Middleton, G.V. (Ed.), Encyclopedia of Sediments and Sedimentary Rocks, pp. 231–234. Kluwer Academic, Dordrecht.
Smith, A.G., Barnes, W.C., 1966. Correlation of and facies changes in the carbonaceous, calcareous, and dolomitic formations of the Precambrian Belt–Purcell Supergroup. Geological Society of America Bulletin 77, 1399–1426.
Steel, R.J., Plink-Björklund, P., Aschoff, J. 2012.Tidal deposits of the Campanian Western Interior Seaway, Wyoming, Utah and Colorado, USA. In: Davis, R.A., Jr., Dalrymple, R.W., (Eds.), Principles of Tidal Sedimentology, pp. 437–471. Springer, New York.

Stewart, E.D., Link, P.K., Fanning, C.M., Frost, C.D., McCurry, M., 2010 Paleogeographic implications of non-North American sediment in the Mesoproterozoic upper Belt Supergroup and Lemhi Group, Idaho and Montana, USA. Geology 38, 927–930.
Stockmal, G.S., Fallas, K.M., compilers, 2015. Geology, Chinook South, Alberta–British Columbia. Geological Survey of Canada, Open File 7476. Map, scale 1:100,000, Report, 48 pp.
Sumner, D.Y., 1997. Carbonate precipitation and oxygen stratification in late Archean seawater as deduced from facies and stratigraphy of the Gamohaan and Frisco formations, Transvaal Supergroup, South Africa. American Journal of Science 297, 455–487.
Sumner, D.Y., Grotzinger, J.P. 2000. Late Archean aragonite precipitation: Petrography, facies associations, and environmental significance. In: Grotzinger, J.P., James, N.P. (Eds.), Carbonate Sedimentation and Diagenesis in the Evolving Precambrian World. SEPM Special Publication 67, pp. 123–144.
Thomson, D., Rainbird, R.H., Dix, G., 2014. Architecture of a Neoproterozoic intracratonic carbonate ramp succession: Wynniatt Formation, Amundsen Basin, Arctic Canada. Sedimentary Geology 299, 119–138.
Trower, E.J., Grotzinger, J.P., 2010. Sedimentology, diagenesis, and stratigraphic occurrence of giant ooids in the Ediacaran Rainstorm Member, Johnnie Formation, Death Valley region, California. Precambrian Research 180, 113–124.
Turner, E.C., 2009. Mesoproterozoic carbonate systems in the Borden basin, Nunavut. Canadian Journal of Earth Sciences 46, 915–938.
Turner, E.C., James, N.P., Narbonne, G.M., 1997. Growth dynamics of Neoproterozoic calcimicrobe reefs, Mackenzie Mountains, Northwest Canada. Journal of Sedimentary Research 67, 437–450.
Turner, E.C., Long, D.G.F., Rainbird, R.H., Petrus, J.A., Rayner, N.M., 2016. Late Mesoproterozoic rifting in Arctic Canada during Rodinia assembly: impactogens, trans-continental far-field stress and zinc mineralization. Terra Nova 28, 188–194.
Wang, Jia., La Croix, A.D., Wang, H., Guo, F., Ren, B., 2019. Linkage between calcirudite lithofacies and storm-generated depositional processes in the Upper Cambrian Series, Shandong Province, eastern China. Sedimentary Geology 391, article 105518, 13 pp.
Wang, Jin., He, Z., Zhu, D., Liu, Q., Ding, Q., Li, S., Zhang, D., 2020. Petrological and geochemical characteristics of the botryoidal dolomite of Denying Formation in the Yangtze Craton, South China: Contraints on terminal Ediacaran “dolomite seas”. Sedimentary Geology 406, article 105722, 17 pp.
Wanless, H.R., 1979. Limestone response to stress: Pressure solution and dolomitization. Journal of Sedimentary Petrology 49, 437–462.
Westphal, H., Munnecke, A., Böhm, F., Bornholdt, S., 2008. Limestone–marl alternations in epeiric sea settings—witnesses of environmental changes or diagenesis? In: Pratt, B.R., Holmden, C. (Eds.). The Dynamics of Epeiric Seas. Geological Association of Canada, Special Paper 48, pp. 389–406.
Westrop, S.R., 1989. Facies anatomy of an Upper Cambrian grand cycle: Bison Creek and Mistaya formations, southern Alberta. Canadian Journal of Earth Sciences 26, 2292–2304.
Whipple, J.W., compiler, 1992. Geologic map of Glacier National Park, Montana. U.S. Geological Survey, Miscellaneous Investigations Series Map I-1508-F, scale 1:100,000.
Whipple, J.W., Connor, J.J., Raup, O.B., McGimsey, R.G., 1984. Preliminary report on the stratigraphy of the Belt Supergroup, Glacier National Park and adjacent Whitefish Range, Montana. In: McBane, J.D., Garrison, P.B. (Eds.), Northwest Montana and Adjacent Canada. Montana Geological Society Guidebook, 1984 Field Conference and Symposium, pp. 33–50.

Whisonant, R., 1987. Paleocurrent and petrographic analysis of imbricate intraclasts in shallow-marine carbonates, Upper Cambrian, southwestern Virginia. Journal of Sedimentary Petrology 57, 983–994.
White, B., 1984. Stromatolites and associated facies in shallowing–upward cycles from the Middle Proterozoic Altyn Formation of Glacier National Park, Montana. Precambrian Research 24, 1–26.
Willis, B., 1902. Stratigraphy and structure, Lewis and Livingston ranges, Montana. Geological Society of America Bulletin 13, 305–325.
Winston, D., 1986a. Sedimentology of the Ravalli Group, middle Belt carbonate and Missoula Group, Middle Proterozoic Belt Supergroup, Montana, Idaho and Washington, in: Roberts, S.M. (Ed.), Belt Supergroup: A Guide to Proterozoic Rocks of Western Montana and Adjacent Areas. Montana Bureau of Mines and Geology, Special Publication 94, pp. 85–124.
Winston, D., 1986b, Middle Proterozoic tectonics of the Belt basin, western Montana and northern Idaho. In: Roberts, S.M. (Ed.), Belt Supergroup: A Guide to Proterozoic Rocks of Western Montana and Adjacent Areas. Montana Bureau of Mines and Geology, Special Publication 94, pp. 245–257.
Winston, D., 1986c. Sedimentation and tectonics of the Middle Proterozoic Belt Basin and their influence on Phanerozoic compression and extension in western Montana and northern Idaho. In: Peterson, J.A. (Ed.), Paleotectonics and Sedimentation in the Rocky Mountain Region, United States. American Association of Petroleum Geologists Memoir 41, pp. 87–118.
Winston, D., 1989. Introduction to the Belt. In: Winston, D., Horodyski, R.J., Whipple, J.W. (Eds.), Middle Proterozoic Belt Supergroup, Western Montana. American Geophysical Union, 28th International Geological Congress, Washington, Field trip Guidebook T334, pp. 1–6.
Winston, D., 1990. Evidence for intracratonic, fluvial and lacustrine settings of Middle to Late Proterozoic basins of western U.S.A. In: Gower, C. F., Rivers, T., Ryan, B. (Eds.), Mid-Proterozoic Laurentia–Baltica. Geological Association of Canada Special Paper 38, pp. 535–564.
Winston, D., 2007. Revised stratigraphy and depositional history of the Helena and Wallace formations, mid-Proterozoic Piegan Group, Belt Supergroup, Montana and Idaho, U.S.A. In: Link, P.K., Lewis, R.S. (Eds.), Proterozoic Geology of Western North America and Siberia. SEPM Special Publication 86, pp. 65–100.
Winston, D., 2016. Sheetflood sedimentology of the Mesoproterozoic Revett Formation, Belt Supergroup, northwestern Montana, USA. In: MacLean, J.S., Sears, J.W. (Eds.), Belt Basin: Window to Mesoproterozoic Earth. Geological Society of America, Special Paper 522, pp. 1–56.
Winston, D., Link, P.K., 1993. Middle Proterozoic rocks of Montana, Idaho and eastern Washington: the Belt Supergroup. In: Link, P.K. (Ed.), Middle and Late Proterozoic stratified rocks of the western U.S. Cordillera, Colorado Plateau, and Basin and Range Province. In: Reed, J.C., Bickford, M.E., Houston, R.S., Link, P.K., Rankin, D.W., Sims, P.K., Van Schmus, W.R. (Eds.), Precambrian: Conterminous U.S. Geological Society of America, The Geology of North America C-2, pp. 487–517.
Winston, D., McGee, D., Quattlebaum, D., 1986. Stratigraphy and sedimentology of the Bonner Formation, Middle Proterozoic Belt Supergroup, western Montana. In: Roberts, S. (Ed.), Belt Supergroup: A Guide to Proterozoic Rocks of Western Montana and Adjacent Areas. Montana Bureau of Mines and Geology, Special Publication 94, pp. 183–195.

Wright, V.P., Cherns, L., 2016. Leaving no stone unturned: the feedback between increased biotic diversity and early diagenesis during the Ordovician. Journal of the Geological Society 173, 241–244.
Yin, A., Kelty, T.K., 1991. Structural evolution of the Lewis plate in Glacier National Park, Montana: Implications for regional tectonic development. Geological Society of America Bulletin 103, 1073–1089.
Zempolich, W.G., Baker, P.A., 1993. Experimental and natural mimetic dolomitization of aragonite ooids. Journal of Sedimentary Petrology 63, 596–606.

Figure Captions

Fig. 3.1. (A) Map of central western North America showing outcrop distribution of Belt Supergroup rocks and location of Glacier and Waterton Lakes national parks (Waterton–Glacier International Peace Park astride the border between Montana and Alberta). (B) Map of the national and Alberta provincial parks showing locations mentioned in the text. 1=Marias Pass; 2=Two Medicine Lake; 3=Rising Sun; 4=Singleshot Mountain; 5=Apikuni Falls; 6=Yellow Mountain; 7=Chief Mountain; 8=Sofa Mountain; 9=Waterton area; 10=northeastern end of Pincher Ridge and adjacent ridges to the south; 11=eastern Syncline Mountain; 12=Syncline Brook; 13=Packhorse Peak and Tombstone Mountain (northwestern Clark Range, British Columbia). Sections were measured at Apikuni Falls (48°48'50"N, 113°38'32"W) and 4 km to the northeast at the base of Apikuni Mountain (48°49'47"N, 113°37'26"W), Sofa Mountain (49°02'06"N, 113°47'16"W), Waterton area (Crypt Lake—49°00'24"N, 113°50'19"W; Bosporus ridge—49°02'53"N, 113°53'50"W; Waterton lakeside—49°02'37"N, 113°54'55"W; Bertha Bay—49°00'57"N, 113°54'37"W; Bertha Creek—49°02'04"N, 113°54'51"W; Akamina Highway—49°03'16"N, 113°55'00"W to 49°04'24"N, 113°57'02"W; Bear's Hump—49°03'26"N, 113°55'10"W); Syncline Mountain (49°21'57"N 114°24'57"W and 49°21'25"N 114°25'10"W), and Pincher Ridge (49°17'15.4"N, 114°04'23.4"W). Mount Boswell in the Waterton area was measured by Hill (1984) who also measured the section at Sofa Mountain, Bosporus ridge, Bertha Creek and Akamina Highway. Jardine (1985) gives a description of the succession at Yellow Mountain, and the Haig Brook–Tombstone Mountain–Waterton succession is described in Fermor and Price (1983).

Fig. 3.2. West-to-east-to-north cross-section across the Belt Basin from Idaho to Glacier National Park, Montana, showing the main subdivisions of the Belt Supergroup and formations in the lower and middle portion (based on the most recent compilation of U.S. nomenclature by Winston, 2016, fig. 1, with additions from Fermor and Price, 1983; revised from: Winston, 1989, fig. 3, 1990, fig. 5; Winston and Link, 1993, fig. 13). The Appekunny Formation has been placed in the Ravalli Group in some schemes (Harrison, 1972; Horodyski, 1983; Whipple et al., 1984). The Wallace Formation was not originally mapped in Glacier National Park (Whipple, 1992). The Belt Supergroup is called the Purcell Supergroup in Canada and the formational nomenclature has some differences (e.g., McMechan, 1981; Höy, 1992; Chandler, 2000). The Haig Brook and Tombstone Mountain formations are exposed in Castle Wildland Provincial Park and adjacent easternmost British Columbia (Fermor and Price, 1983) north-northwest of Waterton Lakes National Park. The thickness of the Haig Brook through Altyn formations is not to scale.

Fig. 3.3. Generalized northwest-to-southeast cross-section showing correlation of the main stratigraphic sections discussed (locations 13, 11, 10, 9, 8, 6 and 5 in Fig. 3.1B). Datum is the base of the Appekunny Formation. Stratigraphy in the Clark Range is from Fermor and Price

(1983); for Syncline Mountain from Fermor and Price (1983) and this study; for Pincher Ridge, Waterton area and Sofa Mountain, this study; for Yellow Mountain from Jardine (1985); and for Apikuni Falls, from White (1984) and this study. Several sections in the Waterton area, described in Hill and Mountjoy (1984) and Hill (1985), are not included.

Fig. 3.4. Salient exposures of the lower Belt Supergroup. HB=Haig Brook Formation; TM=Tombstone Mountain Formation; W=Waterton Formation; Al=Altyn Formation; Ap=Apekunny Formation; G=Grinnell Formation; H=Helena (Siyeh) Formation. (A) The Haig Brook (lower resistant, labelled), Tombstone Mountain (middle recessive) and Waterton (upper slope) formations on the south side of Packhorse Peak above Cate Creek, British Columbia. Photograph courtesy of P.R. Fermor. (B) Upper Waterton Formation forming the headwall of Syncline Brook looking west from Gravenstafel Ridge. Cate Creek is in the valley behind, and the mountain in the middle ground (labelled P) is Packhorse Peak, shown in A. The yellow line marks the base of the Appekunny Formation. (C) Upper Waterton and lower Altyn formations above Upper Waterton Lake on the flank of Mount Richards, south of Bertha Creek (after the 2017 forest fire). The yellow line marks a thrust fault. Photograph taken from an outcrop of lower Altyn Formation, and the valley in the middle ground contains another thrust fault. Two sections were measured in the upper thrust slice, 300 m to the right and 1 km south of Bertha Creek. (D) Altyn Formation exposed on lower flank of Altyn Peak, immediately to the west of Apikuni Falls. The thinner bedded interval in the lower third is the middle Altyn Formation, including broadly lenticular beds consisting of stromatolite patch reefs. The overlying thicker bedded to massive interval is the upper Altyn Formation, consisting mostly of grainstone and oolite. The yellow line marks the base of the overlying Appekunny Formation. (E) Buff- and maroon-coloured lower Altyn Formation and overlying resistant middle and upper Altyn Formation exposed on the northeast side of Sofa Mountain, looking east. The yellow line marks the base of the overlying Appekunny Formation. (F) Pincher Ridge above Drywood Creek showing the interval of Altyn-like dolomite (arrow) within the Appekunny Formation. This part of the Appekunny Formation is repeated by a thrust fault (below the arrow).

Fig. 3.5. Sedimentary constituents. Vertically oriented thin section photomicrographs, plane-polarized light except for C, cross-polarized light. A, B and F are from the Altyn Formation, Apikuni Falls; C is from Altyn-like dolomite in the Appekunny Formation, Pincher Ridge; D and E are from rudstone in the uppermost Waterton Formation, Syncline Brook. (A) Mudstone lamina composed of peloids and micrite (dolomitized) and subangular to angular silt made up of mostly quartz with minor amounts of feldspar. (B) Grainstone composed of micrite, peloids, sand-sized silty micritic intraclasts, intraclasts of grainstone consisting of peloids, radial ooids and intraclasts and quartz sand. (C) Rudstone (with a grainstone matrix) composed of micrite clasts, silicified, rounded to angular, sand-sized oolite, silicified laminated micritic intraclast (upper-centre), silt, and sand consisting of quartz and minor feldspar; grain (arrowed) consists of silicified anhydrite laths. (D) Oolite composed of ooids with concentric cortices (several silicified), micritic intraclasts, and grains of microspar. (E) Sand-sized grain of calcite microspar eroded from molar-tooth structure. Crystals along the margin are replacive megaquartz euhedra. (F) Oolite with ooids having mostly concentric cortices and many have quartz sand grains as nuclei; to the right of centre an ooid has half-moon cortex showing gravitational displacement to the right.

Fig. 3.6. Evidence for evaporites in Grainstone facies in the lower Altyn Formation, Apikuni Falls. Thin section photomicrographs, plane-polarized light. (A) Radiating long blades or prisms of replacive (and perhaps displacive) gypsum replaced by megaquartz composed of

blocky crystals ~30–50 and rarely up to 100 µm across. (B) Cluster of short blades or prisms of gypsum replaced by megaquartz. Individual crystals are also present. Subrounded grain in upper-centre is detrital quartz and those in lower are silicified carbonate (probably ooids) and composed of microquartz. (C) Subrounded sand grain composed of silicified felted anhydrite laths here ~20–100 µm in length but in other grains up to ~300 µm long, replaced by microquartz.

Fig. 3.7. Laminite facies. (A) Waterton Formation at the northeastern side of Syncline Mountain; ~3 m of section are shown. (B) Lower Altyn Formation at Waterton lakeshore; ~10 m of section are shown. (C) Laminated dolomudstone overlying Grainstone facies. Lower Altyn Formation, Apikuni Falls. (D) Laminated dolomudstone; brownish coloration is secondary. Lower Altyn Formation, roadcut at east of Apikuni Falls. (E) Planar- and lenticular-laminated silty dolomudstone. Block of Waterton Formation, Waterton. (F) Planar- and lenticular-laminated dolomudstone. Lower Altyn Formation, Sofa Mountain.

Fig. 3.8. Laminite facies. (A) Scan of polished surface of laminated dolomudstone. Waterton Formation, Waterton lakeside. (B) Laminated dolomudstone with silty laminae. Lower Altyn Formation, Apikuni Falls. (C) Laminated dolomudstone and silty laminae with scattered sand grains. Lower Altyn Formation, Apikuni Falls.

Fig. 3.9. Ribbon facies. Waterton Formation, Waterton area. (A) Outcrop of ribbon limestone (lower half) overlain by dolomudstone of Laminite facies; reddish and orange coloration is secondary. Akamina Highway; scale bar (at lower left) in centimetres. (B) Outcrop of thin-, lenticular and nodular-bedded lime mudstone (grey-coloured) and argillaceous dolomite (buff-coloured). Bertha Creek. (C) Block of thin-, wavy- and lenticular-bedded silty lime mudstone (grey-coloured) and argillaceous dolomudstone (buff-coloured). (D) Block with variably directed combined-flow cross-lamination in the lenses in the middle. (E) Optical scan of acetate peel of thin-, wavy-, lenticular- and nodular-bedded silty lime mudstone (light grey-coloured) and argillaceous dolomudstone (darker grey-coloured). Bertha Creek.

Fig. 3.10. Grainstone facies. Altyn Formation: lower (C, D), middle (A, B, E), all Apikuni Falls except A, Bosporus ridge. (A) Interbedded thin beds of dolograinstone and sandy dolograinstone with planar lamination and combined-flow cross-lamination. Reddish coloration is secondary. (B) Block with medium beds of variably sandy dolograinstone exhibiting multi-directional tabular cross-bedding. (C) Medium bed of sandy dolograinstone with base scoured up to 5 cm into Laminite facies. (D) Laminite facies with thin interbeds of sandy dolograinstone, the lower one with symmetrical ripples. (E) Close-up of block of cross-laminated dolograinstone with varying amounts of admixed siliciclastic sand and granules.

Fig. 3.11. Lenticular bodies and clinoforms in the Altyn Formation. (A) Tabular and gently lenticular, medium to thick beds of Grainstone facies. Upper Altyn Formation, Swiftcurrent Falls 2 km southwest of Apikuni Falls. (B) Grainstone facies comprising a stack of broadly lenticular beds ~10 m thick overlain by ~10 m of northwest-dipping thick clinoform beds (arrow). Middle Altyn Formation, Bosporus ridge (see also Hill, 1985, fig. 5.2). (C) Oolite facies consisting of westward-dipping clinoforms 5 m thick, overlying 4.6 m of planar-bedded oolite. Upper Altyn Formation, Apikuni Falls (see also Pratt, 2017, fig. 5A).

Fig. 3.12. Stromatolite facies. A, B, D–F from the middle Altyn Formation, Apikuni Falls; C from the lower Altyn Formation, Syncline Mountain. (A) Thin-bedded Laminite facies with several thin, lenticular stromatolite patch reefs overlain by thicker bedded Grainstone facies

containing patch reefs ~1 m thick. The flank of one patch reef is marked by its distinct wedging out (arrow). (B) Side view of block of mainly columnar stromatolites conforming to *Baicalia*. Columns at the bottom are upright, in the middle they lean first to the left and then to the right, and at the top they are upright. Scale (lower right) in centimetres. (C) Side view of leaning mostly columnar stromatolites conforming to *Baicalia*. Pocket knife is 9 cm long. (D) Oblique side view of block showing domical stromatolites with elongate outline in plan view, conforming to *Collenia*. Pocket knife is 9 cm long. (E) Side view of block showing columnar stromatolites with hemispherical and gently conical laminae. (F) Thin section photomicrograph of wavy stromatolite laminae consisting of normally graded, variably silty micrite and microspar, and wavy to lenticular dense micrite.

Fig. 3.13. Ribbon facies containing lenses of flat-pebble conglomerate (intraclastic rudstone). Waterton Formation, Waterton area. A is outcrop on the Akamina Highway, B–E, H are blocks, and F and G, Bertha Creek. (A) Intraclasts make up three lenses 20–40 cm wide. (B) Lenticular- and wavy-bedded lime mudstone and dolomite erosively overlain by lenses of intraclasts (lower left, upper left); intraclasts in upper left are oriented upright in a 'rosette' fashion. (C) Four lenses including lens with scoured base (arrow) overlain by a wider lens; in the latter, at the left is a pocket of vertically oriented intraclasts and a bundle of long, shingled intraclasts. (D) Wavy layer showing intraclasts imbricated in opposing directions. (E) Cluster of nodular intraclasts. (F) Hummocky bed of variably oriented intraclasts of various shapes. (G) Lens of lenticular intraclasts and imbricated thin intraclasts. (H) Lens with vertically oriented intraclasts.

Fig. 3.14. Flat-pebble conglomerate (intraclastic rudstone) in Ribbon facies, Waterton Formation, Waterton area. (A) Optical scan of acetate peel showing a bed of lime mudstone (dark-grey) and plane- and cross-laminated silty lime mudstone (light-grey) intraclasts. (B) Slabbed and etched rock sample showing wavy-laminated silty lime mudstone overlain by horizonally oriented lime mudstone intraclasts in a silty lime mudstone matrix, which is in turn erosively overlain by intraclasts in a grainstone matrix. Large intraclasts at left are light-grey in colour due to dolomitization. (C) Optical scan of thin section showing a thin bed of blocky to tabular lime mudstone intraclasts in a dolomitic matrix (dark-grey), sandwiched between thin-bedded silty lime mudstone (light-grey). Dolomite layer at lower left contains a lime mudstone nodule. (D) Optical scan of thin section showing laminated silty lime mudstone overlain by a thin bed of intraclasts in a grainstone matrix, in turn overlain by dolomitic layer (dark-coloured) and cross-laminated silty lime mudstone.

Fig. 3.15. Intraclastic rudstone in Grainstone facies. A and B are lower Altyn Formation, Apikuni Falls; C–E are upper Waterton Formation, Syncline Brook. (A) Lower bed with scattered, subrounded, horizontally oriented flat-pebble intraclasts of Laminite facies, and an upper bed with a layer of flat-pebble intraclasts. (B) Polished surface of angular sandy Laminite facies intraclasts. (C) Fallen block about 2 m thick with intraclasts imbricated mainly indicating current direction to the right, with several sandy grainstone blocks. (D) Fallen block about 2 m thick (up to the left) showing cross-laminated, variably intraclastic sandy grainstone erosively overlain by rudstone with intraclasts imbricated in multiple directions. (E) Fallen block with subangular to subrounded, planar- and cross-laminated sandy grainstone intraclasts, mostly horizontally oriented, in a sandy grainstone matrix.

Fig. 3.16. Rudstone associated with Stromatolite facies. Lower Altyn Formation, Apikuni Falls. (A) Rudstone composed of angular to subrounded granules, pebbles and cobbles of

various shapes of Laminite facies flanking a stromatolite patch reef. (B) Polished surface of angular, blocky to tabular intraclasts.

Fig. 3.17. Stratigraphic distribution of facies types in the main measured sections of the Waterton and Altyn formations arranged northwest (left) to southeast (right). Datum is the contact with the overlying Appekunny Formation. The approximate contact between the Waterton and Altyn formations at Syncline Mountain is inferred on the basis of the lowest beds that record the first sand influx. Sections at Bear's Hump, Bertha Creek, Bertha Bay and Waterton lakeside are in fault-bounded slices. The upper part of the lower Altyn Formation at Apikuni Falls and Sofa Mountain contains common interbeds of Grainstone facies but is shown as Laminite facies because the sandy dolograinstone is allochthonous and dololaminite is the host for these beds. The Grainstone facies of the middle Altyn Formation records mid- to outer platform mixed carbonate–siliciclastic sands reworked by tidal currents. The upper Altyn Formation in the Waterton area also records sand-sized sediments albeit finer grained than those of the underlying unit. The sections at Apikuni Falls and Apikuni Mountain are separated by 4 km, and show how facies vary laterally in the outer platform setting of the upper Altyn Formation in that area.

Fig. 3.18. Hypothetical, simplified west–east cross-section of the carbonate platform during Altyn Formation time, as indicated by outcrop facies plus proxies for the inner platform and coastal region. Tidal flat sabkhas mantled the low-relief shore. Compositionally and texturally mainly mature sand in coastal areas mixed with various types of carbonate sands produced by the carbonate factory. Lime mud was also produced, and much of it was exported onto the shelf and down the ramp. Occasional weak storms reworked the sea bottom. Stromatolite patch reefs accreted in deeper areas, and ooid shoals formed locally. Strong tidal currents reworked sand-sized sediment forming dunes and larger bars in certain parts of the outer platform. Faulting in the basin centre generated frequent tsunamis, and tsunami off-surge transported carbonate and siliciclastic sand seaward from the inner platform, coastal areas and tidal flats. Earthquakes from faulting occurred frequently and also caused common deformation of the sediments (see Chapter 4).

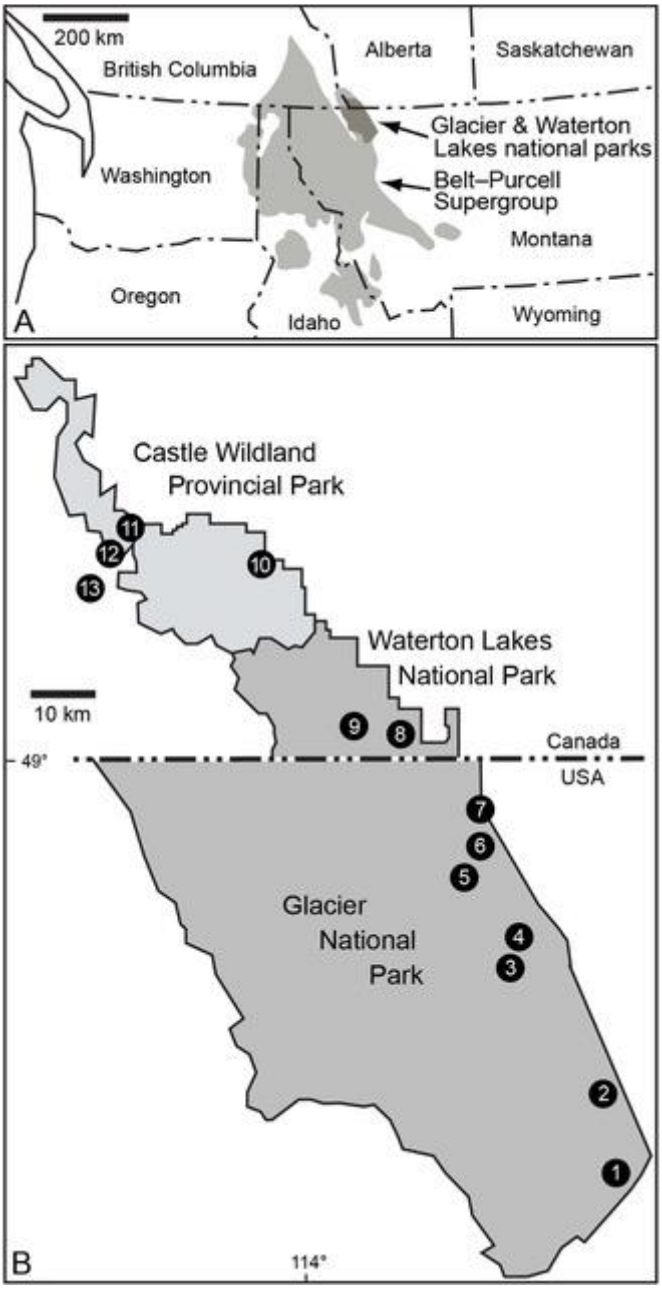
200 km
British Columbia
Alberta
Saskatchewan
Glacier & Waterton
Lakes national parks
Belt–Purcell
Supergroup
Washington
Montana
Oregon
Idaho
Wyoming
A
Castle Wildland
Provincial Park
Waterton Lakes
National Park
10 km
Canada
USA
49°
Glacier
National
Park
B
114°

Fig. 3.1

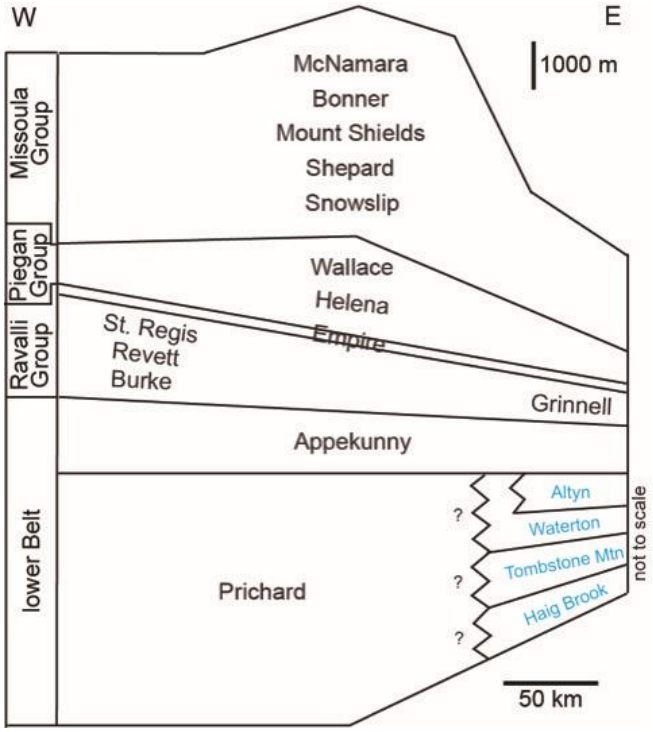
W
E
1000 m
Missoula Group
McNamara
Bonner
Mount Shields
Shepard
Snowslip
Piegan Group
Wallace
Helena
Empire
Ravalli Group
St. Regis
Revett
Burke
Grinnell
Appekunny
lower Belt
Prichard
Altyn
Waterton
Tombstone Mtn
Haig Brook
?
?
?
not to scale
50 km

Fig. 3.2

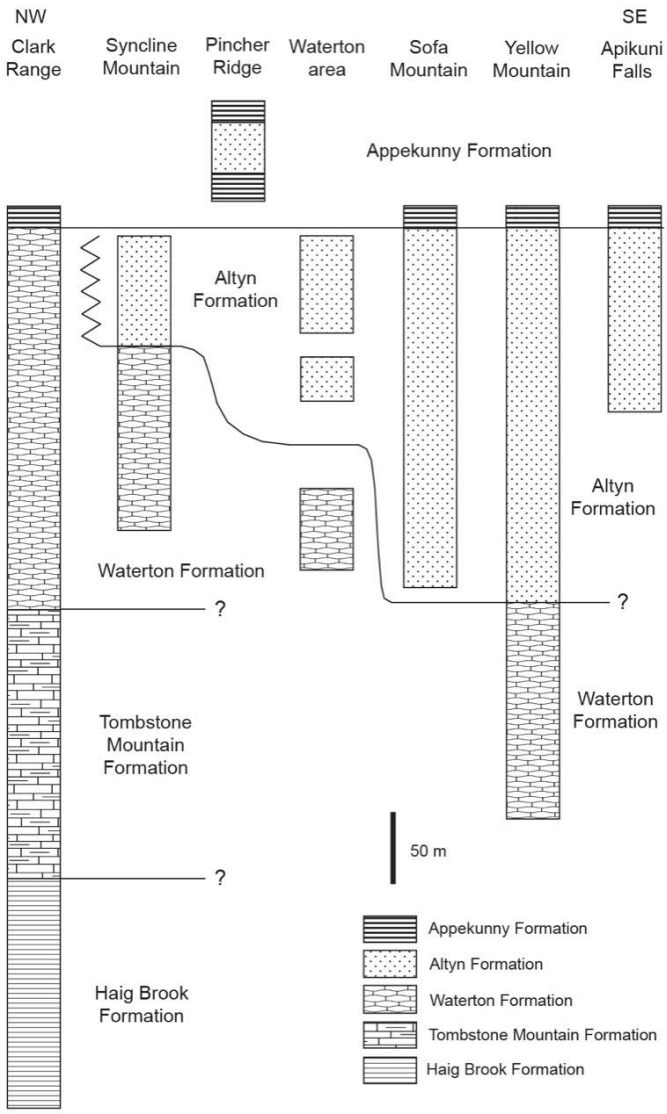
NW
SE
Clark Range
Syncline Mountain
Pincher Ridge
Waterton area
Sofa Mountain
Yellow Mountain
Apikuni Falls
Appekunny Formation
Altyn Formation
Altyn Formation
Waterton Formation
?
?
Tombstone Mountain Formation
Waterton Formation
50 m
?
Haig Brook Formation
Appekunny Formation
Altyn Formation
Waterton Formation
Tombstone Mountain Formation
Haig Brook Formation

Fig. 3.3

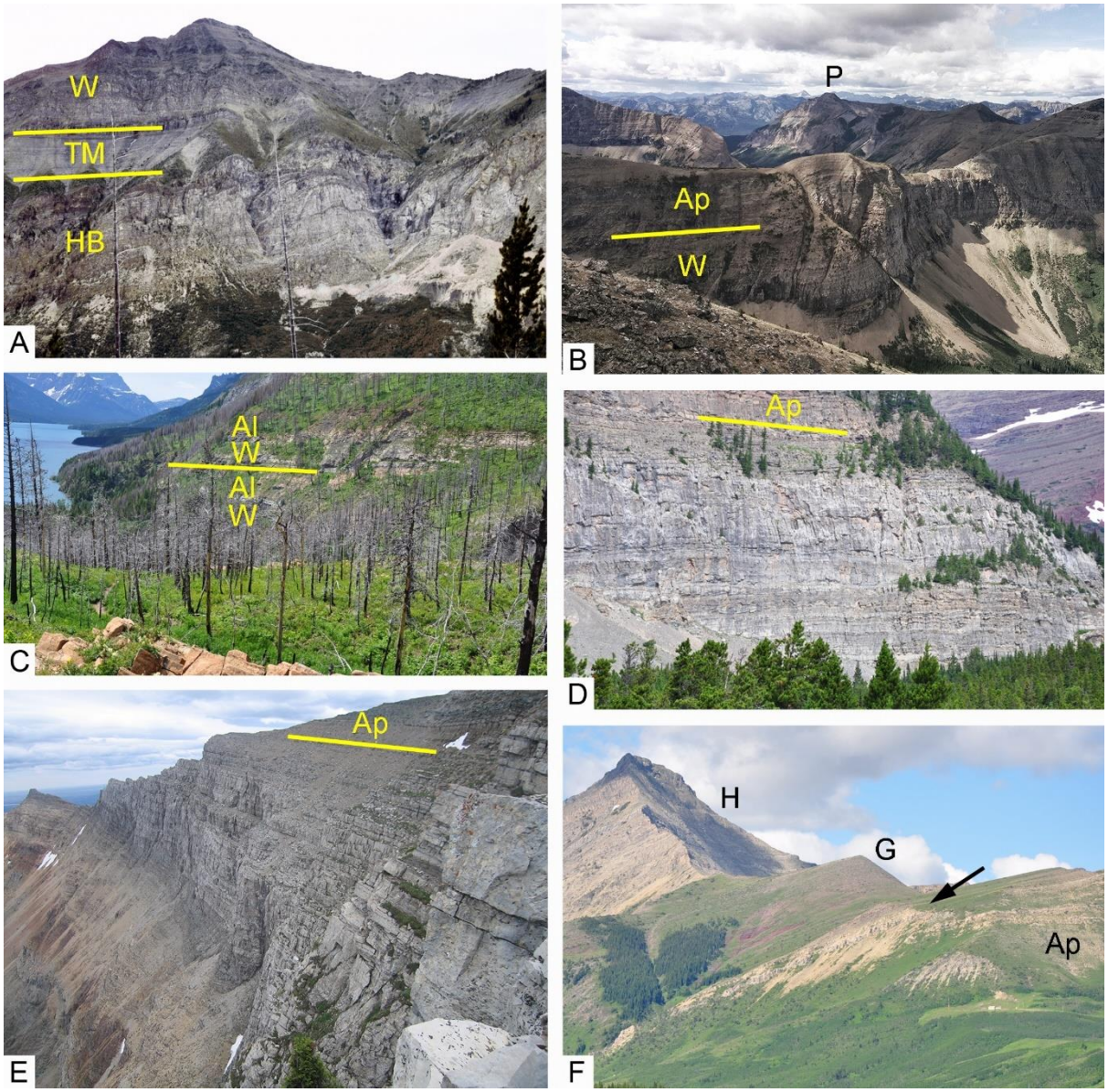

Fig. 3.4.

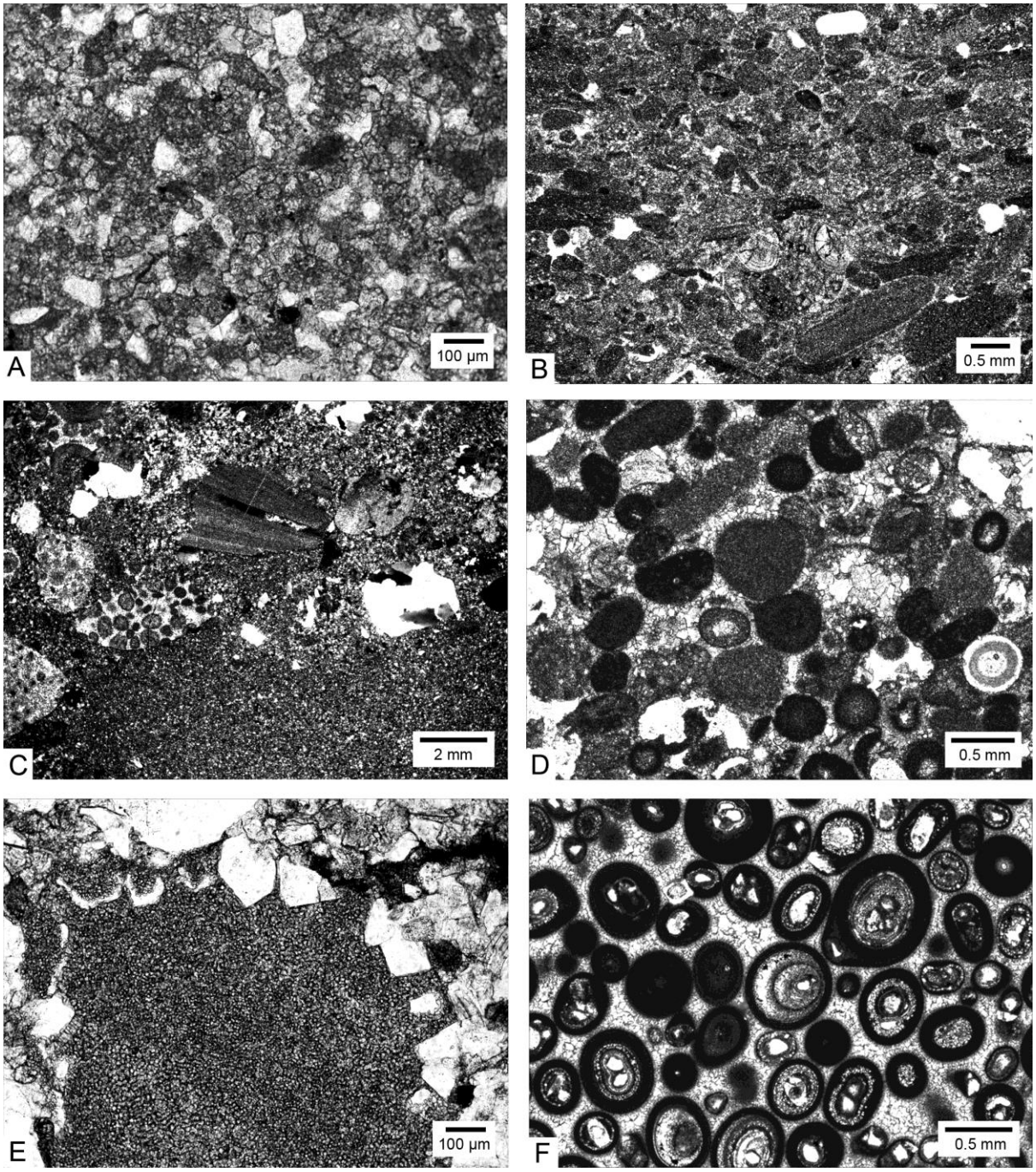

Fig. 3.5.

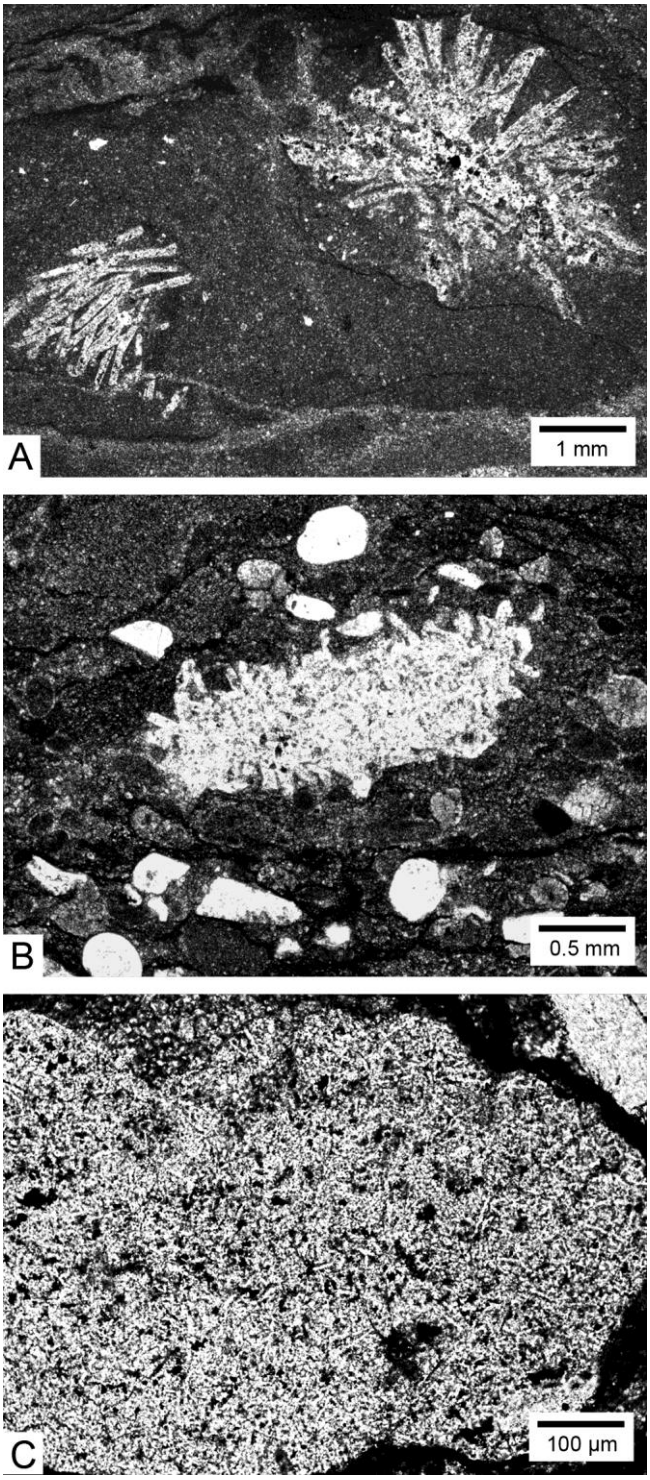

Fig. 3.6

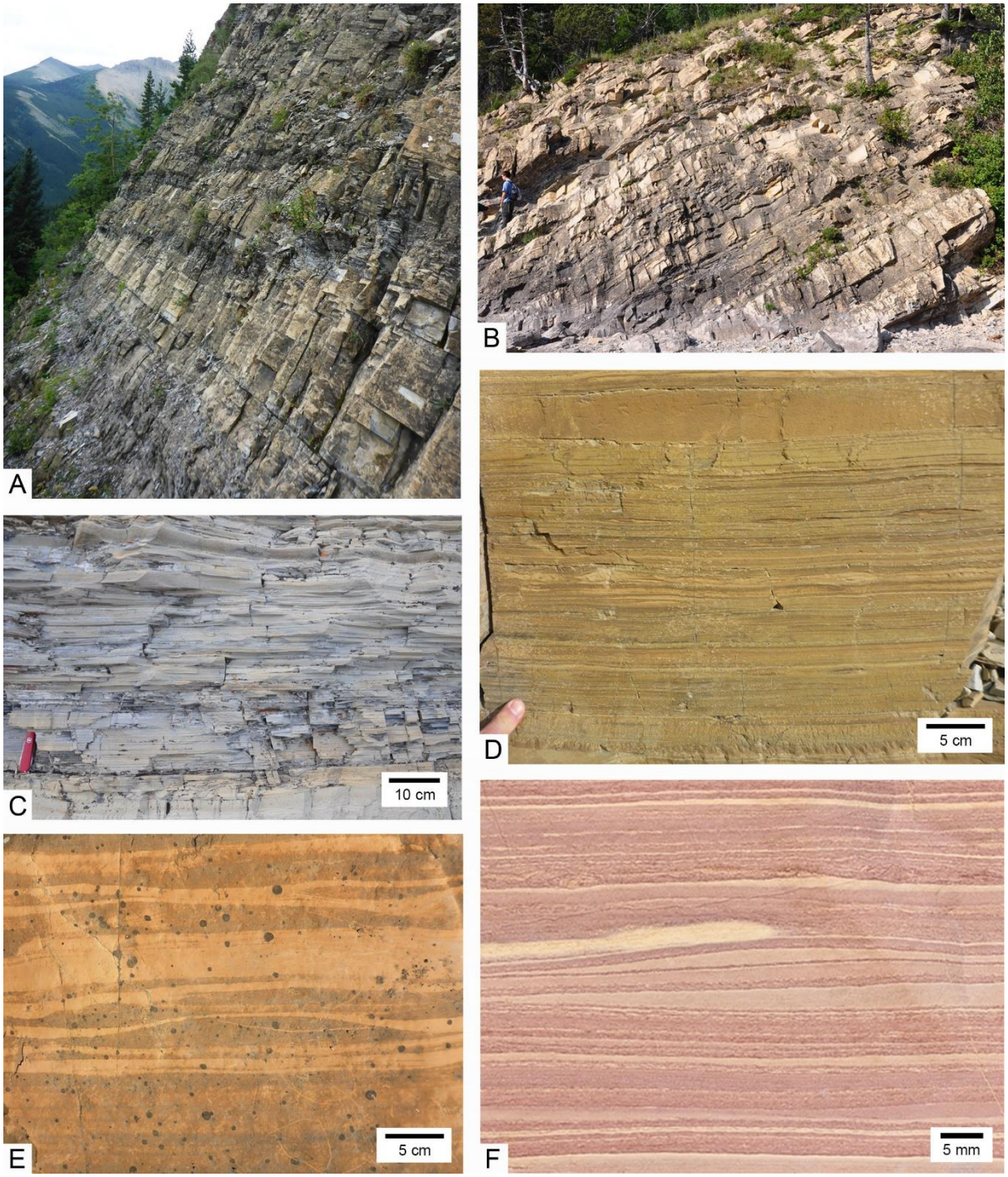

Fig. 3.7

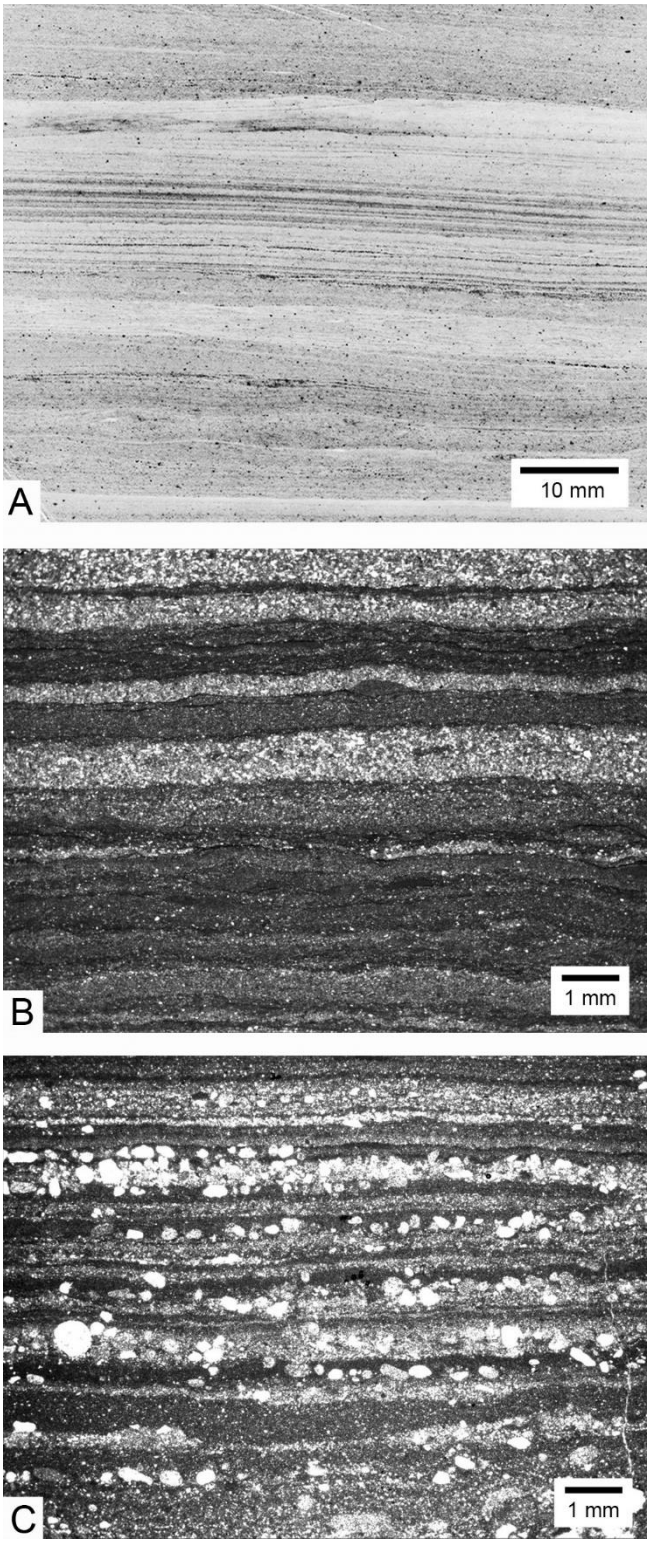

Fig. 3.8

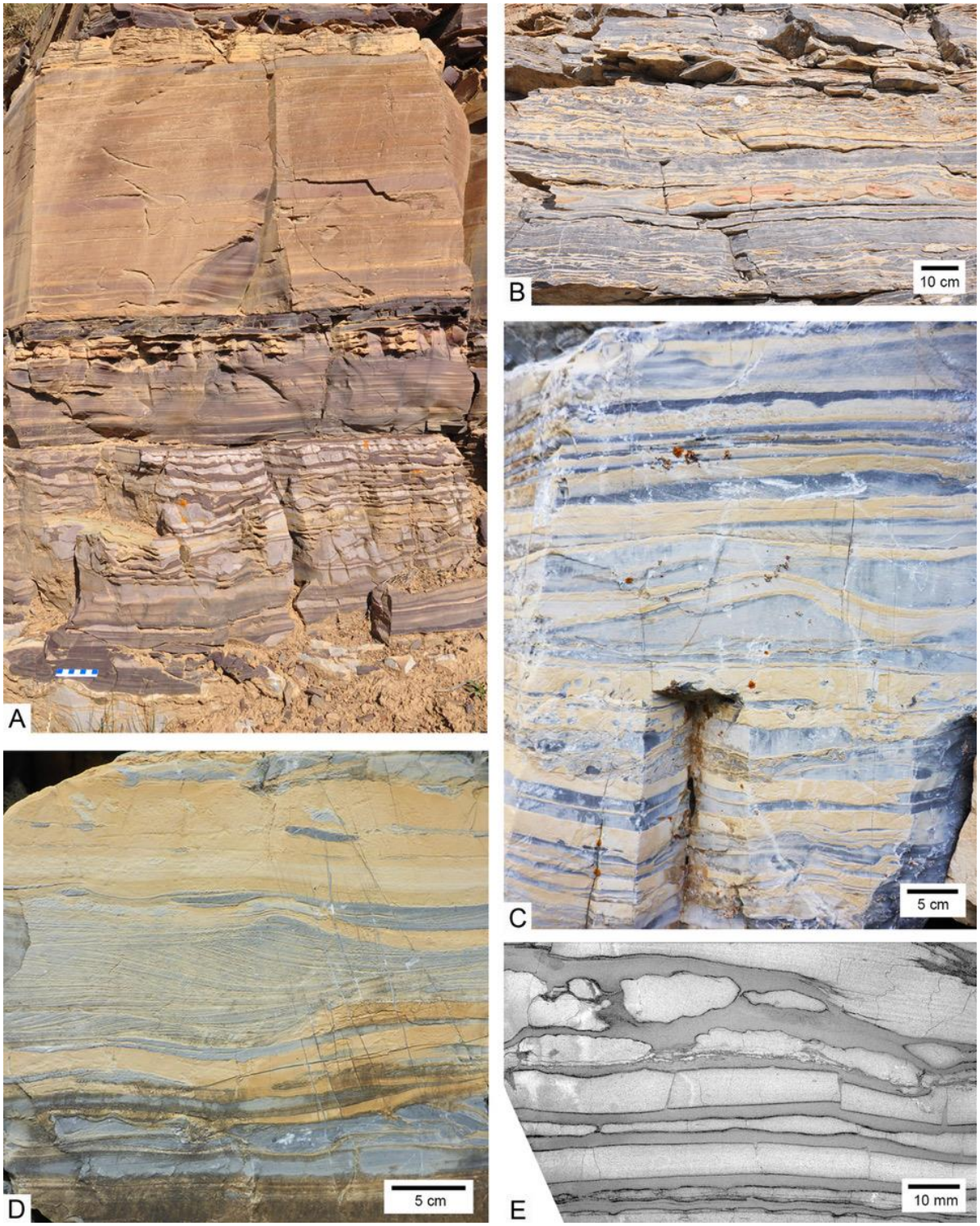

Fig. 3.9

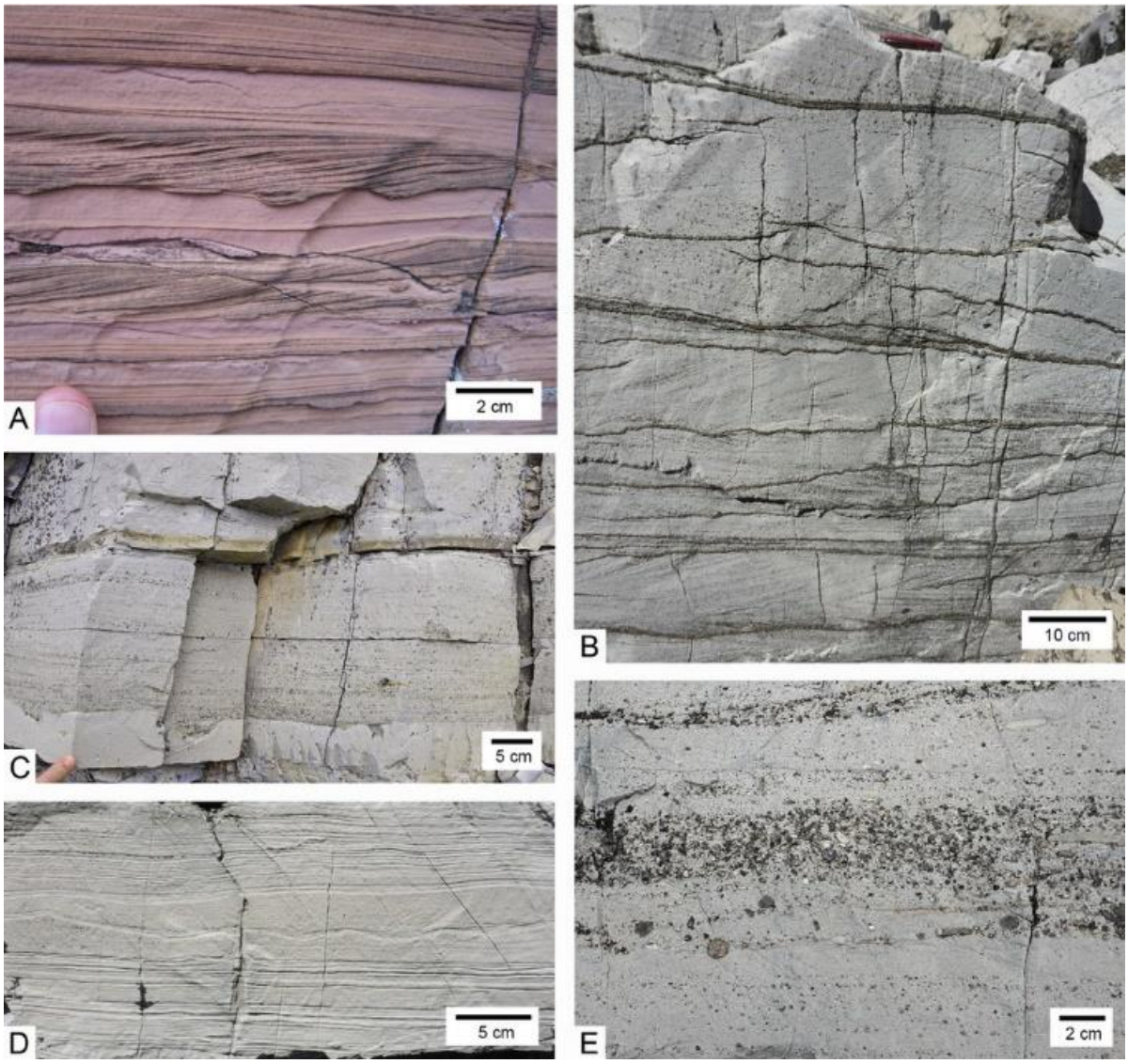

Fig. 3.10

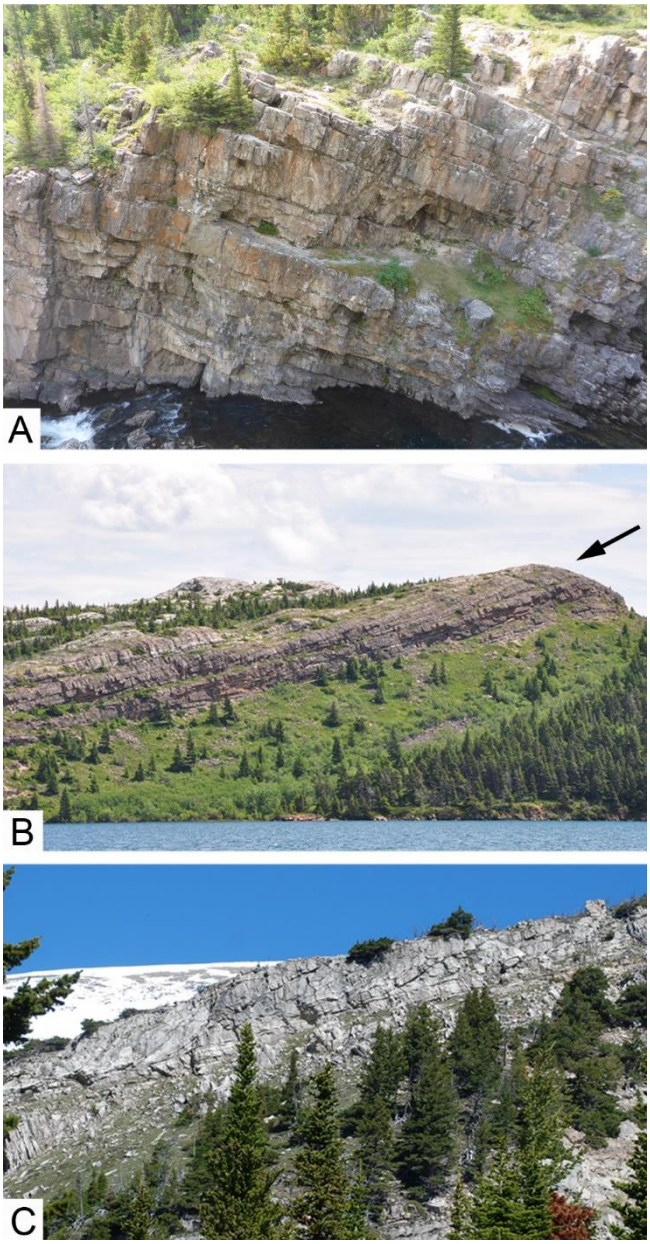

Fig. 3.11

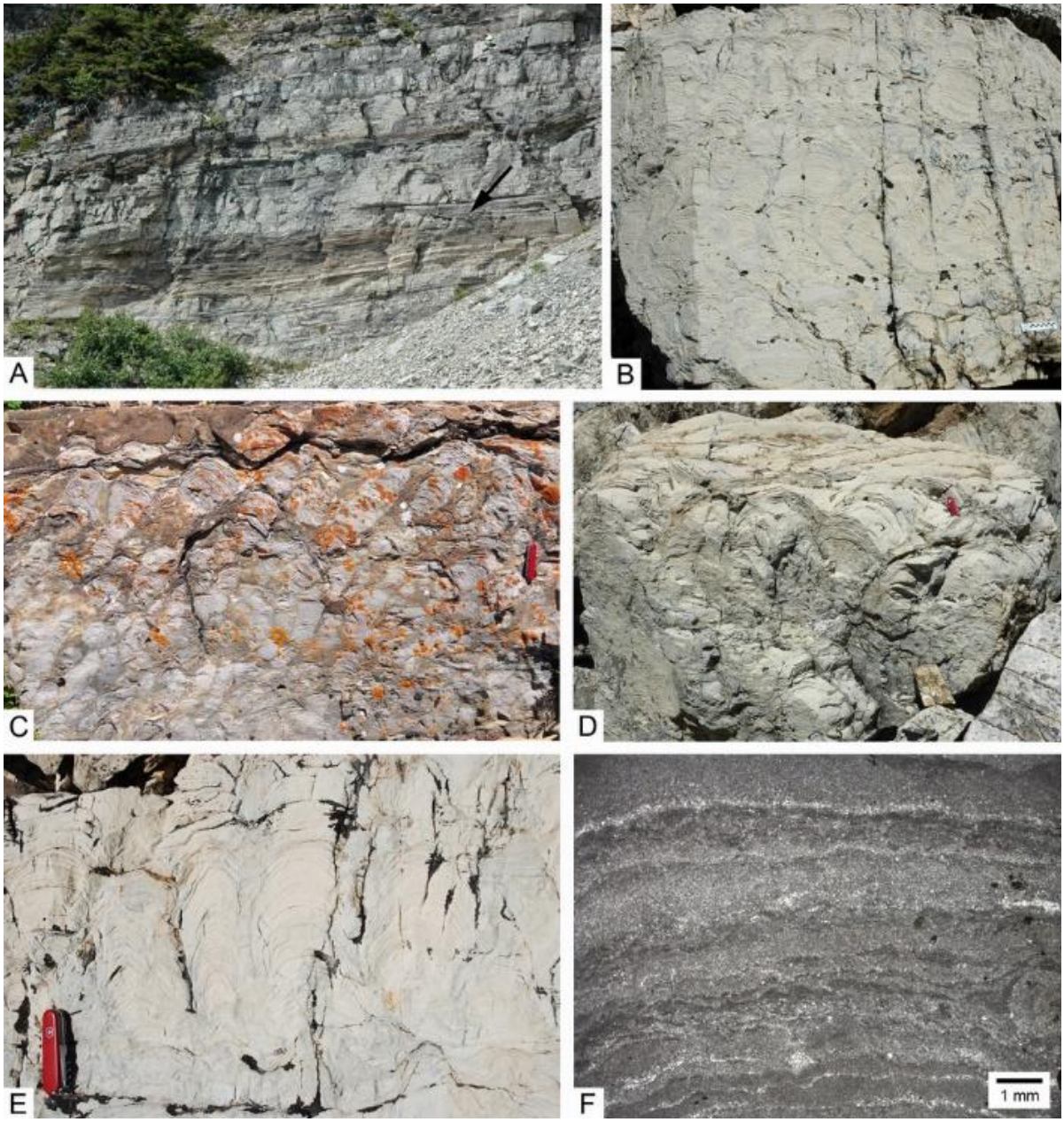

Fig. 3.12

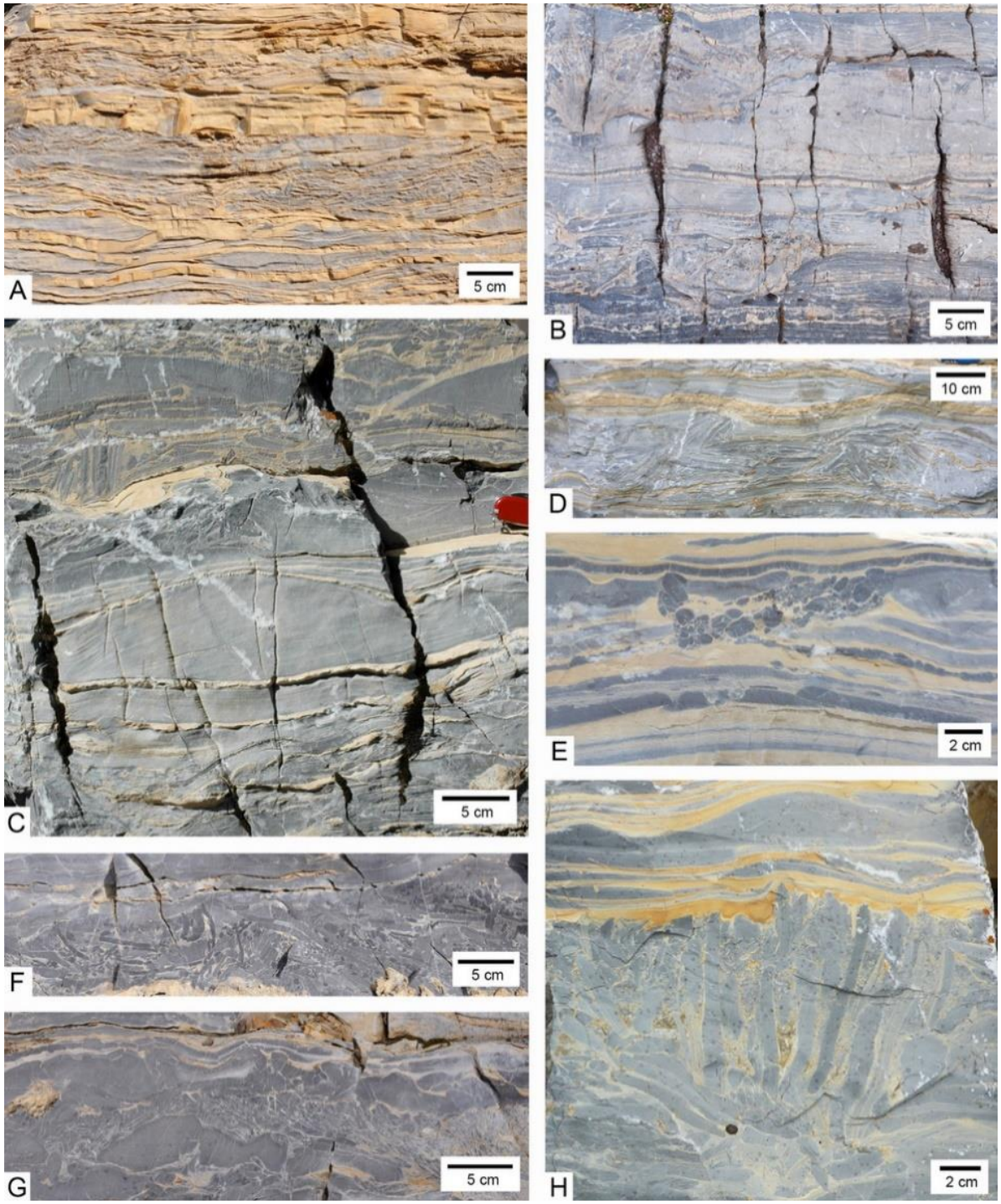

Fig. 3.13

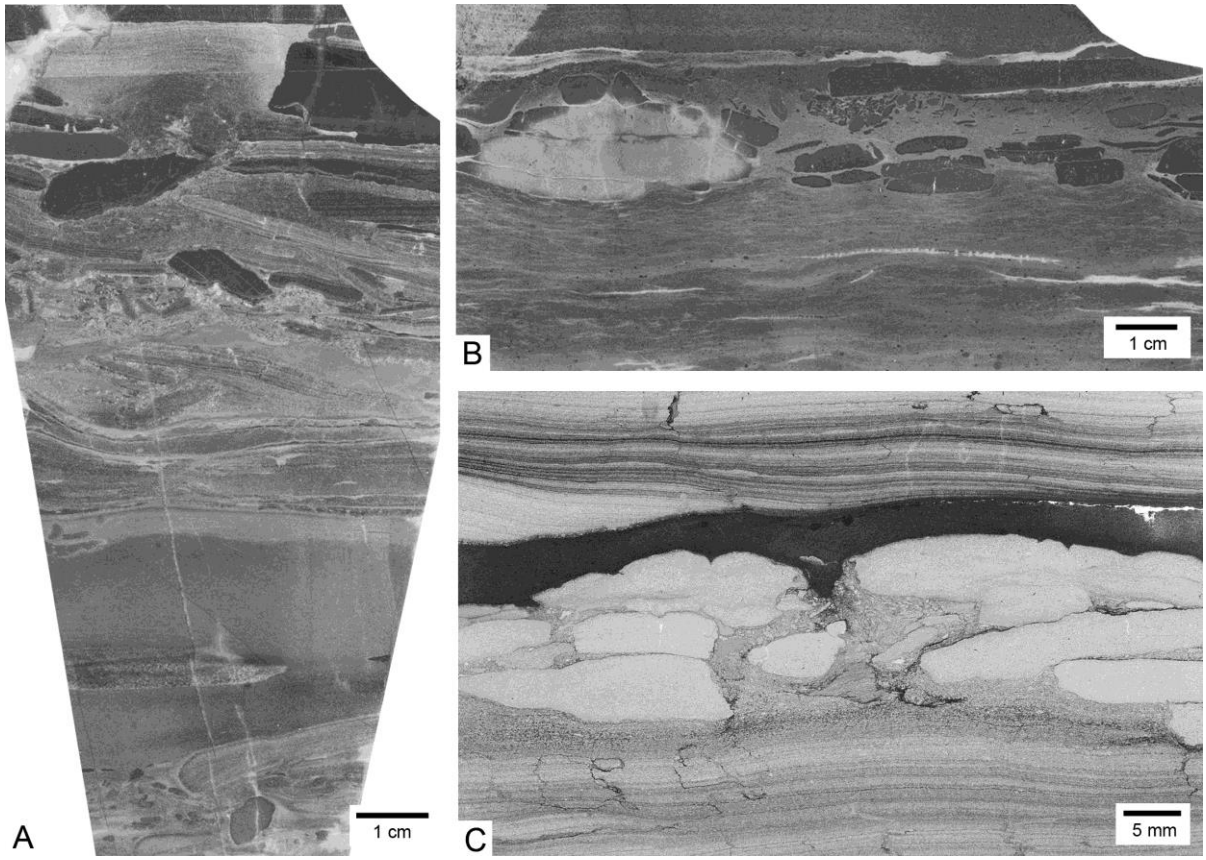

Fig. 3.14

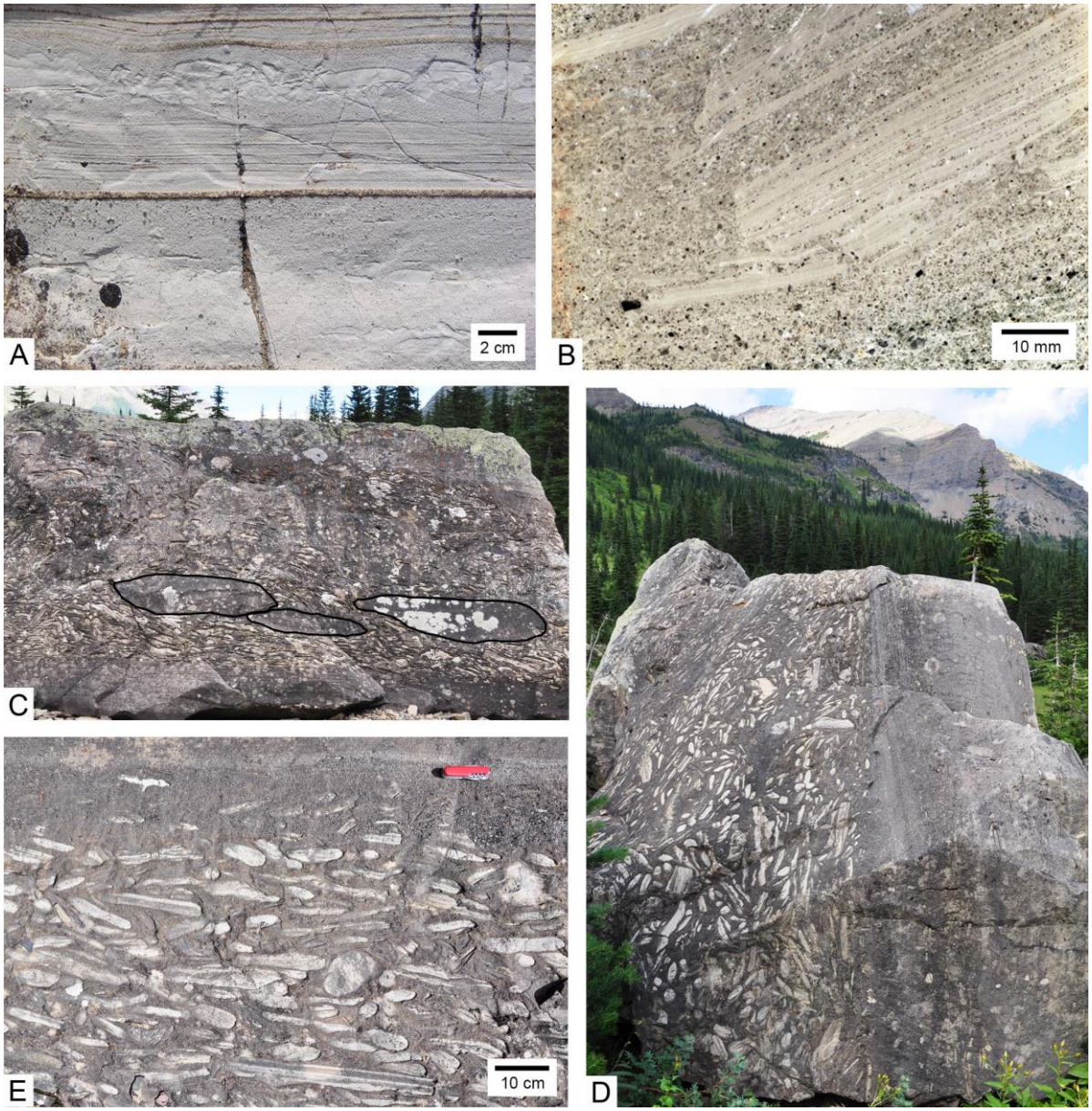

Fig. 3.15

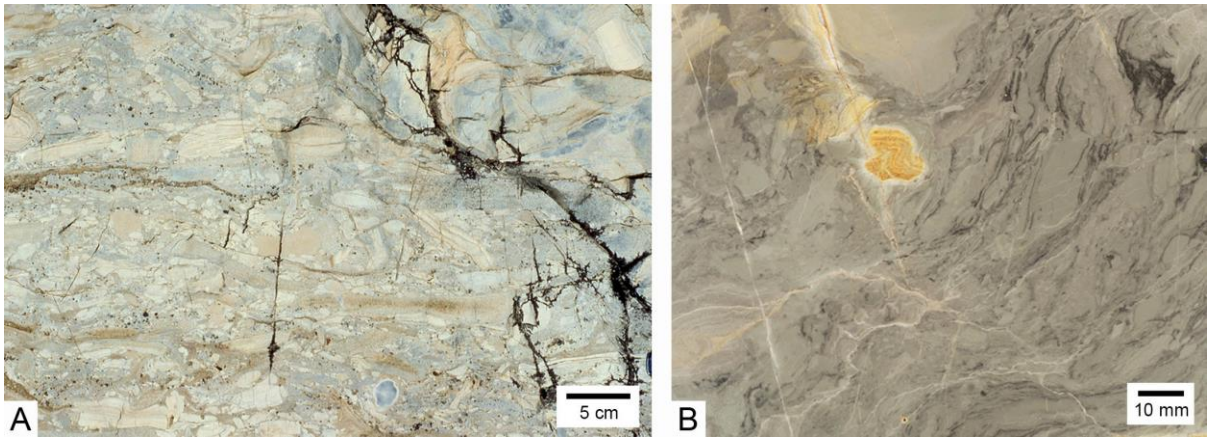

Fig. 3.16

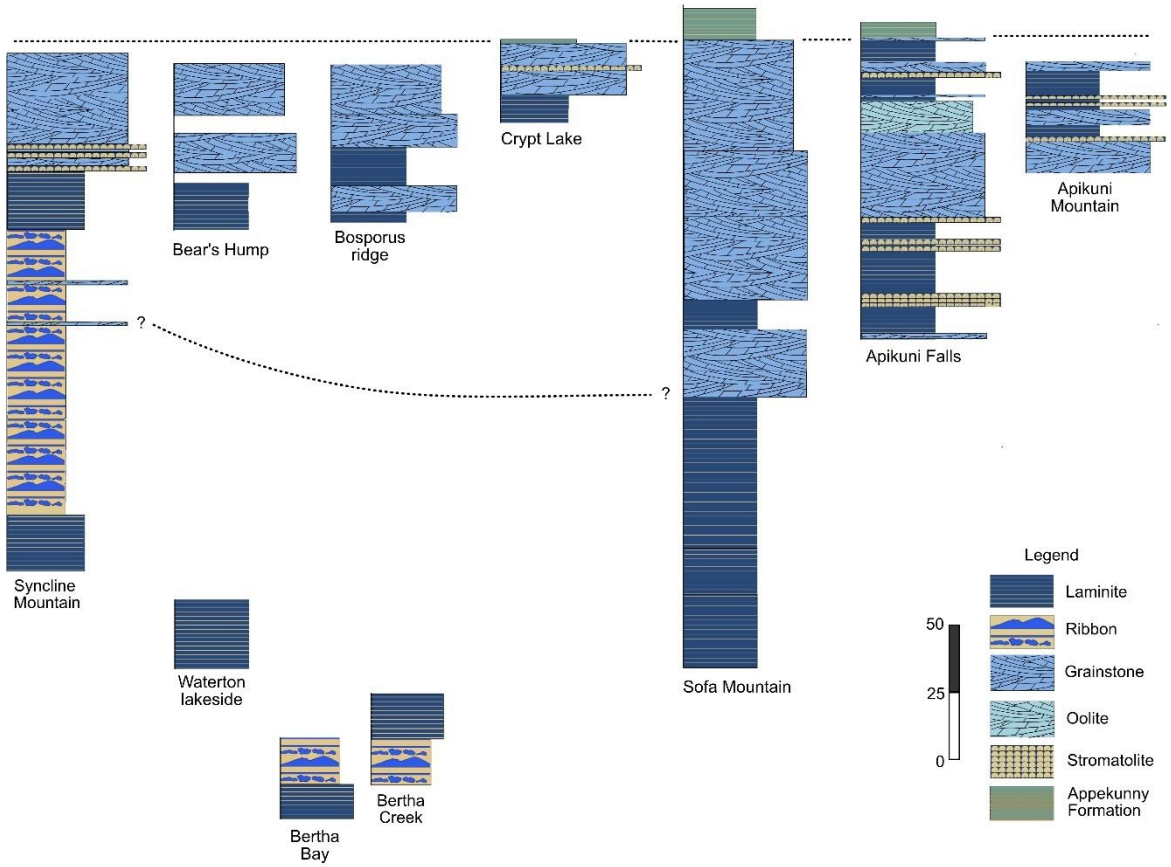
Syncline Mountain
Bear's Hump
Bosporus ridge
Crypt Lake
Apikuni Mountain
Apikuni Falls
Sofa Mountain
Waterton lakeside
Bertha Bay
Bertha Creek
?
?
Legend
Laminite
Ribbon
Grainstone
Oolite
Stromatolite
Appekunny Formation
50
25
0

Fig. 3.17

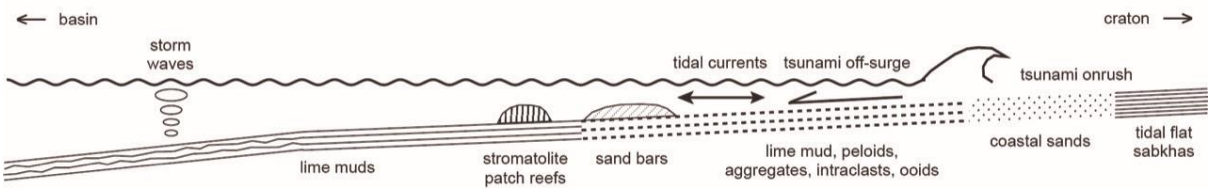
basin
craton
storm
waves
tidal currents
tsunami off-surge
tsunami onrush
lime muds
stromatolite
patch reefs
sand bars
lime mud, peloids,
aggregates, intraclasts, ooids
coastal sands
tidal flat
sabkhas

Fig. 3.18

CHAPTER 4

Synsedimentary deformation

1. Introduction

In situ synsedimentary deformation not due directly to gravitational instability, i.e. deposition and spontaneous failure on a sufficiently inclined slope, has been recognized in many different kinds of deposits and facies. The various types fall into two main categories: brittle deformation and soft-sediment deformation. Examples of the former are cracks, small-scale faults and breccias, while the latter includes small-scale folds and convolute lamination, ball-and-pillow and load structures, sedimentary sills and dikes of various dimensions (injectites), and shear veins, along with other features that involved liquefaction (e.g., Brothers et al., 1996; Pratt, 1998a, b, 2001a, 2002; Bachmann and Aref, 2005; Agnon et al., 2006; Montenat et al., 2007; El Taki and Pratt, 2012; Törő and Pratt, 2015a, b, 2016; Cobain et al., 2015; Mazumder et al., 2016; Egenhoff, 2017; Chatalov, 2017; Hill and Corcoran, 2018; Novak and Egenhoff, 2019; Matysik and Szulc, 2019; Hou et al., 2020). There are also hybrid features, reflecting the range of rheology that sediments can possess by virtue of particle size and shape, composition, cementation, interbedding, burial depth and so on. Although facies-controlled, some of these can be mistaken for primary sedimentary structures, such as shrinkage cracks and dikelets for desiccation cracks (Pratt, 1998a; Pratt and Ponce, 2019). A number of different mechanisms can be entertained for some of these structures in individual situations (e.g., Owen et al., 2011; Owen and Moretti, 2011; Owen and Santos, 2014; Gladstone et al., 2018), but in general most examples can be attributed to syndepositional earthquakes, and consequently they may be termed seismites.

The Belt Supergroup has been shown to be riddled with seismites of various types depending on rock type, including convolute bedding, microfaults, crack arrays due to shrinkage and injection, and molar-tooth structure (Pratt, 1994, 1998a, b, 1999, 2001b, 2017; Pratt and Ponce, 2019). Most of these features have been recognized in other stratigraphic units in other basins and in rocks of other ages. For example, while molar-tooth structure is common in lime mudstones in many Precambrian basins and has been assumed to be only a Proterozoic feature (e.g., James et al., 1998), essentially the same phenomenon has been recorded in Ordovician marine strata (Pratt, 1982, 2011) as well as Cretaceous (Rossetti, 2000; Rossetti and Góes, 2000) and Eocene lacustrine lime mudstones (Törő and Pratt, 2015a, b).

Pratt (1994) recorded abundant seismites in the middle Altyn Formation at Apikuni Falls, and compared their stratigraphic distribution with the stacking pattern of what were then held to be cyclic, shallowing-upward, peritidal facies (White, 1984). This study now rejects that environmental interpretation and shows that the Laminite facies was deposited under relatively low-energy, submerged conditions, while the interbedded sandy Grainstone facies is allochthonous, here considered to be tsunami backwash deposits (see Chapter 3). Nonetheless, the apparent lack of correlation between the seismites and facies still holds true. However, more plausibly it means that relatively proximal seismic activity that produced the seismites was mainly not the same as the fault movements that generated the tsunami events of sufficient magnitude to transport coastal sediment to the offshore depositional locale. This is evidence that the tsunami-generating normal faults were probably located in the basin centre which is thought to have been crossed by several regionally extensive fault systems that led to major differences in subsidence (Winston, 1986a, b). Episodic fault movement involving vertical displacement was presumably responsible.

The purpose of this chapter is to revisit the evidence for synsedimentary deformation in part of the lower Belt Supergroup, in order to better characterize the nature of the structures and their facies-dependence. Besides the fact that not all sediment types were susceptible to deformation, there are additional limitations in getting a sense of how common seismites are in the lowest units, in part because the Haig Brook and Tombstone Mountain formations were not examined in detail, and also because some features are subtle and difficult to discern or are virtually invisible on natural surfaces. For these reasons, the precise stratigraphic occurrence of seismites is not evaluated.

2. Synsedimentary deformation features

These features in the lower Belt Supergroup are subdivided into two groups, soft-sediment deformation features and brittle deformation features. In the former are ball-and-pillow structures, folds, pinch-and-swell structures, veins and dikelets, and molar-tooth structure, while in the latter are cracks, microfaults of various geometries, cataclasites and breccias.

2.1. Ball-and-pillow structures

2.1.1. Description

Ball-and-pillow structures occur sporadically in Grainstone facies and are sandwiched between undeformed beds. The largest comprise an interval 4 m thick in the Altyn-like unit in the Appekunny Formation at Pincher Ridge. There and in the Altyn Formation at Syncline Mountain there are several intervals 0.4–1 m thick containing metre-sized examples (Fig. 4.1A). At Apikuni Falls, in one ~ 20 cm thick interval of interbedded grainstone and laminite in the middle Altyn Formation there are two ball-and-pillow structures nearly side by side. They are subrounded in shape, 40 cm in length, and subcircular to semicircular in vertical cross-section (Fig. 4.1B, C). Seen in vertical cross-section, each consists essentially of one or a series of nested recumbent folds with nearly horizontal fold axes. In one, intraclasts of Laminite facies are present in the inner and outer periphery; those on the outer periphery are folded and separated layers of laminite that underlay the grainstone bed and were caught up. Smaller ball-and-pillow structures in massive grainstone show alternating cusps with upward-pointing laminae separating bowl-shaped zones about 10 cm wide and a few centimetres thick with concave-up laminae (Fig. 4.1D). Some of these also show tilted fold axes.

2.1.2. Interpretation

Ball-and-pillow structures typically develop when a sandy bed sinks into a finer grained substrate due to liquefaction and loss of shear strength of the latter (e.g., Hildebrandt and Egenhoff, 2007; Törő and Pratt, 2015a). Examples in massive grainstone are somewhat different in that they developed in nearly homogeneous carbonate sand, yet with sufficient variation to permit more localized liquefaction. The sand in ball-and-pillow structures retains its original lamination, albeit deformed plastically by folding. Early interpretations ascribed ball-and-pillow structure and smaller load features to the density contrast between the two types of sediment and triggered by the sedimentation itself, causing foundering of the overlying layer into an underlying fluidized layer (e.g., Potter and Pettijohn, 1977; Allen, 1982). However, features such as tilted to horizontal fold axes and the incorporated intraclasts indicate that deformation occurred some time after deposition and after incipient cementation of laminite. This also rules out wave impact which has been proposed for some examples (Alfaro et al., 2002). The ball-and-pillow structures at Apikuni Falls were tilted

sideways but facing opposing directions, suggesting stresses of opposing directions. The nesting of the deformed layers points to protracted deformation or closely timed repetition of the deforming mechanism.

2.2. Folds

2.2.1. Description

Microfolded layers in the silt- and sand-bearing Laminite facies and laminae in Stromatolite facies are common in the lower and middle Altyn Formation and rare in the Ribbon facies of the Waterton Formation. Laterally discontinuous bundles of laminae up to about 5 cm thick are folded and disrupted over lateral distances of up to about 0.5 m (Fig. 4.2A, B). Folds are commonly recumbent and folded segments may be detached and in places stacked against each other. Domical shapes are locally present (White, 1984). Pinch-and-well structures are commonly present in enclosing laminae (see 2.3). In one case where the laminae overlie *Baicalia* stromatolites, the laminae are not just overturned but locally rolled up, and the limbs of the folds are up to about 10 cm in length (Fig. 4.2C). The fine lamination in Laminite facies of the lower Altyn Formation locally exhibits tight recumbent folds (Fig. 4.2D). Larger, more open folds are locally present in the Grainstone facies of the Altyn Formation and Ribbon facies of the Waterton Formation.

In some stromatolite patch reefs in the middle Altyn Formation at Apikuni Falls, *Baicalia* columns are tilted and separated from laterally adjacent columns roughly 20 cm in length by surfaces that are steep fault planes with small displacements. In some cases the stromatolites are compressed against these surfaces making them asymmetric around the growth axis, and the stromatolite laminae show tight undulations with a wavelength of a few millimetres to about 1 cm (Fig. 4.2E–G). Laminae are also locally dilated or cracked (see 2.6).

2.2.2. Interpretation

Folding in the Laminite and Grainstone facies was by intrastratral, lateral compression and bedding-parallel shearing of plastic layers, and affected intervals were bound by intact layers or those that developed pinch-and-swell structures. Domical shapes were misinterpreted as stromatolites (White, 1984). The rolled-up laminae suggest a back-and-forth sliding along bedding planes, and the friction between the deforming laminae and the confining layers was variable during deformation. The folding of laminae in variously oriented stromatolites was probably due to compression in variable directions during the deforming event. Folding of the laminite and microbial laminae attests to an overall plastic rheology at the time of deformation, but local disruption indicates brittle failure (e.g., Törő and Pratt, 2015a, 2016). The plasticity might have been enhanced by microbial binding, but this cannot be demonstrated. The stiffness may have been due to a response akin to strain hardening, say from porosity reduction during folding, or a later deformation event that affected the already deformed interval.

2.3. Pinch-and-swell structures

2.3.1. Description

The laminae in centimetre-thick intervals of the Laminite facies of the lower and middle Altyn Formation are locally pulled apart into small lenses or boudins a few millimetres to about 1 cm in length and up to about 1 mm in thickness, as well as pushed together into small

beads of similar size (Figs. 4.2B, 4.6A). This style of deformation occurs in thin intervals containing microfolds and microthrust faults (see 2.2, 2.7).

2.3.2. Interpretation

These small-scale features are soft-sediment deformation structures indicative of intrastratal shearing in varying directions, which caused somewhat cohesive laminae to be both stretched and compressed (e.g., El Taki and Pratt, 2012; Törő and Pratt, 2015a, 2016). They differ from 'loop bedding' as originally described, which, while also showing extension, consists of larger features and does not exhibit the small-scale boudin or beaded shapes (Calvo et al., 2002).

2.4. Veins and dikelets

2.4.1. Description

Irregular argillaceous vein arrays are locally present in beds of silty lime mudstone of the Ribbon limestone facies in the Waterton Formation in the Waterton area (Fig. 4.3A). Veins are about 100 µm wide, and range from bedding-parallel, to vertical in orientation to interconnected and zigzag in outline. In some cases they extend through the lime mudstone from crack tips.

Some dolomitic laminae in the Ribbon facies of the Waterton Formation contain arrays of closely spaced, short, mainly upward-opening V-shaped cracks about 5 mm long (Fig. 4.3B), or short, variably oriented, interconnected cracks several millimetres in length (Fig. 4.3C). The latter in particular impart a quasi-brecciated aspect to the host lamina. The crack fills merge into the overlying microcrystalline dolomite.

Short, downward- and upward-injected sand-filled dikelets are present in several intervals 1 cm thick in the Laminite facies of the middle Altyn Formation (Fig. 4.3D). The dikes are several millimetres wide and up to 5 mm long. On bedding planes they form polygonal crack networks (White, 1984, fig. 6).

2.4.2. Interpretation

These are various forms of dewatering features involving mobilization, segregation and injection of different grain sizes of sediment, although apart from the clay-filled veins, they are uncommon. Dewatering and clay concentration, probably in microfractures (Ogawa, 2019), took place under shallow burial while the carbonate mud was somewhat stiff due to incipient cementation. The likely mechanism was variably oriented stresses from shaking of the sea floor, which produced irregularly shaped veins which have been observed also in the Helena Formation (Pratt, 2001, fig. 12C; Pratt, 2017, fig. 8F) and elsewhere (El Taki and Pratt, 2012). However, the absence of oriented vein arrays (e.g., Brothers et al., 1996; Grimm and Orange, 1997; Ohsumi and Ogawa, 2008) is evidence that the deformation was not from uni-directional shear stress. The small dolomitic cracks suggest liquefaction and lime mud expulsion at the millimetre scale. The different kinds of features show a facies dependence. The tiny dolomitic veins are evidence for small-scale, upward-directed dewatering that carried with it some lime mud. Short sandy dikelets indicate downward injection of coarse sediment into concomitantly formed shrinkage cracks (Törő and Pratt, 2015a, 2016; Pratt and Ponce, 2019).

2.5. Molar-tooth structure

2.5.1. Description

Only two, 20 cm thick intervals with molar-tooth structure were observed, in a 3 m thick interval of lime mudstone of the Ribbon facies in the Waterton Formation near Bertha Creek. Tapering, microcrystalline calcite-filled veins range in length from less than 1 mm to just over 5 mm, are variably zigzag in shape, and are oriented nearly bedding-parallel, oblique to bedding, and vertical (Fig. 4.4A–C). While absent from the exposed Altyn Formation, well-rounded, sand-sized fragments of molar-tooth microsparry calcite or dolomite are present in many beds of Grainstone as well as Oolite facies and in the Altyn-like dolomite in the Appekunny Formation (see Chapter 3, section 4.1.).

2.5.2. Interpretation

Molar-tooth structure formed by localized, shallow intrastratal dewatering and granular lime mud expulsion from the host lime mud into concomitantly formed fissures (Pratt, 1998b, 1999, 2001a, 2011). The rare occurrence in the Waterton Formation indicates either that the lime mud was only occasionally texturally vulnerable to mobilization during cyclic loading and liquidization, or that the appropriate deformation event occurred rarely. Given the farily common presence of other synsedimentary deformation features, its rarity points to the former explanation. Microsparry grains in allochthonous sandy grainstones in the Altyn Formation indicate that shallower areas to the east were in places characterized by lime mud deposition and subject to this style of deformation, although the host facies is not preserved.

2.6. Cracks

2.6.1. Description

Lenses of planar- and cross-laminated, silty lime mudstone in the Ribbon facies in the Waterton Formation are locally cracked and pulled apart about 1 mm. Cracks are V-shaped, orientation is roughly vertical, and crack margins are more or less straight (Fig. 4.5A). The material filling the cracks is partly dolomitized lime mudstone from the thin interbeds between the cracked lime mudstone lenses. Thin beds may be ruptured and dislodged and the cracks are jagged (Fig. 4.5B). *Baicalia* stromatolite columns in the middle Altyn Formation at Apikuni Falls also exhibit cracks roughly perpendicular to lamination (Figs. 4.2G, 4.5C), as well as separation of hemispherical stromatolite laminae by 1 mm wide cracks (Fig. 4.5D). Some vertically cracked stromatolites have silt in the cracks (Fig. 4.5C), whereas the cracks that jacked apart laminae contain sparry calcite cement (Fig. 4.5D).

2.6.2. Interpretation

These are type I cracks indicating extension and brittle failure in the Ribbon and Stromatolite facies after incipient cementation imparted a degree of stiffness (e.g., El Taki and Pratt, 2012). Failure took place under shallow burial, and in the Ribbon facies was likely favoured by the contrast in rheology between the incipiently cementing lime mud lenses versus argillaceous laminae in between, when sufficiently strong stresses were applied. Cracking and dilation of stromatolite laminae took place when strong stresses were applied after they had become partially lithified so they were no longer prone to small-scale folding (see 2.2).

2.7. Microfaults

2.7.1. Description

Low-angle reverse (thrust) microfaults are locally present in the Laminite facies of the lower and middle Altyn Formation at Sofa Mountain and Apikuni Falls, respectively, which led to rupturing and tilting of layers (Fig. 4.6A). Pinch-and-swell structures are present in adjacent laminae (see 2.3). In some intervals the detachment surfaces are close to being bedding-parallel (Fig. 4.6B). The laminite under several lenticular beds of Grainstone facies shows drag folds and disruption indicating short-distance reverse movement of the coarse bed (Fig. 4.6C). At a number of levels there are larger, metre-scale, fault-bound interbedded laminite and grainstone bodies that have been tilted (Fig. 4.6D), and this is also present in a grainstone unit in the Altyn Formation at Syncline Mountain. In two 10 cm thick beds an array of parallel reverse faults and disruption and lateral translation led to tabular fault blocks (plates) several centimetres thick being stacked obliquely against each other in an en-échelon fashion (Fig. 4.6E, F).

Steep microfaults are present in the Laminite facies of the middle Altyn Formation. Arrays of oblique normal and reverse faults up to ~20 cm in length with displacement of a few millimetres to ~1 cm are locally common in the middle Altyn Formation in zones up to a metre or so in lateral extent. The faults are single fault planes which locally grade into anastomosed cracks. Some intervals up to about 10 cm in thickness exhibit a series of vertically to obliquely oriented faults, closely spaced arrays of steep faults of variable orientation, and arrays of subparallel normal or reverse faults (Fig. 4.7A–E). Displacement is typically a few millimetres. Fault zones in the same unit can switch orientation laterally, and also pass laterally to cataclasite (see 2.8).

2.7.2. Interpretation

The various kinds of small-scale faults are clearly synsedimentary but affected intervals of the Laminite facies of varying thickness after it started to become stiffer and prone to brittle failure. This stiffness would have been due to a combination of confining by overlying laminae plus incipient cementation. Deformation was intrastratal, under a small amount of burial in cases of low-angle reverse faults, and some tens of centimetres with steeper faults given their length. The various orientations of faults and degree of displacement attest to the combination of compression and extension, variable rheology, and possible variable magnitude of the applied stresses (e.g., El Taki and Pratt, 2012; Novak and Egenhoff, 2019). The discordant, metre-scale bodies resemble channel fills to a degree, but are displaced along slide planes (e.g., Knaust, 2000).

2.8. Cataclasites

2.8.1. Description

Thin lenses and laterally discontinuous beds of Laminite facies in the middle Altyn Formation at Apikuni Falls are brecciated into angular, blocky and tabular, granule- and small pebble-sized fragments of laminite in a matrix of sand-sized fragments and micrite (Fig. 4.8A–D). The lamination in the fragments shows variable orientation. Microfaults and disrupted laminae are commonly present in underlying layers (Fig. 4.8B), and in places the breccia passes laterally into arrays of steep microfaults. In at least one case the cataclasite

interval is overlain by mud-supported breccia containing poorly sorted laminite intraclasts (Fig. 4.8C).

2.8.2. Interpretation

These are autoclastic breccias and they indicate intrastratal, bedding-plane shearing and translation causing brittle failure of laminae that had acquired stiffness due to cementation. The equant shape of many fragments and crushed matrix suggests shearing was in multiple directions. The laterally impersistent nature of some cataclasites suggests that once failure was initiated its locale was further exploited such that brecciation was focused in that zone. On a small scale, the confining stress inhibits sliding such that localized stresses exceed grain strength causing breakage (Lucas and Moore, 1986). Similar features have been termed 'concordant breccias' (Kahle, 2002). Associated breccias suggest that in some cases shearing was accompanied by liquefaction and flow of the fragments and finer grained matrix (see 2.9).

2.9. Breccias

2.9.1. Description

A number of beds in the Ribbon facies in the Waterton Formation consist of lenses of granule- and pebble-size, blocky to tabular fragments, i.e. intraclasts, of thin mudstone laminae floating in a structureless, dolomitic mudstone matrix (Fig. 4.9A). The tabular intraclasts are oriented horizontally. Several intervals in the Laminite facies in the middle Altyn Formation at Apikuni Falls, on the other hand, exhibit horizontally oriented, angular, coarse sand- to granule-sized fragments of laminite in a structureless mudstone matrix (Fig. 4.9B–D). In some beds the intraclasts are in grain-to-grain contact (Fig. 4.9D). Many of the laminated intraclasts are microfolded, and in some beds the breccias pass vertically into folded laminae (Fig. 4.9B).

2.9.2. Interpretation

There is no evidence of unidirectional flow or current sorting, so deformation was in situ and took place intrastratally under shallow burial. These breccias point to rupturing of thin beds and laminae and mixing with liquefied lime mud during lateral flow but with only a small amount of overall transport. This argues that there has been bedding-parallel shear stresses that broke up laminae, combined with cyclic ground motion to cause liquefaction of interbedded lime mudstone creating a conglomeratic bed. The folded fragments and transition into microfolded laminae are evidence that during one or more episodes of deformation ductile behaviour evolved into brittle failure and liquefaction. This suggests that stresses became concentrated where rupture took place, rather than strain-hardening whereby laminated intervals became stiffer during the deformation event. It is possible, however, that more than one event affected these intervals. Similar fabrics consisting of fragments in structureless lime mudstone have been described by Kahle (2002) and Sarkar et al. (2014), among others.

3. Discussion

Taken together, these deformation features point to variably directed stresses of sufficient magnitude that acted on beds of sediment after they were deposited and under shallow burial.

The responses to these stresses ranged from loss of shear strength and liquefaction, dewatering, shrinkage and injection, folding, stretching and squeezing, and cracking, faulting and brecciation. Sediments behaved as fluids, deformed plastically or suffered brittle failure. Consequently, different facies exhibit different kinds of deformation features (Fig. 4.10).

A variety of mechanisms has been invoked to deform sediments in subaqueous settings, such as gravitational instability, wave impact, strong tidal bores, rapid sedimentation or subsurface fluid expulsion. However, these features have previously been interpreted to have been triggered by strong shaking of the sea floor by syndepositional earthquakes (Pratt, 1994), and alternative interpretations have been discounted for occurrences in the Belt Supergroup (Pratt, 1994, 1998b, 1999, 2001, 2017; Pratt and Ponce, 2019, as they have in many other comparable units (e.g., Alfaro et al., 2010; El Taki and Pratt, 2012; Törő and Pratt, 2015a, b, 2016; Liu et al., 2016; Mazumder et al., 2016; Rychliński and Jaglarz, 2017; Chatalov, 2017; Novak and Egenhoff, 2019; Pratt, 2019; Matysik and Szulc, 2019; Hou et al., 2020). The Waterton and Altyn formations lack evidence for directed downslope slumping, and these features occur mainly in lower energy facies and formed under the sediment–water interface. Hummocky cross-stratification from strong wave action is essentially absent, and cross-laminated sandy grainstones interpreted to have been worked by tidal currents show no deformation that can be related specifically to these currents. Deformation is post-depositional, such that even with ball-and-pillow structures is not a consequence of the sedimentation event itself. There is no evidence for a subsurface plumbing system that could have led to localized overpressuring and brecciation in, for example, vertical pipes. Hence, these deformation features considered 'seismites'.

Cyclic pore-pressure increase due to earthquake shock, i.e. shaking and loss of shear strength of the granular sediment, possibly modified by subsequent events, before further burial and lithification, accounts for the ball-and-pillow structures. The most likely cause of ductile deformation features, represented by microfolding and pinch-and-swell structures in the Laminite facies, is earthquake-induced, bedding-parallel shear stresses acting on plastic laminae. White (1984) presumed that the laminae in the middle Altyn Formation were bound by microbial mats, and this was thought to have influenced deformation because it made them cohesive (Pratt, 1994). This seems no longer certain without other evidence, but given that water depth may have been within the photic zone (see Chapter 3), microbial biofilms or mats may have been present and could have exerted some influence on rheology. Microfolding of the stromatolite laminae took place before cementation, and microbial material could have aided cohesion before cementation. Judging from the vertical extent of deformed laminae, cementation might not have occurred until 10–20 cm below the accreting surface.

Injection features, including molar-tooth structure, argillaceous veins and dikelets, were caused by mobilization, segregation, dewatering and injection of selective sediment types during shaking,. The rarity of sand-filled dikelets contrasts with the siliciclastic counterparts in the upper Appekunny and Grinnell formations and younger units which contain countless beds deformed in this fashion (Pratt, 1998a, 2017; Pratt and Ponce, 2019). This suggests that interbedded lime mud, silt and sand in the Laminite facies in the middle Altyn Formation was in general not vulnerable to shrinkage during cyclic pore pressure increase and dewatering. The rarity of molar-tooth structure was likely due to the type of lime mud in the platform, in that it was not dominated by granular particles and therefore not prone to mobilization with concomitant shrinkage of the matrix during injection. However, allochthonous particles composed of microspar do indicate that lime muds in the inner platform at times were conducive to the formation of this feature. This changed dramatically with deposition of the younger Helena Formation which is notable for the ubiquity of molar-tooth structure (Pratt, 1998b, 1999, 2001a, 2017).

Earthquake shock including vertical motions and back-and-forth translation causing bedding-parallel shearing created cracks in various relatively stiff lithologies, generated the cataclasites, and reworked brecciated material in a liquefied matrix. Various microfault geometries were due to stresses imposed on Laminite facies at various stages of stiffening due to early lithification.

Based on historical earthquakes, a minimum of M_s =~5.0 is typically considered necessary to trigger liquefaction and sediment mobilization (e.g., Galli, 2000; Papathanassiou et al., 2005), and possibly earthquakes of a greater magnitude were required for inducing brittle failure of the stiffer intervals. Because different facies recorded strong earthquakes with varying degrees of fidelity, this means that using seismites as a proxy seismometer has some limitations (Pratt, 1994, 2001b). Numerous horizons with 'slump folds' and other deformation features have been documented in turbiditic facies of the Prichard Formation (Cressman, 1985, 1989), but the relative abundance of seismites has yet to be determined. Nonetheless, they suggest that the Belt Basin was especially active tectonically from the beginning, which continued while the bathymetry shallowed and subsidence and sedimentation were more or less in balance (Pratt, 2017).

4. Conclusions

Synsedimentary deformation features ascribed to earthquakes, i.e. seismites, are common in the Lower Belt but their abundance reflects most importantly the rheological attributes of the specific sediment. Varying earthquake frequency may have played a role but with the variety of facies present, recognizable seismites are a proxy seismometer, albeit an imperfect one. Nonetheless, they attest to the high degree of syndepositional tectonic activity during the early phases of the Belt Basin. The abundance of seismites in succeeding units indicates that seismicity did not let up, even though the bathymetry of the basin was markedly reduced. It continued to subside at a dramatic rate.

The range of seismite types is comparable to that observed in many other units of Proterozoic and Phanerozoic ages. Some features, however, have not been recognized in the Waterton–Altyn succession. This includes dikes that cross-cut beds at the decimetre to metre scale (e.g. Törő and Pratt, 2016). Others include subparallel shear vein arrays such as sigmoidal features (Neuweiler et al., 1999; Chatalov, 2017). These differences are facies-dependent although the reasons are unclear.

The ever-growing body of literature on synsedimentary deformation features and evaluation of alternative mechanisms is pointing to earthquakes as the most common explanation. This will reveal important insights into the nature and behaviour of sediments and the role of tectonic activity, especially in basins without other evidence for faulting. In addition, a seismic origin for certain features identified as desiccation cracks and tepee structures, if correct, provides important new insight for the interpretation of the depositional setting.

References

Agnon, A., Migowski, C., Marco, S., 2006. Intraclast breccias in laminated sequences reviewed: Recorders of paleo-earthquakes. In: Enzel, Y., Agnon, A., Stein, M. (Eds.), New Frontiers in Dead Sea Paleoenvironmental Research. Geological Society of America Special Paper 401, pp. 195–214.

Alfaro, P., Delgado, J., Estévez, A., Molina, J.M., Moretti, M., Soria, J.M., 2002 Liquefaction and fluidization structures in Messinian storm deposits (Bajo Segura Basin, Betic Cordillera, southern Spain). International Journal of Earth Sciences 91, 505–513.

Alfaro, P., Gibert, L., Moretti, M., García-Tortosa, F.J., Sanz de Galdeano, C., Galindo-Zaldívar, J., López-Garrido, A.C., 2010. The significance of giant seismites in the Plio-Pleistocene Baza palaeo-lake (S Spain). Terra Nova 22, 172–179.

Allen, J.R.L., 1982. Sedimentary Structures Their Character and Physical Basis Volume II. Elsevier, Amsterdam, 662 pp.

Bachmann, G.H., Aref, M.A.M., 2005. A seismite in the Triassic gypsum deposits (Grabfeld Formation, Ladinian), southwestern Germany. Sedimentary Geology 180, 75–89.

Brothers, R.J., Kemp, A.E.S., Maltman, A.J., 1996. Mechanical development of vein structures due to the passage of earthquake waves through poorly consolidated sediments. Tectonophysics 260, 227–244.

Chatalov, A., 2017. Anachronistic and unusual carbonate facies in uppermost Lower Triassic rocks of the western Balkanides, Bulgaria. Facies 63, 24. [19 pp.]

Cobain, S.L., Hodgson, D.M., Peakall, J., Shiers, M.C., 2015. An integrated model of clastic injectites and basin floor lobe complexes: implications for stratigraphic trap plays. Basin Research 29, 816–835.

Cressman, E.R., 1985. The Prichard Formation of the lower part of the Belt Supergroup (Middle Proterozoic), near Plains, Sanders County, Montana. U.S. Geological Survey Professional Bulletin 1553, 64 pp.

Cressman, E.R., 1989. Reconnaissance stratigraphy of the Prichard Formation (Middle Proterozoic) and the early development of the Belt Basin, Washington, Idaho, and Montana. U.S. Geological Survey Professional Paper 1490, 78 pp.

Egenhoff, S.O., 2017. The lost Devonian sequence – Sequence stratigraphy of the middle Bakken member, and the importance of clastic dykes in the lower Bakken member shale, North Dakota, USA. Marine and Petroleum Geology 81, 278–293.

El Taki, H., Pratt, B.R., 2012. Syndepositional tectonic activity in an epicontinental basin revealed by deformation of subaqueous carbonate laminites and evaporites: Seismites in Red River strata (Upper Ordovician) of southern Saskatchewan, Canada. Bulletin of Canadian Petroleum Geology 60, 37–58.

Gladstone, C., McClelland, H.L.O., Woodcock, N.H., Pritchard, D., Hunt, J.E., 2018. The formation of convolute lamination in mud-rich turbidites. Sedimentology 65, 1800–1825.

Grimm, K.A., Orange, D.A., 1997. Synsedimentary fracturing, fluid migration, and subaqueous mass wasting: Intrastratal microfractured zones in laminated diatomaceous sediments, Miocene Monterey Formation, California, U.S.A. Journal of Sedimentary Research 67, 601–613.

Hildebrandt, C., Egenhoff, S., 2007. Shallow-marine massive sandstone sheets and indicators of palaeoseismic liquefaction – An example from the Ordovician shelf of Central Bolivia. Sedimentary Geology 202, 581–595.

Hill, C.M., Corcoran, P.L., 2018. Processes responsible for the development of soft-sediment deformation structures (SSDS) in the Paleoproterozoic Gordon Lake Formation, Huronian Supergroup, Canada. Precambrian Research 310, 63–75.

Hou, Z., Chen, S., Zhang, S., Yang, H., 2020. Sedimentary deformation features as evidence for paleoseismic events in the middle Eocene in the Dongying Depression of the southern Bohai Bay Basin, eastern China. Canadian Journal of Earth Sciences 57, 954–970.

James, N.P., Narbonne, G.M., Sherman, A.G. 1998. Molar-tooth carbonates: shallow subtidal facies of the Mid- to Late Proterozoic. Journal of Sedimentary Research 68, 716-722.

Kahle, C.F., 2002. Seismogenic deformation structures in microbialites and mudstones, Silurian Lockport Dolomite, northwestern Ohio, U.S.A. Journal of Sedimentary Research 72, 201–216.

Knaust, D., 2000. Signatures of tectonically controlled sedimentation in Lower Muschelkalk carbonates (Middle Triassic) of the Germanic Basin. Zentralblatt für Geologie und Paläontologie I 1998, 893–924.

Liu, L., Zhong, Y., Chen, H., Xu, Ch., Wu, K., 2016. Seismically induced soft-sediment deformation structures in the Palaeogene deposits of the Liaodong Bay Depression in the Bohai Bay basin and their spatial stratigraphic distribution. Sedimentary Geology 342, 78–90.

Lucas, S.E., Moore, J.C. 1986. Cataclastic deformation in accretionary wedges: Deep Sea Drilling Project Leg 66, southwestern Mexico, and on-land examples from Barbados and Kodiak Islands. In: Moore, J.C. (Ed.), Structural Fabric in DSDP Cores from Forearcs. Geological Society of America Memoir 166, pp. 89–109.

Matysik, M., Szulc, J., 2019. Shallow-marine carbonate sedimentation in a tectonically mobile basin, the Muschelkalk (Middle Triassic) of Upper Silesia (southern Poland). Marine and Petroleum Geology 107, 99–115.

Mazumder, R., van Loon, A.J., Malviya, V.P., Arima, M., Ogawa, Y., 2016. Soft-sediment deformation structures in the Mio-Pliocene Misaki Formation within alternating deep-sea clays and volcanic ashes (Miura Peninsula, Japan). Sedimentary Geology 344, 323–335.

Montenat, C., Barrier, P., Ott d'Estevou, P., Hibsch, C., 2007. Seismites: an attempt at critical analysis and classification. Sedimentary Geology 196, 5–30.

Neuweiler, F., Peckmann, J., Ziems, A., 1999. Sinusoidally deformed veins ("Sigmoidalklüftung") in the Lower Muschelkalk (Triassic, Anisian) of Central Germany: sheet injection structures deformed within the shallow subsurface. Neues Jahrbuch für Geologie und Paläontologie Abhandlungen 214, 129–148.

Novak, A. Egenhoff, S., 2019. Soft-sediment deformation structures as a tool to recognize synsedimentary tectonic activity in the middle member of the Bakken Formation, Williston Basin, North Dakota. Journal of Marine and Petroleum Geology 105, 124–140.

Ogawa, Y., 2019. Conceptual consideration and outcrop interpretation on early stage deformation of sand and mud in accretionary prisms for chaotic deposit formation. Gondwana Research 74, 31–50.

Ohsumi, T., Ogawa, Y., 2008. Vein structures, like ripple marks, are formed by short-wavelength shear waves. Journal of Structural Geology 30, 719–724.

Owen, G., Moretti, M., 2011. Identifying triggers for liquefaction-induced soft-sediment deformation in sands. Sedimentary Geology 235, 141–147.

Owen, G., Santos, M.G.M., 2014, Soft-sediment deformation in a pre-vegetation river system: the Neoproterozoic Torridonian of NW Scotland. Proceedings of the Geologists' Association 125, 511–523.

Owen, G., Moretti, M., Alfaro, P., 2011. Recognising triggers for soft-sediment deformation: current understanding and future directions. Sedimentary Geology 235, 133–140.

Papathanassiou, G., Pavlides, S., Christaras, B., Pitilakis, K., 2005. Liquefaction case histories and empirical relations of earthquake magnitude versus distance from the broader Aegean region. Journal of Geodynamics 40, 257–278.

Potter, P.E., Pettijohn, F.J., 1977. Paleocurrents and Basin Analysis [2nd edn.]. Springer, Berlin, 425 pp, 30 pls.

Pratt, B.R., 1982. Limestone response to stress: Pressure solution and dolomitization—discussion and examples of compaction in carbonate sediments. Journal of Sedimentary Petrology 52: 323–327.

Pratt, B.R., 1994. Seismites in the Mesoproterozoic Altyn Formation (Belt Supergroup), Montana: A test for tectonic control of peritidal carbonate cyclicity. Geology 22, 1091–1094.

Pratt, B.R., 1998a. Syneresis cracks: subaqueous shrinkage in argillaceous sediments caused by earthquake-induced dewatering. Sedimentary Geology 117, 1–10.
Pratt, B.R., 1998b. Molar-tooth structure in Proterozoic carbonate rocks: Origin from synsedimentary earthquakes, and implications for the nature and evolution of basins and marine sediment. Geological Society of America Bulletin 110, 1028–1045.
Pratt, B.R., 1999. Gas bubble and expansion crack origin of molar-tooth calcite structures in the Middle Proterozoic Belt Supergroup, western Montana—Discussion. Journal of Sedimentary Research 69, 1136–1140.
Pratt, B.R., 2001a. Oceanography, bathymetry and syndepositional tectonics of a Precambrian intracratonic basin: integrating sediments, storms, earthquakes and tsunamis in the Belt Supergroup (Helena Formation, ca. 1.45 Ga), western North America. Sedimentary Geology 141–142, 371−394.
Pratt, B.R., 2001b. Septarian concretions: internal cracking caused by synsedimentary earthquakes. Sedimentology 48, 189–213.
Pratt, B.R., 2002. Tepees in peritidal carbonates: origin via earthquake-induced deformation, with example from the Middle Cambrian of western Canada. Sedimentary Geology 153, 57–64.
Pratt, B.R., 2011. Molar-tooth structure. In: Reitner, J., Thiel, V. (Eds.), Encyclopedia of Geobiology. Springer, Dordrecht, pp. 662–666.
Pratt, B.R., 2017. The Mesoproterozoic Belt Supergroup in Glacier and Waterton Lakes national parks, northwestern Montana and southwestern Alberta: Sedimentary facies and syndepositional deformation. In: Hsieh, J.C.C. (Ed.), Geologic Field Trips of the Canadian Rockies: 2017 Meeting of the GSA Rocky Mountain Section. Geological Society of America Field Guide 48, pp. 123–135.
Pratt, B.R., 2019. Discussion: "Depositional setting of the 2.1 Ga Francevillian macrobiota (Gabon): Rapid mud settling in a shallow basin swept by high-density sand flows" by Reynaud *et al.* (2018) Sedimentology 65, 670–701. Sedimentology 66, 774–776.
Pratt, B.R., Ponce, J.J., 2019. Sedimentation, earthquakes, and tsunamis in a shallow, muddy epeiric sea: Grinnell Formation (Belt Supergroup, ca 1.45 Ga), western North America. Geological Society of America Bulletin 131, 1411–1439.
Rossetti, D.F., 2000. Molar-tooth carbonates: Shallow subtidal facies of the mid- to Late Proterozoic: Discussion. Journal of Sedimentary Research 70, 1246–1248.
Rossetti, D.F., Góes, A.M., 2000. Deciphering the sedimentological imprint of paleoseismic events: an example from the Aptian Codó Formation, northern Brazil. Sedimentary Geology 135, 137–156.
Rychliński, T., Jaglarz, P., 2017. An evidence of tectonic activity in the Triassic of the Western Tethys: a case study from the carbonate succession in the Tatra Mountains (S Poland). Carbonates and Evaporites 32, 103–116.
Sarkar, S., Choudhuri, A., Banerjee, S., van Loon, A.J., Bose, P.K., 2014. Seismic and non-seismic soft-sediment deformation structures in the Proterozoic Bhander Limestone, central India. Geologos 20, 898–103.
Törő, B., Pratt, B.R., 2015a. Characteristics and implications of sedimentary deformation features in Eocene lacustrine and fluvial strata in the Uinta Basin, Utah and Colorado. In: Birgenheier, L., Ressetar, R., Vanden Berg, M. (Eds.), The Uinta Basin and Uinta Mountains: Utah Geological Association Publication 44, pp. 371–422.
Törő, B., Pratt, B.R., 2015b. Eocene paleoseismic record of the Green River Formation, Fossil Basin, Wyoming, U.S.A.: Implications of synsedimentary deformation structures in lacustrine carbonate mudstones. Journal of Sedimentary Research 85, 855–884.

Törő, B., Pratt, B.R., 2016. Sedimentary record of seismic events in the Eocene Green River Formation and its implications for regional tectonics on lake evolution (Bridger Basin, Wyoming). Sedimentary Geology 344, 175–204.
Winston, D., 1986a. Sedimentation and tectonics of the Middle Proterozoic Belt Basin and their influence on Phanerozoic compression and extension in western Montana and northern Idaho. In: Peterson, J.A. (Ed.), Paleotectonics and Sedimentation in the Rocky Mountain Region, United States. American Association of Petroleum Geologists Memoir 41. pp. 87–118.
Winston, D., 1986b. Middle Proterozoic tectonics of the Belt basin, western Montana and northern Idaho. In: Roberts, S.M. (Ed.), Belt Supergroup: A Guide to Proterozoic Rocks of Western Montana and Adjacent Areas. Montana Bureau of Mines and Geology Special Publication 94, pp. 245–257.
White, B., 1984. Stromatolites and associated facies in shallowing-upward cycles from the Middle Proterozoic Altyn Formation of Glacier National Park, Montana. Precambrian Research 24, 1–26.

Figure Captions

Fig. 4.1. Soft-sediment deformation in the form of ball-and-pillow structures in Grainstone facies. (A) Large ball-and-pillow structure. Field of view is 3 m. Upper Altyn Formation, Syncline Mountain. (B) Ball-and-pillow structure with a nearly horizontal axial plane and the hinge facing right, with the lower layers of Laminite facies folded and brecciated at right and the upper layers brecciated at left. Middle Altyn Formation, Apikuni Falls. (C) Three nested ball-and-pillow structures with gently upward- and downward-inclined axial planes and the hinges facing left. From the same horizon and several metres to the right (east) of B. (D) Nested convex-downward laminae separated by upward-pointing cuspate laminae. Upper Altyn Formation (block), Apikuni Falls.

Fig. 4.2. Soft-sediment deformation in the form of folds. A–C, E–G, middle Altyn Formation, Apikuni Falls; D, lower Altyn Formation, Waterton lakeside. (A) Laminite facies with thin bed (middle) containing recumbent microfolds. (B) Sawn surface of Laminite facies showing folded and ruptured laminae, with pinch-and-swell structures in underlying laminae. (C) Top of stromatolite patch reef overlain by rolled up laminae. (D) Thin section photomicrograph (plane-polarized light) of Laminite facies with overturned fold (middle). (E) Brecciated and toppled columnar stromatolites with crumpled lamination. (F) Tilted stromatolite columns with crumpled laminae. (G) Optical scan of thin section of stromatolite laminae showing small-scale folding with cracked layers at top.

Fig. 4.3. Soft-sediment deformation in the form of veins and dikelets. (A) Laminated silty mudstone of Ribbon Limestone facies cut by irregularly vertical argillaceous veins. Waterton Formation, Bertha Creek. (B) Plane-laminated, variably argillaceous dolomudstone of Ribbon limestone facies with a layer containing an array of upward-widening veins. (C) Same sample as B with a different layer containing oblique and crisscrossing veins, grading upward into a breccia-like fabric. (D) Laminite facies showing short dikelets extending downward and upward from sandy grainstone laminae into laminated mudstone. Middle Altyn Formation, Apikuni Falls.

Fig. 4.4. Soft-sediment deformation in the form of molar-tooth structure in Ribbon limestone facies. Waterton Formation, Bertha Creek. (A) Planar-laminated silty lime mudstone (grey) with dolomite nodules (buff), grading upwards into dolomitic silty lime mudstone containing

contorted calcite-filled veins of molar-tooth structure. (B) Optical scan of acetate peel of cross-laminated silty lime mudstone containing dolomite nodule, overlain in turn by dolomite lamina (light-grey) and silty lime mudstone containing short calcite-filled veins. (C) Acetate peel photomicrograph of dolomitic lime mudstone containing inclined and contorted calcite microspar-filled veins. The more dolomitic areas are dark-coloured.

Fig. 4.5. Brittle deformation in the form of cracks. (A) Sawn and etched surface of Ribbon limestone facies showing upward-opening V-shaped cracks in planar-laminated silty lime mudstone. Waterton Formation, Bertha Creek. (B) Ribbon limestone facies containing disrupted beds of silty lime mudstone; cracks are preferentially dolomitized. Waterton Formation (block). (C) Optical scan of thin section of part of columnar stromatolite showing irregular crack oriented roughly at right angles to lamination. (D) Optical scan of thin section of part of columnar stromatolite showing cracked and dilated microbial laminae. C and D, middle Altyn Formation (block), Apikuni Falls.

Fig. 4.6. Brittle deformation in the form of low-angle, reverse (thrust) microfaults in Laminite facies. Lower Altyn Formation, Apikuni Falls. (A) Sawn surface showing microfaults and disrupted layers, with pinch-and-swell structures in underlying and overlying laminae. (B) Thin lenticular interval bound by a nearly bedding-parallel microfaults. (C) Laminite facies erosively overlain by lenticular bed of Grainstone facies, exhibiting translation along the oblique contact at its base forming microfaults. (D) Fault-bound, disrupted and tilted interval of interbedded grainstone and laminite facies. (E) Broadly lenticular bed sandwiched between undeformed Laminite facies, composed of disrupted, imbricated, steeply east-dipping and stacked plates 10 cm wide. (F) Imbricated, gently east-dipping plates, overlain by undeformed Laminite facies.

Fig. 4.7. Brittle deformation in the form of high-angle normal and reverse microfaults in Laminite facies. Middle Altyn Formation, Apikuni Falls. (A) Interval with array of closely spaced left- and right-dipping (west- and east- dipping) microfaults. (B) Interbedded laminite and wave-rippled sandy grainstone with lens of microfaulted laminite. (C) Sawn surface showing steep microfaults. (D) Optical scan of thin section showing closely spaced, steep reverse microfaults. (E) Thin section photomicrograph (plane-polarized light) of nearly vertical, anastomosing microfaults with up to a 0.5 mm throw.

Fig. 4.8. Brittle deformation in the form of cataclastites in Laminite facies. Middle Altyn Formation, Apikuni Falls. (A) Lenses of autoclastic breccia and bounding microfaults and associated microfolds. (B) Sawn surface showing microfaulted and locally, gently folded laminite grading upward into fractured laminate and cataclastite. This is overlain by laminite and in turn by a second cataclastite. (C) Sawn surface showing cataclastite layer overlain in turn by a thin interval of laminite and a breccia of laminite intraclasts in a liquefied lime mudstone matrix. (D) Optical scan of thin section of cataclastite layer sandwiched between undeformed laminae.

Fig. 4.9. Brittle deformation in the form of breccias in a liquefied matrix. (A) Sawn and etched surface showing flat-pebble and brecciated intraclasts in dolomudstone matrix. Waterton Formation, Bertha Creek. (B) Sawn surface of brecciated laminite fragments passing upward into folded laminite. (C) Sawn surface showing laminite fragments in mudstone matrix. (D) Optical scan of thin section showing laminite fragments in a silty mudstone matrix. B–D, middle Altyn Formation, Apikuni Falls.

Fig. 4.10. Summary table showing the occurrence of the various kinds of synsedimentary deformation features (along the left) in the five lithofacies types in the Waterton and Altyn formations (along the top). Molar-tooth structure is also inferred to have formed in inner platform lime muds during deposition of the Altyn Formation, but the host beds are not preserved.

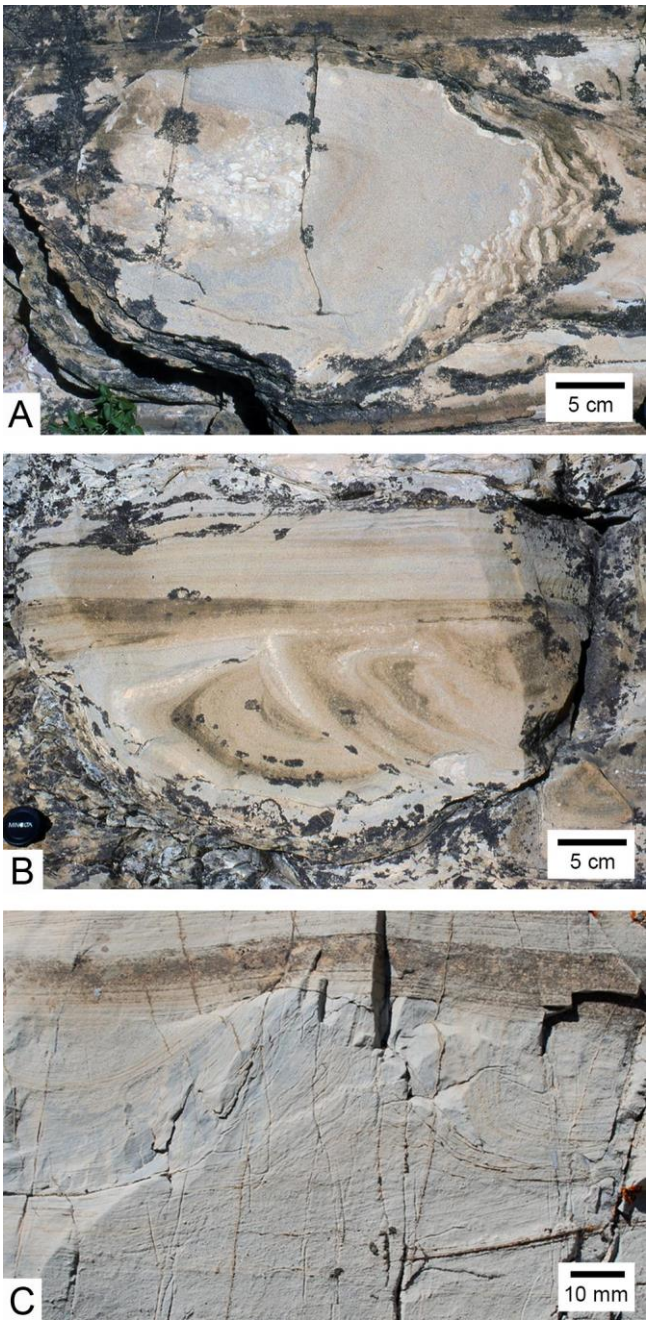

Fig. 4.1

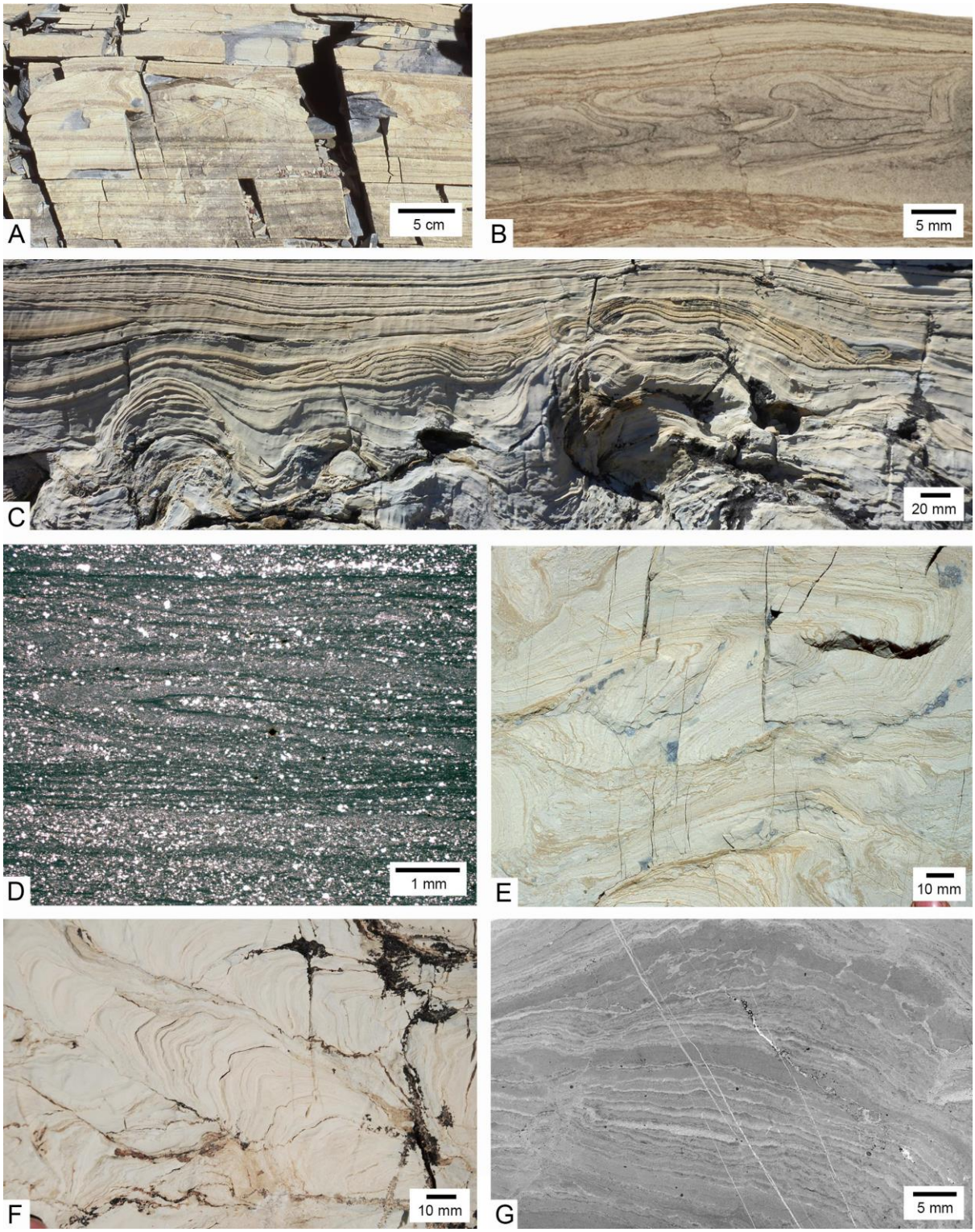

Fig. 4.2

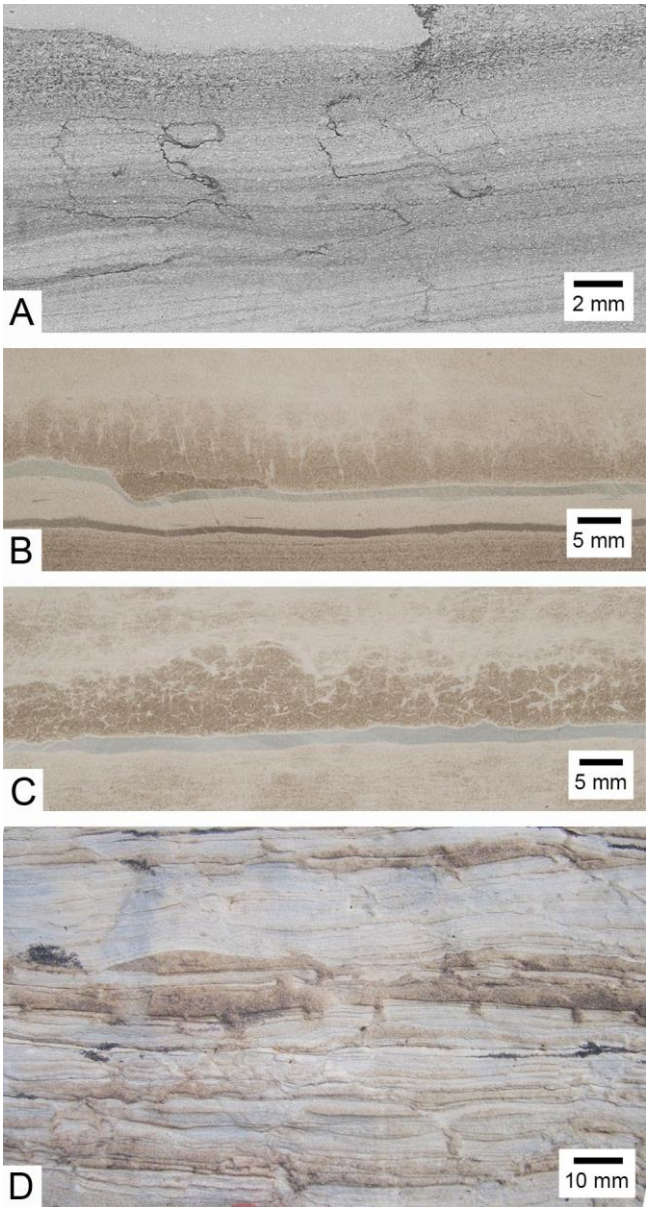

Fig. 4.3

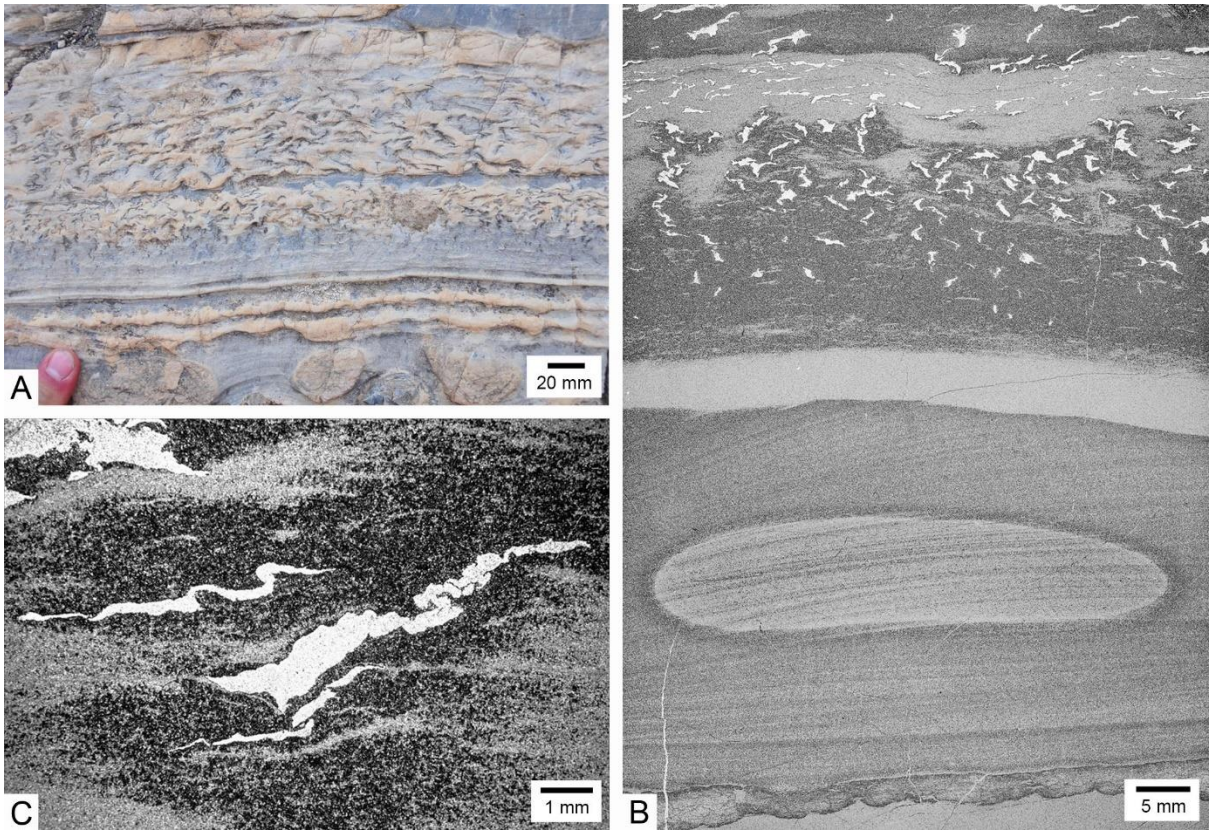

Fig. 4.4

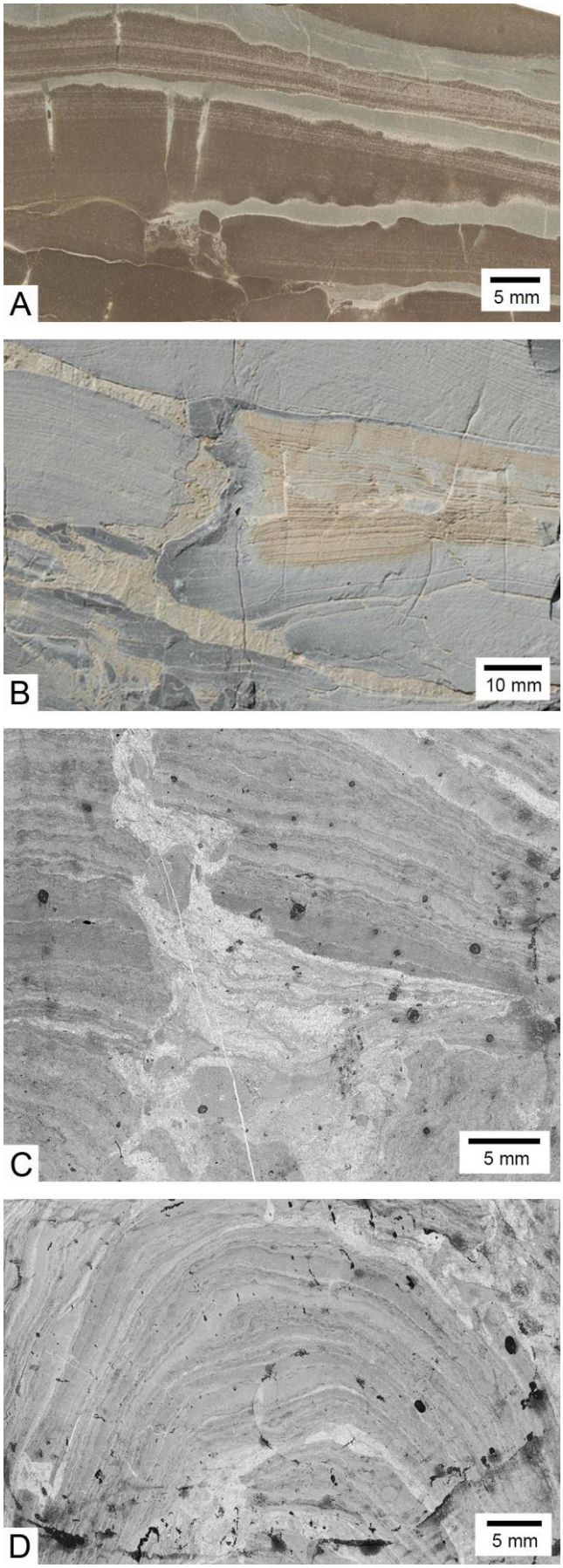

Fig. 4.5

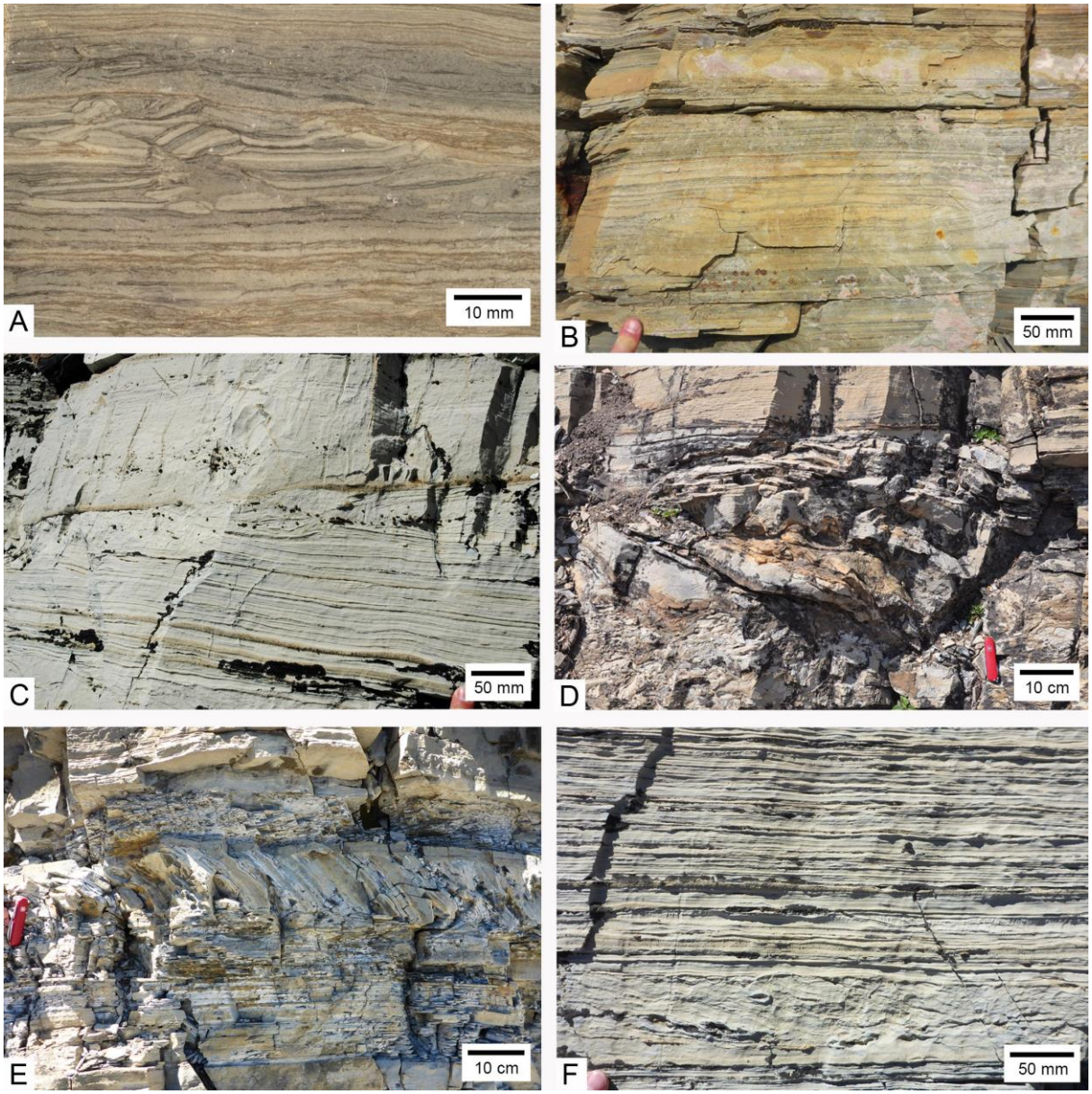

Fig. 4.6

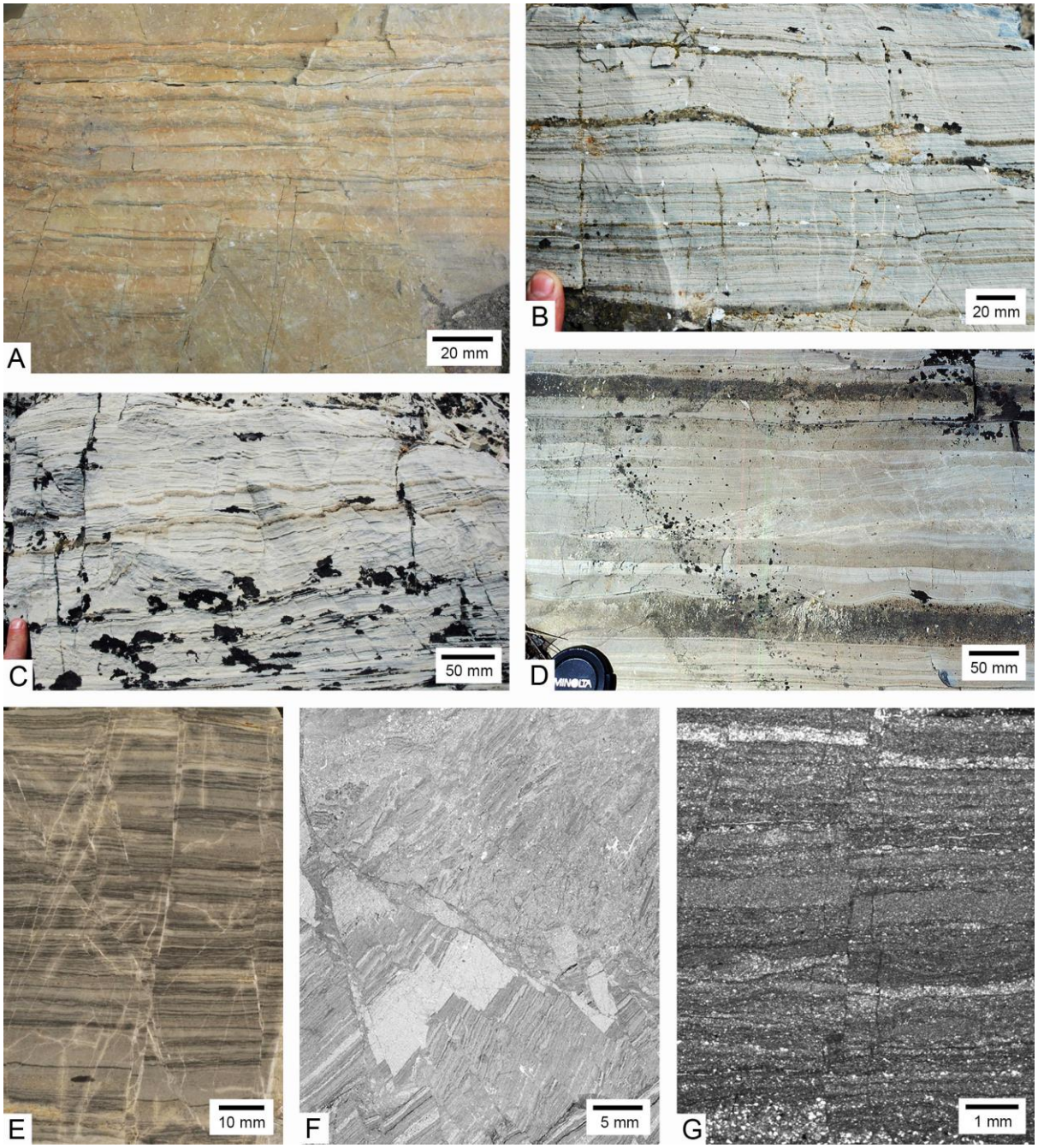

Fig. 4.7

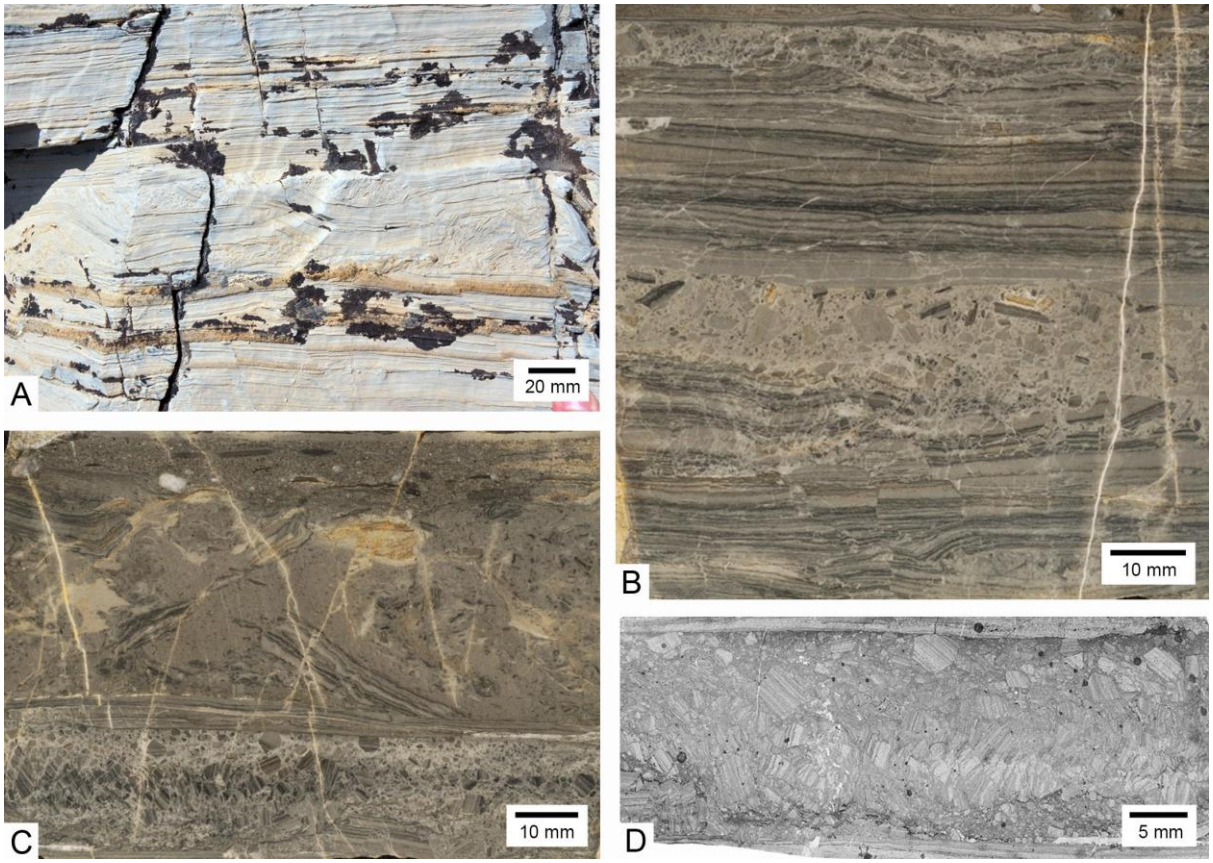

Fig. 4.8

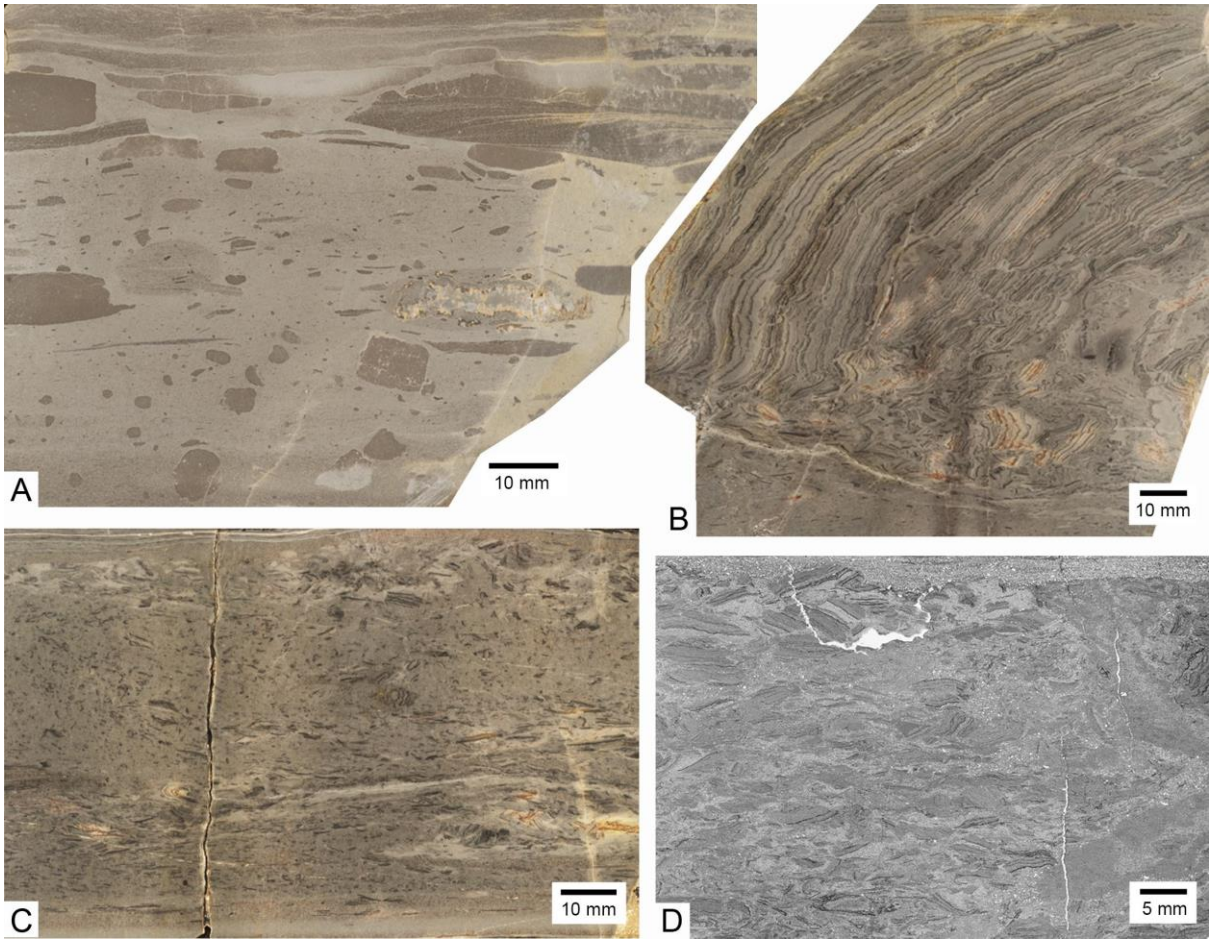

Fig. 4.9

	Laminite	Ribbon	Grainstone	Oolite	Stromatolite
Ball-and-pillow			■		
Folds	■	■			■
Pinch-and-swell	■				
Veins		■			
Dikelets	■				
Molar-tooth		■			
Cracks		■			■
Microfaults	■				
Cataclasites	■				
Breccias	■	■			

Fig. 4.10

CHAPTER 5

Conclusions

1. Accomplishments

This study has tackled two important questions posed by the nearly 1.5 billion-year-old Lower Belt portion of the Belt Supergroup (= Purcell Supergroup in Canada). The first was to elucidate the nature of the controversial 'string-of-beads' feature in mudstones in the lower Appekunny Formation and to test the interpretation that this is the oldest eukaryotic macrofossil in the rock record. Detailed observations showed that it is not a fossil, and also provided new insight on the deposition of the host sediment. A novel mechanism was proposed whereby flocculated clay and clay flakes became bound on a benthic microbial mat with a wrinkled upper surface that lent a quasi-organized aspect to the bound particles. This model has implications for other pre-Cambrian and as well Phanerozoic sedimentation processes. It has been assumed for some time that shallow-marine substrates before the onset of widespread bioturbation in the early Paleozoic were extensively covered by these mats or biofilms and that they must have played important roles in sediment binding, rheology, erosion and so forth. On the other hand, even circumstantial evidence for these coverings has not been strong. This part of the study provides some guidance for what could be looked for in other successions.

The second part of this study was to conduct a sedimentological analysis of the underlying carbonate succession consisting of the Waterton and Altyn formations. These units comprise a carbonate platform seemingly uniquely located in just this, the northeastern part of the Belt Basin, early in its history. These rocks had essentially not been studied since the 1980s, meaning that the time was ripe for a fresh analysis, informed not only by advances in the discipline but also the re-interpretations of younger units by my supervisor, which contrast markedly with the work by others. Stratigraphic relationships and facies description showed that these rocks were not tidal flat deposits, as held by earlier studies, and instead the different sediment types reflect bathymetry and paleogeography of a mid- and outer shelf and ramp setting. Fine-grained carbonate sediment was exported from the shallow carbonate factory, as expected, but as the platform prograded and shallowed, tsunami-induced backwash helped deliver coarse carbonate sediment, coastal siliciclastic sand, and even particles from evaporitic tidal flats out onto the shelf. In the mid-shelf setting, this material was reworked, and the agent of reworking was interpreted to be tides. These tides created dunes and also, in places, migrating sand bars with relief of several metres.

The recognition of stratigraphically frequent 'tsunamites' is new for the Lower Belt platform, but it dovetails with the model proposed two decades ago for the younger carbonate unit that accumulated when the entire basin had shallowed and no longer had much bathymetric relief. This analysis shows that ascribing relatively high-energy deposits to storms, as is routinely assumed, is not necessarily justified, especially once the larger paleoclimatic context is appreciated: the Belt Basin seems to have been an arid region without major storm or hurricane activity.

A further achievement of this study was to interpret thick, cross-bedded grainstones as the deposits of dunes created by variably directed tidal flood and ebb currents. This is the only reasonable mechanism to produce the sedimentary structures in the absence of strong storms, as shown by the absence of hummocky cross-stratification in the Altyn Formation. Moreover, broadly lenticular grainstone beds and units with clinoforms are taken as due to migrating tidal sand bars in parts of the shelf under the right conditions. This is the first time that tidal

deposits are identified in the Belt Basin. It may be that tidal effects diminished as the basin filled in due to the voluminous supply of mud from the west.

While the role of earthquakes in generating synsedimentary deformation features had previously been noted in the Altyn Formation, they had not been described in detail nor recognized in the Waterton Formation. This study accomplishes that and provided evidence that the events that deformed the sediment were not necessarily the same events that generated the tsunamis. This is evidence for a complex structural fabric of the Belt Basin even during its early history. During subsidence, some fault displacements generated tsunamis while other faults, probably even proximal to the platform, generated strong earthquakes only.

While the Belt Basin was a large sea that formed in a unique tectonic setting in an unusually tectonically active setting, the results of this sedimentological work are valuable for at least two reasons: the first being that there are implications for other basins, both pre-Cambrian and Phanerozoic, in which: (1) conventional facies interpretation should be reconsidered; (2) tides may have been more important than appreciated, and if not, why not; and (3) syndepositional tectonic activity may have played a more important role than is recognized.

2. Future research

Geological research is open-ended, and fundamental questions evolve as understanding and technology advance. This study points to some obvious future research directions:
(1) Re-consider the range of so-called 'microbially induced sedimentary structures' (MISS) in order to evaluate the criteria and validity for their recognition.
(2) Re-examine other examples of *Horodyskia* in order to test the proposed model.
(3) Explore the morphology and microstructure of stromatolites throughout the Belt Supergroup and try to relate the differences to environmental changes.
(4) Refine the criteria to distinguish between autochthonous deposits versus allochthonous sediments within carbonate platforms.
(5) Test the assumption that storms are the main high-energy events in shallow-marine settings, and explore instead the possibility that tsunamis were agents of deposition in the offshore.
(6) Explore the intricacies of evaporite formation in tidal flats and coastal areas, and the potential for offshore flow of dense hypersaline brines.
(7) Distinguish between deformation features versus primary sedimentary structures, such as folds versus stromatolites and folds versus tepee structures, in order to develop more fully the appreciation of sediment rheology.
(8) Reinforce the distinction between earthquake-induced cracking and sediment injection in mudstones versus desiccation and gravitational crack filling.
(9) Explore evidence for tides in overlying units and elsewhere, and relate that with notions of a closer moon in the Proterozoic.
(10) Explore the precipitation of silica in marine and peritidal carbonate muds, such as the chert and replaced evaporites in the Lower Belt.
(11) Decipher the nature of dolomitization in the Lower Belt, and especially the mimetic replacement in some facies and not others, and the possibility of later episodes of dolomitization.
(12) Use the Lower Belt to further understand the sedimentological and geochemical evolution of the whole basin, especially how sedimentary processes changed as it shallowed

APPENDIX – MEASURED SECTIONS

A.1. Bear's Hump

Section through middle and upper Altyn Formation measured on the south side of Mount Crandell from scree slope above Akamina Highway up to the top of the "hump". Section is above the Mount Crandell thrust. 49°03'26"N, 113°55'10"W

	Description	Facies	Total Thickness (m)
39.2	Fine- to coarse-grained, sandy dolograinstone. Local intraclasts	Grainstone	84.1
	Fault		
~8	Interbedded sand-bearing, very coarse grained dolograinstone and fissile dolomudstone. Tabular cross-bedded and planar laminated.	Grainstone	44.9
	Fault		
~8	Dark-grey, very coarse-grained, sand-bearing dolograinstone. Trough and tabular cross-bedding and planar laminated.	Grainstone	36.9
~4.5	Interbedded fissile dolomudstone and very-fine grainstone. Tabular and planar laminated.	Laminite	28.9
0.4	Wave-ripple cross-laminated, folded dolomudstone	Laminite	24.4
0.4	Tabular cross-bedded, coarse-grained dolograinstone.	Grainstone	24
0.5	Wave-ripple cross-laminated dolomudstone	Laminite	23.6
	Fault		
~8	Fissile, tabular cross-bedded and wave-ripple cross-laminated, sand-bearing dolomudstone with ruptured laminae.	Laminite	23.1
~7.5	Trough and tabular cross-bedded, dark-grey sand- and ooid- bearing, very coarse grained dolograinstone.	Grainstone	15.1
	Fault		
1.3	Fissile, wave-ripple cross-laminated dolomudstone.	Laminite	8.1
6.8	Interbedded fissile, wave-rippled cross-laminated dolomudstone, up to 0.7 m thick, and coarse-grained dolograinstone bearing planar lamination and tabular cross-bedding (up to 4.2 m thick).	Laminite	6.8

A.2. Bosporus ridge

Section through middle and part of the upper Altyn Formation along ridge on the east side of Upper Waterton Lake south of the Bosporus channel. 49°02'53"N, 113°53'50"W

	Description	Facies	Total Thickness (m)

6	Planar laminated and tabular cross-bedded, very coarse-grained dolograinstone. Light-grey colour. Large sections of ruptured bedding.	Grainstone	63.1
10.2	Trough cross-bedded and planar-laminated, very coarse-grained dolograinstone. Weathered dark-orange and grey colour.	Grainstone	57.1
5.5	Planar laminated and tabular cross-bedded, very coarse-grained dolograinstone. Dark-grey colour.	Grainstone	46.9
11	Interbedded, tabular cross-bedded with planar-laminated, very coarse-grained dolograinstone (1.4–2.1 m thick beds), and thin-bedded wave-ripple cross-laminae dolomudstone.	Grainstone/ Laminite	41.4
10.5	Fissile, grey and red-stained, wave-ripple cross-laminated dolomudstone	Laminite	30.4
15.6	Orange-weathered, coarse-grained sandy dolograinstone with lenses of wave-ripple cross-laminated, nodular dolomudstone. Planar laminated with ruptured laminae and scours.	Grainstone	19.9
4.3	Fissile, grey, wave-rippled cross-laminated dolomudstone.	Laminite	4.3

A.3. Waterton lakeside

Cliffs and beachfront to the southwest of Waterton townsite and campground. The section is in the lower Altyn Formation, which is faulted against 3.82 m of ribbon limestone of the Waterton Formation. 49°02'37"N, 113°54'55"W

	Description	Facies	Total Thickness (m)
28.8	Interbedded beige sand- and silt- bearing dolosiltstone. Wave-ripple cross-laminated and small ruptured laminae.	Laminite	28.8

A.4. Akamina Highway

Multiple sections of Waterton Formation along the Akamina Highway. Sections measured between 49°03'16"N, 113°55'00"W and 49°04'24"N, 113°57'02"W

	Description	Facies	Total Thickness (m)
3.4	Beige and blue-grey dolomudstone and lime mudstone, wave-ripple cross-laminated, chert nodules, and convolute bedding.	Ribbon	20.9
3.1	covered		17.5

0.4	Beige and blue-grey dolomudstone and lime mudstone, wave-ripple cross-laminated, ruptured laminae and chert nodules.	Ribbon	14.4
2.1	Covered		14
1.1	Beige and blue-grey dolomudstone and lime mudstone, wave-ripple cross-laminated, ruptured laminae and chert nodules.	Ribbon	11.9
1.3	Beige and blue-grey dolomudstone and lime mudstone, wave-ripple cross-laminated, ruptured laminae and chert nodules.	Ribbon	10.8
2	Covered		9.5
2.6	Beige and blue-grey dolomudstone and lime mudstone, wave-ripple cross-laminated, ruptured laminae and chert nodules.	Ribbon	7.5
0.6	Covered		4.9
4.3	Beige and blue-grey dolomudstone and lime mudstone, wave-ripple cross-laminated and planar laminated, ruptured laminae and chert nodules.	Ribbon	4.3

	Description	Facies	Total Thickness (m)
3.3	Beige and blue-grey dolostone. Fissile, with wave-ripple cross-laminated.	Laminite	13.1
9.8	Beige and blue-grey dolomudstone and lime mudstone. Small chert nodules, wave-ripple cross-laminated and ruptured bedding.	Ribbon	9.8

	Description	Facies	Total Thickness (m)
14.7	Beige and blue-grey dolomudstone and lime mudstone. Chert nodules, ruptured and wave-ripple cross-laminae.	Ribbon	29.4
14.7	Red- and green- stained dolomudstone. Convolute bedding, chert nodules and ruptured wave-rippled cross-laminae.	Laminite	14.7

A.5. Apikuni Falls

The type ‘section’ of the Altyn Formation on the west side of Mount Apikuni, exposes the middle and upper Altyn Formation. 48°48'50"N, 113°38'32"W

	Description	Facies	Total Thickness (m)
7.2	Green, wave-ripple cross-laminae, argillaceous siltstone with interbedded very coarse, tabular cross-bedding and planar laminae bearing sandstone.	Appekunny Formation	
0.4	Planar laminated dolograinstone.	Grainstone	121.6
8.6	Interbedded, fissile, green-grey argillaceous siltstone and beige dolomudstone.	Laminite	121.2

7.0	Interbedded stromatolite beds, ~3m thick, and sandy dolograinstone with planar lamination. Intraclasts stack up against stromatolite mound.	Stromatolite /Grainstone	112.6
5.8	Fissile, wave-ripple cross-laminated, beige and grey dolomudstone.	Laminite	105.6
1.6	Planar laminated, sandy dolograinstone.	Grainstone	99.8
3.4	Fissile dolomudstone with wave-ripple cross-laminae.	Laminite	98.2
2.3	Interbedded sandy dolograinstone and dolomudstone	Grainstone	94.8
9.5	Very coarse, oolitic dolograinstone. Top section deposited in large clinoforms averaging 5 m thick.	Oolite	92.5
22.4	1.8 m dolomudstone overlain by 20.6 m of coarse sandy dolograinstone.	Grainstone	83
5	1.8 m stromatolite mounds overlain by 1.8 m sandy dolograinstone, overlain by 1.4 m stromatolite mounds. Localised microfaults in grainstone.	Stromatolite	60.6
3	Dolomudstone overlain by sandy dolograinstone. Convolute lamination.	Grainstone	55.6
8.6	Stromatolite biostrome 2 m thick at base. Overlain by 0.6 m interbedded dolograinstone and dolomudstone. Overlain by 6 m of stromatolite bioherms 5 m in diameter, with flanking dolomudstone.	Stromatolite	52.6
7.5	Sandy-dolograinstone. Locally cross-laminated. Scattered interbeds of dolomudstone.	Grainstone/ Laminite	44.1
13.5	*Baicalia* Stromatolite mounds, 1.5 to 3.2 m thick. Interbedded dolograinstone and lesser dolomudstone. Columns locally toppled, intraclastic. Mound at 28 m above base – stromatolites in plan view orientated east-west.	Stromatolite/ Grainstone	38.6
18.4	Interbedded dolomudstone and coarse-grained, locally intraclastic dolograinstone. Locally cross-laminated, microfaulted and convolute laminae.	Laminite/ Grainstone	25.1
1.5	*Baicalia*-bearing stromatolite beds, with intraclastic dolograinstone at base	Stromatolite	6.7
2.6	Interbedded dolomudstone and medium-grained sandy grainstone.	Laminite/ Grainstone	5.2
0.3	Stromatolite patch reef (2m wide) flanked by intraclastic dolomudstone and sandy dolograinstone	Stromatolite	2.6

1.1	Interbedded dolomudstone with medium- to coarse-grained sandy grainstone. Ball-and-pillow structures	Laminite/ Grainstone	2.3
1.2	Medium- to coarse- sandy dolograinstone. Planar- and cross-laminated	Grainstone	1.2

A.6. Apikuni Mountain

Eastern side of Apikuni Mountain, 4 km northeast of Apikuni Falls, exposing upper Altyn Formation. 48°49'47"N, 113°37'26"W

	Description	Facies	Total Thickness (m)
~3	Sand- bearing, planar laminated dolograinstone.	Grainstone	~44.8
2.20	Fissile, dolomudstone with ruptured, wave-ripple cross-lamination.	Laminite	~41.8
~14	Interbedded columnar-branching stromatolite beds and fissile wave-rippled dolomudstone.	Laminite/ Stromatolite	~39.6
5.6	Very coarse-grained, sandy dolograinstone interbedded with thin beds of dolomudstone	Grainstone	~25.6
~6	Columnar-branching stromatolite beds interbedded with dolograinstone and dolomudstone beds.	Stromatolite	~20
~14	Very coarse-grained dolograinstone beds interbedded with dolomudstone beds.	Grainstone	~14

A.7. Crypt Lake north shoulder

Mountainside above the footpath and the Crypt Lake tunnel. Uppermost part of the Altyn Formation into the Appekunny Formation. Access to lower section of the area restricted by request of Parks Canada. The cliff beneath the section shows that grainstones are deposited in decametre-long lenses, up to two metres thick, interbedded with laminite. 49°00'24"N, 113°50'19"W

	Description	Facies	Total Thickness (m)
2.24	Green, wave-ripple cross-laminae argillaceous siltstone with interbedded very coarse quartzite.	Appekunny Formation	
9.4	Very coarse, sandy, tabular cross-bedded dolograinstone interbedded with fissile dolomudstone.	Grainstone	33.5
2.8	Columnar-branching stromatolite beds, with sandy dolograinstone and interbedded thin-bedded dolomudstone.	Stromatolite	24.1
9.2	Sandy, medium- to coarse-grained dolograinstone with interbedded	Grainstone	21.3

	dolomudstone laminae. Wave-rippled, and tabular cross-laminae. Ruptured laminae present, as well as scours and thin infills of black/dark green quartzite (up to 0.6 m deep).		
~6	Covered area with dolomudstone scree. Small (<0.2 m) outcrops of grainstone and laminite.	Laminite	12.1
6.1	Beige-coloured, medium-bedded wavy-laminated dolomudstone, and wavy-laminated interbedded fine- to medium grained sandy dolograinstone beds. Scours (0.1–0.6 m deep) infilled with very coarse grained black/dark green quartzite, overlain by very coarse sandy grainstone (0.2 m thick) at top of grainstone bed.	Laminite	6.1

A.8. Sofa Mountain

Section through the Waterton and Altyn formations follows ridgeline up from between two cirques on the north side of Sofa Mountain. The lowest 40 m of the section is a fault bound slice of the Appekunny Formation. 49°02'06"N, 113°47'16"W

	Description	Facies	Total Thickness (m)
~6.5	Interbedded, green and purple argillaceous silt- and very fine sandstone.	Appekunny	
2	Interbedded, very coarse quartzite with fissile, green argillaceous siltstone.	Appekunny	
41.2	Light-grey sandy, planar cross-bedded, medium-grained dolograinstone 0.8–3 m thick. Fault 3 m from the top.	Grainstone	236.2
46.4	Sandy, planar cross-bedded, very coarse-grained dolograinstone.	Grainstone	195
4.3	Light-grey, sandy, tabular cross-bedded fine-grained dolograinstone.	Grainstone	148.6
5.1	Grey sandy, tabular cross-bedded with planar laminated, very coarse-grained dolograinstone.	Grainstone	144.3
25.6	Dark-grey, tabular and trough cross-bedded, very coarse grained dolograinstone.	Grainstone	139.2
~31	Medium to thick bedded dolograinstone beds with interbedded dolomudstone. Increasing sand content throughout section. 10 m beneath main cliff: ~2 m thick, wavy lenticular laminite overlain by 1.5 m of	Grainstone	113.6

	medium- to coarse-grained, intraclastic doloarenite.		
5.2	Beige dolomudstone with intraclasts and very fine sand lenses.	Laminite	82.6
~15	Fissile, beige dolomudstone with planar bedding and wave-ripple cross-laminae. Red-stained laminae in sporadic beds. Sandy grainstone beds appearing around 10 m, with increasing sand content throughout section.	Laminite	77.4
16.3	Fissile, beige wave-ripple cross-laminae dolomudstone with red-stained silt-bearing laminae packages.	Laminite	62.4
21.1	Fissile, interbedded beige and blue-grey, silt-bearing and wave-ripple cross-laminated dolomudstone.	Laminite	46.1
~25	Fissile, interbedded beige and blue-grey, heavily folded, brecciated and ruptured dolomudstone. Most of section covered by scree.	Laminite	~25
	Fault; uppermost Waterton exposed laterally in cirque.		
~10	Medium to thick lenticular beds of very fine to medium grained sandstone. Low relief hummocky cross-bedding with mud interbeds. *Horodyskia* found in muds, with the beds containing scattered injection dykelets and small crack networks.	Appekunny (fault bound)	
~15	Medium to thick-bedded very fine to medium grained sandstone and argillaceous mudstone with dolomite beds. Planar to tabular cross-laminated, with large ripples.	Appekunny (fault bound)	
~15	Medium to thick-bedded, laminated dolomite. Interbedded with green sandstone and mudstone (interspersed and sporadic). Sporadic disrupted laminae, domes up to 10s of metres in thickness and folded beds.	Appekunny? (fault bound)	

A.9. Bertha Bay

Stream cut on the east side of Mount Richards, about 500 m south of the Bertha Bay campsite. 49°00'57"N, 113°54'37"W

	Description	Facies	Total Thickness (m)
14.7	Beige and blue-grey dolomudstone and lime mudstone, chert nodules, wave-ripple cross-laminae and ruptured laminae.	Ribbon	29.4

14.7	Silt- and fine sand-bearing dolomudstone. Convolute bedding and ruptured wave-ripple cross-laminae.	Laminite	14.7

A.10. Bertha Creek

Thrust fault-bounded section of the Bertha Lake trail; base of section faulted against middle Altyn grainstone. 49°02'04"N, 113°54'51"W

	Description	Facies	Total Thickness (m)
10	Thin-bedded, fissile, dolomudstone.	Laminite	39
5	Covered. Surface scree is dolomitic laminite.		29
2	Thin-bedded, fissile, dolomudstone.	Laminite	24
3	Thin- to medium-bedded, wave-rippled, nodular, intraclastic dolomudstone and lime mudstone. Folded laminae. Intraclastic flat pebble conglomerate (clasts up to 30 mm in length).	Ribbon	22
3	Covered		19
3	Medium-bedded, wave-rippled, nodular, intraclastic and folded dolomudstone and lime mudstone.	Ribbon	16
	Joint plane		
2	Medium-bedded, wave-rippled, nodular, intraclastic and folded dolomudstone and lime mudstone.	Ribbon	13
5	Thin- to medium-bedded, wave-rippled, nodular, intraclastic dolomudstone and lime mudstone. Folded laminae. Molar-tooth structure beds at base and 3 m into unit.	Ribbon	11
1	Medium-bedded, nodular, dolomudstone and lime mudstone.	Ribbon	6
5	Medium planar-bedded and cross-laminated, medium- to coarse-grained dolograinstone. Fault bound	Grainstone	5

A.11. Syncline Brook stream cut.

Stream cut expose part of Upper Altyn Formation on the east side of Syncline Mountain, ~1 km southwest of section on Syncline Mountain. 49°20'58"N, 114°25'10"W

	Description	Facies	Total Thickness (m)
2.5	Sandy, very coarse ooid-bearing dolograinstone.	Grainstone	21.6

19.2	Sandy dolograinstone 1.5–4.2 m thick, interbedded with fissile beds of dolomudstone 0.2–0.8 m thick.	Grainstone/ Laminite	19.2

A.12. Syncline Mountain

Waterton formation and Altyn formation exposed on ridge on northeastern side of Syncline Mountain. Lower part (92.5 m) of section measured on northeastern side, and upper part on southeastern side. Measured in two stages. 49°21'57"N 114°24'57"W and 49°21'25"N 114°25'10”W

	Description	Facies	Total Thickness (m)
17.5	Medium- to thick-bedded sandy dolograinstone. Medium- to coarse-grained, with ball-and-pillow structures.	Grainstone	193.5
14.5	Medium-bedded lime mudstone interbedded with medium-bedded grainstone. Lateral variation in dolomitization. At top, 0.5 m thick stromatolite mound (10m wide). Limestone and grainstone beds effected by ball-and-pillow deformation (up to 2 m thick). Local, possible, small scale hummocky cross-lamination.	Grainstone	176
9	Thin- to medium-bedded grainstone, affected by up to 1 m thick ball-and-pillow structures and convolution bedding. Variably sandy with medium- to coarse-grained beds with small intraclasts (1–5 cm).	Grainstone	161.5
13	Three domal and branching stromatolite moundss up to 2m thick, interbedded with fine- to medium-grained dolograinstone beds up to 0.5m thick.	Stromatolite	152.5
22	Planar-laminated, wave-rippled microcrystalline dolomite. Localised cross-lamination and 1cm deep scours.	Laminite	149.5
35	60 cm of medium-bedded, planar-laminated sandy grainstone containing 1cm deep scours and wave ripples. Overlain by 34.4 m of thin- and wavy-bedded and nodular lime mudstone, localised cross-lamination, some interbedded sandy, laminated dolomite intervals (between 0.5–1 m thick)	Ribbons	127.5
69	Thin- and wavy-bedded nodular dolomudstone and lime mudstone, with local cross-lamination.	Ribbon	92.5

2.5	Locally thick-bedded lime mudstone (microspar) with cm-scale cross-lamination.	Ribbon	23.5
21	Planar-laminated, dolomudstone, common thin lenticular-bedding due to wave ripples	Laminite	21

A.13. Pincher Ridge

Tongue of Altyn-like facies on Pincher Ridge, measured above Drywood Creek, in Appekunny Formation and previously identified as Siyeh Formation in the Chinook South map. 49°17'15.4"N 114°04'23.4"W

	Description	Facies	Total Thickness (m)
7	Interbedded, thin-bedded,argillaceous dolomudstone and fine-grained dolograinstone. Planar and trough cross-lamination (paleocurrents to N and NE).	Appekunny	71
7	Covered.	Appekunny	64
26	Thick-bedded coarse sandy grainstone with ball-and-pillow structures grading into covered, sporadic beds of interbedded coarse- and finer-grained grainstone. 10 cm deep scours and hummocky and swaley cross-stratification at top.	Grainstone	57
18	Medium- to thick- bedded, sandy dolograinstone with rare, interbedded, thin beds of wavy-laminated dolomudstone and up to decametre thick ball-and-pillow structures.	Grainstone	31
13	Thin- to medium- bedded, variably sandy dolograinstone. Small scale hummocky cross-stratification, tabular and lenticular bedding. Large scours (up to 20 cm deep), infilled with symmetrical ripples.	Grainstone	13